
# The Pursuit of Causality in Multivariate Statistical Control of Aluminium Smelting Cells

**Marco Alexander Stam**

A thesis submitted in fulfilment of the requirements for the degree of
Doctor of Philosophy in Engineering

The University of Auckland
October 2011

# Abstract

Aluminium smelting cells are operated at the limit of their capability by the adaptation of increasingly higher line current and the requirement of maximum flexibility in energy input and raw materials used. Poor controllability and observability limit both energy efficiency and productivity of pot lines under these varying inputs. Based on several key hypotheses which are developed and tested here, a new control approach is demonstrated for smelting cells, to tackle the cell variability over a wide range of time scales and in a way which reduces this variation over time.

In the present thesis a novel control scheme has been tested on 10 industrial cells. These results are compared to the period before the test and to a group of 10 reference cells. The control philosophy is based on the determination of cell-specific natural behaviour envelops using Hotelling $T^2$ statistic and cause-specific detection of abnormalities. A sludge cycle is identified as one of the main self-accelerating destabilising mechanisms in smelting cells driving substantial variations in liquid bath mass up to 50%. This overrides the self-regulating side wall ledge mechanism, and moves the liquid bath mass and chemistry out of the optimum operating range.

The natural behaviour envelops are based on a moving window of the interchanging of the bath temperature, liquidus point and the rate of alumina accumulation to allow maximum flexibility. The size and shape of these ellipsoidal envelops are characteristic of the presence or absence of bath mass variation through the above sludge cycle. These envelops allow multivariate detection of abnormalities and this detection is combined with online Pareto and root cause analyses. This cell control scheme has been demonstrated to improve the quality of decision-making. Identification of causes of abnormality and their correction or removal through this system allows continuous improvement on a daily basis.

For the test cells, the employment of the new control philosophy presented in this thesis has resulted in a higher current efficiency (+2.0%, p=0.075) and significantly lower energy consumption (-0.42 kWh/kg, p=0.034) for 2008 compared to 2007. The new control scheme has been implemented for all cells on both pot lines at Aldel in 2009. In the future, further control system improvements to alumina feeding, along with extension of the multivariate control approach and incorporation of human decision guidance will have even greater implications for the flexibility of smelter operation under the constrained global electricity market conditions prevailing.

# Acknowledgements

"I'm working on a dream" – Bruce Springsteen (2009)

The journey of this thesis started during the first superheat user meeting in South Africa (March 20-23, 2005). At the farewell dinner, a research project was founded. It was a step in uncertainty. Not only the scientific and industrial challenges were adventurous, but also the collaboration with a group of international partners has broadened my view to the world. From time to time it drew heavily on my energy, but the spirit to finish it was always there.

During this journey the support of friends and colleagues was encouraging and meaningful to me. In this respect I would like to thank my supervisor, colleague and friend Professor Mark Taylor for his support, outstanding knowledge and drive. Innumerable moments of intense discussions about life, sports and above all smelting technology were alternated with a good glass of wine or beer. I'd also like to thank his wife Florence for her support. Thirdly I am grateful to Professor John Chen. As co-supervisor he is very knowledgeable in the field of process control and aluminium smelting. He helped me with the scientific foundation of the thesis and to find my way within the university.

Furthermore, I owe much to my colleagues at Aluminium Delfzijl. Albert Mulder spent a lot of time in programming my never-ending flow of new ideas. Especially the 3D representation of the natural behaviour envelops took the best out of him. All regular and also special process measurements were controlled by Sikke van Dellen and his team. I thank them for their great contribution. Without measurements, there are no results. I am grateful to the management team of Aluminium Delfzijl for their interest and support.

This research has been partly financed by Heraeus Electro-Nite. I had great contacts with Renuka Rodrigo. He was already present in the early stage of this work and we had several constructive discussions and generated a lot of ideas. Above all we enjoyed many breakfasts in the "Slurp Bar" at the Campus and dinners in good restaurants in Auckland or Groningen. Further, I thank Rik Kelchtermans and Peter White for their contribution. We were lucky to meet each other in several interesting places around the world.

Also I would like to thank the people from the Light Metals Research Centre at the University of Auckland. A warm welcome was part of my time at the Centre. I liked presenting my work to the staff, researchers and students during my seminars. Twice I participated in the yearly Christmas Party, full of sports, food and drinks. Their team spirit is catching. Especially I am grateful to Nazatul, who helped me with the PCA and PLS analyses. I also like to thank Song for our discussions about human decision making. These talks were always interesting and

sometimes full of nonsense. Furthermore, I thank Wei, Linus, Pascal, Pretesh, Jenny and Marcus for their help and great times in Auckland.

In addition, I would like to thank friends and family. Although the topic of my research is way out of their daily lives, they were always interested in my work and curious about my stories. I had energetic discussions about several topics. Mostly my thesis was only a starting point of these talks. In this respect I liked the lectures about modern philosophy at the University of Groningen. I always look for synergies with other disciplines.

This journey brought me to several places in the world. At the age of eleven I already dreamt of a trip to New Zealand. A book in the library drew my attention due to the enormous variety in landscapes and nature. I was very lucky to spend two holidays in New Zealand. Both trips were awesome, above all due to the company of my wife Maartje. I would like to express my deepest feelings to her. She helped me to develop myself into a much broader personality and interests. During the work of this thesis she was always open for valuable advices and supported me to finish it.

Marco Stam
Groningen, December 2010

# Table of Contents

# List of Figures

# List of Tables

# Nomenclature

| Variable | Description | Unit |
|---|---|---|
| $\tau$ | Coefficient of Cell Construction related to Age | day |
| $\chi^2$ | Chi-squared Statistic | - |
| $\sigma^2_{TB}$ | Temperature Variance | - |
| $\sigma^2_{TBTL}$ | Temperature-Liquidus Covariance | - |
| $\sigma^2_{TL}$ | Liquidus Variance | - |
| $\eta_{AA}$ | Anode Reaction Overvoltage | V |
| $\eta_{AC}$ | Anode Concentration Overvoltage | V |
| $\eta_{CC}$ | Cathode Concentration Overvoltage | V |
| $\Delta t_{A,i}$ | Average Travel Time of Plunger A | s |
| $\Delta t_{B,i}$ | Average Travel Time of Plunger B | s |
| $\Delta V$ | Voltage Adjustment | V |
| $a$ | Activity | - |
| $A_{bath\text{-}sludge}$ | Interfacial Electrolyte/Sludge Area | $m^2$ |
| $acd$ | Anodic Current Density | $A \cdot cm^{-2}$ |
| $ACD$ | Anode Cathode Distance | cm |
| $age$ | Cell age | day |
| $[Al_2O_3]$ | Alumina Concentration in Electrolyte | wt% |
| $[Al_2O_3]_{sat}$ | Alumina Saturation Concentration in Electrolyte | wt% |
| $A_{ledge}$ | Side Ledge Area | $m^2$ |
| $[AlF_3]$ | Aluminium Fluoride Concentration in Electrolyte | wt% |
| $[AlF_3]_{target}$ | Target Aluminium Fluoride Concentration in Electrolyte | wt% |
| $Anode_{insertion\text{-}height}$ | Anode Insertion Height | mm |
| $Anode_{reference\text{-}height}$ | Anode Reference Height (Marking on Anode Rod) | mm |
| $Beam_0$ | Beam Position at Reference Point | mm |
| $Beam_{actual}$ | Actual Beam Position | mm |
| $[CaF_2]$ | Calcium Fluoride Concentration | wt% |
| $[CaO]$ | Calcium Oxide Concentration in Alumina | wt% |
| $CE$ | Current Efficiency | - |
| $CR_{Al2O3}$ | CUSUM of Ratio of Alumina Fed to Cell | - |
| $CR_{Al2O3,\ previous}$ | Previous CUSUM of Ratio of Alumina Fed to Cell | - |
| $e(t)$ | Function of PID Controller | - |
| $E^0$ | Reaction Potential at Standard Conditions | V |
| $E_{Al}$ | Energy Consumption | $kWh \cdot kg^{-1}$ |
| $Energy_{acc}$ | Energy Accumulation | $J \cdot s^{-1}$ |

| | | |
|---|---|---|
| $Energy_{in}$ | Energy In | $J \cdot s^{-1}$ |
| $Energy_{out}$ | Energy Out | $J \cdot s^{-1}$ |
| $Energy_{prod}$ | Energy Production | $J \cdot s^{-1}$ |
| $E_{rev}$ | Decomposition Potential | V |
| $F$ | Faraday Constant | $C \cdot mol^{-1}$ |
| $F_{AlF3}$ | $AlF_3$ Addition | $kg \cdot day^{-1}$ |
| $F_0$ | Base Addition of $AlF_3$ related to Cell Age | $kg \cdot day^{-1}$ |
| $h_B$ | Heat Transfer Coefficient between Electrolyte and Ledge | $J \cdot m^{-2} \cdot °C^{-1} \cdot s^{-1}$ |
| $H_{bath}$ | Bath Height | cm |
| $H_{liq}$ | Calculated Total Liquid Height | mm |
| $H_{metal}$ | Metal Height | cm |
| $I$ | Current | kA |
| $k_a$ | Base Addition of $AlF_3$ | $kg \cdot day^{-1}$ |
| $k_{Al2O3}$ | Alumina Mass Transfer Coefficient | $m^{-2} \cdot s^{-1}$ |
| $k_b$ | Coefficient of Cell Construction related to Base Addition | $kg \cdot day^{-1}$ |
| $k_c$ | $AlF_3$ Concentration Coefficient | $kg \cdot wt^{\%-1} \cdot day^{-1}$ |
| $[KF]$ | Potassium Fluoride Concentration | wt% |
| $kg_{Al2O3}$ | Mass of Alumina Fed to Cell | $kg \cdot h^{-1}$ |
| $k_L$ | Liquidus Temperature Coefficient | $kg \cdot °C^{-1} \cdot day^{-1}$ |
| $k_{liq}$ | Voltage Coefficient for Liquidus Temperature | $V \cdot °C^{-1}$ |
| $K_P$ | Constant of PID Controller | $s^{-1}$ |
| $k_{SH}$ | Voltage Coefficient for Superheat | $V \cdot °C^{-1}$ |
| $k_{SH\text{-}trend}$ | Voltage Coefficient for Trend in Superheat | $V \cdot °C^{-1}$ |
| $k_T$ | Bath Temperature Coefficient | $kg \cdot °C^{-1} \cdot day^{-1}$ |
| $k_{volts}$ | Voltage Coefficient | $°C \cdot V^{-1}$ |
| $[LiF]$ | Lithium Fluoride Concentration | wt% |
| $M_{Al}$ | Molecular Mass of Aluminium | kg |
| $M_{Al2O3}$ | Molecular Mass of Alumina | kg |
| $Mass_{acc}$ | Mass Accumulation | $kg \cdot s^{-1}$ |
| $Mass_{in}$ | Mass In | $kg \cdot s^{-1}$ |
| $Mass_{out}$ | Mass Out | $kg \cdot s^{-1}$ |
| $Mass_{prod}$ | Mass Production | $kg \cdot s^{-1}$ |
| $[MgF_2]$ | Magnesium Fluoride Concentration | wt% |
| $MH_{cal}$ | Calculated Metal Height | mm |
| $n$ | Number of Electrons Involved in the Electrode Reaction | - |

| | | |
|---|---|---|
| $[Na_2O]$ | Sodium Oxide Concentration in Alumina | wt% |
| $OA$ | Number of Overfeeds | - |
| $P_{Al}$ | Production Rate of Aluminium | $kg \cdot h^{-1}$ |
| $PB$ | Pinballing | $°C^{2/3}$ |
| $q$ | Heat Transfer from Bulk Electrolyte to Electrolyte/Ledge Boundary Layer | $J \cdot s^{-1}$ |
| $R$ | Gas Constant | $J \cdot mol^{-1}K^{-1}$ |
| $R_{Al2O3}$ | Ratio of Alumina Fed to Cell | - |
| $R_{anode}$ | Anode Resistance | mΩ |
| $R_{bubble}$ | Gas Bubble Resistance | mΩ |
| $R_{cathode}$ | Cathode Resistance | mΩ |
| $R_{dissolution}$ | Rate of Alumina Dissolution | $wt\% \cdot s^{-1}$ |
| $R_{electrolyte}$ | Electrolyte Resistance | mΩ |
| $R_{ext}$ | External Resistance | mΩ |
| $R_{pseudo}$ | Pseudo Cell Resistance | μΩ |
| $S$ | Estimated Covariance Matrix | - |
| $SH_{measured}$ | Measured Superheat | °C |
| $SH_{number\text{-}days}$ | Number of Days in Slope of Superheat | - |
| $SH_{target}$ | Target Superheat | °C |
| $t$ | Time | h |
| $T$ | Temperature | K |
| $T^2$ | Hotelling $T^2$ Statistic | - |
| $T^2_{UCL}$ | Upper Control Limit of Hotelling $T^2$ Statistic | - |
| $T_B$ | Bath Temperature | °C |
| $T_{B,previous}$ | Previous Bath Temperature | °C |
| $T_{B\text{-}avg}$ | Average Bath Temperature | °C |
| $TC_{Al2O3}$ | Theoretical Consumption Rate of Alumina | $kg \cdot h^{-1}$ |
| $T_{corrected}$ | Corrected Bath Temperature | °C |
| $T_d$ | Derivative Time of PID Controller | s |
| $T_i$ | Integral Time of PID Controller | s |
| $T_L$ | Liquidus Temperature | °C |
| $T_{L,previous}$ | Previous Liquidus Temperature | °C |
| $T_{L\text{-}avg}$ | Average Liquidus Temperature | °C |
| $T_{L\text{-}target}$ | Target Liquidus Temperature | °C |
| $TP_{Al}$ | Theoretical Production Rate Aluminium | $kg \cdot h^{-1}$ |
| $UF$ | Underfeed Duration | $h \cdot day^{-1}$ |
| $v_{A,i}$ | Average Travel Speed of Plunger A | s |
| $V_{avg}$ | Average Cell Voltage | V |

| | | |
|---|---|---|
| $v_{B,i}$ | Average Travel Speed of Plunger A | s |
| $V_{cell}$ | Cell Voltage | V |
| $V_{dev}$ | Natural Voltage Band | V |
| $V_{ellipsoid}$ | Ellipsoid Volume | $°C^2$ |
| $V_{extrapolated}$ | Voltage Intercept | V |
| $V_{setpoint}$ | Setpoint Voltage | V |
| $y(t)$ | Output of PID Controller | - |

# Abbreviations

| Variable | Description | Unit |
|---|---|---|
| *AC* | Anode Changing | - |
| *AE* | Anode Effect | $(cell \cdot day)^{-1}$ |
| *AEERR* | Anode Effect Error | $(cell \cdot day)^{-1}$ |
| *AEKWH* | Anode Effect Energy High | $(cell \cdot day)^{-1}$ |
| *Al2O3H* | CUSUM(Alumina Ratio) High | $(cell \cdot day)^{-1}$ |
| *Al2O3L* | CUSUM(Alumina Ratio) Low | $(cell \cdot day)^{-1}$ |
| *Aldel* | Aluminium Delfzijl B.V. | - |
| *AlF3ERR* | General Hardware Problems $AlF_3$ Feeding | $(cell \cdot day)^{-1}$ |
| *ANHGH* | Anode Set Too High | - |
| *ANOFF* | Anode Drop Off/Clad Failure | - |
| *ANSLP* | Slipped Anode | - |
| *ANSPA* | Automatic Spike Detection | $(cell \cdot day)^{-1}$ |
| *ANSPM* | Spike Detection Measurement Team | - |
| *ANSPS* | Spike Detection Shift Operators | - |
| *BHCALC* | Bath Height Calculation Error | $(cell \cdot day)^{-1}$ |
| *BHH* | Bath Height Calculation High | $(cell \cdot day)^{-1}$ |
| *BHL* | Bath Height Calculation Low | $(cell \cdot day)^{-1}$ |
| *BR* | Beam Raising | - |
| *BVDEC* | Bath Volume Decrease | $(cell \cdot day)^{-1}$ |
| *BVINC* | Bath Volume Increase | $(cell \cdot day)^{-1}$ |
| *CBAN* | Plunger hits Anode | $(cell \cdot day)^{-1}$ |
| *CBDIST* | Slow Plunger | $(cell \cdot day)^{-1}$ |
| *CBERR* | General Hardware Failure $Al_2O_3$ Feeding | $(cell \cdot day)^{-1}$ |
| *CBSPK* | Plugged Feeder | $(cell \cdot day)^{-1}$ |
| *CD* | Current Drop/Outage | $(cell \cdot day)^{-1}$ |
| *CLMVH* | Clamp Voltage High | - |
| *FA* | $Al_2O_3$ Feed Intervention | - |
| *FAC* | $Al_2O_3$ Feed Intervention after AC | - |
| *HOTAH* | Out of Control Behaviour (Hotelling $T^2$) | $(cell \cdot day)^{-1}$ |
| *HOTAL* | Target Region (Hotelling $T^2$) | $(cell \cdot day)^{-1}$ |
| *LIQH* | Liquidus High | $(cell \cdot day)^{-1}$ |
| *LIQL* | Liquidus Low | $(cell \cdot day)^{-1}$ |
| *LM* | Load Management or Power Modulation | - |
| *NP* | Noise High | $(cell \cdot day)^{-1}$ |

| | | |
|---|---|---|
| *OACURV* | Reaction of Cell Resistance to Overfeed | $(cell \cdot day)^{-1}$ |
| *OAERR* | Number of Overfeed Low | $(cell \cdot day)^{-1}$ |
| *PBH* | Pinballing: High Process Velocity | $(cell \cdot day)^{-1}$ |
| *SHH* | Superheat High | $(cell \cdot day)^{-1}$ |
| *SHL* | Superheat Low | $(cell \cdot day)^{-1}$ |
| *TEMPH* | Temperature High | $(cell \cdot day)^{-1}$ |
| *TEMPKH* | Temperature Critical High | $(cell \cdot day)^{-1}$ |
| *TEMPKL* | Temperature Critical Low | $(cell \cdot day)^{-1}$ |
| *TEMPL* | Temperature Low | $(cell \cdot day)^{-1}$ |
| *TOTAN* | Total Number of Anode Failure Events | - |
| *TOTEV* | Total Duration of Events | $(cell \cdot day)^{-1}$ |
| *TP* | Metal Tapping | - |

# Chapter 1 Introduction

This chapter describes the underlying motivation and background for the development of a multivariate causally based control system for aluminium smelters (Section 1.1). In addition, a brief review of the basic principles of the electrolytic reduction of aluminium oxide, which is the main component of the smelting process, is given (Section 1.3). Furthermore, Section 1.4 presents the outline of the thesis.

## 1.1 Motivation and Background

There is a strong pressure to push aluminium smelters towards maximum value for all stakeholders, but both the direction and goal are continuously under discussion and are strongly influenced by rapid changes in economic and environmental circumstances. While the development of cell technology has taken place incrementally, primarily through changing cell dimensions and increasing line current, the current and energy efficiency of the smelting process haven't significantly improved over the last thirty years (Welch and Keniry, 2000). For example the rate of improvement in terms of energy efficiency as well as carbon consumption per tonne of metal produced has slowed down considerably, which indicates that the same or even more causes that contribute towards efficiency losses are still embedded in the process. Today power modulation is imposed on smelter operations because of the availability and price of electricity. Furthermore, there is a gradual degradation and variability in the quality of some of the raw materials used in the process. All these factors add further to the already complex interplay of parameters that affect the control of the process making efficiency improvements difficult.

Process intensification through line current increase has exacerbated the interactions of the various parameters, and imbalances must be sensed quickly and their causes corrected or removed in a timely manner to maintain aluminium smelting cells within their most efficient operating window, or move them quickly to a new economically viable operating region. Advanced control of a type not previously employed is necessary in order to run smelters at these new and challenging required conditions. Causes of variation must be continually identified and removed in the aluminium smelting process using a new control approach - if the cost and energy intensity of the production is to be reduced to sustainable levels in this carbon-sensitive, global economy.

The need for new control strategies is also linked to the necessity to reduce energy usage and to increase the flexibility of energy use (Brant Filho *et al.*, 1992; Stam and Schaafsma, 2007). Power modulation redistributes the energy input into the smelter over time according to the actual and forward prices of electricity. Under these conditions the current is reduced

or even switched off for a particular period of time resulting in large deficiencies in energy input and therefore a deterioration of the process stability. For example a day-night rhythm contains lower and higher line current during day and night respectively. Moreover, existing smelter resource and environmental footprints in many communities will not be tolerated because they are seen as cost and environmental burdens to the community (Moors, 2006; SavingIceland.org, 2009). Rapid and flexible changes in smelter operating conditions are increasingly required to satisfy both regulatory changes and community perceptions.

In this thesis the development of a new multivariate causally based control system has been carried out and tested on an industrial scale. The interactive multivariate nature of the smelting process is incorporated into the new control philosophy in order to improve the quality of decision-making, including automated control actions and human decisions. The research goals are concerned with the scientific investigation of the underlying interrelated system dynamics, the detection of cell abnormalities and process deterioration mechanisms. Through these studies a holistic causally based process control philosophy is developed for aluminium smelting cells. The industrial experiments focus on the application of the control model in reduction lines to improve the overall smelter performance.

The experimental work reported in this thesis was carried out at Aluminium Delfzijl B.V. (Aldel) in the Netherlands. In order to remain competitive within European power prices and environmental regulations, a hugely complex retrofit of the base technology was carried out. All cells were upgraded with new integrated-cradle shells and a high electrical and thermal conductivity lining design, pneumatic dense phase system for alumina transport, alumina and $AlF_3$ point feeders, individual micro-computers and modern dry-scrubber technology. The busbar systems and cells were originally designed for 100 kA and 120 kA respectively. However, the cells are running today at an average of 147 kA including a day-night rhythm of 5 kA without magnetic field modifications to the busbar configuration. This requires a new process control philosophy which focuses on continual identification of abnormalities and variable operating envelop dependent on the daily economics of metal production and sale (Stam *et al.*, 2007).

## 1.2 Aluminium

The earth's crust consists of approximately 8% of aluminium compounds of which bauxite deposits contain up to 60% aluminium oxide composites. Bauxite is composed of one or more aluminium hydroxide complexes plus silica, iron and titanium oxides as the main impurities and must be treated chemically in order to produce alumina (aluminium oxide or $Al_2O_3$).

In the Bayer Process as much aluminium hydroxide compounds and as little impurity oxides as possible are dissolved in caustic soda at high pressure and temperature to form a sodium aluminate solution. After filtration of the insoluble oxides, gibbsite (aluminium tri-hydroxide) is precipitated by seeding and nucleation. The last step in the Bayer Process is calcination of gibbsite into smelter grade alumina. Then aluminium is produced by electrolytic reduction of alumina (Section 1.3). In practice 2 tonnes of alumina, itself extracted from 4 tonnes of bauxite, is required to produce 1 tonne of aluminium.

Nowadays aluminium is used in a broad range of different products. It is used to a large extent in the transport industry because of its high strength to weight ratio (33% less than steel) and good formability. Due to lower construction weight and/or an increase in the mass of transported goods, fuel consumption and $CO_2$ emissions per kilometre are both reduced. For similar reasons aluminium is used in packaging and the building industries. Beside the advantage of low weight, aluminium has excellent corrosion resistance and is easily recycled, requiring only 5% of energy needed for production of the primary metal (Green, 2007). Aluminium is a good conductor of heat as well as electricity. Heat exchangers for the automotive industry and of course most of existing bus bar systems in aluminium smelters are made of aluminium.

## 1.3 Electrolytic Reduction of Alumina

Methods of producing aluminium were only discovered in the early 19$^{th}$ century, but it took another hundred years before a commercially viable industrial production process was invented. In 1886 Charles Hall (USA) and Paul Héroult (France) invented simultaneously and independently of each other an electro-chemical process to produce aluminium. A diagram of a typical aluminium smelting cell is shown in Figure 1.1. Alumina is dissolved in a molten electrolyte, which is a mixture of cryolite ($Na_3AlF_6$) and other fluoride additives (e.g. $AlF_3$, $CaF_2$, $MgF_2$), and is decomposed in an electrolytic process to give liquid aluminium (Grjotheim and Kvande, 1993). The positive electrode (anode) of the electrolytic cell is made of carbon and the pool of already produced aluminium acts as the negative electrode (cathode). Oxygen from alumina is discharged at the anode where it reacts immediately with the carbon anode to produce carbon dioxide ($CO_2$). The primary reaction is given by Equation 1.1.

$$Al_2O_3(sol) + \frac{3}{2}C(s) \rightarrow 2Al(l) + \frac{3}{2}CO_2(g) \tag{1.1}$$

A brief explanation of the basic principles of the electrolytic reduction of alumina is outlined in Sections 1.3.1 to 1.3.6. In order to achieve maximum process stability and efficiency these

basic principles have to be well understood, not only individually, but also their interactions. In this respect these complex multivariate interactions are exacerbated by the employment of power modulation, increased line current and increased variability of the physical quality and impurity content of the raw materials from different supplier sources.

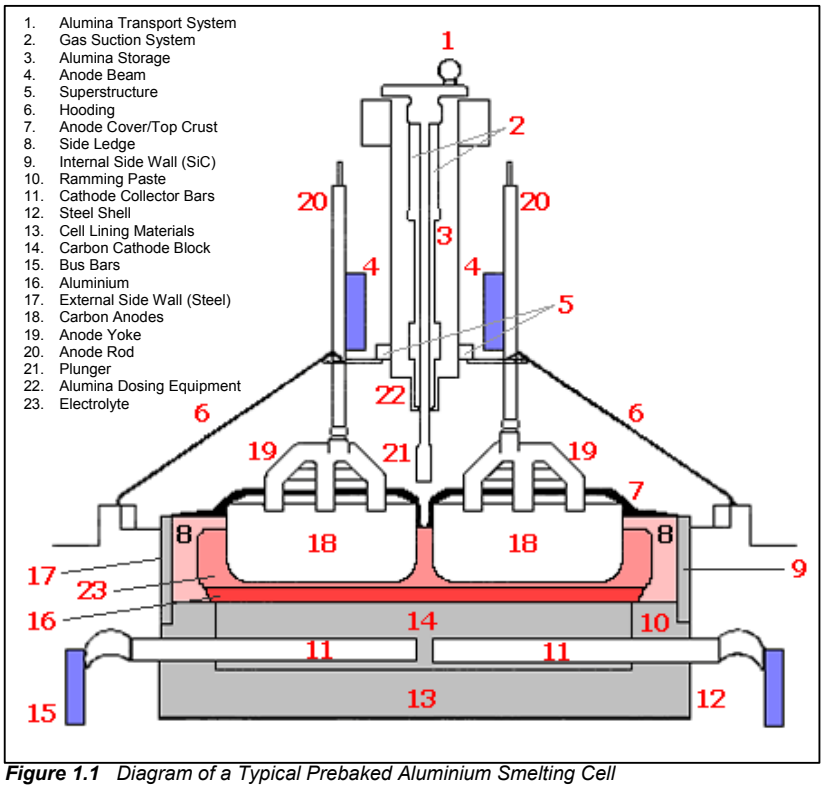


***Figure 1.1*** *Diagram of a Typical Prebaked Aluminium Smelting Cell*

### 1.3.1 Current Efficiency

According to Faraday's law the theoretical electrolytic production rate of liquid aluminium ($TP_{Al}$) is proportional to the amount of current ($I$) passed through a smelting cell and time ($t$) as shown in Equation 1.2.

$$TP_{Al} = \frac{M_{Al}}{nF} \cdot I \cdot t = 0.3356 \cdot I \cdot t \qquad (1.2)$$

Where, $M_{Al}$ is the molecular mass of aluminium, $n$ is the number of electrons transferred in the reaction and $F$ is the Faraday constant. As in every technical electrolytic process, there are losses leading to a lower output than the theoretically calculated amount. Current efficiency *(CE)* is the ratio between the actually produced aluminium ($P_{Al}$) and the theoretical production as shown in Equation 1.3.

$$CE = \frac{P_{Al}}{TP_{Al}} \tag{1.3}$$

The predominant mechanism for the reduced production rate is the partial back reaction of the aluminium produced with dissolved $CO_2$ according to Equation 1.4 (Grjotheim and Kvande, 1993).

$$Al(sol) + \frac{3}{2}CO_2(sol) \rightarrow \frac{1}{2}Al_2O_3(sol) + \frac{3}{2}CO(g) \tag{1.4}$$

The traditional explanation for the back reaction consists of a sequence of events including the chemical dissolution of aluminium at the metal-electrolyte interface and the subsequent transfer into the electrolyte, the mass transfer of dissolved aluminium through the electrolyte and on to the anode gas interface, followed by the oxidation of aluminium (Figure 1.2) (Thonstad *et al.*, 2001). Another pathway is the direct entrainment of aluminium droplets and gas bubbles in the electrolyte (bath) and aluminium respectively (Zhang *et al.*, 1991). Both mechanisms are strongly influenced by the interactions between the electrolyte temperature, the composition of electrolyte and the associated turbulence due, in a large part, to the release of the anode gas (Graduate Certificate Course, 2003).

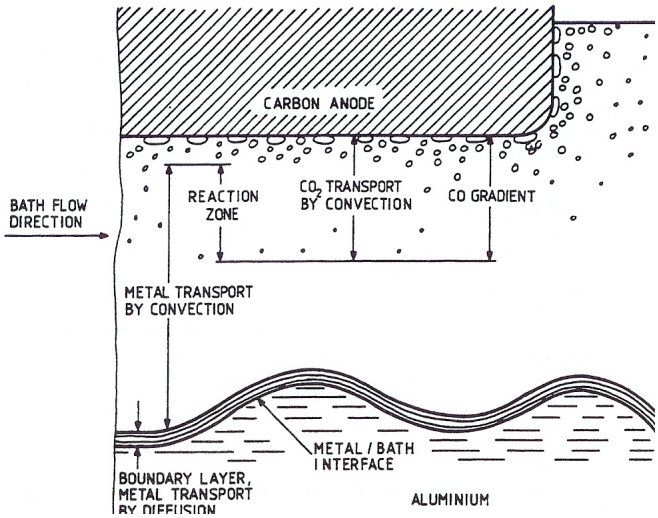


***Figure 1.2*** *Mechanism of Back Reaction (Grjotheim and Kvande, 1993)*

It is generally recognized that in the operation of an aluminium smelting cell, the most efficient operating zone is associated with maximum process stability (Welch, 1998). The turbulence in the bath and metal pad increases the mass transfer of dissolved metal into the electrolyte, which is accelerated by the pumping action of large bubbles of gas that are being released.

Moreover, metal solubility in the electrolyte is determined by the electrolyte temperature and its composition. The influence of the electrolyte composition is described in Section 1.3.3. The complex interactions between electrolyte temperature, electrolyte composition and turbulence are exacerbated by the employment of power modulation, increased line current and increased variability of the raw materials used. Advanced control is required to overcome the corresponding deterioration in the process stability and hence to improve the current efficiency.

Other mechanisms which play a relatively minor role in lowering the current efficiency are the oxidation of other species dissolved in the electrolyte (e.g. $Al_4C_3$, CO, C), electrical short-circuiting at the anode, electronic conduction (e.g. Na-ions), cyclical oxidation-reduction behaviour of multivalent impurities (e.g. P, V), metal losses into the cell lining and other physical losses (Thonstad *et al.*, 2001).

### 1.3.2 Cell Voltage

An electrochemical cell is used for producing chemical reactions that require an applied electrical potential to proceed. The cell voltage may be considered to be made up of three groups as shown in Equation 1.5 (Grjotheim and Kvande, 1993). The magnitude of the individual components is shown in Figure 1.3 (Haupin and Kvande, 2001).

$$V_{cell} = E_{rev} + [\eta_{CC} + \eta_{AA} + \eta_{AC}] + [I \cdot (R_{anode} + R_{bubble} + R_{electrolyte} + R_{cathode} + R_{ext})] \qquad (1.5)$$

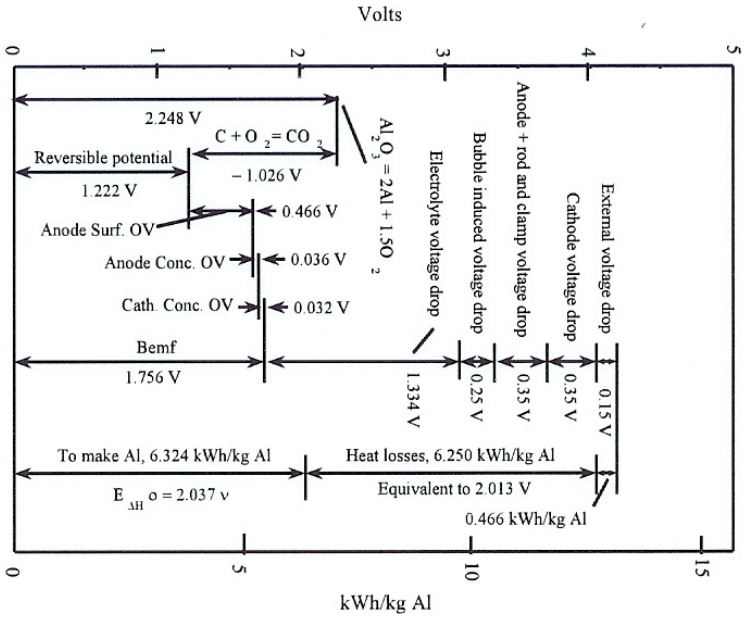


***Figure 1.3*** *Typical Voltage Drops in Aluminium Smelting Cell (Haupin and Kvande, 2001)*

The first group consists only of the decomposition potential *($E_{rev}$)* for the reaction given by Equation 1.1. This decomposition potential *($E_{rev}$)*, for reversible and non-standard conditions, is calculated using the Nernst relationship as shown in Equation 1.6.

$$E_{rev} = E^0 - \frac{RT}{nF} \cdot \ln\left( \frac{a_{CO_2}^{3/2} \cdot a_{Al}^2}{a_{Al_2O_3} \cdot a_C^{3/2}} \right) \tag{1.6}$$

Where, $E^0$ is the standard potential at standard conditions, $T$ is the electrolyte temperature, the notation *'a'* is used to denote activities of the products and reactants and $R$ is the universal gas constant. The activities of aluminium and carbon are unity, because they are pure substances. The activity of $CO_2$ is close to unity and the alumina concentration is the only variable in the decomposition voltage.

The second group in the overall cell voltage consists of the reaction and concentration overvoltages and is temperature dependent (Grjotheim and Kvande, 1993). Polarisation at the carbon anode has a reaction or activation overvoltage *($\eta_{AA}$)* and a concentration *($\eta_{AC}$)* component. The reaction overvoltage makes a significant contribution to the cell voltage and is approximately 0.47V. The anode concentration voltage *($\eta_{AC}$)* is only important at low alumina concentrations. Furthermore, sodium ions are responsible for about 95% of current transport through the electrolyte. The concentration overvoltage at the cathode *($\eta_{CC}$)* is due to a higher concentration of sodium ions at the metal-electrolyte interface compared to the bulk electrolyte. This counter-voltage is dependent on the interfacial turbulence and therefore process stability.

The third group in the cell voltage is the ohmic heat generation due to the resistance imparted by various sections of the cell (Equation 1.5) (Grjotheim and Kvande, 1993). Here, $R_{anode}$, $R_{electrolyte}$, $R_{bubble}$, $R_{cathode}$ *and* $R_{ext}$ are the resistances of anode, electrolyte, gas bubble layer, cathode and all external conductors respectively. Anode, cathode and external resistances are affected by the line current combined with dimensions and material properties. The electrolyte resistance depends on the conductivity, electrode areas, anode cathode distance (ACD) and the volume of gas bubble present. The bubble resistance dominates electrolyte resistance at low ACD.

The smelting process needs energy to produce aluminium and to keep the electrolytic cell at the reaction temperature. The theoretical energy requirement, which can be calculated based on thermodynamics, demonstrates a need of 6.32 kWh per kg aluminium at a current efficiency of 96% and electrolyte temperature of 960°C (Figure 1.3) (Haupin and Kvande, 2001). Specific energy consumption *($E_{Al}$)* is calculated by the energy input divided by the

amount of metal produced (Equations 1.2 and 1.3) and is given by Equation 1.7 (Grjotheim and Kvande, 1993).

$$E_{Al} = \frac{V_{cell} \cdot I \cdot t}{P_{Al}} = 2.98 \cdot \frac{V_{cell}}{CE} \tag{1.7}$$

Current efficiency is strongly affected by the process stability associated with the underlying system dynamics (Section 1.3.1). The process stability is also inversely related to the anode cathode distance. The ACD in aluminium smelting cells is indirectly controlled by the overall cell voltage and a lower ACD results in an increase in the partial back reaction due to magnetically induced turbulences in the metal pad (Section 1.3.5) and a decrease in the distance between the anodic and cathodic reaction areas as shown in Figure 1.2. The individual voltage components including the dependency on electrolyte temperature, electrolyte composition and turbulence determine the actual electrolyte voltage drop and therefore the ACD (Figure 1.3). In this respect the most efficient operating zone is a compromise between the current efficiency and the cell voltage given maximum productivity and minimum energy consumption respectively, as demonstrated by Equation 1.7.

### 1.3.3 Electrolyte Composition

Cryolite is the only electrolyte used in the industrial production of primary aluminium. This is due to its suitable characteristics in terms of alumina solubility, electrical conductivity, relatively low melting point, inert properties related to metal purity (except for sodium contamination) and integrity in the presence of other materials like carbon, impurities and aluminium. One of the major disadvantages of cryolite melts is the steep liquidus curve in the region of interest when represented on the phase diagram for the NaF-$AlF_3$ system (Figure 1.4) (Solheim and Sterten, 1997). The steep gradient of the curve leads to difficulties in controlling the liquidus temperature.

In order to obtain the required electrolyte characteristics, excess $AlF_3$ is added to the industrial cryolite. Excess $AlF_3$ reduces the metal solubility in the electrolyte and lowers the liquidus temperature. A lower temperature will also reduce the metal solubility in the electrolyte (Table 1.1). Lower metal solubility in the electrolyte improves the current efficiency as discussed in Section 1.3.1. Moreover, the density of the electrolyte is lowered resulting in a better natural separation of the metal and electrolyte. However, a higher $AlF_3$ concentration decreases the alumina solubility and electrical conductivity.

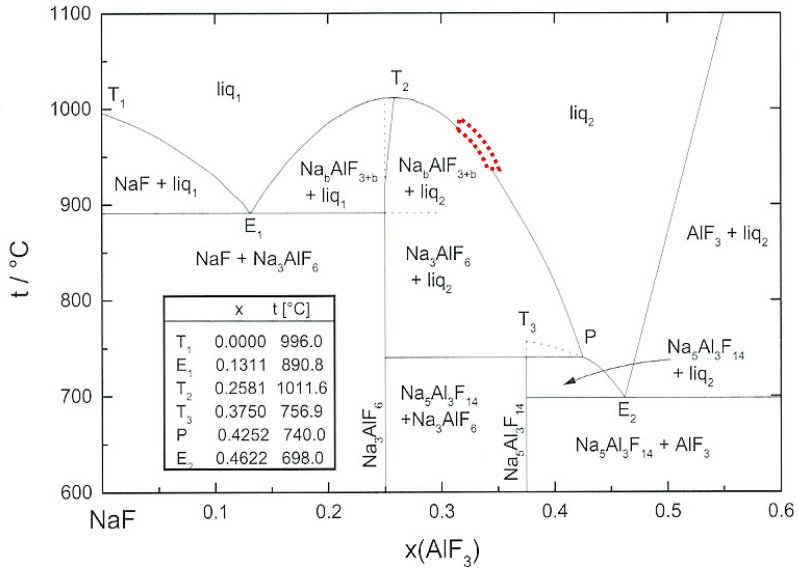


***Figure 1.4*** *Phase Diagram NaF – $AlF_3$ (Solheim and Sterten, 1997)*

In Table 1.1 other additives found in industrial cryolite melts are listed with their effects on the chemical and physical properties (Taylor, 1997). $CaF_2$ and $MgF_2$ occur naturally due to their origin as oxides in smelter grade alumina (Section 4.2.2). Both substances increase the density of electrolyte and therefore decrease the density difference between electrolyte and aluminium. The contribution of $MgF_2$ in modern cells is negligible due to a low concentration of approximately 0.3 wt%. Most other additives will significantly contaminate the metal and/or they are unstable in the given chemical environment.

| | **$Al_2O_3$ Sol.** | **Electrical Cond.** | **Density** | **Viscosity** | **Liquidus Point** | **Metal Sol.** | **Surface Tension** | **Vapour Pressure** |
|---|---|---|---|---|---|---|---|---|
| **$AlF_3$** | ↓ | ↓ | ↓ | ↓ | ↘ | ↓ | ↓ | ↑ |
| **$CaF_2$** | ↓ | ↓ | ↑ | ↗ | ↓ | ↓ | ↑ | ↓ |
| **$Al_2O_3$** | - | ↓ | ↓ | ↗ | ↓ | ↓ | ↘ | ↓ |
| **$MgF_2$** | ↓ | ↓ | ↑ | ↑ | ↓ | ↓ | ↑ | ↓ |
| **Temp** | ↑ | ↑ | ↓ | ↓ | - | ↑ | ↓ | ↑ |

***Table 1.1*** *Additives and Corresponding Chemical and Physical Properties (Taylor, 1997)*

The optimum operating region as represented by the red box in Figure 1.4 is a compromise between these properties and is strongly dependent on the control of mass and energy balance within tight limits (Section 1.3.4). An increased variability in the quality of alumina results in a decrease in the stability of the ensuing electrolyte composition. In addition, power modulation and increased line current further deteriorates the compensational stability of the electrolyte leading to a higher variability in the liquidus temperature.

### 1.3.4 Mass and Energy Balance

The principle of conservation of mass and energy leads to a mass and energy balance which is given by Equations 1.8 and 1.9 respectively (Westerterp *et al.*, 1993).

$$Mass_{accumulation} = Mass_{in} - Mass_{out} + Mass_{production} \tag{1.8}$$

$$Energy_{accumulation} = Energy_{in} - Energy_{out} + Energy_{production} \tag{1.9}$$

These equations are only applicable to an appropriately defined system with corresponding boundary conditions. In the case of a steady-state situation where accumulation of mass and energy is equal to zero, the overall process performance can be examined by using average data. In this thesis the effectiveness of the new control philosophy is examined based on a long term industrial trial to eliminate short term mass and energy imbalances (Section 4.1).

In Figure 1.5 a simplified mass and energy balance of a smelting cell is shown based on Equation 1.1, where inputs are at room temperature and outputs at cell temperature (Bruggeman, 1998). However, a smelting cell is seldom in steady-state conditions, not at least because some of the processes are continuous and others are carried out in a batch-wise manner. Hence, the cell process states are dynamic, leading to complicated interaction patterns between the mass and energy balance.

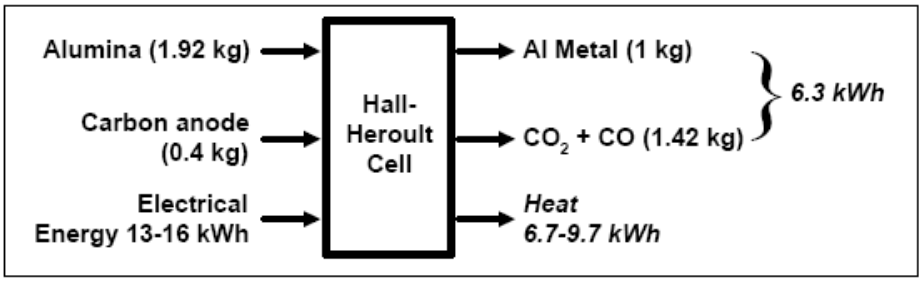


***Figure 1.5*** *Steady State Mass and Energy Balance of a Smelting Cell (Bruggeman, 1998)*

The energy balance of a smelting cell is designed based upon the pre-determined operating targets such as the optimal current and energy consumption. Consequently other features like anode dimensions, anode yoke design, cover thickness and composition, gas suction rate, and cell and building ventilation characteristics have to be taken into account in order to maintain stable operation (Section 2.1.2). Adjustments to the energy balance are necessary in the case of an increase in the line current, which is often compensated for in terms of heat generation by lowering the voltage. The specific energy consumption decreases according to Equation 1.7, if the deterioration of the current efficiency at lower ACD operation is limited (Section 1.3.2).

Energy input is the result of the total electrical potential across the cell combined with the line current according to Equation 1.5 as well as combustion of anode carbon within the cell. The oxidation of anodes contributes to the energy input to the cell by increasing the temperature of the anodes and through this the superheat of the electrolyte (Equation 1.10). Superheat is the difference between the electrolyte and liquidus temperature (Section 2.1.2).

$$C(s) + O_2(g) \rightarrow CO_2(g) \tag{1.10}$$

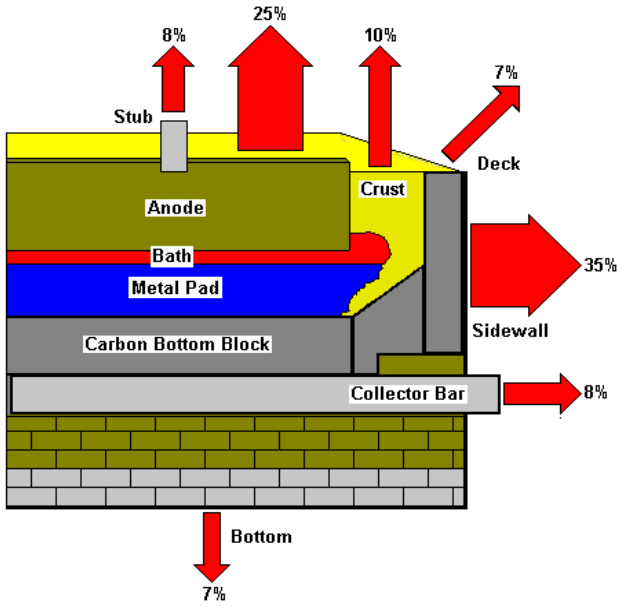


***Figure 1.6*** *Percentage Heat Losses of a Smelting Cell (Alusuisse Electrolysis Seminar, 1998)*

The above energy inputs are used in the long term (energy accumulation is zero in Equation 1.9) for metal production enthalpy through the cell electrochemical reaction and the side reactions, and the heat dissipation from the cell. In Figure 1.6 the percentage heat losses from the various parts of the cell are shown. Approximately 50% of the total heat losses are dissipated at the top of a smelting cell, while only 15% is lost via the cathode bars and bottom of the cell. The heat loss rate at the top of a cell is measured in the range of 120-150 kW per daily tonne of aluminium produced, whereas heat losses at the bottom and collector bars are responsible for 45-70 kW per daily tonne of aluminium (Welch and Keniry, 2000). The remaining heat is transferred through the side and end walls of the cell and is sensitive to changes in temperature and superheat. Sidewall losses can vary between 60 and 90 kW per daily tonne of aluminium. In case of power modulation this part of the heat loss is naturally adjusted by the rapid freezing of side ledge. This leads to a large shift in mass balance due to preferential precipitation of cryolite out of the melt as can be explained by using the phase diagram in Figure 1.4.

### 1.3.5 Magnetic Fields

Large magnetic fields are generated by virtue of the direct current flow in the bus bars around the cells and the accompanying electromagnetic forces are due to the combination of these fields with the electrical current flow in the molten aluminium. The ensuing distortion of the metal pad and flow velocities are a consequence of the intensity and direction of both current flowing through a smelting cell and magnetic field at particular points within that cell. The movement of metal and electrolyte is a complex process which can be described by the Navier-Stokes equation. This process is influenced by factors such as bubble release, liquid viscosities, coupling between metal and electrolyte in respect to their properties, pressure effects due to metal heaving, channel geometry and ledge profile (Cooksey *et al.*, 2009).

Figure 1.7 demonstrates the interactions between the energy balance and the magnetic stability within a smelting cell. The shape of the side ledge is determined by the heat losses at the side wall and the liquidus temperature. A direct link with the mass balance (electrolyte composition) is introduced. The side ledge profile influences the cathodic current density as the side ledge doesn't conduct electrical current; the extent of side ledge will affect the magnetic stability as it could induce horizontal current to flow.

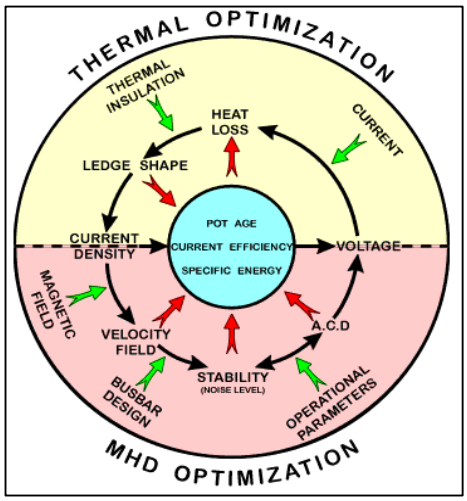


***Figure 1.7*** *Interactions between Energy Balance and Magnetic Stability (Alusuisse Electrolysis Seminar, 1998)*

Moreover, the corresponding magnetic stability affects the turbulence in the metal pad which is directly linked to current efficiency (Section 1.3.1). Since the process is dynamic, the ledge profile always fluctuates around a mean and therefore it becomes important to ensure that process variations are minimized to achieve maximum electromagnetic stability (Grjotheim and Kvande, 1993). The effect of undissolved alumina on the electromagnetic stability of a cell is discussed further in Section 2.1.1.

The anode cathode distance also has a significant impact on the magnetic stability. At Aldel, an average ACD of 45 mm is found for normal operation. In order to investigate the magnetic stability of the cells a test was carried out in which the ACD was reduced in steps of 2 mm per 30 minutes. A reduction of 15 mm was reached at 17:01. Figure 1.8 shows extreme oscillations in the current for an individual anode, measured indirectly by a voltage drop, at a reduced ACD of 15 mm. The observed periodic oscillations are in the range of 40 seconds, which is a typical indication of electromagnetic instabilities (metal pad roll). Although this is an extreme example, electromagnetic stability under normal operating conditions is also subject to variations in ACD and hence the current efficiency (Section 1.3.2). From theoretical consideration of Ohm's law the industry trends towards power modulation, increased current and greater variability in raw materials should have the detrimental effect on reducing anode cathode distance in aluminium smelting cells which would adversely affect the electromagnetic stability (Section 5.1.1.3).

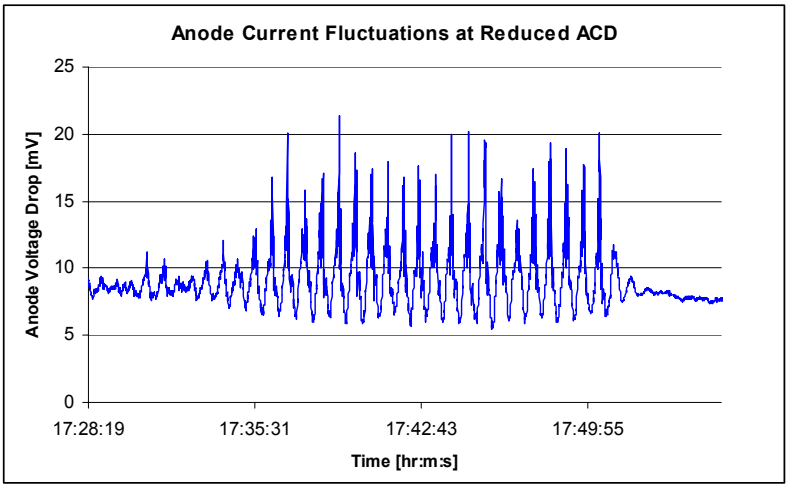


***Figure 1.8*** *Individual Anode Current Fluctuations at a Reduced ACD of 15 mm at Aldel*

### 1.3.6 Discrete Events – Batch-Wise Operations

The aluminium smelting process is a continuous process as far as the current is concerned with the current flowing through the line and metal is produced according to Equations 1.2 and 1.3. However, a significant number of discrete events or batch-wise processes are necessary. Metal is removed from a smelting cell periodically, typically every 24 to 60 hours. Alumina feeding is semi-continuous with modern point feed technology providing the addition of discrete quantities of alumina (1-2 kg per dump) to the liquid electrolyte (Section 2.1.3).

As shown in Equation 1.1 prebaked carbon anodes are consumed during the aluminium smelting process and spent anode butts have to be removed at regular intervals. When spent anode butts are taken out of a cell, some anode cover material is removed as well.

Therefore new anodes have to be redressed. These batch-wise operational practices result in large deviations from steady-state operation and therefore result in significant temporal variations in the mass and energy balance (Welch, 1998).

The proper execution of these operational practices is observed to influence process stability and associated current efficiency (Andrews *et al.*, 2005). An increased variability in the physical characteristic and impurity contents of the alumina sourced from different suppliers has been linked to deterioration in the control of the concentration within a given range and the electrolyte composition (Homsi, 2001). Moreover, power modulation introduces large deficiencies in energy input to the cells resulting in large swings in energy and mass balance. These imbalances directly affect alumina feeding and anode changing (Section 2.1.3). Higher line current initiates higher electromagnetic instabilities, especially as the ACD is reduced to maintain the energy balance (Sections 1.3.4 and 1.3.5). Beside the magnetic influences, the mass balance is also affected by an increased alumina feeding rate caused by running the operation at increased line current.

## 1.4 Outline of the Thesis

Chapters 2 and 3 are concerned with the literature review and development of the theoretical foundation of this research respectively. Chapters 4 and 5 describe the experimental design of the new causally based control philosophy with the accompanying results and discussion. Chapter 6 gives the conclusions and suggestions for further developments.

The literature review in Chapter 2 summarizes previous developments and understanding of the aluminium smelting process, along with process control and statistics applied to other industrial processes. Some recent developments in measurements and control of aluminium smelting cells are also included.

In Chapter 3 the theoretical development of this thesis is explained. A better understanding of interactions between the mass and energy balance including the effectiveness of alumina dissolution in smelting cells is derived. This is then applied to improving the control in the present global situation of rapidly changing economical and environmental circumstances. Advanced use of the Hotelling $T^2$ statistic is employed to determine the natural behaviour envelops for individual cells in order to distinguish between in and out of control behaviour (Chen and Taylor, 2005).

Causes of variation are determined through online problem-solving techniques such as Pareto and root cause analysis. The statistical definition of natural process behaviour and subsequent detection of special cause variation provides new, real time information related

to both ongoing process states and state changes of the cell within the multidimensional control envelop. This knowledge results in corrective actions as apposed to symptomatic control, which prevents overreaction in both the control in the energy balance and electrolyte composition.

Chapter 4 describes the experimental design undertaken in this thesis including the relevant operational constraints imposed through performing experiments in the industrial process. In this respect variations in the energy input and variations in the supply and hence properties and purity of raw materials are inevitable in industrial experiments. The statistical basis and the equipment and instruments involved in the experiments are also discussed. Results and discussion are presented in Chapter 5, while the conclusions and further developments are presented in Chapter 6.

# Chapter 2 Literature Review

In this chapter a literature review is presented to provide an overview of the knowledge about process control strategies in aluminium smelting in general and an understanding of the aluminium smelting process in particular. Sections 2.1.1 to 2.1.4 of this chapter focus on investigations undertaken in the area of alumina feed control, mass and energy balance control, discrete events within a continuous process and liquid electrolyte mass. Sections 2.2.1 to 2.2.7 discuss control strategies and statistical methods applied in the chemical and metallurgical industries. In the last part of this chapter, Sections 2.3.1 and 2.3.2 review new developments in measurements and process control to improve the ability to control the aluminium smelting cells. The constraints in existing control strategies regarding the ability to deal with continuous changing conditions like line current, power modulation and raw materials used are discussed.

## 2.1 Aluminium Smelting Process

### 2.1.1 Alumina Feeding

Alumina is the single largest raw material input into a smelting cell. Due to increased line current the mass of alumina fed to a cell per day is now almost equal to the amount of liquid mass available for dissolution (Martin *et al.*, 2008). Effective feeding and dissolution is critical to maintaining the target alumina concentration band and electrolysing it efficiently. It is also pivotal in the control of heat balance, as well as avoidance of anode effects and sludge formation (Taylor *et al.*, 1990). The essential requirements during alumina feeding are effective transport into the electrolyte, rapid dispersion in the electrolyte, rapid dissolution as small alumina grains and finally uniform mixing of the dissolved alumina in the electrolyte (Graduate Certificate, 2008). The saturation solubility in industrial electrolytes is typically in the range of 5-6 wt%. Electrolyte additives and impurities generally lower the solubility of alumina in the bath (Section 1.3.3).

The design of feeders with respect to electrolyte flow characteristics, coupled with a stable anode cover and transport of alumina along the surface of electrolyte in the feeding channel are essential for good dissolution (Purdie, 1995). The dispersion of alumina in the electrolyte during feeding due to a combination of electrolyte movement (Section 1.3.5) and gas bubble flow characteristics is another determinant of good dissolution (Moxnes *et al.*, 1998). In addition, transition alumina with a high internal surface and structural hydroxyl content will essentially blow apart when added to the electrolyte, if the grains are initially well dispersed (Metson *et al.*, 2005). The gas release due to this explosion will actually aid dispersion and supports rapid dissolution of alumina. This is if agglomeration of the alumina grains with

frozen electrolyte is prevented in the seconds after alumina addition. A high alpha content (no hydroxyl groups in its structure) has the reverse effect because of the absence of gas evolution.

Beside moisture and alpha content, there are several other alumina properties that are important for its dissolution in the electrolyte (Taylor, A., 2004). In terms of particle size distribution, coarser fractions are favoured as there are problems with the dissolution of finer particles linked to freezing and aggregation. Furthermore, the morphology of alumina particles is a function of the Bayer process and affects the attrition index of the particles as they are handled. An increased variability in the quality of alumina used results in a decrease in the controllability of the target alumina concentration band in the smelting process. More knowledge is required to understand the development of structural features during calcination of Bayer Gibbsite to produce smelter grade alumina (Perander *et al.*, 2008).

Together with the ability to dissolve alumina in the electrolyte, the dissolution rate is also important for the reduction operation. What limits the alumina dissolution rate is the amount of sensible heat that is available in the electrolyte before it freezes onto the alumina (Wai-Poi *et al.*, 1994). Without natural mixing as described previously, freezing will retard alumina dissolution significantly, because the total energy required for preheat, dissolution and volatile evolution is substantial (up to 2000 kJ/kg) (Taylor *et al.*, 1990). Studies show also a relatively long duration for the dissolution process to take place, including its distribution under all anodes within a cell (Thonstad *et al.*, 2001). In order to ensure alumina dissolution is continuously maintained, the smelting cell must also have sufficient superheat (typically 8-10°C) to allow the liquid electrolyte mass transfer of the sensible heat. In this respect power modulation results in large deficiencies in energy input with a corresponding decrease of the sensible heat available for dissolution.

The initial endothermic heat supply to maintain the chemical dissolution rate within poorly dispersing alumina additions may not be supported by interfacial convection from the melt and localized freezing will occur - resulting in a smaller overall temperature decrease of the bulk electrolyte (Taylor *et al.*, 1986). The main consequence of incomplete alumina dissolution is sludge formation on the cathode. The composition of sludge is different from liquid electrolyte and consists of 40-70% alumina, 0-5% $AlF_3$, and cryolite saturated with dissolved alumina (Taylor *et al.*, 1990). The measured solidification temperature of sludge is almost invariant at 948 - 954°C. The dissolution of alumina from sludge into the electrolyte is likely to be controlled by the access of fresh electrolyte to the sludge (Equation 2.1 and Figure 2.1) (Grjotheim and Kvande, 1993; Whitfield *et al.*, 2004).

$$R_{dissolution} = k_{Al_2O_3} \cdot A_{bath-sludge} \cdot \left([Al_2O_3]_{sat} - [Al_2O_3]\right) \quad (2.1)$$

Where, $k_{Al2O3}$ is the mass transfer coefficient, $A_{bath\text{-}slduge}$ is the effective interfacial electrolyte/ sludge area, $[Al_2O_3]_{sat}$ is the saturation concentration of alumina and $[Al_2O_3]$ is the actual alumina concentration in the bulk electrolyte. The saturation concentration is a function of the electrolyte temperature and composition.

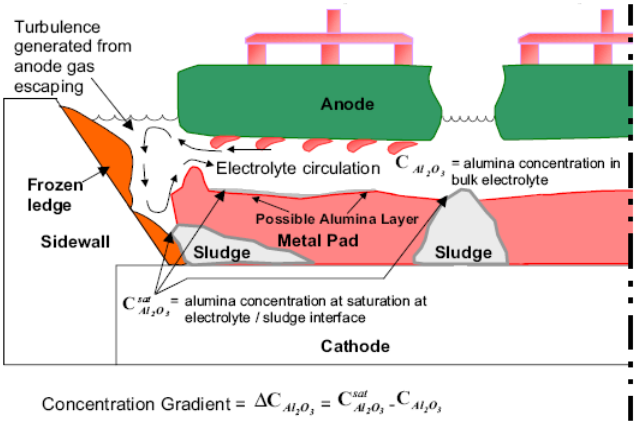


***Figure 2.1*** *Mechanism of Back Feeding in Aluminium Smelting Cells (Whitfield et al., 2004)*

Most alumina feeding control philosophies are based on the molten electrolyte's resistance dependency on the alumina concentration (Welch, 1965). The decomposition potential $(E_{rev})$, anode polarisation $(\eta_{AC})$, bubble resistance and electrolyte resistance $(R_{electrolyte})$ vary with alumina concentration in the bulk electrolyte and are sensitive to the anode current density (Equation 1.5). Alumina feed control is normally based on resistance or pseudo-resistance $(R_{pseudo})$ in order to filter out current fluctuations (Equation 2.2). The pseudo-resistance is derived from the cell voltage and voltage intercept $(V_{extrapolated})$ of cell voltage versus current extrapolated from a small change in line current to zero current (Kvande and Haupin, 2000). Although not technically correct, the voltage intercept is often referred to the $B_{emf}$ which is made up of the decomposition potential and overvoltages.

$$R_{pseudo} = \frac{V_{cell} - V_{extrapolated}}{I} \tag{2.2}$$

Demand feed or an underfeed/overfeed strategy for alumina feed control is used in modern point feed cells (Bearne, 1998). In both cases alumina is fed to the cell at a reduced feed rate leading to a decline in alumina concentration and therefore an increase of the pseudo-resistance. A period of underfeed ends at a fixed alumina concentration and a period of overfeed starts. Demand feed is controlled by a fixed resistance change (ΔR), whereas underfeed/overfeed strategy switches at a given slope (dR/dt) and/or the second derivative of the cell pseudo-resistance ($d^2R/dt^2$). In the latter case the alumina concentration is subject to increased variability at increased line current due to a rise in the alumina depletion rate.

The main assumption is that changes in alumina concentration due to the applied feeding strategy have a significantly higher effect on the resistance than changes in anode-cathode distance (ACD) or external resistances. This sets a lower limit for feeding rate, otherwise other effects like variations in metal production, anode consumption or even thermal effects dominate changes in the resistance. The upper feeding rate limit is linked to alumina dissolution and determines the maximum concentration band. The shape of the curve of cell pseudo-resistance *(R)* versus alumina concentration varies with anode-cathode distance *(ACD)*, alumina concentration *([$Al_2O_3$])*, temperature *(T)*, aluminium fluoride concentration *([$AlF_3$])*, anodic current density *(acd)* and other factors. This is conceptually described as a chain differentiation of partial derivatives in Equation 2.3. Therefore a deterioration of the controllability of the alumina feeding is introduced by the employment of power modulation due to a varying ACD, temperature, bath chemistry and current density over time.

$$\frac{dR}{dt} = \frac{\partial R}{\partial T}\cdot\frac{dT}{dt} + \frac{\partial R}{\partial [Al_2O_3]}\cdot\frac{d[Al_2O_3]}{dt} + \frac{\partial R}{\partial ACD}\cdot\frac{dACD}{dt} + \frac{\partial R}{\partial [AlF_3]}\cdot\frac{d[AlF_3]}{dt} + \frac{\partial R}{\partial cd}\cdot\frac{dacd}{dt} + \ldots \tag{2.3}$$

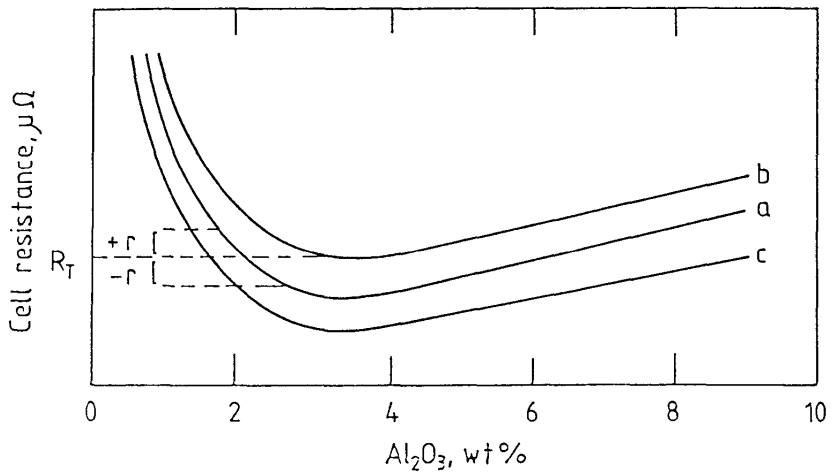


***Figure 2.2*** *Resistance versus Alumina Concentration (Grjotheim and Kvande, 1993)*

The characteristic variation of pseudo-resistance allows the alumina feed strategy to target an average alumina concentration, although the actual slope, $\partial R/\partial[Al_2O_3]$, is unique for every resistance curve as is shown in Figure 2.2 (Grjotheim and Kvande, 1993). Curves *c*, *a,* and *b* represent the curvature at increasing ACD. It is hypothesised that the presence of an alumina layer at electrolyte-metal interface leads to significant differences between theoretical and measured pseudo-resistance curves (Figure 2.1). There is evidence for this layer is also dependent on the electrolyte temperature (Whitfield *et al.*, 2004).

The mass and duration of overfeeding and underfeeding are specified as control settings. An increase of the underfeed rate will lead to a longer time in underfeed given the same endpoint in alumina concentration. If the overfeed rate is increased, the range of the alumina concentration in the cycle will increase, average concentration will shift towards higher value and a longer time in underfeed will be found. Broadening the regulation bandwidth of the cell voltage will lead to a decrease in the average alumina concentration due to a higher ACD operation (=less beam down movements), but will not change over/underfeed duration.

The lowest alumina concentration is set by proximity to the anode effect concentration. When the bulk concentration of alumina in the electrolyte falls below a critical value, typically below 1.5%, an anode effect will occur (Taylor, Welch *et al.*, 1984). The anode effect is characterized by an abrupt sudden and rapid increase in cell voltage. The wettability of the bottom anode surfaces decreases with decreasing alumina content in the electrolyte resulting in combination of de-wetting and increased coverage of the anode surface by gas bubbles. The anode effect occurs when the local current density exceeds the critical limiting current density resulting in the evolution of greenhouse gases like $CF_4$ and $C_2F_6$.

The highest alumina concentration is influenced by the alumina dissolution effectiveness along with the cell pseudo-resistance characteristic. As demonstrated in Figure 2.2 control of the alumina concentration is lost in case of a positive relationship between the alumina concentration and pseudo-resistance, which is represented by the region on the right side of the minimum in the resistance curve. By their design, both a demand feed as well as underfeed/overfeed control strategies initiate extra feeding of alumina under these conditions resulting in an acceleration of sludge formation (Bearne, 1998). Furthermore, the rate of alumina dissolution is reduced according to Equation 2.1, which also leads to more sludge formation.

### 2.1.2 Mass and Energy Balance

The mass and energy balance are defined by Equations 1.8 and 1.9 respectively. Several control parameters can be used to optimize the steady state mass and energy balance like target settings for the cell voltage, temperature and chemistry (combined as superheat), electrolyte and metal level, anode cover and suction rate. However, the smelting process is rarely in a steady state equilibrium due to the necessity for frequent batch-wise operations like alumina feeding, metal tapping, anode changing and anode covering (Section 1.3.6). The frequency of these operational activities and hence the associated impact to the mass and energy balance increases at increased line current. Moreover, power modulation results in large deficiencies in the energy input to a cell as demonstrated in previous work (Stam and Schaafsma, 2007).

#### 2.1.2.1 $AlF_3$ Balance

As described in Section 2.1.1 tight control of the mass of alumina in the bulk electrolyte is necessary to control the smelting process efficiently. Secondary mass balance control focuses on constant aluminium fluoride mass within the cell. Aluminium fluoride in modern technologies with a dry-scrubber is most particularly used to neutralise sodium oxide *($Na_2O$)* and calcium oxide *(CaO)* content of alumina used (Equation 2.4 and 2.5) (Drengstig, 1997).

$$3Na_2O + 4AlF_3 \rightarrow 2Na_3AlF_6 + Al_2O_3 \quad (2.4)$$

$$3CaO + 2AlF_3 + \rightarrow 3CaF_2 + Al_2O_3 \quad (2.5)$$

Therefore the steady state base addition *($k_a$)* of aluminium fluoride is proportional to the amount of alumina fed to a cell based on line current *(I)* and current efficiency *(CE)* (Kloetstra and Stam, 2001). Notwithstanding this, changes in $AlF_3$ additions are required at increased line current and during power modulation. For example, at Aldel, Equation 2.6 represents the $AlF_3$ base addition, in which the demand for an excess $AlF_3$ concentration in the bath is taken into account through the last term in the equation (Graduate Certificate Course, 2003).

$$k_a = I \cdot CE \cdot (34.3 \cdot [Na_2O] \cdot + 19 \cdot [CaO] + 0.49 \cdot [Na_2O] \cdot [AlF_3]) / 124.08 \quad (2.6)$$

The carbon cathode and lining are important in the accumulation of sodium in the smelting cell (Sølie and Øye, 1994). The mass of aluminium fluoride in a cell is enriched in the early phase of its lifetime due to sodium uptake in the cathode blocks and ramming paste. Exposing cathodic ramming paste to the electrolyte during normal operation is also expected to absorb sodium. The additions to maintain constant $AlF_3$ mass *($F_0$)* have to be adjusted for cell age *(age)* and the type of cathode blocks used. This gives an exponential relationship with the steady state base additions *($k_a$)* and cell construction *($k_b, \tau$)* represented by a mirror image of the sodium uptake, for example as represented in Equation 2.7. The above constants in this equation are influenced by the cathode type and are regularly fitted against the actual data in order to optimize their values as shown in Figure 2.3.

$$F_0 = k_a - k_b \cdot \exp(\frac{-age}{\tau}) \quad (2.7)$$

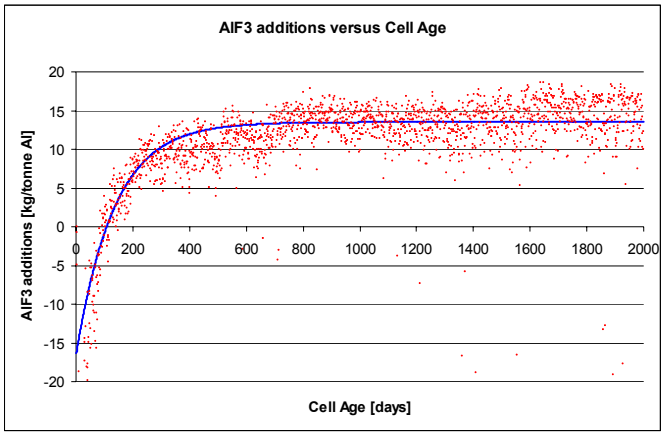


***Figure 2.3*** *$AlF_3$ Additions versus Cell Age at Aldel*

In modern smelters the fluoride emissions, mainly as HF and $NaAlF_4$, are captured using the primary alumina in a dry-scrubbing system (Equations 2.8 to 2.11). Moisture in the air (10-30%), water and structural hydroxyls (50-70%) are the main source for HF evolution from smelting cells (Hyland *et al.*, 2004). The vapour pressure of electrolyte increases with an increase in the temperature, superheat and $AlF_3$ concentration (Thonstad *et al.*, 2001). Holes in the anode cover can increase fugitive emissions by a factor of 2-3 and therefore increase the $AlF_3$ consumption significantly (Dando, 2004).

$$2AlF_3(g/diss)+3H_2O(g)\rightarrow 6HF(g)+Al_2O_3(s/diss) \quad (2.8)$$

$$3NaAlF_4(g)+3H_2O(g)\rightarrow 6HF(g)+Al_2O_3(s)+Na_3AlF_6(s) \quad (2.9)$$

$$3Na_5Al_3F_{14}+6H_2O\rightarrow 5Na_3AlF_6+2Al_2O_3+12HF \quad (2.10)$$

$$3Na_5Al_3F_{14}\rightarrow Na_3AlF_6+2NaAlF_4 \quad (2.11)$$

The fluoride is returned to the cells as secondary alumina. Although the gas collection efficiency is close to 100% in the case of well designed operational practice, the cells will see an averaged fluoride concentration on the alumina returning from the dry-scrubbing system (Karlsen *et al.*, 1998). Therefore some variations in $AlF_3$ additions are required to correct the net balance between individual cell losses and the average fluoride input via secondary alumina.

For the most part mass balance control in aluminium smelting cells is based solely upon concentration measurements. Therefore, considerable caution needs to be exercised when $AlF_3$ additions are also being used to compensate for a change in electrolyte composition. Equation 2.12 is an example of a linear correction of $AlF_3$ additions *($F_{AlF3}$)* based on bath temperature and chemistry analysis (Kloetstra and Stam, 2001). Specification limits around the bath temperature (±5°C) and $AlF_3$ concentration (±1%) are used to incorporate ensuing

process variations artificially. In addition, a minimum and maximum number of $AlF_3$ additions per cell per day are introduced with the amount added over the last 8 days also being taken into consideration.

$$F_{AlF3} = F_0 + ([AlF_3] - [AlF_3]_{target}) \cdot k_c + (T_{measured} - T_{target}) \cdot k_T \quad (2.12)$$

In order to avoid overcorrection for the $AlF_3$ concentration instead of the mass of $AlF_3$ in the cell, the $AlF_3$ additions are switched to a minimum number of additions per day per cell when the $AlF_3$ concentration exceeded a critical upper limit. Under these process conditions for more than 2 days soda ash is only added to restore sufficient alumina solubility as shown in Table 1.1 (Equation 2.13).

$$3Na_2CO_3 + 4AlF_3 \rightarrow 2Na_3AlF_6 + Al_2O_3 + 3CO_2 \quad (2.13)$$

A range of different approaches in the control of aluminium fluoride concentration/mass in smelting cells have been published. A linear regression model was proposed for $AlF_3$ mass balance calculation taking into consideration historical $AlF_3$ additions and a time lag reaction (Entner, 1992). Daily analyses of the electrolyte composition are needed to measure $AlF_3$ concentration as an input parameter to the model. Other techniques, e.g. fuzzy logic or neural networks, use the relationship between the electrolyte temperature and composition to predict the $AlF_3$ concentration and subsequent additions (Meghlaoui and Aljabri, 2003). These strategies are rather static due to the absence of chemical and physical information as they are based on historical examined process conditions. Therefore these models are less useful under rapidly changing conditions such as increased line current, power modulation and increased variability of the quality of the raw materials used.

#### 2.1.2.2 Energy Balance and Sidewall Dynamics

The steady state energy balance described in Section 1.3.4 assumed no changes in cell energy input or cell heat losses. However, a cell is seldom in steady-state conditions, not at least because some of the processes are continuous and others are carried out in a batch-wise manner (Section 1.3.6). Changes in the energy balance are most immediately reflected in a change in the superheat of the molten electrolyte and therefore a change in heat transfer through the sidewall ledge (Taylor, 1984). The heat transfer at stationary conditions in a smelting cell through the side and end walls is proportional to the difference between the electrolyte and liquidus temperature and hence the superheat. The convective heat transfer from the bulk electrolyte *(q)* to the electrolyte-ledge boundary layer is given by Equation 2.14.

$$q = h_B \cdot A_{ledge} \cdot (T_B - T_L) \tag{2.14}$$

Where, $h_B$ is the heat transfer coefficient between the electrolyte and side ledge, $A_{ledge}$ is the total area of side ledge, $T_B$ is the electrolyte temperature and $T_L$ is the temperature at the ledge-bath interface.

This driving force connects the energy balance with the mass balance due to melting and freezing of the side ledge with corresponding composition changes in the electrolyte (Figure 2.4) (Taylor, 1997). Heat losses from the bottom of the cell are relatively constant in response to changes in process conditions, since they are governed primarily by conduction through the cathode and insulating layers. This is similar for the heat losses at the top of a cell provided that the cover and drafting remain uniform.

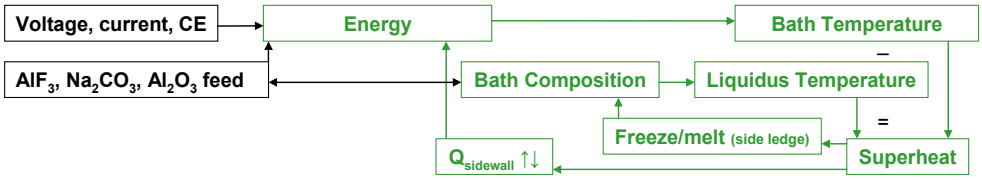


***Figure 2.4*** *Self-Regulation of Mass and Energy Balance via Side Ledge (Taylor, 1997)*

Recent control models are based on the interaction between the mass and energy balance via the side ledge (Kloetstra and Stam, 2001; Rieck *et al.*, 2003). For example, if the energy input into a cell increases, bath temperature rises and an increase of the superheat will occur. The increase in the heat dissipation to the sidewall and corresponding melting of side ledge dampens the final temperature response to the original increase in energy input. This reaction via the side ledge is an internal self-regulating mechanism, which stabilizes the process eventually at a new state (Figure 2.4). The resultant state is defined by a new bath composition and heat losses at a different liquid bath mass (increased in this case).

Similarly, if the amount of the $AlF_3$ additions into a cell increases, liquidus temperature decreases and a temporary increase of the cell superheat will occur. The increase in heat dissipation to the sidewall and corresponding melting of side ledge dampens the final liquidus temperature response to the original increase of $AlF_3$ additions. However, in both cases (energy input and $AlF_3$ addition) this phenomenon is not valid if side ledge is not present, in which case bath temperature or chemistry are directly affected by differences in energy or mass balance according to its heat capacity or mass additions.

The heat balance of a smelting cell is designed for a particular (range in) line current. Once the cell is built, the bottom losses are governed by the operational temperature and thermal

conductivity of materials and dimensions used such as the isolation and fire bricks, cathode blocks, collector bars and ramming paste (Figure 1.6). Thermal and electrical models have been developed to specify the geometry of the cell lining in order to maintain the target heat balance and corresponding isotherms within the lining.

The total area available for heat transfer through the sides is influenced by the total liquid level and liquid flow characteristics. Metal height control is often used to fine-tune heat losses and is of particular importance for ledge/ridge formation at the cathode surface. In general, higher heat losses are connected to higher metal levels and vice versa resulting in a direct link with the magnetic stability of the process (Bruggeman, 1998). For example a lower metal level will increase the horizontal current density in the metal, and the magnitude and impact of the electromagnetic forces in a reduced metal mass increasing velocity and metal heave. An increase of the heat transfer coefficient due to higher metal velocities dampens the intended effect of a reduced metal height to reduce the overall cell heat losses. In case of ledge/ridge formation under the anodes due to an energy imbalance, horizontal current components can result in large metal pad instabilities (Section 1.3.5).

#### 2.1.2.3 Top Heat Losses and Cell Ventilation

Heat losses from the top of a smelting cell are significantly influenced by anode, yoke and rod dimensions. With increasing line current, larger anode and pin sizes have to be employed to dissipate more heat at the top of a cell. Poor anode cover/crust retention is another source of heat loss from the top of a smelting cell. Anode cover is a mixture of blended alumina and crushed (solidified) bath material, which contains alumina at or above saturation. The composition of crushed bath consists of 2 phase mixtures: cryolite ($Na_3AlF_6$) and chiolite ($Na_5Al_3F_{14}$). The chiolite fraction in liquid bath with an $AlF_3$ concentration of 12% is approximately 27%, whereas the proportion in crushed bath can contain up to 70% chiolite by weight (Taylor *et al.*, 2004). Softening and melting of chiolite is a major weakening mechanism in anode cover containing a mixture of crushed bath and alumina (Taylor *et al.*, 2004). Chiolite melts incongruently in the range of 695-730°C (Figure 1.4).

The thickness and composition of the anode cover determines the heat transfer through the top of a cell. The main parameters for controlling the thermal conductivity of the anode cover are the particle size distribution of the blend and the ratio of crushed bath versus alumina (Taylor, 2007). The integrity of anode cover is controlled by maximum heat transfer before it melts and collapses and operational practices like dressing and redressing. In case of an increase in line current the associated anode cover thickness and composition require some adjustments to increase the heat losses through the top of a cell. Furthermore the anode cover acts as a protection against air-burn of anodes and it minimizes fugitive emissions.

The duct gasses of dry-scrubber operated cells are responsible for approximately three quarters of top heat extraction from smelting cells (Abbas *et al.*, 2009). Hooding and superstructure contribute 18% and 5% of heat losses at the top respectively. The ventilation characteristics around a smelting cell and within the building affect the heat dissipation and transfer to the surroundings. Ventilation is necessary to cool a smelting cell to maintain sufficient ledge to protect sidewall lining against corrosive electrolyte and to assure good temperature conditions within the building (Holt *et al.*, 1999).

A reduction of the air and steel temperature of 77°C and 98°C respectively were achieved with a new ventilation design at Aldel (Figure 2.5) (Stam and Kloetstra, 2004). The direction of airflow along the cells changed the way that heat dissipation through the vents is forced away from the side of the cell, this being a better design in respect to the gas collection efficiency (Karlsen *et al.*, 1998). This new design was developed to counteract a substantial increase in line current which would have had a serious impact on heat balance (Section 4.2.1.1). It actually resulted in a growth in the average ledge thickness (+16%) due to improved cooling. A clear relation was found between a reduction of the total heat dissipation into the building (calculated from the cell heat loss minus the heat extraction by the dry-scrubber) and the average airflow through the roof as shown in Table 2.1 (Stam *et al.*, 2007).

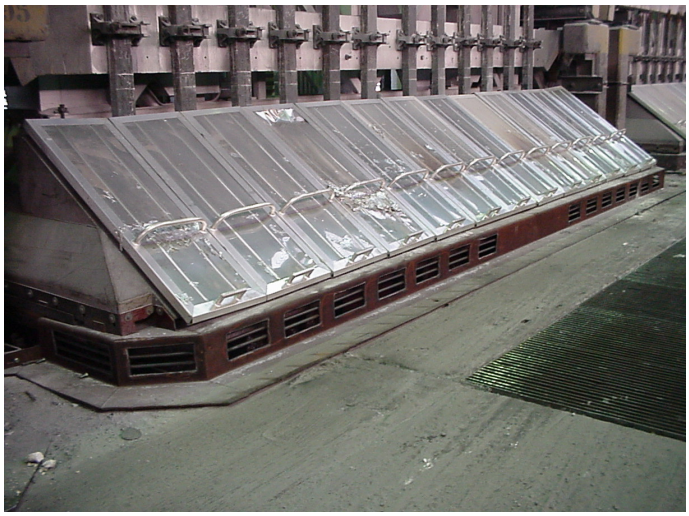

***Figure 2.5*** *Improved Ventilation Design at Aldel (Stam and Kloetstra, 2004)*

| | Heat Dissipation Per Pot [MWh/day] | Air Velocity Roof [m/s] |
|---|---|---|
| **2001** | 6.33 | 0.723 |
| **2002** | 6.37 | 0.788 |
| **2003** | 6.32 | 0.720 |
| **2004** | 6.11 | 0.590 |
| **2005** | 6.04 | 0.476 |
| **$R^2$** | **0.9678** | |

***Table 2.1*** *Heat Dissipation versus Roof Airflow per Year at Aldel (Stam et al., 2007)*

### 2.1.3 Discrete Events in Aluminium Smelting Cells

#### 2.1.3.1 Alumina Feeding

In modern smelting cells alumina is fed via point feeders with doses of 1-2 kg per dump. As described in Section 2.1.1 the alumina concentration is mainly controlled by demand or underfeed/overfeed strategies. Variations in the alumina concentration lead to cycling of the electrolyte temperature, which is typically of the order of 5-8°C (Taylor and Welch, 2004; Iffert, 2007). Figure 2.6 shows the cyclic decrease and increase in the temperature during overfeeding and underfeeding respectively due to the associated variations in the ensuing energy demand (Section 2.1.1) (Iffert, 2007). The superheat also shows a cyclic behaviour of 2-3°C in relation to the overfeed/underfeed strategy. However, these short term observations are influenced by longer term state changes. The increasing trend in the bath temperature in combination with a decreasing average alumina concentration indicates the presence of a surplus of energy in the cell prior to the test (Figure 2.6).

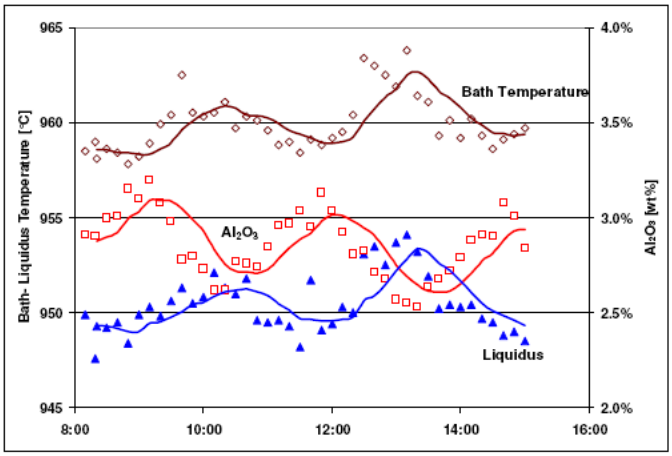


***Figure 2.6*** *Bath and Liquidus Temperature during Alumina Feeding (Iffert, 2007)*

When the bulk concentration of alumina in electrolyte falls below a critical value, an anode effect will occur (Section 2.1.1). During an anode effect the cell voltage can rise up to 30-40V, which leads to an excessive heat input to the cell. This extra heat causes a rapid melting of the side ledge (~7.5 mm/min), which retards the rapid rise of bath temperature (Taylor, 1984). Most control strategies automatically increase the alumina feeding rate, which also slows down the increase of the bath temperature. Mass and energy balance adjustments based on measurements just after anode effects must be avoided to prevent overcompensation.

### 2.1.3.2 $AlF_3$ Feeding

In modern smelting cells aluminium fluoride is fed via point feeders with doses of 2-4 kg per dump. As described in Section 2.1.2.1 the $AlF_3$ balance is particularly tuned to the sodium and calcium oxide content of the alumina used. Figure 2.7 shows the response of the bath and liquidus temperatures after a large addition of 100 kg $AlF_3$ to a cell (Rye *et al.*, 2001). It was found that the major part (67 kg) dissolved rapidly. The base addition of $AlF_3$ at Aldel is only 12.6 kg per tonne of aluminium (=14 kg·day$^{-1}$ at 147 kA) (Figure 2.3). Combined with the application of $AlF_3$ point feeders, it is assumed in this thesis that all added $AlF_3$ is dissolved

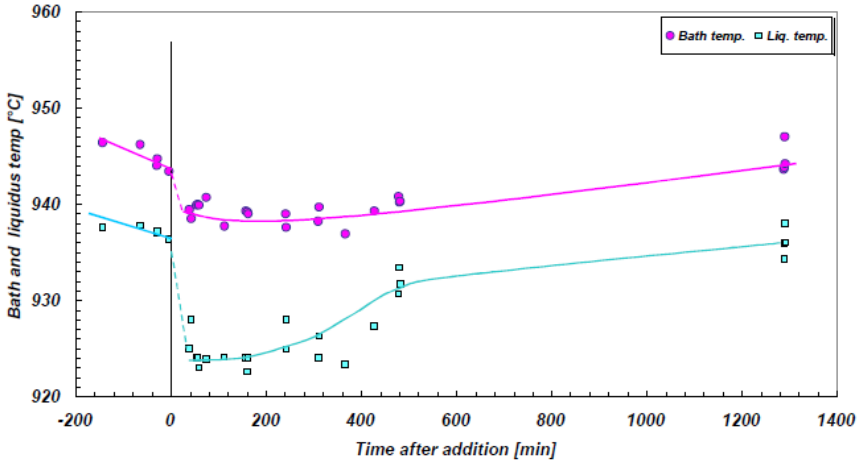


***Figure 2.7*** *Bath and Liquidus Temperature after addition of 100 kg $AlF_3$ (Rye, 2001)*

### 2.1.3.3 Anode Changing

Anode changing introduces a major disturbance to the energy balance in a smelting cell (Welch, 1998). A substantial amount of energy is removed from a cell with the hot butt, and the resultant cavity and cleaning of the open bath result in increased radiant heat losses. The immediate thermal demand by the introduction of a new anode is considerable followed by an extra heat demand for the new anode cover material. Excessive localized freezing of electrolyte to the anode surface causes temperature and compositional variability due to a reduced bath volume. These effects are exacerbated at increased line current due to larger anodes and/or a higher frequency of anode changing. Cell mixing characteristics as well as the anodic current distribution will be affected leading to further process instabilities.

A correlation between the anode setting rota and current and energy efficiency have been found (Iffert, 2007). A rota based on one single row or two rows alternating between the inner and outer side of a cell result in one or two temperature front(s) moving through the cell respectively, creating cold spots, high variation in the anodic current distribution, high noise

and therefore continuous changes in the anode cathode distance. Another rota is based on an equal distribution of the average anode age per quarter of a cell. The first rota is designed for anode cover integrity, whereas the latter rota results in equal current distribution. In this respect a random anode rota has a positive effect on the current efficiency due to the absence of thermal waves throughout the cell.

#### 2.1.3.4 Anode Covering

Anode covering is directly linked to anode changing. Anodes are mostly covered within a time range of 2-10 hours after changing, which depends on crust formation around the newly set anode(s). The cover integrity plays an important role in heat balance as well as environmental performance. Heat balance influences are related to thickness, composition and particle size distribution of anode cover material (Section 2.1.2.3). At increasing line current anode cover thickness is minimized to release as much heat as possible through the top of a cell. This can lead to a rising sensitivity to variations in the relative thickness and therefore heat losses.

#### 2.1.3.5 Beam Raising

Beam raising is necessary, because of its downwards adjustment as anodes are consumed. When the beam approaches the lowest limit, an extra beam is placed on top of the cell superstructure. The anodes are connected to the temporary beam and the original beam can be raised. An even anodic current distribution in aluminium smelting cells is very important in order to achieve maximum current and energy efficiency. There are two main reasons for current imbalances after beam raising, being sagging beams due to large and heavy anodes and high clamp voltage drops caused by alumina flowing from the top of the anode beam in between beam and rods during beam raising.

#### 2.1.3.6 Metal Tapping

Aluminium settles down at the bottom of a cell and is removed following a fixed routine, in which the tapping and anode setting routine are tuned to each other. The mass of tapped metal produced is now up to 3 tonnes per day in high current cells and this has implications on the thermal stability. On the one hand the amount of tapped metal per batch as a fraction of its inventory in the cell is an important factor in the variation of the heat capacity and electrical current density in the metal. On the other hand variations in metal height influence heat fluxes through the side wall. This variation can be up to 35% in case of retrofitted old technologies running at substantial higher line current than their original design values.

The metal inventory is controlled by metal height and the amount of tapped metal. At Aldel, the metal height is calculated based the insertion height of anodes and measured height of the anode beam (Equation 2.22). The amount of tapped metal is fixed for a successive number of days and is adjusted according to long-term variations in the current efficiency. The interval between tapping moments is minimized to reduce the ensuing variability.

#### 2.1.3.7 Power Modulation

In order to reduce the overall energy costs aluminium smelters investigate different methods of power modulation in which the energy intake is redistributed over a given time interval (Section 1.1). These strategies lead to an inconsistent energy input to the smelting process and disrupt the mass and energy balance significantly (Section 2.1.2). Line current reduction or interruptions are generally used to reduce energy consumption during periods of the day when power charges are expensive. These events can occur with or without a prior warning.

Precautionary mass and energy balance adjustments like an increase of the cell voltage and alumina feeding are used to counteract the ensuing system dynamics and promote a quick recovery of the smelting process to its original state. However, determination of the process state after power modulation based on the existing process sensitivity is hindered by rapid changes in the liquid bath mass. When unexpected events occur corrective measures are needed afterwards such as a temporary increase of line current for a given period of time, preferably related to the impact and duration of power modulation.

### 2.1.4 Liquid Bath Mass

Limited studies have been published about the dynamic behaviour of the liquid bath mass in aluminium smelting cells (Iffert, 2007). However, it is assumed that changes in superheat are the main cause of variation in the amount of liquid electrolyte within cells. According to Equation 2.14 the thickness of sidewall ledge is controlled by the rate of convection heat transfer from the bulk electrolyte. Frozen ledge acts as a thermal buffer allowing changes in the amount of heat transferred through the sidewall by melting or freezing. In this respect 35 kWh/cm of energy is accumulated in the side ledge (Welch, 1998).

Measurements of the amount of liquid bath mass in industrial cells show large fluctuations indicating a process variability of more than 50% (Iffert, 2007). This automatically leads to large errors in bath chemistry control in smelting cells when adjustments in $AlF_3$ additions are based on $AlF_3$ concentration measurements (Section 2.1.2). Figure 2.8 shows the relationship between the bath inventory and bath level. The bath height is measured with the iron rod method and is controlled independently of other variables (Section 2.3.1.3). In addition, superheat is added as a third parameter to show the impact of superheat on the

amount of liquid bath mass measured in the cell (a larger bubble volume represents a higher superheat). Based upon Equation 2.14 a proportional relationship between superheat and bath inventory is expected, but a weak correlation between bath levels and inventory and between superheat and inventory were found (Iffert, 2007).

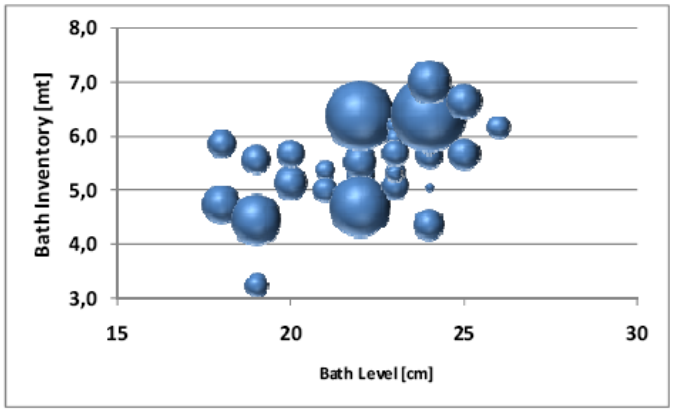


***Figure 2.8*** *Relation between Bath Mass and Bath Height (Iffert, 2007)*

## 2.2 Process Control and Statistical Methods

Section 2.2 discusses an overview of control principles and applied statistical methods in comparison to traditional engineering compensatory control where deviation from target is minimized without explicitly addressing the cause of variation. Many control models are based on a “back to target” philosophy like PID controllers used in simple single-input/single-output (SISO) or more sophisticated multi-input/multi-output (MIMO) systems as described in Section 2.2.4. Fuzzy logic and neural networks are founded on non-discrete or heuristic relations between inputs and outputs, but they still manipulate process parameters in order to bring them back to their target setpoints as described in Section 2.2.5.

Continuous improvement techniques (for example SPC) have been integrated into control systems to address causes of variation in a broad range of industrial processes. Instead of compensatory control actions these methods are focused on the removal or elimination, and/or correction of these root causes. Statistical process control is used to distinguish between common-cause and special-cause variation to avoid inappropriate actions. In this technique the main control objective shifts from a 100% control of outputs to signalling potential input or process problems prior to major excursions or product rejections.

### 2.2.1 Common-Cause and Special-Cause Variation

Process variation is embedded in dynamic systems and can be divided into common-cause and special-cause variations (Shewhart, 1931). Natural or common-cause behaviour of

processes is characterized by a mix of phenomena and mechanisms acting within the system constantly of which the ensuing variation is predictable probably due to its normal distribution or historical reproducibility. Although some of these variations are highly mechanised (e.g. feeding of alumina) and have been classified as structural variation, together they still represent a natural behaviour of the combined variation (Jounier, 1994).

Under these circumstances the system is statistically in control and only carefully designed experimentation can be used to reduce the variability. The tendency of target-based control strategies to 'tamper' with processes in statistical control is a main driver of increased variation. On the other hand special-cause variation is statistically unpredictable, whereby abnormal discrete events suddenly arise and disturb natural process behaviour. These events actually represent the improvement opportunities in complex processes, because the dominant causes can then be found through a detailed investigation of the underlying mechanisms.

The origin of statistical process control traces back to Deming's 14 points famously stated in "Out of the Crisis" (Table 2.2) (Deming, 1982). In parallel to this the development and application of univariate control charts in industrial processes occurred, but this was not applied to great effect until the power to change the work of individuals through their use - Deming's points 3, 5, 10 and 11 - began to be understood (after they revolutionised industry in Japan).

| | |
|---|---|
| 1 | Create constancy of purpose |
| 2 | Adopt the new philosophy |
| 3 | Cease dependence on mass inspection to achieve quality |
| 4 | Minimize total cost, not initial price of supplies |
| 5 | Improve constantly the system of production and service |
| 6 | Institute training on the job |
| 7 | Institute leadership |
| 8 | Drive out fear |
| 9 | Break down barriers between departments |
| 10 | Eliminate slogans, exhortations, and numerical targets |
| 11 | Eliminate work standards (quotas) and management by objective |
| 12 | Remove barriers that rob workers, engineers, and managers of their right to pride of workmanship |
| 13 | Institute a vigorous program of education and self-improvement |
| 14 | Put everyone in the company to work to accomplish the transformation |

***Table 2.2*** *Deming's 14 Key Principles for Management for Transforming Business Effectiveness (Deming, 1982)*

Traditional control charts such as Shewhart charts, cumulative sums (CUSUM) and exponentially weighted moving averages (EWMA) are used to monitor key measurements on the final product for quality control purposes individually. A control chart (individual - moving range for example) is made of single point measurements, a central line indicating the mean,

and an upper and lower control limit in this case defined by the mean variability over time, point to point (Johnson, 1994). These limits are calculated based on a fixed number of standard deviations, or a defined probability of a data point or pattern within the chart. The power of such charts is that non-random, or special variation is very quickly apparent and signals to the chart owner that the process is no longer in statistical control.

These techniques can therefore be used to differentiate between stable processes varying naturally within given boundary conditions, drifting processes experiencing long-term change away from these conditions and processes growing towards higher variability. In this respect additional rules provide extra information to detect out-of-control behaviour like the detection of a bias, trend or oscillation (Nelson, 1984). The upper and lower control limits are set at $3\sigma$ above and below the centre line respectively. The control chart is divided into 6 zones, each zone being $1\sigma$. The upper half of the chart is referred to as A (outer third), B (middle third) and C (inner third) (Table 2.3), whereas the lower half is taken as the mirror image. By finding special-causes, systematically long-term improvements in the process and in product quality can be achieved by eliminating causes or improving the process or its operating procedures. In order to reduce common-cause variation a wide range of different statistical techniques are available, usually based upon analysis of variance (ANOVA) methods.

| Rule | Description |
|---|---|
| 1 | One point beyond Zone A |
| 2 | Nine points in a row in Zone C or beyond |
| 3 | Six points in a row steadily increasing or decreasing |
| 4 | Fourteen points in a row alternating up and down |
| 5 | Two of three points in a row in Zone A or beyond |
| 6 | Four out of five points in a row in Zone B or beyond |
| 7 | Fifteen points in a row in Zone C (above and below centre line) |
| 8 | Eight points in a row on both sides of centre line with non in Zones C |

***Table 2.3*** *Nelson Rules for Additional Detection of Out-of-Control Behaviours (Nelson, 1984)*

### 2.2.2 Causality and Control

As described in Section 2.2.1 causality and control can be closely linked by an event (cause) followed by another event (detected process effect) which is the direct consequence of the first. If applied immediately when the evidence of the first event is still available, root cause analysis is an effective set of problem-solving methods and is widely applied to identify process abnormalities systematically. The practice is predicated again on Deming's thinking that problems are best solved by attempting to correct or eliminate root causes as opposed to merely addressing symptoms (or tampering, as he called it). By eliminating causes, and implementing only corrective measures, recurrence of a variation will be minimized, but

complete prevention by a single intervention is not always possible. An iterative process is necessary to achieve continuous improvement.

In order to implant continuous improvement in organisations Deming developed the so-called System of Profound Knowledge (Deming, 2000). The layout of profound knowledge appears in four parts, all related to each other: appreciation of a system, knowledge about variation, theory of knowledge, and psychology. The first part deals with better understanding of underlying processes to determine the system complexity and interdependency. Sections 3.1.1 to 3.1.5 discuss the theoretical development of the process mechanisms studied in this thesis. The second part of the philosophy refers to a better understanding about common-cause and special-cause variations and provides knowledge about the direction of improvement (Sections 3.2.1 and 3.2.2). The third part incorporates continuous learning supported by Deming's PDSA-cycle (plan, do, study, act) that creates a systematic approach to reduce process variability over time. This is embedded in the formulation of the new control approach undertaken in Section 3.3. Finally, knowledge about human nature stimulates collaboration of all people involved (Section 3.3.3.2).

Over the last two decades both Six Sigma and Lean Production systems have been implemented successfully into a wide range of businesses to improve their performances. Six Sigma was implemented by Motorola in the 1980's and is a method to improve quality of process outputs by identifying and removing causes of defects and process variation (Section 3.3.2) (Gupta, 2004). For example a process chain of 100 sub-processes with a success rate of 99% each will finally lead to an overall success rate of only 36.6%. A breakthrough approach to Six Sigma was developed in 2000, which incorporates an iterative problem-solving method called DMAIC (define, measure, analyze, improve and control) inspired by Deming's PDSA cycle (Gupta, 2004). A prerequisite is the unconditional commitment of management to achieve sustained quality improvements (Deming's first and probably most important point).

Lean Manufacturing uses a refined set of Deming's learning's about production, derived from the Toyota Production System (TPS) in Japan. It focuses on maintaining and maximizing flow with an integrated production chain, often referring back to its original design (Womack and Jones, 2003). The objectives are to eliminate waste and to design out overburden and inconsistency. Seven different categories of waste are distinguished: transportation, inventory, motion, waiting, overproduction, over processing and defects. The critical starting point of lean thinking is value, which is defined by the customer. Flow must be created within the total production chain based on demand from the customers. Finally, all individual steps will lead to a perfection of the total production chain.

Both Six Sigma and Lean Manufacturing make use of a broad range of techniques to find root causes of process abnormalities such as Failure Mode and Effect Analysis (FMEA), Cause & Effect (Fish Bone) Diagrams, Cause Mapping, Pareto Charts or Juran Diagrams, Measurement System Analysis (MSA), Fault Tree Analysis, 5 Whys and others (Chapter 2, Gupta, 2004).

Quality management systems (e.g. ISO 9001) have been introduced to achieve customer satisfaction through consistent products and services which meet customer expectations. These systems adopt documentation consistent with statistical control of processes but do not encompass or enact the principles of improvement described above, which must be embedded in the actual control of the processes. In general quality management systems have had short lives in operating production facilities because they cannot be relied upon for these daily control tasks. However, suppliers to key sectors must comply with the main elements such as systematic business approach including full traceability of all underlying processes. The automotive industry has introduced the ISO/TS16949 certificate, in which above-mentioned techniques are obligatory in process monitoring and continuous improvement (ISO/TS16949: Quality Management Systems, 2002). Aldel is an ISO/TS16949 company.

In this respect efficient smelter operation requires a detailed and well considered design of all discrete events, human interactions, control actions and their mutual relations. The large distances between production units or cells in an aluminium smelter affects the ability to control tasks within the smelting process, e.g. modern smelter with an annual capacity of 500.000 tonnes of primary metal contain up to 500 cells and 5 kilometres of building lengths. These smelters need advanced and highly automated supervision of their cells in order to run the process at highest efficiencies.

The sequence of operational activities (flow) also influences performance. In order to reduce measurement variability due to operational activities sufficient time between these operations and measurement is taken place (Section 2.3.1.5). In case of an outage or reduction in the line current measurements and/or interpretation have to be related to history of energy input to the cell. Based on a continuous flow of activities with a predictable impact to the process a working sequence of measurements, metal tapping, anode changing and anode covering is used in the aluminium industry. After alumina feeding the anode setting rota has the biggest influence on this schedule due to its utmost major impact on the ensuing mass and energy balance (Section 2.1.3).

Moreover, accuracy and consistency of these operational practices are very important to limit system variability and therefore wrong control actions. At Aldel, the management system prescribes procedures for running all smelter operations including task-specific workplace

instructions. These instructions have been developed in collaboration with the operators in order to define “best practices” and uniformity in the five shifts operation. Well designed procedures and accompanying operator skills for operational practices like anode changing, anode covering and metal tapping result in low and predictable influences to the ensuing system dynamics. Maximizing line current, application of power modulation and deterioration of raw materials underline the necessity to optimize standard operations. A well designed control strategy is able to compensate limited variability in mass and energy balance.

At Aldel, process audits are carried out to check the performance related to standards and feedback is given to the operators. Figure 2.9 demonstrates a daily audit of the number of holes in the crust and the average cover height after anode changing (10 cells/day). The control targets for the number of holes and cover height are 0 per cell and 7 cm respectively. These process parameters are important for maintaining good environmental performance and heat balance (Section 2.1.2). In this case both the variation and average cover height reduces over time; this being a requirement when an increase in line current occurs.

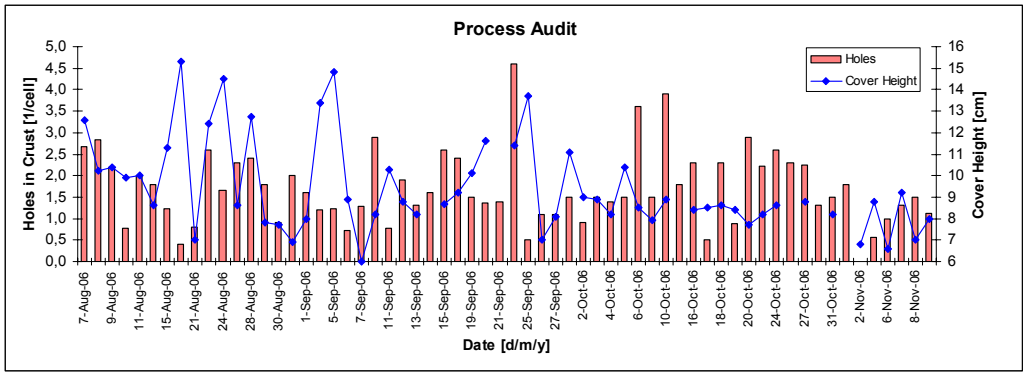


***Figure 2.9*** *Daily Audit of Holes in the Crust and Cover Height after Anode Changing at Aldel*

### 2.2.3 Compensatory versus Corrective Control

A general shift in the quality management systems towards corrective actions instead of a compensatory approach can be observed from implementation of Lean Six Sigma into a broad range of industries (Torremans, 2008). Corrective control actions are focused on the detection of causes of abnormalities in order to correct or remove them and to bring the process back to its operating window. A preventative action is undertaken to avoid non-conformances and is a proactive process to identify opportunities for improvement rather than a simple reaction to problems or complaints after they have been raised.

As described in Sections 2.2.1 and 2.2.2 different techniques regarding root cause analysis are available to support and improve decision-making in industrial processes. However, application of these methods within strong interactive multivariate processes can lead to

incorrect control actions as described by Type I and II errors. From a statistical point of view a Type I error or false alarm rejects the null hypothesis when it is true, whereas a Type II error fails to reject the null hypothesis when it is false (Taylor *et al.*, 2007). The occurrence of a false alarm can result in incorrect control actions. More care is needed for failed alarms, because potential harmful process conditions are not being detected.

Despite observed trends towards a more corrective control approach, compensatory control is still used as the main control strategy in industrial processes globally. This approach is undertaken to respond to an assumed single cause of variation, because this cause was identified by the control system designer. However, when a mix of causes is acting the compensatory controller can become ineffective since these causes are not addressed by the control action. Compensatory control is used successfully in intensively measured processes with good sensory characteristics where only known causes of variation are acting. These control models can be empirical (black box), based on physio-chemical laws (grey box) or grounded on full physical understanding of the underlying process (white box). However, limited process monitoring is inherent to the aluminium smelting process, mainly due to the highly corrosive characteristics of the electrolyte used (Section 2.3).

Under particular circumstances compensatory control actions avoid severe damage to the process or its surroundings due to effective counter measures to input variables. For example losing sidewall ledge in aluminium smelting cells is of high concern and temporary reduction of heat input could protect the cell against a sidewall and cell failure. However, such counter measures, for example a reduction in cell voltage or an increase in $AlF_3$ additions only suppress short term variations and do not remove the root cause. In this respect automatic control actions can hide the abnormality leading to a substantial worse process excursion afterwards. These control actions can also initiate extra process variation, because they adjust the mass and energy balance symptomatically. Detailed knowledge and better understanding of underlying sub-processes is necessary to distinguish between single causes acting within a system and to describe their interaction (black $\rightarrow$ white box model).

### 2.2.4 Proportional Control

The application of a proportional-integral-derivative (PID) controller is used in process control in a wide range of industries and corrects a deviation between a measured variable and its desired setpoint (Creemers *et al.*, 1987). PID controllers adjust processes rapidly according to their deviation in order to keep the detected deviation minimal. The proportional factor is designed for a linear response, whereas the integral and derivative actions are designed to respond quickly and dampen any overshoot respectively. The output $y(t)$ of a general PID controller is given by Equation 2.15, where $T_i$ is the integral time and $T_d$ is the derivative time.

$$y(t) = K_P \cdot \left( e(t) + \frac{1}{T_i} \int_0^t e(\tau) d\tau + T_d \frac{de}{dt}(t) \right) \quad (2.15)$$

Proportional control *(P)* is applied to the aluminium smelting process as shown in Equation 2.12. In this case aluminium fluoride control is proportional to the deviation of measured and target $AlF_3$ concentration as well as measured and target electrolyte temperature. This philosophy allows adjustments in $AlF_3$ additions to imbalances in the concentration due to individual fluoride losses per cell (Section 2.1.2). However, since there is no additional check on the root cause of the concentration imbalance, changes in $AlF_3$ additions are also applied in case of ledge movement due to heat imbalances. Proportional control then becomes compensatory rather than corrective.

In Equation 2.12 the measured temperature was not used directly to calculate the fluoride additions (Kloetstra and Stam, 2001). This was done in order to avoid overreaction of the control system. Equation 2.16 incorporates a correction of the bath temperature *($T_B$)* based on extra energy input due to abnormal operating voltages, which is based on the average voltage *($V_{avg}$)* related to the setpoint voltage *($V_{setpoint}$)* accounting for a natural band *($V_{dev}$)* calculated for the period between two successive measurements. A second adjustment is the introduction of a band around bath temperature to incorporate natural variation due to discrete events as described in Section 2.1.3. Another option is to use predictable measurement errors related to operational practices (structural variation) to correct the input into the control model, e.g. a specific correction according to recent changed anode can be used (Figure 2.10) (Stevens McFadden, Welch *et al.*, 2001).

$$T_{corrected} = T_B - k_{volts} \cdot (V_{avg} - V_{setpoint} - V_{dev}) \quad (2.16)$$

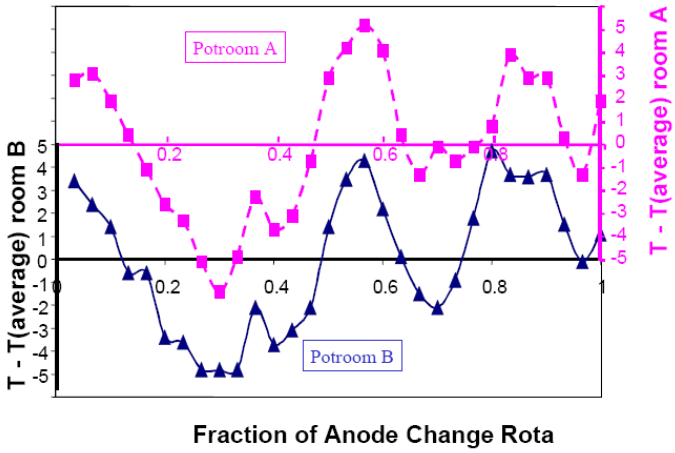


***Figure 2.10*** *Structural Variation Related to Anode Changing (Stevens McFadden, Welch et al., 2001)*

As stated in Section 2.1.1 SISO control is also applied in alumina feed control, which is achieved using interferential sensors $\Delta R$, dR/dt and/or $d^2R/dt^2$. These utilize the impact of alumina concentration on anode polarization voltage and hence cell resistance (Figure 2.2). The problem associated with this approach is the requirement for significant filtering of cell resistance due to noisy voltage signals leading to major time delays, assumption of a constant relationship between $\Delta R$ and alumina concentration and assumption of a time invariant dependency of the depletion rate of alumina in case of dR/dt and/or $d^2R/dt^2$ control (Stevens McFadden, Bearne *et al.*, 2001).

In the above examples automatic control actions are applied to correct a deviation between a measured value and its setpoint. These PID controllers assume the causes of the variation. For example a correction of the measured temperature is linked to the deviation between the cell voltage and setpoint (Equation 2.16). However, the overall voltage contains a number of different components (Equation 1.5). These components vary with the process conditions as described in Section 1.3.2, not necessarily resulting in an extra energy input and therefore affect the bath temperature. Likewise variations in voltage or resistance are not only caused by variation in the alumina concentration as demonstrated in Equation 2.3.

### 2.2.5 Model-Based Control

Fuzzy logic, neural networks and empirical models have been applied to improve the control in a wide range of industrial processes. This section presents a brief summary of these models in relation to the requirement for maximum flexibility under the rapidly varying economic and environmental circumstances as discussed in Section 1.1.

Fuzzy logic is based on rules of the form “if…then” that convert inputs to outputs, one fuzzy set to another (Kosko *et al.*, 1993). This technique has been applied to aluminium fluoride control to predict the concentration in electrolyte as discussed in Section 2.1.2 (Meghlaoui and Aljabri, 2003). Prior to the implementation of fuzzy logic control, a fuzzy set has been determined based on historical measurements and calculations in order to connect the measurements and predictions. Further, three regions (“cold”, “normal” and “warm” as represented by three different colours) are defined as given by Figure 2.11. In these regions the $AlF_3$ concentration is set to a particular value (e.g. if temperature is “cold” then [$AlF_3$] = 14%). Thereafter the $AlF_3$ concentration has been predicted based on a temperature measurement and the fuzzy model using the corresponding weighing factors (y-axis).

However, fuzzy sets identification is based on a historical survey of the underlying system dynamics for given boundary conditions. In addition, these fuzzy sets are defined for group averages and therefore introduce deviations when used for individual cells. Moreover, this approach ignores individual variation between cells and inevitable process variations in

superheat and the uncertainty in the determination of the $AlF_3$ concentration as described in Section 2.3.1.2. Due to the static characteristics of the fuzzy set, these models can't be applied to rapid varying circumstances like power modulation, increased line current and increased variability in the quality of the raw materials used.

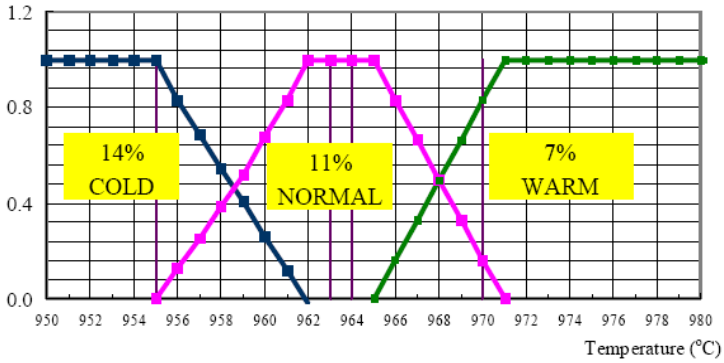


***Figure 2.11*** *Example of Fuzzy Logic Set for $AlF_3$ control (Meghlaoui and Aljabri, 2003)*

A fuzzy logic strategy has also been developed for resistance (ACD) and alumina feed control (Li *et al.*, 2001). In this case a combination with an expert system is used because it has the properties of being able to use precise as well as heuristic knowledge and also have the flexibility to modify and expand information in its knowledge base. The controller requires self-adjustment and self-learning abilities to deal with non-linear and time-varying characteristics. Tests at smelters have shown an accurate, robust and stable control system which results in higher production efficiencies but process parameters are still manipulated in order to bring them back to their target setpoints, without knowing the cause of variation.

Expert system approaches are also being attempted in the aluminium industry in combination with fuzzy logic and failure mode and effect analysis tools (Berezin *et al.* 2005). FMEA is an analytical method used to identify potential abnormalities with their effect, frequency and detection rate (Section 2.2.2). The FMEA method is used to prioritize both "sick" cells and dominant failure mechanism in the pot line. After that continuous improvement is supported by removing causes of abnormality on a daily basis. The authors claim a better efficiency by timely diagnosis of cells. However, no qualitative figures are published.

In general, an artificial neural network is built on a number of simple processing elements (Cheng, 1997). These elements are often structured with a sequence of layers. These layers are linked by weights, which are adapted by supervised or unsupervised learning. A neural network consists of an interconnected architecture among the elements, a transfer function to establish the relation between inputs and outputs and a learning algorithm. This technique

is also applied to SPC control charts and is capable of detecting unnatural patterns to assist in the correction of specific-cause variation.

A neural network has been applied to identify significant control parameters in the aluminium smelting process (Frost and Karri, 2000). Originally 12 process parameters were selected as potential neural network inputs for prediction, while 2 outputs were used. In order to find the correlation between inputs and outputs detailed data acquisition was carried out. Based on this only 5 network inputs contribute to the prediction which are cell stability (39.3%), cell identification (10.9%), cell efficiency (10.5%), sludge level (19.8%) and current flow (19.4%). This outcome confirms that the most efficient operating zone is associated with maximum process stability as discussed in Section 1.3.1 and the need for good control of the alumina concentration in aluminium smelting cells (Section 2.1.1).

A recent approach in control of smelting cells is the application of Linear-Quadratic-Gaussian control as a first step towards Model-based Predictive Control (Stevens McFadden, 2007). An LQG-controller, designed using a linear state-space model or system description of the process, is made up of a state estimator (Kalman filter) and an optimal state feedback controller. The state-controller is designed to minimize variation in controlled variables and control actions according to a set of relative weightings defined by the designer.

Multivariable control of temperature, bath height and superheat using LQG-control principles predicts a reduction in standard deviation of 20% for temperature, 25% for liquidus, 22% for the $AlF_3$ concentration, 23% for superheat and 10% for bath height over that achieved with the existing control system. Regarding the implementation of sensors, no benefit was found for the use of measurements of alumina concentration, or individual cell duct flow rate, temperature or heat losses as feed forward variables in a multivariable model-based controller. No industrial experiments are published to confirm the predicted improvement in process stability. The LQG-control approach does, however, underline the necessity of a multivariate control approach for aluminium smelting cells.

### 2.2.6 Multivariate Statistical Projection Methods

In Section 2.2.1 the application of univariate control charts is considered to be an important factor in the overall reduction of process variation in industrial processes. These control charts can not be used in interrelated processes as shown in Figure 2.12 (MacGregor and Kourti, 1995). In this example tracing of variables $y_1$ and $y_2$ individually will not detect a process abnormality, represented by the points $\otimes$ in the diagram, because they stay within the upper and lower control limits of both univariate control charts. If these charts are combined incorporating the correlation between both variables, it is clearly seen that these particular points represent out of control behaviour.

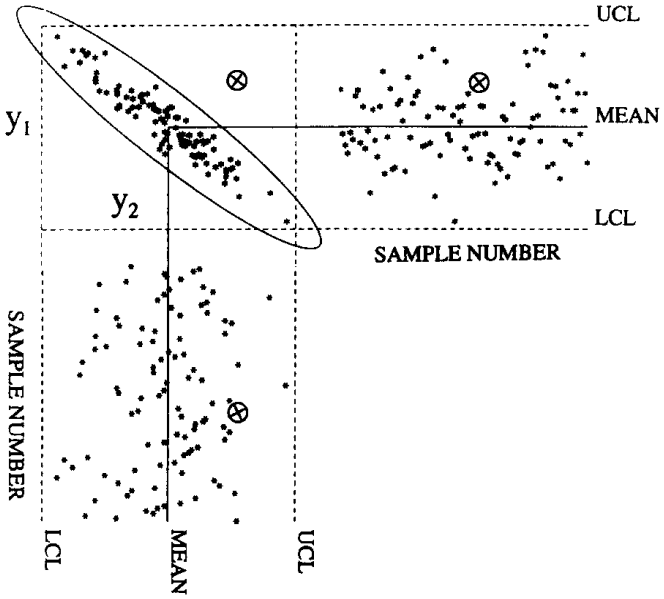


***Figure 2.12*** *Multivariate Process Control (MacGregor and Kourti, 1995)*

To overcome false alarms in the control of largely interrelated processes, multivariate extensions of these univariate control charts have been developed based on Chi-squared *($\chi^2$)* and Hotelling statistic *($T^2$)* respectively. Given a (*q x 1*) vector of measurements *y* on *q*, normally distributed variables with an in-control covariance matrix $\Sigma$, it is possible to test whether vector $\mu$ of the means of these variables is at its desired target $\tau$ by computing the statistic as shown by Equation 2.17.

$$\chi^2 = (y-\tau)^T \Sigma^{-1} (y-\tau) \tag{2.17}$$

This statistic will be distributed as a central Chi-squared distribution with *q* degrees of freedom if $\mu=\tau$. A multivariate control chart can be constructed by plotting $\chi^2$ versus time with an upper control limit given by $\chi^2_\alpha(q)$, where $\alpha$ an appropriate level of significance. All points lying on the ellipse in Figure 2.12 would have the same $\chi^2$ value and this chart detects, as a special event, any points lying outside of the ellipse (Section 3.2.1.2). When the in-control covariance matrix $\Sigma$ is not known, it must be estimated from a sample of *n* past multivariate observations as shown in Equation 2.18.

$$S = (n-1)^{-1} \sum_{i=1}^{n} (y_i - \bar{y})(y_i - \bar{y})^T \tag{2.18}$$

When new multivariate observations *(y)* are obtained, then Hotelling's $T^2$ statistic is given by Equation 2.19.

$$T^2 = (y-\tau)^T S^{-1}(y-\tau) \tag{2.19}$$

The upper control limit based on Hotelling's $T^2$ statistic is given by Equation 2.20,

$$T^2_{UCL} = \frac{(n-1)(n+1)q}{n(n-q)} F_\alpha(q, n-q) \tag{2.20}$$

Where, $F_\alpha(q, n\text{-}q)$ is the upper control limit of the F-distribution with $q$ and $n$-$q$ degrees of freedom at confidence interval $\alpha$. A two dimensional system of Hotelling $T^2$ statistic versus time allows application of simple SPC charts to detect abnormalities. Once an abnormality is found, further investigation is necessary to determine which variables are responsible for it. Various statistical techniques (e.g. CUSUM, EWMA techniques) can then be applied to individual variations to analyze in detail what is causing the abnormality (Section 2.2.1).

In case of highly correlated data combined with a nearly singular covariance matrix $\Sigma$, Principal Component Analysis (PCA) can be used to reduce the dimensionality of the system (MacGregor and Kourti, 1995). The first principal component (PC1) of measurements $y$ is defined as that linear combination $t_1 = p_1^T y$ that has maximum variance subject to $|p_1| = 1$. The second principal component (PC2) can be derived similarly and is uncorrelated with PC1 due to its orthogonal character and explains the next greatest amount of variation (Roffel, 2008). Additional principal components are defined in the same way. Once a PCA model is established, based on statistically in control variation, process behaviour can be referenced against this model.

Partial Least Squares (PLS) is a regression method and is used to correlate input parameters to output or quality measures (Kourti *et al.*, 1996). Given two matrices, an $(n \times m)$ process variable matrix $X$ and a $(n \times q)$ matrix of corresponding outcome matrix $Y$, the variation in $Y$ can be explained by variation in $X$. The major advantages of using these multivariate projection methods are the ability to handle large numbers of highly correlated variables, measurement errors and missing data. Processes can easily be monitored in reduced spaces with conventional univariate SPC charts by using lower dimensional systems.

Due to the multivariate interrelated characteristics the aluminium smelting process and inconsistency of data gathering of different parameters, the application of these projection methods has a huge potential to improve process control in smelting cells (Majid *et al.*, 2009). Recently, PCA has been applied to determine out of control behaviour using it as a daily diagnostic tool (Tessier *et al.*, 2009). It is demonstrated that PCA is able to detect problems faster than ordinary SPC techniques resulting in faster corrective actions and

therefore avoiding significant lowering in current and energy efficiencies. Some disadvantages are the requirement for historical data to build up a reliable model and the specificity of that model for particular setpoints (i.e. line current, or alumina or anode supply) to define the operating window. These issues have not yet been addressed.

### 2.2.7 Other Techniques

Process Analytical Technology (PAT) is a grouping of techniques for providing analysis and control of manufacturing processes based on timely measurements of critical quality parameters and performance attributes of raw and in-process materials to assure predefined end-product quality at the completion of the process (U.S. Department of Health and Human Services *et al.*, 2004). The concept aims at understanding the process by defining their critical performance attributes and monitoring them in a timely and preferably by inline and online manner. Quality and availability of reliable data is essential as disturbances like noise, outliers or abnormalities, jumps, drifts, fluctuations and missing data are embedded in most industrial processes.

PAT transforms relevant data sources such as process data, sensory data and end-product quality data with the use of multivariate analysis tools (e.g. PCA, PLS) into a unique process fingerprint indicating the natural behaviour of the process. Studies have been carried out to use chemical imaging to determine specific process characteristics using different sensors. For example an in-line control system for measuring the thickness of a protective layer on metal sheets is developed with the use of interference and reflectance spectroscopy (Kessler and Kessler, 2008). Application classification or data reduction by PCA was necessary for real-time measurements and therefore development of a control system.

A similar technique was applied to predict the alumina composition of anode cover and to investigate the impact from variations induced by differences in alumina properties and crushed bath content (Tessier *et al.*, 2008). Textural features have been extracted from images of anode cover using Grey Level Co-occurrence Matrices (GLCM) texture algorithm. PLS predictions gave a good correlation with laboratory measurements in the texture features of the alumina properties and crushed bath.

Another attempt to improve the measurability and sensitivity of a process is based on sensor data fusion (Crowley and Demazeau, 1993). This is a combination of sensory data and data derived from disparate sources in order to design an accurate, complete and dependable detection method. A broad range of different combinations between hardware sensors, soft sensors based on intelligent data acquisition, historical sensor data and others provide cause-specific information. In this thesis, soft sensors are developed to improve cause-specific detection of abnormalities (Section 3.2).

## 2.3 Developments in Measurements and Control in Aluminium Smelting Cells

Compared with other chemical industries there are many major constraints in the reactor design and chemicals used in the aluminium smelting process. The main solvent (cryolite) is highly corrosive and therefore gives substantial restrictions to materials that can be used in the cell (reactor) construction and devices that can be used to control the process. Currently there are no continuous online (industrial) measurement tools available for the determination of existing process conditions like the bath temperature and composition. Consequently practitioners are forced to use indirect or discrete measurement methods, particularly for alumina feed and bath chemistry control.

### 2.3.1 Process Measurements

#### 2.3.1.1 Electrolyte Temperature

Temperature measurements in the aluminium smelting process are most commonly carried out with ordinary thermocouples. Type K - protected with a steel sheath - is widely used in bath temperature measurements due its availability with relatively low costs. However, Type K thermocouples have inherent instabilities at high temperatures due to “short-ranged ordering” induced inhomogeneity and shows a measurement bias from 3 up to 10°C (Wang *et al.*, 2006). This bias can not be eliminated through a pre-calibration. In addition, chemical corrosion of the thermocouple deteriorates the integrity over time. Type S thermocouples are constructed with a 100% Pt wire and a 90% Pt/10% Rh wire and are calibrated using a gold bridge melting at 1064.43°C. With this system, Type S thermocouples, especially if used in a disposable manner, exhibit more reliable data within the highly corrosive environment in a smelting cell.

As described in Section 2.1.3 discrete events like anode changing and alumina feeding lead to spatial variations in bath temperature. The large mass of metal contained in cells produces a greater thermal inertia in the metal pad than the bath and is partly isolated or dampened from the impact of frequent alumina additions. A 3-6°C lower metal temperature compared to the electrolyte temperature was found (Whitfield *et al.*, 2004). Although the metal temperature does follow the alumina feed cycle, it is partially resistant to the abrupt changes in the bulk electrolyte. The difference between bath and metal temperatures are relatively constant during demand and underfeed, but falls dramatically during overfeed. However, no improvements to the control of the smelting process have been published.

### 2.3.1.2 Electrolyte Composition

XRD is usually applied in aluminium smelters to analyse $AlF_3$ and $CaF_2$ concentrations. It is used to characterize heterogeneous solid mixtures to determine the relative abundance of crystalline compounds. Diffraction occurs when the dimensions of the diffracting objects are comparable to the wavelengths of radiation (Atkins, 1990). Typically, a bath sample is taken in a fixed sequence in relation to the operating cycle together with the bath temperature. Obtaining a representative sample of the industrial electrolyte is very difficult because the rate of cooling of the sample determines the amount of different phases created and this affects the results ascertained by XRD (Rolseth *et al.*, 1998). The rate of cooling mainly depends on the workmanship of the operator during sampling and the geometry (size, shape, material) of the sampler itself.

As demonstrated in Figure 2.4 both the electrolyte and liquidus temperatures are important parameters in the control of the aluminium smelting process. The difference between the two gives the electrolyte's superheat, which can be used as a diagnostic as well as control parameter. There have been a lot of attempts to empirically determine temperatures of primary crystallisation by thermal analysis of bath samples (Thonstad *et al.*, 2001). The best prediction of the liquidus temperature is considered to be the SINTEF-equation and is given by Equation 2.21 (Thonstad *et al.*, 2001).

$$\begin{aligned} T_L = {} & 1011 + 0.5\cdot[AlF_3] - 0.13\cdot[AlF_3]^{2.2} - \frac{3.45\cdot[CaF_2]}{1+0.0173\cdot[CaF_2]} \\ & + 0.124\cdot[AlF_3]\cdot[CaF_2] - 0.00542\cdot\left([AlF_3]\cdot[CaF_2]\right)^{1.5} \\ & - \frac{7.93\cdot[Al_2O_3]}{1+0.0936\cdot[Al_2O_3] - 0.0017\cdot[Al_2O_3]^2 - 0.023\cdot[AlF_3]\cdot[Al_2O_3]} \\ & - \frac{8.90\cdot[LiF]}{1+0.0047\cdot[LiF]+0.0010\cdot[AlF_3]^2} - 3.95\cdot[MgF_2] - 3.95\cdot[KF] \end{aligned} \tag{2.21}$$

Where, $T_L$ is the liquidus temperature in degrees Celsius and the square brackets denote the weight percent of the components in the system $Na_3AlF_6$-$AlF_3$-$CaF_2$-$Al_2O_3$-LiF-$MgF_2$-KF. The equation is valid for compositions of $AlF_3$, $CaF_2$, LiF lower than 20 wt%, and $MgF_2$, KF lower than 5 wt%, and alumina concentration up to saturation.

There are some major disadvantages using the predicted liquidus temperature for control purposes. In the first place there is an analytical lead time needed for bath sampling and analysis which leads to a delay in decision-making. The inherent uncertainty in the liquidus prediction using the SINTEF type of equation is expected to be 2°C for $AlF_3$-rich bath compositions (i.e. [$AlF_3$] >10 wt%) (Wang *et al.*, 2006). However, the key factor appears to be the precision of the bath analysis. Furthermore, it is suggested that some of the trace

elements reduce the liquidus temperature more in an acidic melt than in pure cryolite and it was hypothesised that aluminium carbide leads to a reduced liquidus temperature, which is estimated to be 4.8°C/wt% of $Al_4C_3$ by a maximum solubility of 1 wt% in normal bath (Moxnes *et al.*, 2006).

In order to overcome these prediction uncertainties it is advantageous to measure liquidus temperature directly (Verstreken and Benninghoff, 1996). A liquidus probe (Cry-O-Therm) has been developed recording the thermal response of a cooling sample at a frequency of 10 Hertz (Figure 2.13). A Type S thermocouple with low thermal mass is used to measure the electrolyte and liquidus temperature. The thermocouple is plasma coated with copper to enable the thermocouple to survive chemical attack by liquid bath during immersion. Another critical design feature is vibration of the sample during a measurement to avoid supercooling. A cardboard tube is used as a protective carrier and stimulates turbulence within the measuring hole to obtain a representative bath sample and increased heat transfer to the probe (Figure 2.13). The superheat is calculated as the difference between the electrolyte and liquidus temperature. The liquidus temperature is determined based on the change in slope of the cooling curve representing the complete solidification of the sample.

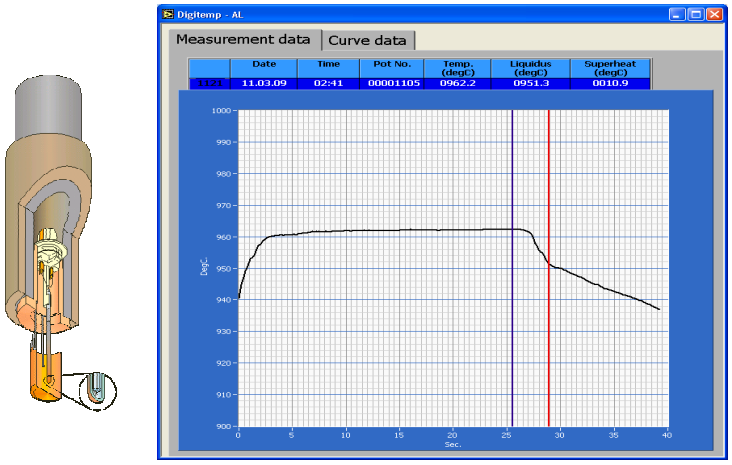


***Figure 2.13*** *Temperature and Liquidus Measurement with Cry-O-Therm*

The observed discrepancy in the commonly used Type K thermocouple and difficulties with prediction of liquidus temperature and superheat has been confirmed experimentally by own measurements. Figure 2.14 shows the relationship between the measurements of the bath temperature carried out in a number of cells with a Type K thermocouple versus a calibrated Type S thermocouple (Section 2.3.1.1). The black lines represent the perfect match between the two couples. These measurements demonstrate an average difference of 7.8°C between the Type K and S couple with an increased deviation from low to high temperature regions.

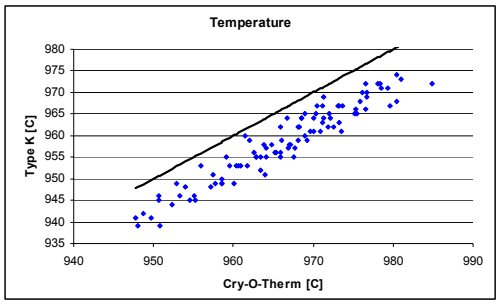


***Figure 2.14*** *Type K versus Type S Thermocouple*

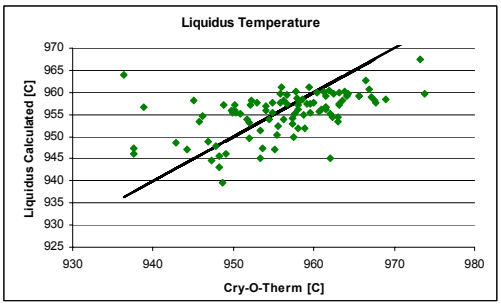


***Figure 2.15*** *Measured versus Calculated Liquidus*

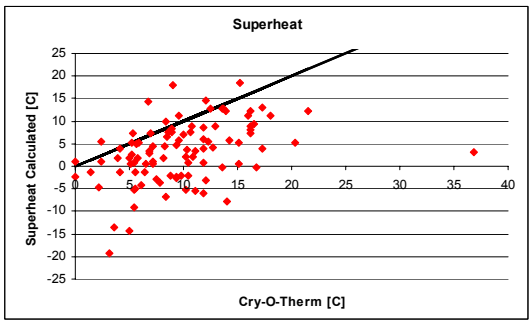


***Figure 2.16*** *Measured versus Calculated Superheat*

A representative calculation of the liquidus temperature in industrial circumstances is not possible as given by Figure 2.15. Usually an average alumina concentration or estimation based on the feeding cycle is used in the calculation. The spread increases from high to low temperature zones, which indicates an increased uncertainty in bath sampling as well as alumina concentration. In the case of superheat, no useful correlation is found between calculated and measured values; in fact superheat calculated from bath composition even gave some negative superheat values, which is physically impossible (Figure 2.16). Given errors in the liquidus prediction using equations one major advantage of direct measurement using the Cry-O-Therm sensor is that it gives both the bath and liquidus measurement with a single thermocouple thus reducing the overall errors in the measurement. All bath, liquidus and superheat measurements in this thesis have been carried out with the Cry-O-Therm system.

### 2.3.1.3 Liquid Levels and Inventories

Liquid level control in smelting cells is performed by individual bath and metal height measurements using an iron rod. The iron rod is dipped through the liquid until it touches the cathode surface and is taken out after 3-5 seconds. The metal height is measured by the distance from the bottom of the rod to the interface defined by the different cooling characteristics of the two liquids (metal and electrolyte), whereas the bath level is measured by the distance from this interface to the top of frozen material. More recently, these measurements have been done from the top of the cell to avoid errors with localised bottom

erosion (especially when the measuring hole is located near the tapping hole) or in the vicinity of bottom sludge/ridge. Individual cell conditions like carbon dust formation, high temperatures and high bath densities can significantly influence the accuracy.

As discussed in Section 2.1.4 measurements of the amount of liquid bath mass in industrial cells revealed large fluctuations and therefore a weak correlation between bath levels and inventory were found. Liquid bath mass measurements are performed using a tracer method in which a well-defined amount of tracer material is dissolved in the electrolyte. The difference between the background concentration and the measured concentration after the addition of the tracer provides the liquid bath mass. The liquid bath mass is determined using a strontium carbonate ($SrCO_3$) tracer (Purdie, 1993; Iffert, 2007). The strontium concentration is determined with ICP-OES. The determination of the metal volume and mass in smelting cells is achieved using a copper based tracer. Both methods are not applied in regular process control strategies.

#### 2.3.1.4 Cell Bottom Condition

Bottom voltage drop is measured regularly in smelting cells to determine the cathode condition. A common method of voltage drop measurements includes the use of a pointed iron rod. The rod is immersed to touch the bottom of the cell and the voltage drop measurement is taken across the cathode lining and the external bus-work. The measurements provide information about cathode condition versus cell age and cathode materials from different suppliers. The disadvantages of this method is the local influence of cathode conditions such as sludge formation, ridge, erosion or other damages to the cathode surface at the location of measurements. A combined temperature and bottom voltage sensor has been developed to avoid these disadvantages (White *et al.*, 2001). After a temperature measurement performed with a Type S thermocouple as described in Section 2.3.1.1, the sensor is lowered in the metal pad and a cathode voltage drop measurement is taken. This method gives an average bottom voltage as measured across the metal pad and external bus-work and it demonstrates a high accuracy and repeatability. This is used to detect potential sludge formation or ridge building during cell operation.

#### 2.3.1.5 Measurement Accuracy

Process measurements mentioned above are all affected by operational practices carried out in the smelting cell. Alumina feeding, metal tapping, followed by anode changing have an increased impact on the measurements (Section 2.1.3). The moment of measurement is important and therefore a fixed point in the operational cycle will provide the lowest and most predicable influence to the system dynamics. Over and under feeding of alumina respectively result in a decrease and an increase of both bath temperature and superheat

due to changes in the requirement for pre-heat and dissolution of alumina (Figure 2.6). Metal tapping reduces the heat losses via the side wall and give a temporary rise in both bath temperature and superheat according to Figure 2.4.

After alumina feeding, anode changing has the most impact to mass and energy balance of all operational actions (Section 2.1.3). Bath and liquidus temperature measurements have a strong dependency on the position of recent anodes being changed related to the measuring position. For example an anode change close to the measuring hole substantially gives a lower reading of the electrolyte and liquidus temperature due to local cooling (Figure 2.10). On the other hand an anode change far from the measuring hole gives a falsely higher reading of the bath and liquidus temperature due to a rise in anode current density and therefore heat generation in the middle of the cell. Bath and metal height measurements are also affected by anode changing. Local variations in metal curvature due to redistribution of anode current flow lead to a different partition of bath and metal levels.

Power modulation gives another variation to the process measurements (Section 4.2.1.2). A day-night schedule gives a decrease followed by a rise in bath and liquidus temperature during day and night respectively. The timing of measurements and corresponding control actions should be at a fixed point in the overall process cycle. Other situations that are more unpredictable such as current outages or reductions of the line amperage, will result in non representative measurements of the overall process.

### 2.3.2 Advanced Sensing Techniques

This section discusses advanced sensing techniques applied to improved control of the aluminium smelting process.

#### 2.3.2.1 Process Conditions

As can be derived from the inaccuracy associated with the current iron rod method for liquid level measurements, other attempts have been published to overcome existing uncertainties in determination of the metal level. One method is based on a calculation using the insertion height of the anodes and measured height of the anode beam (Guðmundsson, 1999). This method has been modified and applied to Aldel (Figure 2.17).

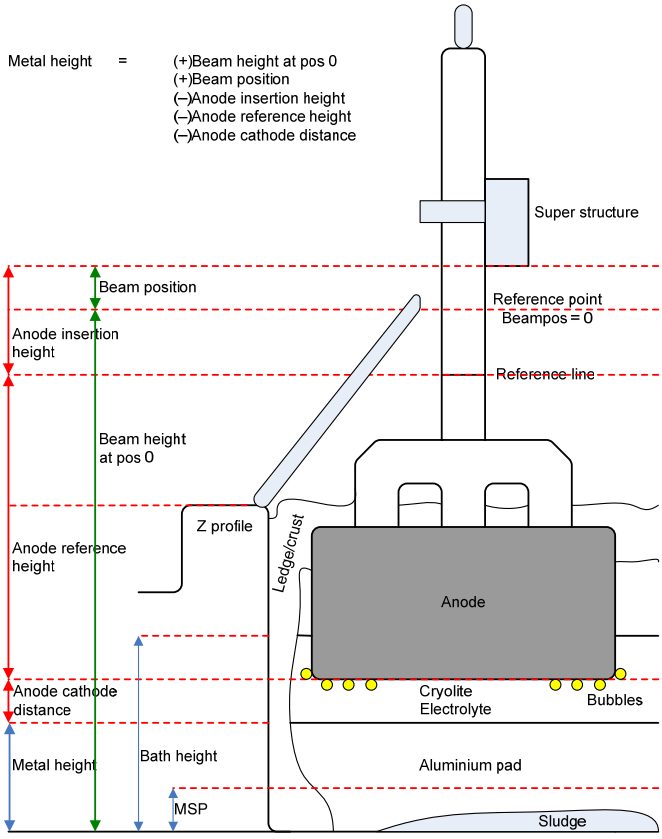


***Figure 2.17*** *Metal Height Calculation based on Insertion Height and Beam Position*

The metal height calculation *($MH_{cal}$)* is based on upper *($Beam_0$)* and actual beam position *($Beam_{actual}$)*, anode insertion *($Anode_{insertion\text{-}height}$)* and reference height *($Anode_{reference\text{-}height}$)* and the anode cathode distance *(ACD)* as given by Equation 2.22. The difference between the calculated metal height and metal setpoint *(MSP)* is the height of metal for tapping (Section 2.1.3.6).

$$MH_{cal} = Beam_0 + Beam_{actual} - Anode_{insertion-height} - Anode_{reference-height} - ACD \quad (2.22)$$

The anode insertion height is calculated based on the insertion height from previous day and the anode burn rate, whereas the ACD is estimated by a fixed value adjusted with the deviation from cell voltage against setpoint voltage. Then the average metal height is calculated regardless of variation in local cathode conditions, temporal metal heave due to recent anode change and errors incorporate in the iron rod method or process conditions like hot cells.

A comprehensive Six Sigma study was performed to compare both methods, i.e. the iron rod and anode beam position (Bearne and Whitfield, 2005). Although reduced variations were achieved for both methods through identifying and reducing the causes of variation, it was

proven that the metal height determination using the anode beam position was more suitable for control. Differences in anode burn rate and beam movements in relation to anode setting have been identified as the main determining factors for variations in metal height calculation. Interference from routine operations was identified as another source of variation. However, the calculation was found to be acceptable in terms of repeatability and reproducibility.

A method for measuring temperature and electrolyte level using a plunger from the alumina feeding mechanism has been developed for application in the AP50 technology (Vanvoren *et al.*, 2001). The concept requires an integrated thermocouple in the plunger; the plunger is dipped into the electrolyte for a particular period of time. The bath temperature is extrapolated from the temperature reading as the plunger is extracted from the bath prior to it reaching the final temperature to ensure sufficient lifetime of the device. The bath temperature used for control actions is calculated based upon a number of successive measurements, after which adjustments to the cell resistance are sent to the cell controller automatically. The disadvantages of this method are high capital investment costs and the incorporation of uncertainties in the prediction of the temperature by extrapolation and chemical attack of the couple (Section 2.3.1.1).

As in the case of bath temperature, bath level is also measured using the plunger. The liquid level is determined by lowering the plunger from upper position down to the liquid level. The potential between plunger and cell is measured continuously in order to determine direct contact of plunger with liquid electrolyte. Simultaneously, the displacement of the plunger from upper position to liquid bath is measured, thereby the liquid level can be calculated. Bath level can be estimated based on liquid level and calculated metal height as described previously. In case of AP50 technology solid bath is fed to the cell according the calculated bath height. In this thesis a method is developed to predict the liquid level in smelting cells using the average velocity of the plunger and the associated travel time until the plunger makes an electrical circuit with the bath as described in Section 3.2.2.2.

#### 2.3.2.2 Process Abnormalities

Recent publications have demonstrated the use of “smart” feeders to detect process abnormalities in alumina feeding, but these attempts were actually modifications to developments from the early 1980’s (Hvidsten and Rye, 2007; Ferreira *et al.*, 2008; Dupas, 2009). Several options exist for position sensing like electrical contact with molten bath (as discussed above), electro/mechanical end position switches and proximity switches. Process errors such as hard crust, plunger sticking in the feedhole and heavy build-up of material under plunger can be detected. Technical issues are related to loss of air supply, broken wires, switches, etc. Anode effects and heavy sludge formation can be limited using these

sensing techniques, if, and only if they are incorporated into a control strategy which detects and investigates abnormalities in cell behaviour. In fact this comment can be applied to most sensing techniques in aluminium smelting, and its lack of application is responsible for ineffectiveness of existing sensors in the aluminium industry. Section 3.2.2.1 describes the development of several soft sensors to detect abnormalities regarding alumina feeding and anode setting.

Advanced sensing methods to improve controllability of alumina feeding are linked to measurements of individual anode currents (Keniry and Shaidulin, 2008). Identification of spatial variation in alumina concentration by early warning of anode polarization at specific regions though the individual anode currents can be used to optimize alumina feeding in order to avoid anode effects. More uniform alumina distribution in the cell will lead to improved cell performance. This creates the possibility to adjust the average alumina concentration without an increased anode effect frequency, avoid an increase in sludge levels and a reduced anode spike frequency which will lead to reduced deviations in ACD (Moxnes *et al.*, 2009). Moreover, individual anode current differentiate between magnetic instabilities caused by a thermal imbalance, low ACD operation or instabilities caused by defective anodes (Keniry and Shaidulin, 2008). The main disadvantage to the use of individual anode currents is high capital investment costs if not already present in the existing micro-computers.

***Figure 2.18*** *Example of an Anode Spike at Voerdal*

Investigations have shown that some anode pairs are more sensitive to spike formation than others (Rolofs and Wai-Poi, 2000). Spike formation at corner anodes is promoted and affected by the location of alumina point feeders, carbon dust collection related to metal circulation and extra local cooling by the side and end walls (Figure 2.18). A clear relation was found between the amount of carbon dust with spike formation. A substantial increase of line current creates a higher sensitivity for energy imbalances due to larger bath mass variations, lower liquid bath mass and consequently an increased sensitivity to anode setting.

Figure 2.19 shows multi-way principal component analysis to observe the movement of data towards process conditions indicating an anode spike (Majid *et al.*, 2009). The first principle components (t[1]) and (t[2]) are enough to analyse the important variance in the data set. Process data is collected under in-control conditions, which are used as reference to monitor future abnormalities. Monitoring new data by referencing to historical normal data is the basis of the underlying data-driven multivariate statistical method. Data including an anode spike present moved in a different direction than data with anode spike absent. An anode spike trajectory provides an early warning system, which can be used to remove the spike prior to major process excursions. An improved understanding of anode performance in the cell enables optimizing anode insertion heights and setting patterns in order to improve the overall current distribution, and therefore current efficiency and anode consumption (Section 2.3.2.1).

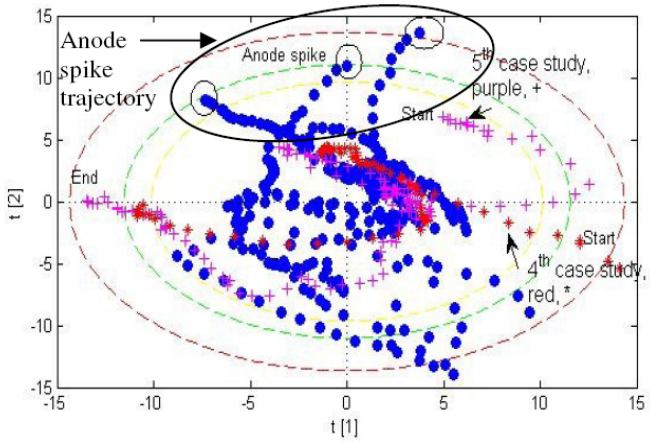


***Figure 2.19*** *Early Warning System for Anode Spike Detection (Majid et al., 2009)*

Individual duct temperature measurements allow better mass and energy balance control, because additional information is available to detect cells with abnormal behaviour. A study has been carried out to locate cells with poor anode cover integrity by searching for high duct temperatures (Dando, 2004). It was found that exhaust duct temperature can vary by more than 50-60°C corresponding to exhibited open holes in the crust. Pot tending and anode cover integrity play an important role in fluoride emission and heat losses from cells, not only leading to better cell performance, but also dry-scrubber operation. Although no benefit was found for the use of measurements of individual duct flow rate, temperature or heat losses as feed forward variables in a multivariable model-based control approach, this is probably due to these sensors not being incorporated in the detection of abnormalities in cell behaviour (Stevens McFadden, 2007).

# Chapter 3 Theoretical Development

As demonstrated in this chapter the aluminium smelting process has strong interactive multivariate characteristics with limited process observability. A prevailing sludge cycle is hypothesised as one of the main self-accelerating destabilising mechanisms interfering with the sidewall freeze/melt self-regulating mechanism as depicted in Figure 2.4. The responses are non-linear, vary over a wide range of time scales and interactions between the different mechanisms are found to lead to complex dynamics (Section 3.1). Section 3.2 evaluates consequences of the application of classical control theory for controlling smelting cells and develops a multivariate causally based control approach using Hotelling $T^2$ statistics and advanced detection of abnormalities. Section 3.3 derives a module-based architecture based on this approach in control of the smelting process.

## 3.1 Process Mechanisms

The sidewall freeze/melt self-regulating mechanism is part of the natural behaviour of the smelting process, and preserves sufficient internal stability to control variation in the bath temperature and mass on an industrial scale within limits (Figure 2.4). However, process intensification through line current increase has exacerbated other interactions. In particular, intensification of alumina feeding in a reduced liquid bath mass due to application of larger anodes at higher line current leads to increased mass and energy imbalances (Section 1.3.3). Operational abnormalities such as anode spikes and deformations also have the tendency to increase due to an increased variation in alumina concentration throughout the cell and an increased generation of carbon dust leading to the lowering of the average anode cathode distance (Moxnes *et al.*, 2007).

In addition, inconsistent energy input through power modulation has introduced another destabilizing mechanism interfering with the internal self-regulating mechanism (Stam and Schaafsma, 2007; Eisma and Patel, 2009). Under these circumstances the line current is reduced or even switched off for a particular period of time resulting in large energy deficiencies. Moreover, a deterioration of the quality of alumina and anodes and increased range of supply have increased the variability of the inputs (Wai-Poi and Welch, 1994). These items, separately as well as interactively, lead to a new control objective, which requires the diagnosis of these more unpredictable process dynamics, as well as much greater process robustness and advanced detection of abnormalities within the natural behaviour envelop of each cell.

### 3.1.1 Sludge Cycle

Alumina is the single largest raw material input into a smelting cell. As described in Section 2.1.1 the essential requirements during alumina feeding are effective transport into the electrolyte, rapid dispersion in the electrolyte, rapid dissolution as small alumina grains and finally uniform mixing of the dissolved alumina in the electrolyte. The largest contributions to the total energy demand are energy associated with pre-heat of alumina to bath temperature and heat of dissolution (Wai-Poi *et al.*, 1994). The total amount of energy involved in the alumina feeding adds up to a contribution of the thermal effects on the energy balance in the range of 1500 to 2100 kJ/kg. The main consequence of incomplete alumina dissolution is the formation of bottom sludge.

In this thesis it is hypothesised that a small bias in sludge formation versus back feeding leads to a mass and energy imbalance. This imbalance can be worsened by increased line current, employment of power modulation and increased variability in raw materials. In case of regular line current variation regarding power modulation alumina feeding should respond to the actual line current. As derived from Equation 1.2 according to the primary reaction (Equation 1.1.), the theoretical alumina consumption ($TC_{Al2O3}$) is proportional to the amount of current ($I$) passed through a cell and time ($t$) given by Equation 3.1.

$$TC_{Al_2O_3} = \frac{M_{Al_2O_3}}{nF} \cdot I \cdot t = 0.634 \cdot I \cdot t \tag{3.1}$$

Where, $M_{Al2O3}$ is the molecular mass, $n$ is the number of electrons transferred in the reaction and $F$ is the Faraday constant (Section 1.3.1). This approach also incorporates the current efficiency as alumina consumption is proportional to the theoretical consumption multiplied by the current efficiency *(CE)*. A dimensionless process variable for the alumina feeding is derived, which is independent of the line current. The alumina consumption ratio *($R_{Al2O3}$)* is calculated by the amount of alumina fed to a cell by the alumina point feeders *(kg of $Al_2O_3$)* divided by the alumina consumption (Equation 3.2).

$$R_{Al_2O_3} = \frac{kg_{Al_2O_3}}{TC_{Al_2O_3} \cdot CE} \tag{3.2}$$

In order to detect a short term mass accumulation or depletion of alumina related to a long term fixed current efficiency, the CUSUM of the ratio of alumina fed to a cell *($CR_{Al2O3}$)* is used (Equation 3.3) (Johnson, 1994).

$$CR_{Al_2O_3} = CUSUM\left(\frac{kg_{Al_2O_3}}{TC_{Al_2O_3} \cdot CE}\right) \tag{3.3}$$

Higher sludge formation than back feeding automatically results in an increase in alumina additions generated by the alumina control logic (Equation 2.3). This will favour more sludge formation leading to the start of a sludge cycle as follows:

1. A smelting cell is initially running at target bath temperature and chemistry with limited sludge formation and back feeding. Energy input and demand changes as described earlier due to various operational practices and other disturbances. If sludge formation becomes slightly favoured at a particular moment, more alumina will be fed to the cell due to the alumina control logic and unchanged depletion rate.

2. Higher sludge formation than back feeding will affect the alumina control strategy. If the start of the overfeeding period is triggered by a fixed increase in resistance (ΔR), a reduction of minimum alumina concentration will occur over time due to a lowering of the maximum concentration after overfeeding (Section 2.1.1). In case of a feeding strategy based on triggering with dR/dt and/or $d^2R/dt^2$, no change in minimum concentration is expected due to a fixed triggering point based on slopes.

3. Both bath temperature and chemistry will be affected by extra alumina additions. The temperature decreases due to a higher energy requirement for pre-heating and (partly) dissolution of alumina as is shown in Figure 2.6 and the $AlF_3$ concentration increases due to freezing of cryolite out of the bulk electrolyte onto alumina and onto the sidewalls as can be explained by using the phase diagram in Figure 1.4. This will lead to a reduction of liquid bath mass within the cell. The balance between sludge formation and back feeding shifts towards higher sludge formation.

4. A reduction in liquid bath mass also affects the alumina control strategy through increasing the rate of alumina concentration decrease. No change in minimum alumina concentration will be found in a fixed ΔR strategy, because the start of the overfeeding period is triggered by a fixed change in resistance. In the case of triggering with dR/dt and/or $d^2R/dt^2$, the minimum alumina concentration will slowly shift towards higher values. Faster changes in alumina concentration due to lower bath mass result in an earlier trigger for overfeeding based on the target slopes (Equation 2.3). The same consequence is observed at increased line current due to a rise in the alumina depletion rate (Section 2.1.1). Sludge formation is accelerated by a reduction of the driving force of alumina dissolution (Equation 2.1).

5. Under these circumstances the control system may try to compensate for the above process imbalance with an increase of the cell resistance, which is partly connected to the energy deficit caused by the extra alumina additions. The control system may also reduce the $AlF_3$ additions in order to keep the cell around its target values, but the lower $AlF_3$ additions will create a mass imbalance on the long run resulting in cyclic process behaviour (Figure 3.1) (Tandon *et al.*, 2007). Figure 3.2 shows the development of the CUSUM of the ratio of alumina fed to a cell as calculated in Equation 3.3 and the CUSUM of $AlF_3$ additions. The increase in the CUSUM of the ratio of alumina fed to the cell is followed by a decrease in the CUSUM of $AlF_3$ additions as part of ordinary control actions to compensate for the above described mechanism of sludge formation.

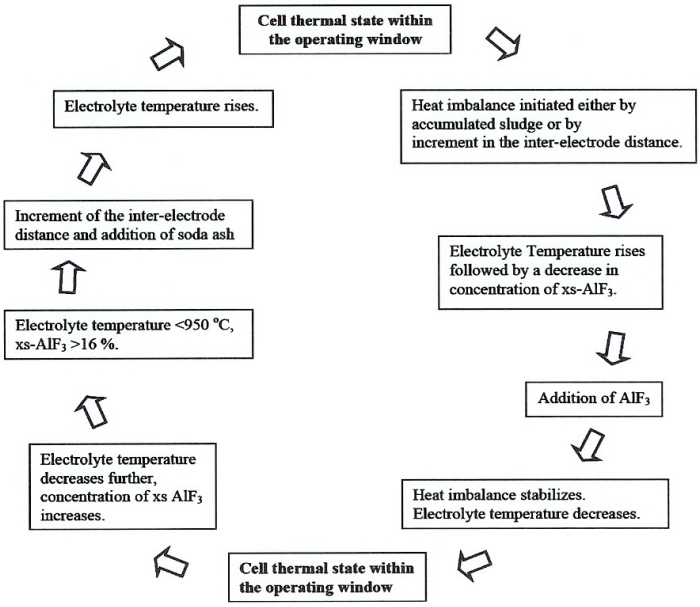


***Figure 3.1*** *Cycle of Cell Thermal State and Compensatory Actions (Tandon et al., 2007)*

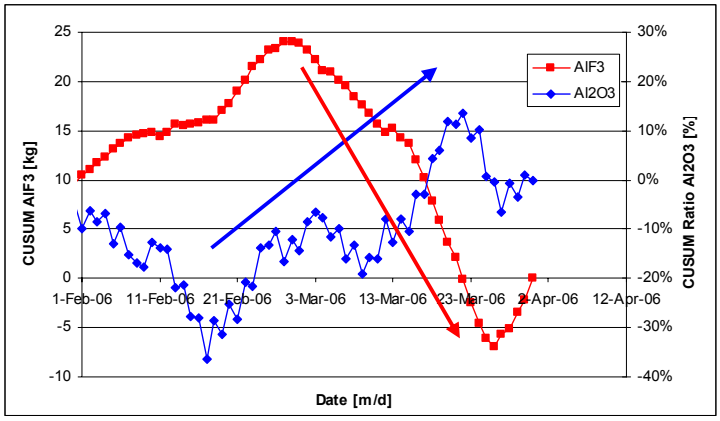


***Figure 3.2*** *Development of CUSUM($AlF_3$) and CUSUM(Alumina Ratio) at Aldel*

6. The combination of sludge formation and decreasing liquid bath mass leads to lower alumina concentration operation with a reducing concentration range for both a fixed ΔR strategy and in case of slope triggering. Ultimately a higher frequency of anode effects is expected.

7. Further sludge formation stimulates extra alumina additions. The amount of sludge will increase and settles down at the cathode surface. This will push the metal upwards leading to a falsely high metal level and increased heat losses through the sidewall due to a larger contact area and higher thermal conductivity. On the other hand a higher metal height will also push the bath mass upwards out of the bath-metal interface hollow and therefore the relation between bath height and liquid bath mass will be disturbed (Figure 2.8).

8. The control system continues to compensate the process shift with increases in the cell resistance and a reduction of $AlF_3$ additions. The alumina saturation concentration will reduce due to higher $AlF_3$ concentration and lower temperature as shown in Figures 3.3 and 3.4 respectively. Further sludge formation is accelerated by a lower driving force of alumina dissolution as given by Equation 2.1. The liquidus temperature will decrease with increased $AlF_3$ concentration resulting in further cooling of the cell if the bath temperature is artificially kept high with extra voltage.

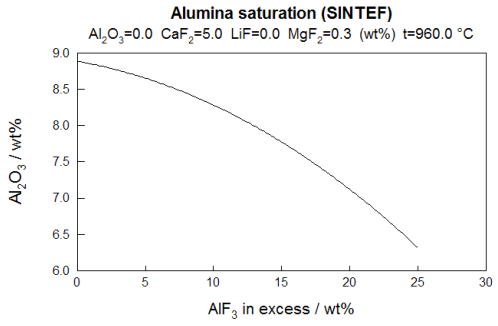


***Figure 3.3*** *Alumina Sat. vs. $AlF_3$ Conc. (Sintef, 2009)*

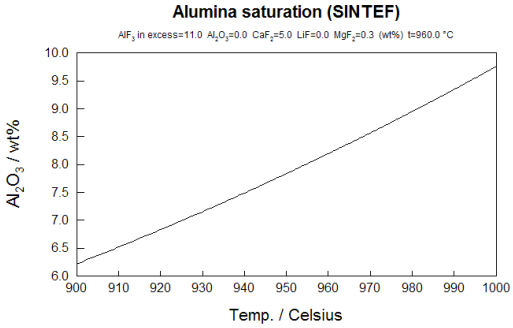


***Figure 3.4*** *Alumina Sat. vs. Temp. (Sintef, 2009)*

9. If the process shift related to the ensuing control actions is approximately at the same speed, a large shift in the liquid bath mass and average alumina concentration can occur without detection. Limited reductions in $AlF_3$ additions based on the requirement of $AlF_3$ related to the alumina quality as suggested by Kloetstra and Stam (Section 2.1.2) will accelerate sludge formation due to a decrease of the alumina dissolution rate at lower bath and liquidus temperatures (point 8).

10. A higher metal level will lead to increased metal tapping. This can either result in fast responses to the ensuing system dynamics when tapping on height or slower responses

when tapping on fixed weight. A reduced metal mass results in a higher current density in the metal leading to higher Lorenz forces within the metal path (Section 2.1.2). Finally, higher metal velocity combined with a slightly increased metal curvature will favour back feeding. Modern magnetically compensated cells or technologies operating at high metal levels suppress this mechanism.

11. Sludge accumulates in particular areas in a cell related to the metal flow characteristics and location of point feeders. Sludge tends to accumulate under the corner anodes. Low metal levels in the corners will bring the corner anodes onto the sludge/ridge (Section 2.3.2). Finally, the cell changes from sludge formation to back feeding at a minimum bath and metal mass with other possible triggers of bath temperature, electromagnetic instability, anode/sludge contact halfway through the sludge cycle as a result of sludge accumulation, low temperature and ACD, plus compensatory control actions.

12. Sludge level breaks through the metal pad and direct contact between sludge and fresh electrolyte increases the rate of back feeding (Figure 2.1). The combination of dilution of the $AlF_3$ content through an increase of the liquid bath mass and a release of “stored” cryolite within the sludge/bath mixture raises the operating bath temperature and reduces the $AlF_3$ concentration substantially. Reverse control actions like a reduction of the resistance, an increase of $AlF_3$ additions and lower metal tapping are ineffective due to the large mass of re-dissolving sludge. These control actions persists setting up the cell for a further cycle in temperature/$AlF_3$ later.

13. The combination of back feeding and increasing liquid bath mass leads to higher alumina concentration operation with a wider concentration band for an alumina control strategy based on a fixed ΔR (Section 2.1.1). A strategy based on slope triggers results in lower alumina concentration operation with an increasing concentration band. In both cases long alumina search or underfeeding periods will identify these conditions.

14. As indicated in point 12, an overshoot in control actions regarding temporary process conditions is of high risk, because a decrease in the cell resistance combined with an increase of $AlF_3$ additions accelerate cooling of the cell. A commonly used strategy in aluminium smelters to minimize the resistance in case of low noise levels has the same effect. These control actions can initiate the start of another sludge cycle.

This sludge cycle has interactive multivariate characteristics (Figure 3.5) (Stam *et al.*, 2008). Alumina feed control consists of an indirect strategy in which the alumina concentration is derived from the behaviour of the pseudo-resistance over time. Decoupled relation of the alumina concentration in the liquid bath from the inventory on the cathode surface where

sludge/ridge collects gives rise to this cycle. In addition, a mixture of different control actions can either accelerate or suppress the detection and intensity of the sludge cycle.

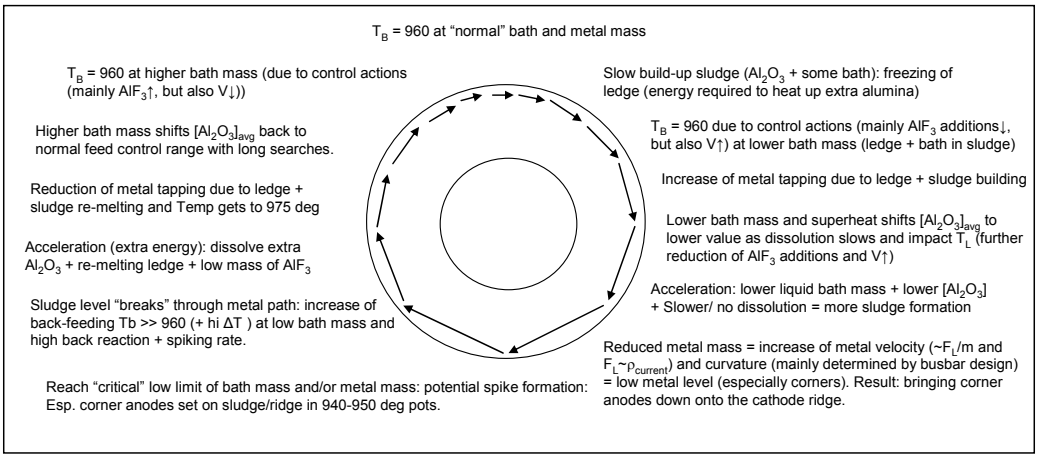


***Figure 3.5*** *Cycle of Sludge Formation and Dissolution (Stam et al., 2008)*

Increased line current also impacts on the above cycle. At higher amperage, larger anodes are required to maintain a desired anodic current density. Therefore the amount of liquid bath mass will decrease while alumina addition increases, which affects the balance between sludge formation and back feeding. Moreover, frequent changes in alumina type changes the dissolution characteristics of the material (Wai-Poi and Welch, 1994). The structural features of alumina are related to the dissolution effectiveness in the aluminium smelting process, but more knowledge about these dissolution kinetics need to be embedded in the control system (Section 2.1.1).

Evidence supporting the derivation of the cycle described above is presented in Figures 3.6 to 3.9, where the alumina additions, power input and liquidus temperature are presented both individually, then as CUSUM to show the inventory effect (Stam *et al.*, 2007). Although many of the changes in the direction and magnitude of the slope are linked to power modulation events (>100 MWh/day), there is a dominant effect of alumina additions resulting in the long-term variation in the liquidus temperature and power input. In 2 cases (July 24$^{th}$ and September 26$^{th}$) an increase in the CUSUM of the total amount of alumina fed is found at a minimum of the energy input indicating the start of the sludge cycle possibly due to a deficiency in energy available for dissolution.

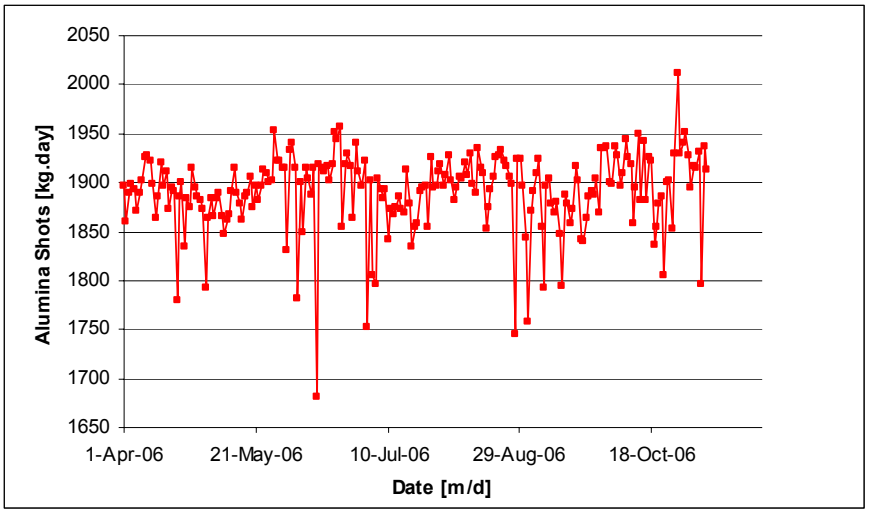


***Figure 3.6*** *Average Alumina Additions at Aldel (April 1st – November 8th, 2006)*

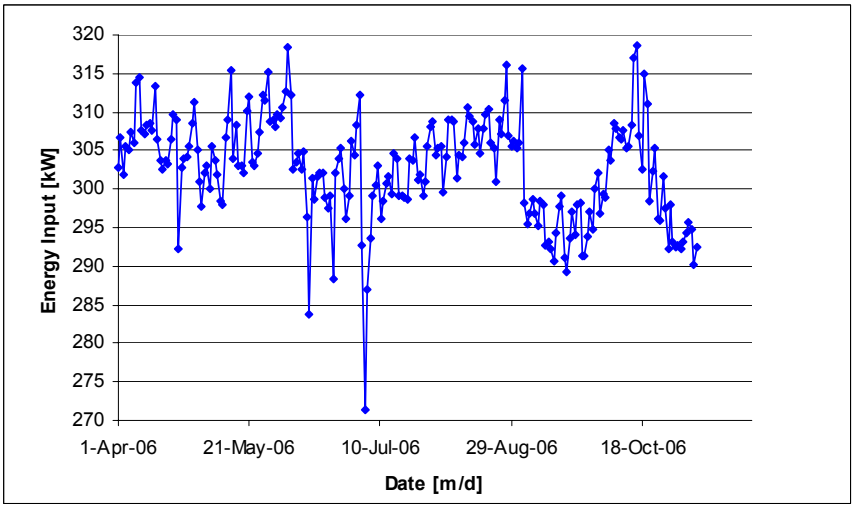


***Figure 3.7*** *Average Power Input at Aldel (April 1st – November 8th, 2006)*

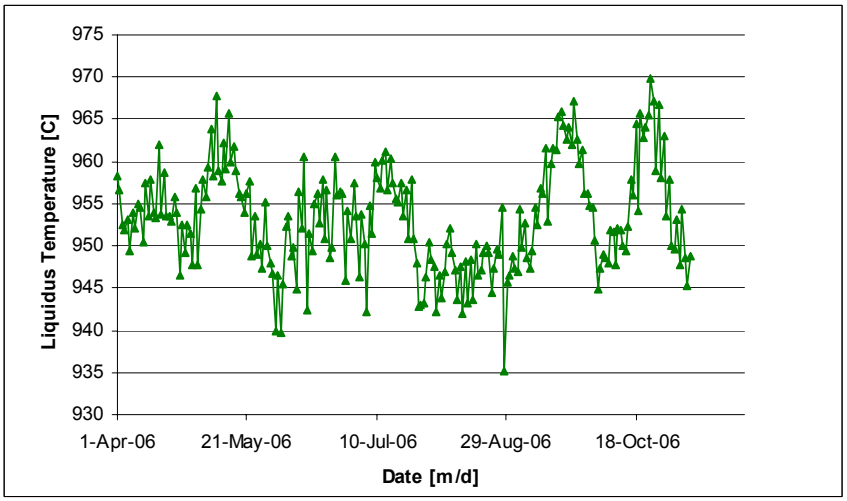


***Figure 3.8*** *Average Liquidus Temperature at Aldel (April 1st – November 8th, 2006)*

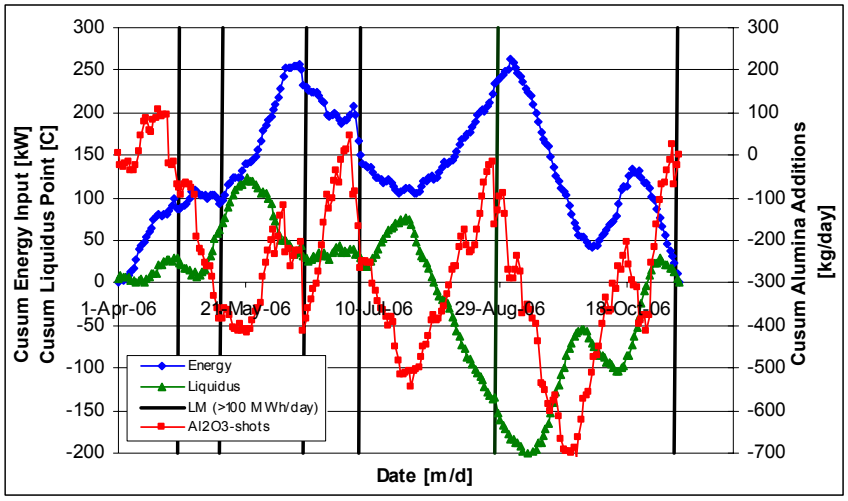


***Figure 3.9*** *Cusum of Energy Input, Liquidus and $Al_2O_3$ Additions at Aldel (Stam et al., 2007)*

### 3.1.2 Self-Regulating and Self-Accelerating Mechanisms

As described in Section 2.1.2 regulation of fluoride imbalances from secondary alumina is achieved by corrective $AlF_3$ additions. In modern cells with dry-scrubber technology, the $AlF_3$ consumption is mainly determined by the sodium and calcium oxide content in the alumina used. Most control systems use energy balance regulation via cell resistance as primary control on bath temperature, whereas mass balance is controlled as a secondary control mechanism.

These control systems only focus on the liquid bath zone and are too simple for advanced control of a smelting cell because sludge formation is inevitable given the present industrial process conditions as discussed in Section 3.1.1. Therefore sludge formation and sludge dissolution are important mechanisms, which are directly linked to the mass and energy balance. The composition of sludge is different from liquid bath and consists of 40-70% alumina, 0-5% $AlF_3$, and cryolite (Section 2.1.1).

The interaction of sludge with the side ledge movement mechanism gives another important factor that influences process variability. For example in case of sludge formation due to partially undissolved alumina feed, both mass and energy balance are affected by the extra alumina additions due to the ensuing alumina feeding strategy (Section 3.1.1). Energy demand increases due to extra feeding and results in a decrease in bath temperature and superheat. Simultaneously $AlF_3$ concentration increases due to freezing of cryolite out of the bulk electrolyte. A higher $AlF_3$ concentration in combination with lower temperature and superheat further decreases the alumina dissolution rate.

Figure 3.10 is an extension of the self-regulating side ledge mechanism depicted in Figure 2.4 (Stam *et al.*, 2008). The self-accelerating mass and energy imbalance mechanism represented by the red arrows interferes with the dampening effect of the side ledge energy adjustments. Depending on the origin of sludge formation or sludge dissolution, these processes can have slow or very rapid velocity. In Figure 3.10 the processes at the bottom of a cell, along with additions to the bath, are integrated into the system being studied.

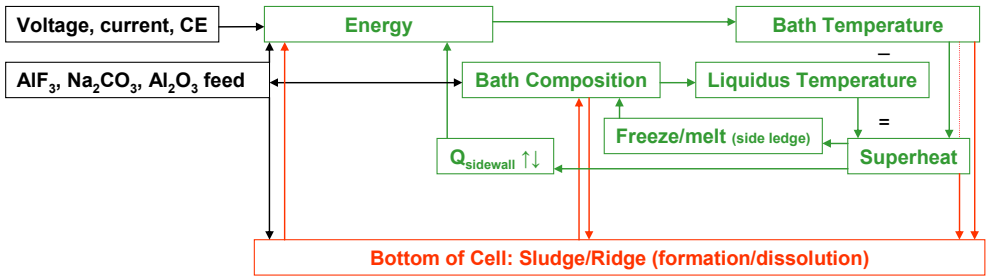


***Figure 3.10*** *Sludge Cycle Integrated in Self-Regulating Mechanism via Side Ledge (Stam et al., 2008)*

The interaction of anode cover with the mass and energy balance is expected to have similar positive feedback behaviour as bottom sludge in control of the aluminium smelting process (Figure 3.11) (Stam *et al.*, 2008). Anode cover is made up of crushed (solidified) bath and alumina (Section 2.1.2.3). The thickness and composition of the anode cover determines the heat transfer through the top of a cell. Destabilisation of the anode cover can ultimately result in collapsing of cover, which results in severe mass and energy imbalances. The interaction of anode cover with the mass and energy balance is not being studied in this work.

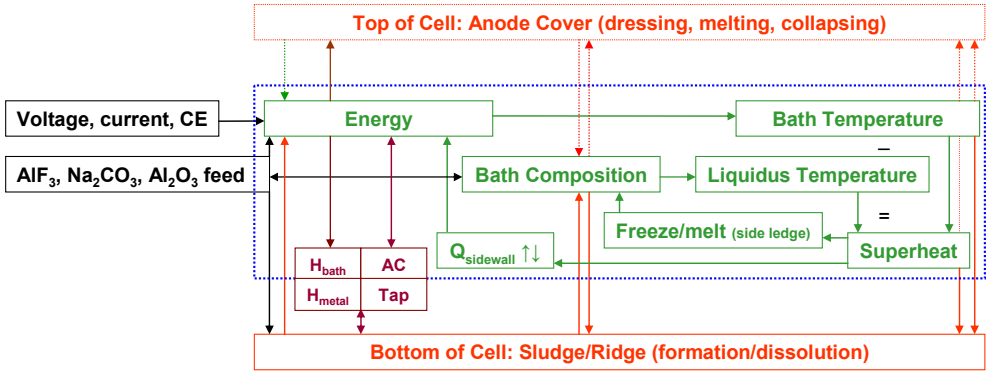


***Figure 3.11*** *Integrated Self-Regulating and Self-Accelerating Mechanisms in a Smelting Cell (Stam et al., 2008)*

Figure 3.11 also integrates the most important cell operations in relation to mass and energy balance - anode changing (AC), metal tapping (TP), bath ($H_{bath}$) and metal ($H_{metal}$) height/mass control - into the system dynamics. Large variations in the mass and energy balance will occur during and direct after operational activities like anode changing and metal

tapping (Section 3.1.3). Redressing after new anodes are being set determines the heat losses at the top of a cell. The underlying interactions are exacerbated at increased line current, the employment of power modulation and increased variability in raw materials used.

Stable liquid level control - both bath and metal height individually as well as combined - is essential. As discussed in Section 2.1.1 the total liquid level sets the conditions for effective transport of alumina along the electrolyte surface and rapid dispersion into the electrolyte. On the other hand heat transfer and partially direct radiation from the top of the liquid level determines the stability of the anode cover by its liquidus temperature. Sufficient superheat and bath height provides good dissolution characteristics for alumina, whereas the rate of back feeding of sludge into the reaction zone is influenced by the metal height (Figure 2.1).

### 3.1.3 Incorporation of Discrete Events in Overall System Dynamics

Despite being a continuous electrolysis process, most sub-processes in a cell like alumina feeding, anode setting, anode covering, beam raising and metal tapping are conducted batch-wise by operators and are controlled by univariate control loops. Alumina feeding has the highest frequent contribution to changes in mass and energy balance. As discussed in Section 2.1.1 pre-heating and dissolution of alumina is strongly endothermic. The amount of alumina fed is an important factor and can vary from 1 kg per dump per minute for modern point-feed cells up to 400 kg per 3-4 hours in case of side break technology.

Figure 3.12 shows the influence of the alumina feeding strategy applied at Aldel to the mass and energy balance. In order to reduce the impact of alumina feeding to the ensuing system dynamics at higher line current and power modulation, the total mass fed during overfeed and duration has been minimized. However, a concentration change of more than 0.5% is necessary to achieve a reliable and controllable alumina feeding strategy (Section 2.1.1).

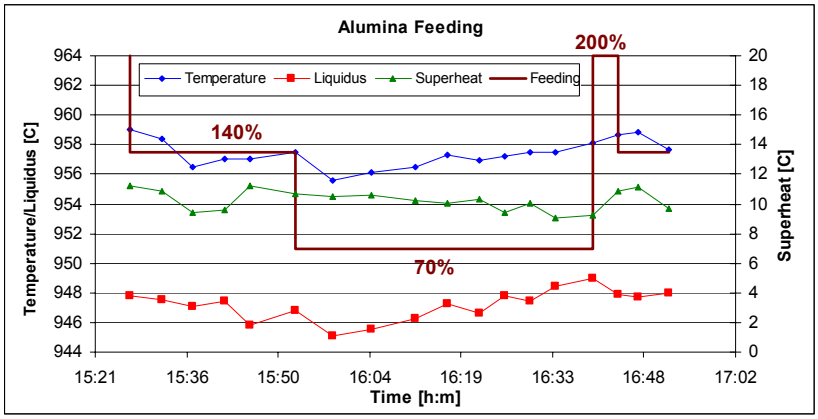


***Figure 3.12*** *Impact of Alumina Feeding on Mass and Energy Balance at Aldel*

Originally a control strategy with an overfeed rate of 200% for 15 minutes and 140% for 45 minutes was used. In order to reduce the extra alumina additions during the overfeed period, this schedule was adjusted to 200% for 5 minutes and 130% for 25 minutes, which results in a fixed amount of 18.5 kg above the nominal alumina feed. With this, the impact to the bath and liquidus temperature is limited to only 4°C, while a temporary decrease of the superheat of 2°C is found. By these adjustments to the control strategy the mass of overfeed was cut by 62% and the impact on the tendency for triggering a sludge cycle should also reduce (Section 2.1.3).

Anode changing has the single largest impact to mass and energy balance of all operational actions apart from feeding of alumina (Section 2.1.3). In modern prebaked cell technology, anode changing follows a fixed routine, and the mass of cold anode(s) introduced to the electrolyte can reach up to 1500 kg. Excessive freezing of electrolyte will occur under new set anode(s) and can take up to 24-48 hours to completely re-melt and thermally equilibrate. This leads to an imbalance in the current distribution and temperature distribution within a cell and affects the overall cell performance. Special control settings such as a temporary increase in the cell resistance in combination with adjustments to the alumina feeding are introduced to counteract negative consequences of anode changing.

Figure 3.13 demonstrates the impact of a double anode change close to the measuring hole at Aldel. A drop in bath temperature and liquidus point of 6.2°C and 8.3°C respectively were measured. The rise in the superheat can be explained by freezing of cryolite from the bulk electrolyte resulting in an increase in $AlF_3$ and $Al_2O_3$ concentrations. Furthermore, a temporary increase of the target resistance and a reduction of alumina feeding are applied as special control settings during anode changing. Normally a recovery period of 24-48 hours is measured in the anode current distribution. This means that the same bath temperature measured after ca. 8 hours represents a lower bath mass as is confirmed by the lower average superheat.

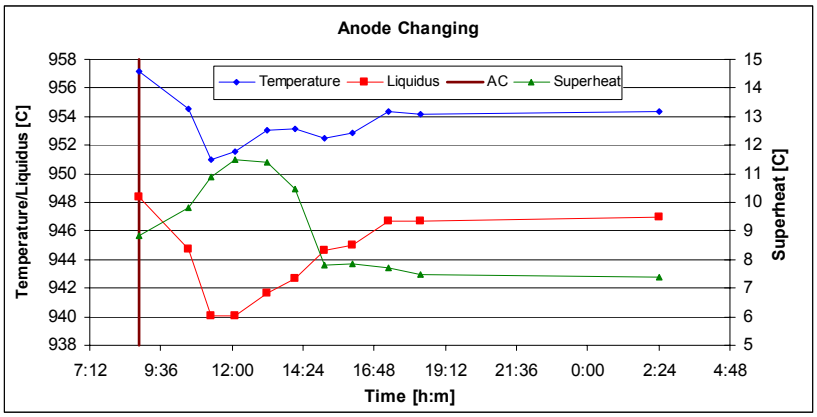


***Figure 3.13*** *Impact of Double Anode Changing on Mass and Energy Balance at Aldel*

### 3.1.4 Short Term Process Variations and Overall System Dynamics

The presence of a dominant sludge cycle (Section 3.1.1), with both self-regulating and self-accelerating mechanisms (Section 3.1.2) and discrete events (Section 3.1.3) within the aluminium smelting process greatly increases complexity and reduces predictability - both of the process and its response to control actions. Linearity assumptions in control logic are not appropriate and a multivariate SPC approach is necessary. In this respect future process states are closely linked to previous conditions and the development of ensuing system dynamics over time.

However, investigations in aluminium smelting are mainly focused on short term effects as shown in some studies about the mechanisms involved in sludge formation and dissolution (Whitfield *et al.*, 2004; Iffert, 2007). Figures 3.14 to 3.16 shows results of an isolated experiment in which both extremes in alumina feeding - heavy overfeed of 130% for 4 hours and zero feed - were investigated (Iffert, 2007). Table 3.1 show the main parameters involved in the mass and energy balance control related to the three experimental stages (start at 8:30, end of overfeeding at 12:30 and end of zero feed at 15:30).

Bath temperature remained constant throughout the overfeeding period, while the liquidus temperature showed a significant decrease resulting in a rise in the superheat (Figure 3.14). According to the self-regulating mechanism depicted in Figure 2.4 an increase in superheat leads to increased heat losses through the side and end walls. On the other hand high superheat provides good alumina dissolution characteristics. The amount of extra alumina fed (114 kg) is almost equal to the increase in alumina mass in the cell (Table 3.1). Under these circumstances - high superheat and heavy overfeeding - a constant bath temperature is most likely a result of an energy surplus within the cell prior to the experiment.

The period of zero feed is characterized by a steady increase in the temperature combined with a fast increase in the liquidus temperature leading to an overall decrease in the cell superheat (Figure 3.10). Based on an alumina consumption rate of 95 kg per hour a back feeding rate of 20-30 kg $Al_2O_3$ per hour has been found. The existence of significant back feeding during zero feed is confirmed by the limited decrease in the bath mass which is in contrast to the large drop in superheat. This is in line with the energy surplus within the cell prior to the experiment as identified during the heavy overfeed period, which also indicates prevailing sludge dissolution conditions. These observations show that short term process variations are embedded in longer term state changes. Therefore the investigations in this thesis are based upon long term experiments.

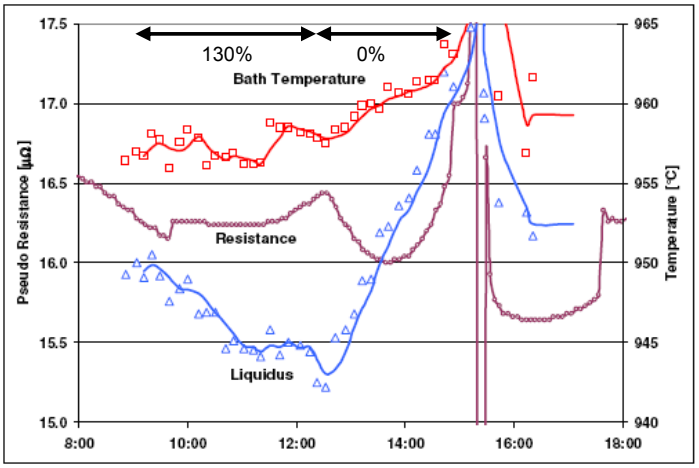


***Figure 3.14*** *Bath and Liquidus Temperature at 130% and Zero Feed (Iffert, 2007)*

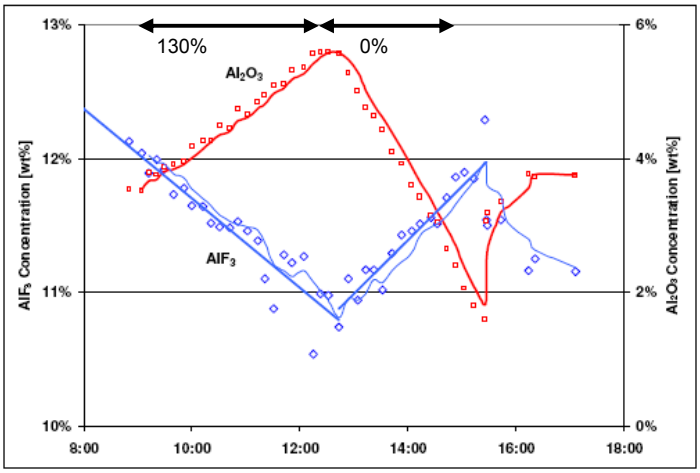


***Figure 3.15*** *$Al_2O_3$ and $AlF_3$ Concentration at 130% and 0% Feed (Iffert, 2007)*

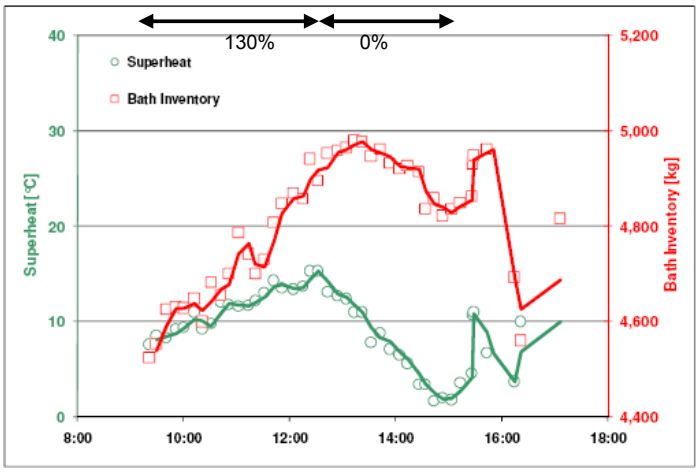


***Figure 3.16*** *Superheat and Bath Inventory at 130% and 0% Feed (Iffert, 2007)*

| | 8:30 | 12:30 | 15:30*) | h:min |
|---|---|---|---|---|
| **Bath Mass** | 4533 | 4970 | 4829 | kg |
| **$AlF_3$** | 544 | 536 | 579 | kg |
| **$Al_2O_3$** | 159 | 278 | 77 | kg |
| **$Na_3AlF_6$+$CaF_2$+…** | 3830 | 4156 | 4173 | kg |
| **Temperature** | 957 | 958 | 965 | °C |
| **Liquidus** | 951 | 942 | 963 | °C |
| **Superheat** | 6 | 16 | 2 | °C |

**) Just before the Onset of the Anode Effect*

***Table 3.1*** *Mass and Energy Balance Measurements during 130% and 0% Feed (Iffert, 2007)*

### 3.1.5 Liquid Bath Mass Variations

As discussed in Sections 3.1.1 to 3.1.4 the reaction zone of an aluminium smelting cell is subject to continuous changes in the liquid bath mass (volume), creating a major constraint in the ability to control the process. Most existing control strategies ignore bath mass with respect to bath chemistry and alumina feed control because of their reliance on $AlF_3$ concentration measurements or derived alumina concentrations respectively (Section 2.1.2). Therefore changes in energy balance are often compensated for changes in $AlF_3$ additions.

The self-regulating mechanism via side ledge as shown in Figure 2.4 is a well understood process. The thickness of the side ledge is controlled by the rate of convection heat transfer from electrolyte and is determined by the superheat (Equation 2.14). However, large and rapid variations in liquid bath mass have been observed in aluminium smelting cells (Figure 3.16). Both speed as well as magnitude of changes can't be explained by the mechanism via side ledge. As hypothesised in Section 3.1.1 a prevailing sludge cycle induces continuous variations in the liquid bath mass.

Low temperature operation ($T_B$<954°C) - especially for a longer period of time - will result in freezing of sludge at the cathode surface (ridge formation). Once cathode ridge is formed - depending on the heat balance design of a cell – it undergoes a slow transformation in its chemical composition due to the formation of corundum. This causes a more permanent redistribution of current leading to deterioration in electromagnetic stability as discussed in Section 1.3.5. In this situation bath material is isolated from the liquid bath zone. Extra bath needs to be added in order to maintain the mass balance under these particular conditions. As described liquid bath mass variations are not only linked to the superheat, but are also connected to variations in both bath and liquidus temperature.

Control of bath levels in smelting cells is confounded because bath height is part of the cyclic mechanisms described above (Section 3.1.2). In general the bath level should represent the total liquid bath mass in a cell, but variations in the ledge thickness and shape affect this

relation. Studies show a weak correlation between the measured bath height and liquid bath mass (Figure 2.8). In this thesis it is hypothesized that one reason for this poor relationship is a prevailing sludge cycle which changes the wetted perimeter of the liquid bath and its height. Depending on the origin of sludge formation or dissolution, this leads to various timescales in variations in the liquid bath mass and height. Low bath levels result in problems with alumina feeding and high levels lead to iron contamination of metal due to stub attack.

## 3.2 Control Theory Development

Classical control theory advocates manipulation of inputs in order to bring the outputs of a system to their targets in order to maintain the desired process conditions (Section 2.2). These controllers regulate inputs in a systematic, but empirical manner. The basic problem here is that the controller assumes the cause of variation and compensates for it, rather than diagnosing and trying to remove the cause in each case. The fact that real causes of variation are not removed in this control paradigm means that apparently successfully automated processes deteriorate over time as more causes of variation are introduced (Brisk, 2004). Especially in complex processes, this leads to a new control objective which requires better understanding of the natural behaviour of the process and advanced detection of abnormalities. The following control strategy and system attempt to address this new control objective.

### 3.2.1 Multivariate Control Approach for Aluminium Smelting Cells

As demonstrated in Section 3.1 the aluminium smelting process has strong interactive multivariate characteristics. Under these conditions a given input can affect more than one process output, a given output is affected by multiplicity of inputs and the impact from inputs to outputs is often via the influence of other outputs. In addition, the highly corrosive characteristics of the industrial electrolyte preclude the continuous monitoring of important parameters like bath temperature and composition (Section 2.3). Finally, various time lags in process responses such as the occurrence of an anode effect within seconds, up to long-term influences of an anode setting rota, which is typically in the range of 24 to 30 days, are a major constraint in further improvements.

The complex system dynamics require a more holistic rather than a reduced parameter control approach. Unfortunately at present, most sub-processes are still controlled individually and independently by univariate control loops like alumina feeding, bath composition, temperature, metal height, bath height, total liquid height, anode setting and cover, anode current distribution, noise and suction rate of dry-scrubber. Most of these

parameters are originally tuned according to their design values, but setpoints have to be optimized iteratively due to increased line current, the employment of power modulation and increased variability in the quality of the raw materials used.

#### 3.2.1.1 Stabilizing Inputs under Univariate Control

Following Deming's thinking reduced variation in the face of these complex system dynamics dominated by univariate control loops is more likely to be achieved by stabilizing individual input variables rather than manipulating them continually. Stable inputs in relation to their targets result in small disturbances in the mass and energy balance of a cell. However, some variation in control inputs is needed in order to correct variations in the current and energy efficiency. In order to avoid the accumulation of small adjustments over time additional restrictions on control actions are required to prevent overcorrection.

##### 3.2.1.1.1 Alumina Feed Control

In this respect continuous tracing of the alumina feeding over time is essential to limit the occurrence of the sludge cycle (Section 3.1.1). As discussed the alumina feeding should respond to the actual line current, which is highly important in case of regular line current variation regarding power modulation. In order to detect a short term mass accumulation or depletion of alumina related to a long term fixed current efficiency, the CUSUM of the ratio of alumina fed to a cell $(CR_{Al2O3})$ is used (Equation 3.3). The CUSUM is calculated based on a short time interval related to a long-term average. In this calculation 6 hours are taken for the purpose of a direct intervention to the existing alumina control strategy, in which temporary influences within the operating cycle (e.g. cover material falling into a cell due to anode change) are excluded.

Furthermore, alumina feeding is also adjusted to prevailing sludge formation, discrete events like anode changing and anode effects as described in Section 2.1.3:

- Automatic control actions like a temporary reduction of alumina feed and/or temporary increase of the resistance in order to restore sufficient dissolution brings a cell back in its optimum operating window.
- The impact of an anode change close to a feeder hole on the dissolution effectiveness can be reduced by redistribution of the alumina feed over other point feed locations.
- Extra alumina additions in case of the occurrence of an anode effect are minimized, whereas the termination procedure is optimized to accelerate gas release from under the anodes.

#### 3.2.1.1.2 Aluminium Fluoride Control

As described in Section 2.1.2 aluminium fluoride is used in secondary mass balance control and is most particularly used to neutralise sodium and calcium oxide content of alumina used. Although $AlF_3$ additions are needed to correct individual fluoride emissions and cathode influences, considerable caution needs to be exercised when $AlF_3$ additions are also being used to compensate for a change in bath composition. Equation 3.4 is a further development of Equation 2.12 and contains a linear correction of $AlF_3$ additions based on average liquidus temperature measurements (Stam and Kloetstra, 2004).

$$F_{AlF3} = F_0 + k_L \cdot (T_{L-avg} - T_{\text{liq-target}}) \tag{3.4}$$

Where, $F_{AlF3}$ is the calculated amount of $AlF_3$ additions per day, $F_0$ represents base addition with respect to cell age, line current and alumina analysis (Equations 2.6 and 2.7), $k_L$ is the feeding constant, $T_{L\text{-}avg}$ is the average liquidus and $T_{L\text{-}target}$ is the target liquidus temperature. In order to dampen overcompensation of the control system resulting in a mass imbalance over time, an average liquidus temperature over the last 3 measurements, a minimum and maximum number of $AlF_3$ additions per day and an upper and lower control limit in CUSUM of $AlF_3$ additions over 8 days are used.

#### 3.2.1.1.3 Pseudo-Resistance Control

The energy balance is controlled by electrical energy input (through pseudo-resistance) and heat losses (Section 2.1.2). The pseudo-resistance is used as a primary control of the energy balance and has an upper and lower control limit. These limits are set according to alumina feeding which allows under/overfeeding without changes of the anode beam position. The resistance follows the cell's unique pseudo-resistance curve and the beam is only adjusted if the cell resistance breaks through one of these limits (Figure 2.2).

In general the setpoint of the pseudo-resistance is tuned to the line current and cell specific characteristics (individual cathode and lining conditions) influencing cell stability and heat losses. Figure 3.17 shows a two dimensional operating window of bath temperature and $AlF_3$ concentration for running the smelting process efficiently (Taylor, 1997).

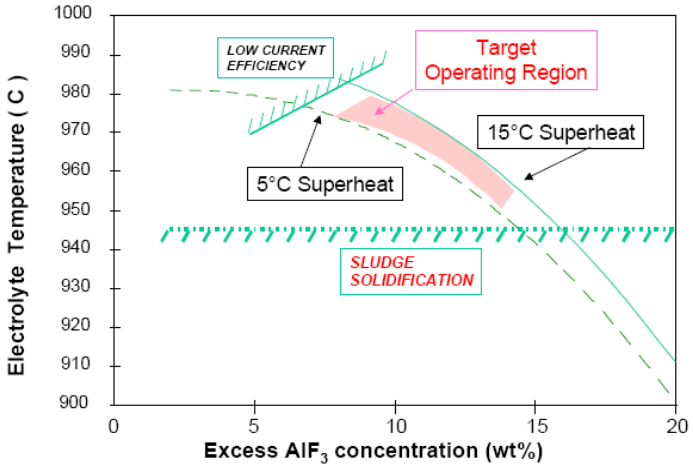


***Figure 3.17*** *Operating Window for Good Cell Performance (Taylor, 1997)*

On the one hand this window is restricted by a lower and upper electrolyte temperature limit corresponding to the sludge solidification temperature and low current efficiency operation respectively. On the other hand the target operating region is limited by a lower and upper superheat limit due to alumina dissolution and maintaining a protective side wall ledge respectively. Based on this the energy balance is controlled by temporary adjustments in cell voltage *(ΔV)* as given by Equation 3.5 (Stam and Kloetstra, 2004).

$$\Delta V = k_{liq} \cdot (T_{\text{liq-target}} - T_{liq-avg}) + k_{SH} \cdot (SH_{\text{target}} - SH_{measured}) + k_{SH-trend} \cdot slope(SH_{number-days}) \quad (3.5)$$

Where, $k_T$, $k_{SH}$, $k_{SH\text{-}trend}$ are the voltage constants, $T_{L\text{-}target}$ and $SH_{target}$ are the liquidus and superheat target respectively, $T_{L\text{-}avg}$ is the average liquidus temperature, $SH_{measured}$ is the measured superheat and $slope(SH_{number\text{-}days})$ is the slope of superheat over a given number of days. The first and second term are introduced to compensate for small deviations in heat generation and losses. The third term responds to a potential trend in superheat and avoids overcompensation.

The operating voltage band is limited by a minimum and maximum setpoint voltage and the calculation of temporary voltage adjustments *(ΔV)* is also restricted by a lower and upper limit. These limits are individually adaptable, because caution is needed when lowering voltage due to increased sensitivity to electromagnetic stability and operational activities (Section 1.3.5). Lowering the setpoint voltage is prevented at high noise operation and sludge formation is detected by above-mentioned CUSUM of ratio of alumina fed to a cell.

This strategy incorporates relatively strong control actions within given boundary conditions as a combination of both high liquidus temperature and high superheat and both low liquidus

temperature and low superheat due to proportional control (Section 2.2.4). Although these actions are partially compensatory in origin, they are undertaken to minimize the duration of a cell in an unwanted operating region which would trigger both excessive freezing/melting of protective sidewall ledge or sludge formation leading to long-term process instabilities (Section 2.2.3).

The combination of high liquidus temperature and low superheat and vice versa result in a dampened reaction in voltage adjustments. Under the first conditions it prevents lowering the cell voltage, which would normally lead to sludge formation due to a low superheat and in the second case it avoids losing ledge at a low liquidus temperature by suppressing a voltage increase. An extreme low liquidus temperature triggers soda ash additions to increase the alumina solubility by reducing the $AlF_3$ concentration in order to break the self-accelerating sludge cycle, which is considered to be the primary driver of variation (Section 3.1.1).

#### 3.2.1.2 Natural Behaviour Envelops

The application of the highly restricted univariate control loops above reduces process variations induced by the compensatory characteristics of the classical control philosophy (Section 2.2.4). However, more flexibility in increased line current, the use of power modulation and increased variability in raw materials used is now required due to rapid varying economical and environmental conditions. Specific control strategies are needed to manage combinations of these new circumstances, leading to the necessity of a multivariable supervisory control approach above the univariate controllers (Section 2.2.6).

It has been found by Chen and Taylor (2005) that Hotelling $T^2$ statistic is an appropriate multivariate control charting and analysis method to use in these circumstances. For the two variables bath temperature and liquidus temperature Hotelling $T^2$ multivariate statistic is given by Equation 3.6.

$$T^2 = \frac{\sigma_{T_B}^2 \sigma_{T_L}^2}{\sigma_{T_B}^2 \sigma_{T_L}^2 - \sigma_{T_B T_L}^2} \left[ \frac{\left(T_B - T_{B-avg}\right)^2}{\sigma_{T_B}^2} + \frac{\left(T_L - T_{L-avg}\right)^2}{\sigma_{T_L}^2} - \frac{2\sigma_{T_B T_L}\left(T_B - T_{B-avg}\right)\cdot\left(T_L - T_{L-avg}\right)}{\sigma_{T_B}^2 \sigma_{T_L}^2} \right] \quad (3.6)$$

Where, $T_B$ is the bath temperature, $T_{B\text{-}avg}$ is the average bath temperature, $T_L$ is the liquidus temperature, $T_{L\text{-}avg}$ is the average liquidus temperature, $\sigma^2_{TB}$ is the temperature variance, $\sigma^2_{TL}$ is the liquidus variance and $\sigma^2_{TBTL}$ is the temperature-liquidus covariance.

The upper control limit for the Hotelling $T^2$ value given by Equation 3.6 is calculated using the F-statistic table and is given by Equation 3.7.

$$T^2 = \frac{p(n-1)}{(n-2)} F_\alpha \tag{3.7}$$

Where, $p$ is the number of variables (p=2 for a two dimensional system), $n$ is the number of data points, $F_\alpha$ is the F statistic for a significance level of $\alpha$ with degrees of freedom for numerator=$p$ and degrees of freedom for denominator=$n$-2. A two dimensional natural behaviour envelop can be derived by substituting Equation 3.7 into Equation 3.6 for a given confidence interval. Figure 3.18 shows an operating ellipse of a typical cell at Aldel derived from the measured bath and liquidus temperatures over a period of 3.5 months at a confidence interval of 95% (Stam *et al.*, 2007).

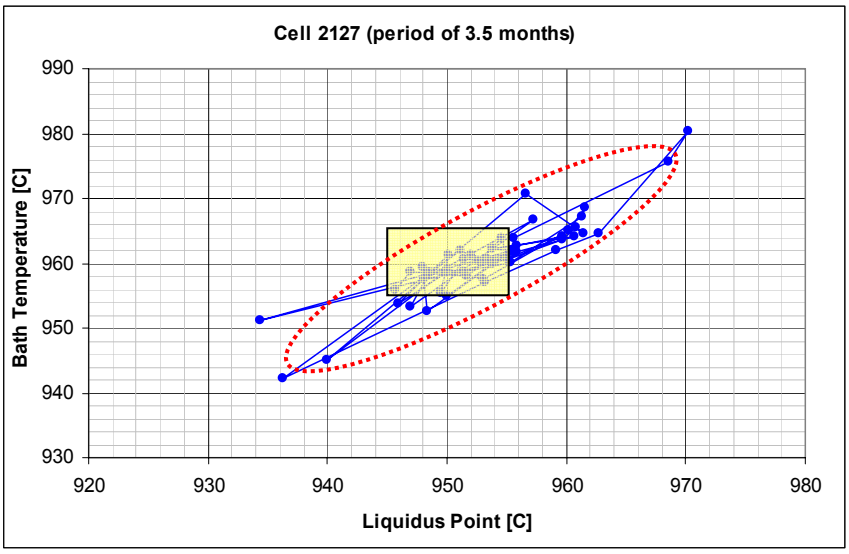


***Figure 3.18*** *2D Natural Behaviour Envelop of a Smelting Cell at Aldel (Stam et al., 2007)*

Without understanding the relationship between the bath and liquidus temperature in the multivariate operating space, control actions based on fixed targets and deviations, quickly lead to incorrect responses. The application of specification limits for these variables (e.g. yellow region) as used in the 9-box approach illustrate the fallacy of univariate control in the aluminium smelting process (Rieck *et al.*, 2003). In fact natural behaviour of the system is well outside the specification region and is actually defined by the elliptical surface as shown by the red dotted line.

This representation is also a powerful tool in the detection of Type I and II errors (Section 2.2.3). Type I errors or false alarms are points outside the yellow box, but inside the elliptical surface. These points are statistically in-control, but because they are outside of the yellow box, control actions would be initiated by a univariate controller leading to overreaction (or 'tampering' as Deming named it). The second type refers to variability that is considered in univariate systems to be in-control, but is in fact outside of statistical control. This

corresponds to the upper left part of the yellow box, which is outside of the ellipse and indicates high superheat operation (14-20°C) with the risk of losing sidewall ledge protection and eventually collapsing top crust.

The sludge cycle postulated in Section 3.1.1 demonstrates the importance of alumina feed as part of natural cell behaviour. The CUSUM of the ratio of alumina fed to a cell is used to take current variations and mass accumulation or depletion into account. The natural behaviour envelop as drawn in Figure 3.18 is extended with alumina feed to improve the ability to control the smelting process more efficiently. Equation 2.17 can be rewritten in a quadratic form to specify a three dimensional envelop as given by Equation 3.8.

$$T^2 = \begin{bmatrix} x & y & z \end{bmatrix} \begin{bmatrix} A & D/2 & E/2 \\ D/2 & B & F/2 \\ E/2 & F/2 & C \end{bmatrix} \begin{bmatrix} x \\ y \\ z \end{bmatrix} = Ax^2 + By^2 + Cz^2 + Dxy + Exz + Fyz \tag{3.8}$$

Where, *A* is the bath temperature variance, *B* is the liquidus temperature variance, *C* is the CUSUM(alumina ratio) variance, *D* is the temperature-liquidus covariance, *E* is the temperature-CUSUM(alumina ratio) covariance, *F* is the liquidus-CUSUM(alumina ratio) covariance, *x* is the temperature, *y* is the liquidus and *z* is the CUSUM(alumina ratio).

In drawing the ellipsoid it is required to determine the semi-principal lengths and orientation of axes in relation to the Cartesian space. The axis lengths of the ellipsoid can be calculated with eigen values and the orientation with eigen vectors. Equation 3.8 is transformed in a standard ellipsoid formula by dividing all parameters by $T^2$. The eigen values $(\lambda)$ can be derived using the third order unit matrix $(I_n)$ by solving Equation 3.9:

$$\det(S_1^{-1} - \lambda I_n) = \det \begin{bmatrix} a-\lambda & b & c \\ d & e-\lambda & f \\ g & h & i-\lambda \end{bmatrix} = 0 \tag{3.9}$$

The third order equations give 3 $\lambda$-values. The solutions represent only real values, because the axes of the ellipsoid are orthogonal. Note that this is a symmetric matrix, and therefore 3 eigen values $(\lambda_1, \lambda_2, \lambda_3)$ and 3 orthogonal (and thus linearly independent) eigen vectors are found. According to the definition of a standard ellipsoid the length of the axes can be calculated as $1/\sqrt{\lambda_1}$, $1/\sqrt{\lambda_2}$ and $1/\sqrt{\lambda_3}$. The *a*-semi-principal axis equals the longest length and the *c*-semi-principal axis equals the shortest. The ellipsoid volume $(V_{ellipsoid})$ is calculated using Equation 3.10. Since the individual lengths of the three axes of the ellipsoid are known, eigen vectors can be determined (Equation 3.11).

$$V_{ellipsoid} = \frac{4}{3} \cdot \pi \cdot a \cdot b \cdot c \tag{3.10}$$

$$\begin{bmatrix} a-\lambda & b & c \\ d & e-\lambda & f \\ g & h & i-\lambda \end{bmatrix} \begin{bmatrix} x_1 \\ x_2 \\ x_3 \end{bmatrix} = \begin{bmatrix} 0 \\ 0 \\ 0 \end{bmatrix} \tag{3.11}$$

The three dimensional natural behaviour envelop for a cell is gathered from both calculated lengths and angles of the three axes in the Cartesian space. Bath and liquidus temperatures are measured simultaneously and in a fixed routine, whereas the CUSUM of the ratio of alumina fed to the cell is monitored continuously. Based on a 95% confidential interval the natural behaviour envelop of every cell can be derived as presented in Figure 3.19.

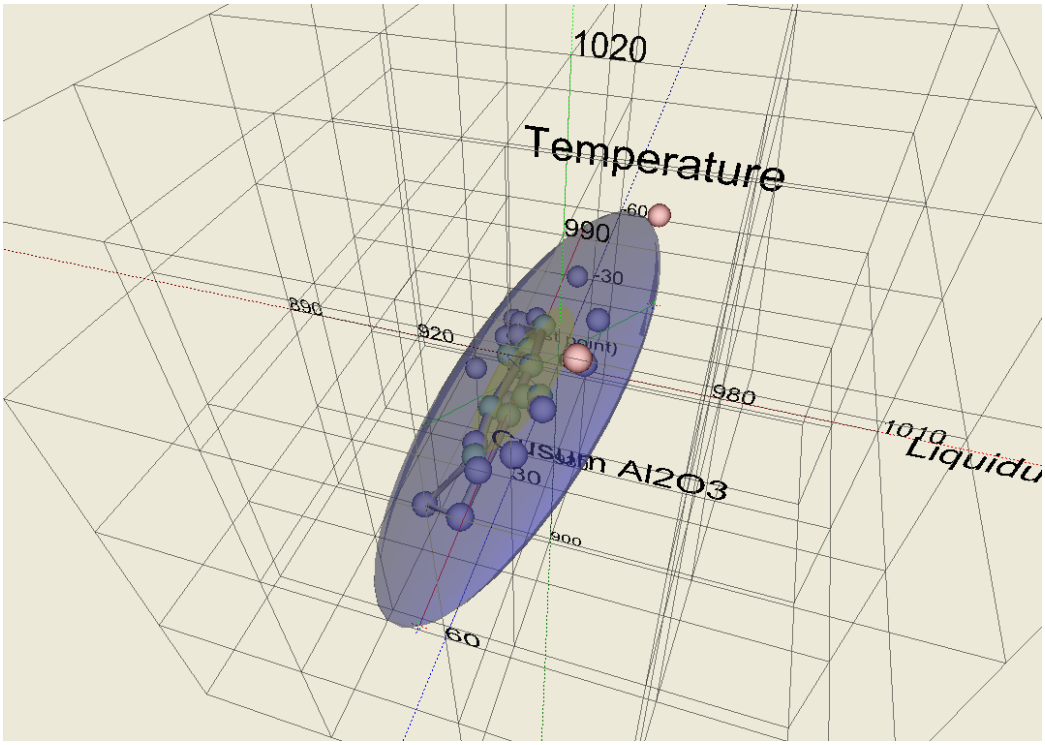


***Figure 3.19*** *3D Natural Behaviour Envelop of a Smelting Cell at Aldel*

### 3.2.1.3 Preventing Impropriate Control Actions

In this thesis it is proposed that control of the aluminium smelting process will be improved by the introduction of an intermediate step between process measurements and control actions, which shifts control away from compensatory behaviour towards corrective or preventive control actions. Natural or common-cause variation occurs where no dominant

cause is acting and a mix of causes results in a basically random pattern of variation inside the ellipsoidal Hotelling envelop (Section 2.2.1).

In Figure 3.19 the blue ellipsoid represents statistically in-control conditions based on the 95% confidence interval. A region in the core of the ellipsoid (yellow ellipsoid) has been introduced to allow for quantifiable, minor process variations due to inevitable measurement errors and short term alumina feeding variation (green dots). The blue dots in between both ellipsoids are statistically in-control and include the univariate control strategies, which are considered to be part of the overall system.

Special-cause variation may happen where a statistically significant, non-random pattern of variation indicates that one dominant cause is influencing the smelting process at that time which is normally not prevailed. Out of control behaviour is calculated with Hotelling $T^2$ statistic at a 95% confidence interval and is represented by the red dots in Figure 3.19. An improvement in process stability by the elimination of these outliners should result in a continuous shrinking of the ellipsoid volume over time. With use of Hotelling $T^2$ statistic, Type I and II errors caused by the interaction between bath temperature, liquidus temperature and alumina feeding are avoided.

Structural variation is recently recognized as a third class of variation, where non-random variation is taking place routinely through the action of the physical and chemical laws and the way the process is operated (Section 2.2.1). Structural variation in smelting cells is connected to discrete events (Section 2.1.3). In this respect the anode setting sequence has a significant influence on measured bath and liquidus temperature (Section 3.1.3). Different studies demonstrate a predictive pattern of temperature measurements as a function of position in the anode setting rota (Stevens McFadden *et al.*, 2001; Iffert, 2007).

The measured impact of the anode setting rota on the bath temperature deviation as shown in Figure 2.10 can be used to define a correction factor to prevent impropriate control actions. However, the application of this type of correction is restricted to stable operating process conditions, because changes in the anode setting rota, line current and raw materials affect the shape and size of the correction curve. Moreover, the curve is validated on average measurements leading to potential errors when applied to individual cells due to cell specific circumstances. In this thesis these structural variations are therefore incorporated in the unique natural behaviour envelop calculated for every cell individually.

The position of a cell in the natural behaviour envelop is important. However, the trajectory of the cell through the ellipsoid, including very rapid movements between one position and another can also constitute out of control behaviour. High process velocity or “pinballing” *(PB)* could indicate either the existence of an abnormality or overcompensation of the

univariate control system (Gao *et al.*, 2007). The magnitude of "pinballing" within the Cartesian space is calculated by the shortest distance between the current and previous measurement points as given by Equation 3.12.

$$PB = \sqrt{\left(T_B - T_{B,previous}\right)^2 + \left(T_L - T_{L,previous}\right)^2 + \left(CR_{Al_2O_3} - CR_{Al_2O_3,previous}\right)^2} \quad (3.12)$$

Where, $T_B$, $T_L$ and $CR_{Al2O}$ are the actual bath temperature, liquidus temperature and CUSUM(alumina ratio) respectively, and $T_{B,previous}$, $T_{B\text{-}previous}$ and $CR_{Al2O3\text{-}previous}$ are the previous bath temperature, liquidus temperature and CUSUM(alumina ratio) respectively. The determination of a long-term trajectory within the 3D natural behaviour envelop could provide information about existence of structural variation as demonstrated in Figure 2.10.

### 3.2.2 Corrective Control

Distinction between common-cause, special-cause and eventually structural-cause variation as explained in Section 3.2.1.3 addresses the interactive multivariate characteristics of the smelting process into the control strategy in a way designed to reduce these causes over time, rather than compensate for them. Following the earlier discussions of Deming's System of Profound Knowledge (Section 2.2.2), this section derives an advanced detection of process abnormalities based on potential failure mechanisms to identify these abnormalities as early as possible. The detection is preferably done prior to Hotelling $T^2$ statistic alarm, because one individual abnormality could lead to a range of successive other failure mechanisms.

Root cause analysis using different methods of problem-solving is then used to diagnose cause-specific abnormalities systematically (Section 2.2.2). For example the mechanism of alumina feeding and bath mass variation within the aluminium smelting process lead to defined failure mechanisms or abnormalities. Then Pareto analysis gives information about frequency and duration of occurrence of these defined process abnormalities. An online early warning system based on real measurements and soft sensing was developed to detect specific-cause variation in the following sections.

#### 3.2.2.1 Alumina Feed Abnormality Sensing

The requirements of availability and reliability of alumina feeding systems are extremely tight as modern smelters with a production of 500,000 tonnes per annum have up to 30 alumina dumps per second. In order to track the status of alumina feeding and dosing equipment, at Aldel, pot control units send information to the overall host computer (Stam *et al.*, 2008).

In Figure 3.20 the configuration is drawn schematically. Main signals are 1) “plunger down” *($t_{start}$)*, 2) “plunger up” *($t_{liquid}$)*, triggered via closure of an electric circuit when the plunger hits the liquid level and 3) “no feedback”, which is set after a certain time period. Travel time *($t_{travel}$)* of each plunger (time between “plunger down” and “plunger up”) and subsequently difference in travel time between both plungers are traced continuously. The anode beam positions *($x_A$, $x_B$)* and the average speed of the plungers *($v_{A,i}$, $v_{B,i}$)* can be used to calculate the metal height (Section 3.2.2.2).

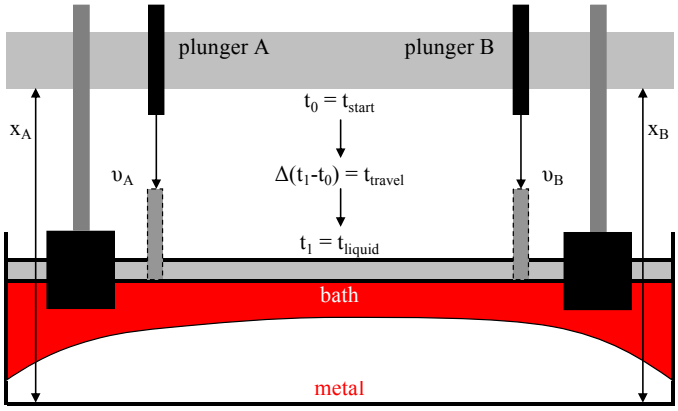


***Figure 3.20*** *Schematic Representations of Beam and Plunger Positions (Stam et al., 2008)*

By using this principle different process abnormalities related to alumina feeding can be detected with individual soft sensors:

a) *“Plunger hits anode”*: detected by a sudden step change in the travel time between 2 plungers after anode change around feeder holes and needs a fast response by the operator to reposition the anode without ensuing anode effects and/or alumina build-up around and on top of anodes.
b) *“Low liquid level”*: detected by a long travel time or no feedback (failure) and can result in problems in getting alumina into the cell and “plugged feeder holes” afterwards.
c) *“Slow plunger”*: detected by a drift of the travel time away from its average and can also lead to “plugged feeder holes”.
d) *“Plugged feeder hole”:* detected by a noisy signal of the individual travel time due to a restriction in the plunger operation.

Anode effects should be treated as an unwanted process abnormality in modern point feed technology. Different causes of anode effects can be sorted out like beam raising, anode changing, metal tapping, cold cells and/or power modulation. In other occasions or in case of repeatable and/or high energy anode effects, a detailed investigation at the cell needs to give the correct cause of abnormality. Blockages of the detection of repeatable anode effects are necessary in case of power modulation to avoid wrong control actions.

A track of a positive CUSUM of alumina shots over time is a good measure for the existence of sludge formation (Equation 3.3). Additional information is gathered by tracing the reaction of the cell resistance to the alumina feed control logic. A clear indication of alumina feeding problems can be found if the resistance doesn't decrease in a given timeframe during and directly after overfeed. Leakage of alumina from dosing devices or alumina bunkers results in a low number of alumina shots fed to the cell.

### 3.2.2.2 Liquid Bath Mass Abnormality Sensing

With the use of the positions at both ends of the anode beam $(x_A, x_B)$ shown in Figure 3.20, the metal height can be calculated continuously (Equation 2.18). The estimation of the average total liquid level ($H_{liq}$) is obtained with multiplication of the travel time $(\Delta t_{A,i}, \Delta t_{B,i})$ and the average speed of the plungers $(v_{A,i}, v_{B,i})$ at a given number of plunger movements $(i)$ (Equation 3.13).

$$H_{liq.} = average\left(\frac{1}{2i}\cdot\left(\sum_i (v_{A,i}\cdot\Delta t_{A,i}) + \sum_i (v_{B,i}\cdot\Delta t_{B,i})\right)\right) \tag{3.13}$$

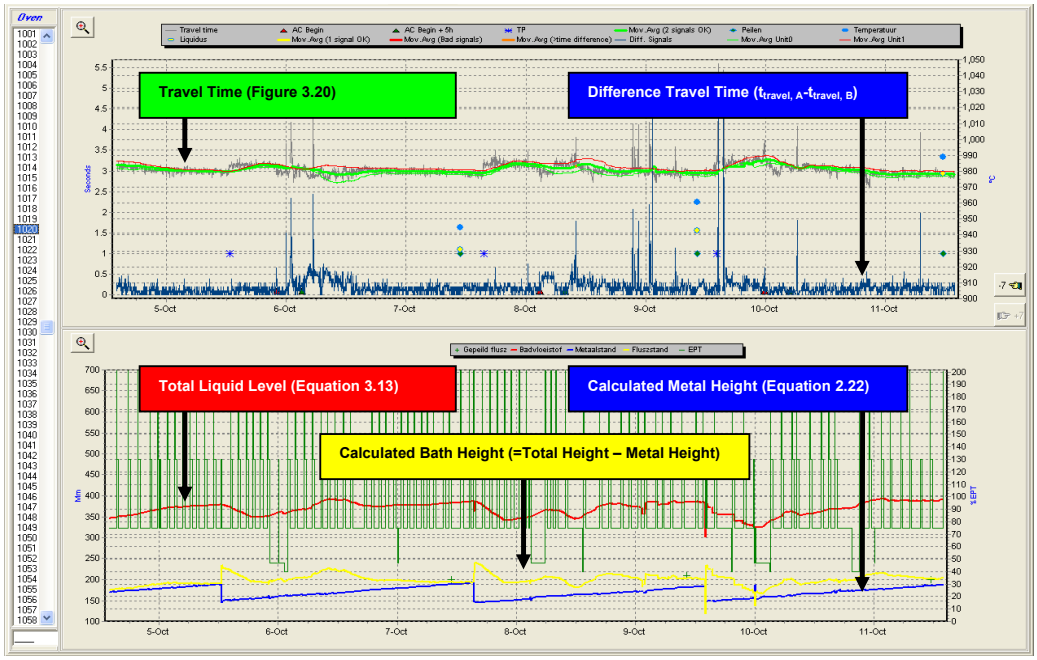


***Figure 3.21*** *Determination of Liquid Levels in a Smelting Cell with Use of Plungers at Aldel*

As developed at Aldel, the average speed of plungers is tuned to the travel time and manual measurements of the total liquid height over a longer time period. The bath height is determined as a difference between the total liquid level and the calculated metal height (Figure 3.21). Discrete events like anode changing, metal tapping and beam raising are

excluded in the calculation of the bath height. Tracking the difference between the measured and calculated metal and bath height respectively provide extra possibilities in abnormality detection.

Bath mass variations cannot be measured on a regular basis and bath height is normally used for the determination of abnormalities. In case of sludge formation with corresponding decrease of the liquid bath mass automatic control actions result in a steady increase of the resistance and a reduction of the amount of $AlF_3$ fed (Section 3.1.1). An increase of CUSUM of alumina fed and a decrease of CUSUM of $AlF_3$ additions simultaneously could indicate a reduction of the liquid bath mass and vice versa (Figure 3.2). This enables the development of a soft sensor to detect an increase or decrease in the bath mass indirectly (Section 2.2.7).

#### 3.2.2.3 Anode Abnormality Sensing

Continuous registration of the beam position and alumina dumps are also helpful in detection of anode spikes. An anode spike can be detected by repeatable beam up movements due to short circuiting. In addition, short circuiting leads to a rapid increase in heat generation within the ACD due to increased local resistance and a reduction in current efficiency. Therefore a combination of a step change in bath temperature combined with a reduction of the CUSUM of the alumina feed ratio is also an indication of an anode spike. Although the temperature is measured at a much lower frequency than the online alumina feed ratio (normally once per day or even once per two days), a crosscheck of both items gives a reliable soft sensor for the detection of anode spikes.

Moreover, continuous monitoring of travel time of individual plungers provides information about the accuracy of anode setting (Section 3.2.2.1). The difference in travel time between the individual plungers is calculated and if there is a sudden step change it can be concluded that an anode is positioned in the point feed hole under the plunger (“plunger hits anode”). This requires a fast response by the operator to reposition the anode without ensuing anode effects and/or alumina build-up around and on top of anodes.

## 3.3 Formulation of Control Model

The formulation of the new control model for smelting cells presented in this section uses the framework of Deming’s “System of Profound Knowledge” (Section 2.2.2). It incorporates multivariate statistical determination of individual cell process states combined with cause-specific detection of abnormities identifying corrective control actions. Online Pareto and root cause analyses allow continual focus on the most important contributions to variation and elimination of these causes respectively, and generate continuous improvements on a daily

basis. In general stable process inputs with restricted compensatory characteristics are applied in the multivariate controllers although control actions are prevented in the case of cell abnormality detection.

### 3.3.1 Determination of Overall Process State

Hotelling $T^2$ statistic determines three (or more if required for diagnostics) dimensional natural behaviour envelops for individual cells (Section 3.2.1.2). This process state is calculated with a predefined moving window of bath and liquidus temperature measurements combined with the CUSUM of the ratio of alumina fed to a cell. A period of 30 measurements - typically 2 anode rotas - is taken to eliminate short term process variations and incorporate medium term variations like a continuous increase in the line current and variations in raw material. Online computation of the number of alumina shots allow fine-tuning of the existing process conditions in between successive temperature measurements. The ellipsoid volume at 95% confidence interval (Equation 3.10) and the orientation of the natural behaviour envelop in Cartesian space are both computed (Equation 3.11).

The overall process state is divided into three operating zones. Points within the ellipsoid are in control, because they represent the normal structural and common cause variation inherent in the 'batch operated' smelting process. Measurements outside this normal behavioural envelop are defined as out of control (Section 3.2.1.3). A third region in the core of the ellipsoid has been introduced to allow for quantifiable, minor process variations due to inevitable measurement errors and short term alumina feeding variation. This region acts as a natural, no-action region inside the normal behavioural envelop and no univariate control actions occur here apart from normal alumina feeding regulation.

### 3.3.2 Abnormality Detection

As a first stage, an abnormal process state is detected by Hotelling $T^2$ statistic as described in Section 3.2.1.2, which discriminates between normal and out of control behaviour. Pinballing - defined as unacceptable process velocity exceeding a particular threshold value - also indicates out of control circumstances (Section 3.2.1.3), but based on velocity of the process trajectory. However, in both cases no direct information of the origin of abnormality is provided and therefore root cause analysis is necessary to identify the cause of variation.

In the second stage, cause-specific detection and diagnosis of abnormalities give an independent identification of potential failure mechanisms; preferably before serious process excursions have taken place. Cause-specific events are defined, which are founded on either direct signalling or indirect derivation using soft sensors indicating specific process circumstances. However, detection is not always possible due to limited process sensitivity

or specificity, or the need of a preparatory phase in order to build up a time evolution of the sensed signal to fingerprint the presence of particular causes.

Sections 3.3.2.1 to 3.3.2.4 develop the detection and identification algorithms for process abnormalities for the overall process state, anode conditions, alumina and $AlF_3$ balance and liquid mass respectively. Under particular process conditions additional preconditions - mostly indicated by blockages - are defined in order to avoid false alarms. Especially periods after discrete events like anode changing (AC), metal tapping (TP), beam raising (BR), a current drop (CD) and load management/power modulation (LM) are excluded in the abnormality detection.

#### 3.3.2.1 Overall System Dynamics

Table 3.2 summarizes a number of abnormalities or events, based on predefined criteria, related to the overall system dynamics. The first 4 events provide general information about the stability of the overall system dynamics. HOTAL represents the region in the core of the ellipsoid allowing for quantifiable, minor variations due to inevitable measurements errors and short term alumina feeding variation (Figure 3.19). Regarding these inevitable variations this region is defined as the target operating zone. Moreover, HOTAH and high pinballing (PBH) signal out of control behaviour. The total duration of events (TOTEV) is monitored for every individual cell to register the time that the cell is out of its optimum operating zone.

| Process Abnormality | Criterion | Block | Event |
|---|---|---|---|
| Target Region (Hotelling $T^2$) | <2 (25% confidence interval) | | HOTAL |
| Out of Control Behaviour (Hotelling $T^2$) | >6 (95% confidence interval) | | HOTAH |
| Pinballing: High Process Velocity | >30 | | PBH |
| Total Duration of Events | 1/cell·day | | TOTEV |
| Temperature Low | <945°C | | TEMPL |
| Temperature Critical Low | <930°C | | TEMPKL |
| Temperature High | >980°C | | TEMPH |
| Temperature Critical High | >990°C | | TEMPKH |
| Liquidus Low | <935°C | | LIQL |
| Liquidus High | >970°C | | LIQH |
| Superheat Low | <2°C | | SHL |
| Superheat High | >20°C | | SHH |
| Noise High | >0.2 μΩ | | NP |
| Current Drop/Outage | Current Decrease >80 kA | | CD |

***Table 3.2*** *Events Related to the Overall System Dynamics*

As the rest of the events are a result of abnormal process behaviour, these events signal out of control circumstances without cause-specific information. These events are derived from the operating window for good cell performance as depicted in Figure 3.17. In case of

abnormalities in the bath temperature 2 different levels of events - e.g. high and critical high temperature events - are defined according to the seriousness and potential hazardous effects of these abnormalities to the ensuing process stability. However, these events can only be used as indicative triggers for out of control behaviour as they have one dimensional characteristic. In addition, high cell noise and current drops are monitored online.

#### 3.3.2.2 Anode Conditions

Table 3.3 lists several abnormalities connected to anode conditions or associated working practices during anode changing. Most of these abnormalities are detected by shift operators or members of a specialist measurement team and provide cause-specific information, e.g. the anode current distribution is measured to detect too high/too low setting of new anodes, anode spikes, slipped anodes, burn offs or clad failures. As described in Section 3.2.2.3 also automatic detection of anode spikes and abnormalities in anode setting are determined. In these cases additional blockages in the detection of abnormalities are introduced to avoid Type I errors or false alarms (Section 2.2.3).

| Process Abnormality | Criterion | Block | Event |
|---|---|---|---|
| "Plunger hits Anode" | $t_{travel}$ <1 seconds | AC<1 hour | CBAN |
| Automatic Spike Detection | $\Delta(T_{measured}-T_{previous})>15°C$<br>$CR_{Al2O3}<-20\%$ | AC<8 hours<br>BR<8 hours | ANSPA |
| Spike Detection Measurement Team | Anode Current>7.5 kA | | ANSPM |
| Spike Detection Shift Operators | Anode Current>7.5 kA | | ANSPS |
| Slipped Anode (Lower than Original Mark) | Anode Current>7.5 kA | | ANSLP |
| Anode Drop Off/Clad Failure | Anode Current<1.0 kA | | ANOFF |
| Anode Set Too High | Anode Current<3.0 kA | | ANHGH |
| Clamp Voltage High | >20 mV | | CLMVH |
| Total Number of Anode Failure Events | | | TOTAN |

***Table 3.3*** *Events Related to Anode Conditions*

#### 3.3.2.3 Alumina and $AlF_3$ Balance

Table 3.4 summarizes cause-specific events related to abnormalities in the alumina and $AlF_3$ balance control. A first group of events detects problems with the hardware of the alumina and $AlF_3$ feeding equipment (Section 3.2.2.1). CBERR events signal hardware failures of the alumina feeding equipment. As the $AlF_3$ additions are added to the cell via one of the alumina feeder holes hardware failures are also detected for the $AlF_3$ additions (AlF3ERR). Moreover, plugged feeder holes (CBSPK) and slow plungers (CBDIST) are distinguished.

| Process Abnormality | Criterion | Block | Event |
|---|---|---|---|
| General Hardware Failure $Al_2O_3$ Feeding | No Feedback from Plunger | AC<1 hours<br>CBAN | CBERR |
| "Plugged Feeder" | Noisy Signal from Plunger | See CBERR | CBSPK |
| Slow Plunger | $t_{travel}$ >5 seconds | See CBERR | CBDIST |
| General Hardware Problems $AlF_3$ Feeding | No Feedback from Plunger | See CBERR | AlF3ERR |
| CUSUM(Alumina Ratio) High | >105% | LM<8 hours<br>AC<8 hours<br>CD<8 hours<br>ANSPA<96 hours<br>ANSPM<96 hours<br>ANSPS<96 hours | Al2O3H |
| CUSUM(Alumina Ratio) Low | <85% | See Al2O3H | Al2O3L |
| Reaction of Cell Resistance to Overfeed | <80% Overfeeds are OK | AC<6 hours | OACURV |
| Number of Overfeed Low | <5/day | See OACURV | OAERR |
| Anode Effect | - | | AE |
| Anode Effect Error | >2 AE's in last 96 h | CD<96 hours<br>BR<96 hours<br>LM<96 hours<br>OAERR<6 hours | AEERR |
| Anode Effect Energy High | >100 kWh in last 8 h | | AEKWH |

***Table 3.4*** *Events Related to Alumina and $AlF_3$ Balance Control*

The second group of events determines abnormalities in alumina feeding. Accumulation or depletion of the mass of alumina within a smelting cell are determined by the development of the CUSUM of the ratio of alumina fed to a cell over time (Al2O3H, Al2O3L). These events allow the detection of the sludge cycle as described in Section 3.1.1. More specifically, the reaction of the cell resistance to overfeed can be used to detect sludge formation (OACURV) in an early stage (no decline in resistance within a predefined time frame). Contrary OAERR indicates sludge dissolution circumstances based on a low number of overfeeds per day. A third group of events is connected to anode effects (occurrence, frequency and energy).

#### 3.3.2.4 Liquid Bath Mass

In Table 3.5 a number of abnormalities in liquid bath mass control are listed. The first three events are linked to the detection of abnormalities in the calculated bath height (Equation 3.12). As described in Section 3.2.2.2 a soft sensor is developed to detect large variations in liquid bath mass (BVINC, BVDEC). This sensor is based on predefined behaviour indicated by the CUSUM of alumina ratio fed to a cell and the CUSUM of $AlF_3$ additions (Figure 3.2). With the use of the new control model, this sensor will be less effective due to additional interventions to the alumina feeding in case of alumina accumulation. Also, more stable $AlF_3$ additions will retard triggers of large variations in liquid bath mass.

| Process Abnormality | Criterion | Block | Event |
|---|---|---|---|
| Bath Height Calculation Error | $\Delta\|(BH_{measured}-BH_{calc})\|>5$ cm | | BHCALC |
| Bath Height Calculation Low | $BH_{calc}<10$ cm | | BHL |
| Bath Height Calculation High | $BH_{calc}>30$ cm | | BHH |
| Bath Volume Increase | $CR_{Al2O3}<-20\%$<br>$CR_{AlF3}>20$ kg | ANSPA<1776 hours<br>ANSPM<1776 hours<br>ANSPS<1776 hours | BVINC |
| Bath Volume Decrease | $CR_{Al2O3}>20\%$<br>$CR_{AlF3}<-20$ kg | See BVINC | BVDEC |

***Table 3.5*** *Events Related to Liquid Mass Control*

### 3.3.3 Control Responses

Control models based on manipulation of process settings in response to recent process measurements and observations are widely applied in industrial processes (Section 2.2.3). However, three different stages in control theory can be distinguished as shown in Figure 3.22 (Taylor and Chen, 2007). The first step is the determination of the overall process state. In this thesis Hotelling $T^2$ statistic is used to define natural behaviour envelops for individual cells as described in Section 3.1.1.

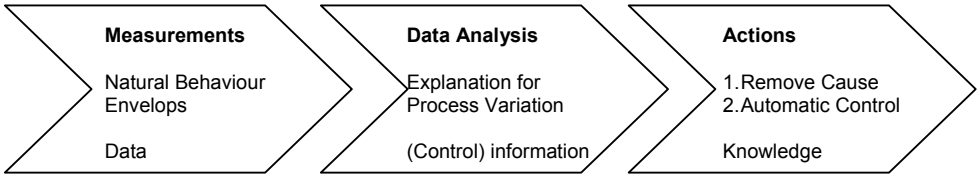


***Figure 3.22*** *Three Basic Steps in Process Control (Taylor and Chen, 2007)*

The second step exposes the causes of variations, whereas observed variation (step 1) is always a combination of measurement (represented by operator and method) and process variation. Hotelling $T^2$ statistic and pinballing are applied to discriminate between normal and out of control behaviour (Section 3.2.2). In order to fingerprint specific causes of abnormality advanced detection is developed for the overall system dynamics, anode conditions, alumina and $AlF_3$ balance, and liquid bath mass.

In the third step control interventions lead to correction or removal of causes of variation with the help of advanced detection of process abnormalities (plungers keep hitting anodes, etc). Automatic control actions tune process settings to maintain the cell in its optimum operating region as discussed in Section 3.3.3.1. Also, human interventions are required to remove the underlying cause and restore normal process conditions (Section 3.3.3.2).

#### 3.3.3.1 Automation

As discussed in Section 3.3.1 three different operating zones are defined. Points within the core of the three dimensional natural behaviour envelop are in the target operating zone, because the process variation is traced back to measurement errors plus short term feeding variation. Being in balance also requires a low process velocity (no pinballing). Under these conditions the cell voltage, $AlF_3$ additions and alumina feeding are set at their setpoints. This approach dampens changes in control inputs due to latency or time lags in the cell responses. Statistical determination of this target zone eliminates Type I errors due to univariate proportionally based control (Section 3.2.1.2).

Points outside the ellipsoid are statistically out of control and under these circumstances automatic control actions are blocked and the cell voltage and $AlF_3$ additions are also set to their targets ($V_{target}$ and $F_0$ respectively) to avoid overcorrection and allow the dominant cause to be removed. Root cause analysis is needed to detect the cause of abnormality. Independently of the status of a cell in its natural behaviour envelop, a protocol of advanced mechanical and other detection of abnormalities runs continuously to detect these conditions as early as possible (Section 3.3.2). The only allowed control action is the addition of soda at a low average liquidus temperature to avoid long residence time in this process state, because of its harmful effect to the underlying process conditions (Section 3.1.4).

The third zone, which is the space in between the natural and normal structural behaviour envelop based on 95% confidence interval, represents statistically in control conditions, although not at optimum process state. Under these circumstances automatic control actions have compensatory characteristics to adjust process settings and move the cell back to the above-mentioned target zone. In general cell voltage and $AlF_3$ additions are controlled according to Equations 3.4 and 3.5 respectively, incorporating multiple restrictions to avoid overcompensation as discussed in Section 3.2.1.1.

Additional damping or blockages of these compensatory control actions are introduced, even within the normal behaviour envelop, in case of specific abnormal process circumstances (Table 3.6). Abnormal process velocity detected by pinballing is defined as out of control and these cells are treated likewise (Section 3.2.1.3). Recent anode effects, power modulation, anode spikes, sludge formation, and large shifts in the liquid bath mass also block automatic control actions. These blockages are introduced to avoid overcompensation leading to an unwanted process shift in the mass and energy balance afterwards.

Alumina feeding is controlled according to the univariate, pseudo-resistance based logic, coupled with a strategy to prevent accumulation of alumina (Al2O3H) and/or incorrect reaction of the cell resistance to overfeed (OACURV). Under these conditions automatic

interventions to the alumina feeding strategy (FA) as a temporary reduction of the total amount of alumina fed to the cell (-15%) and an increase in cell voltage (+80 mV for 6 hours) to restore sufficient dissolution are activated.

| Automatic Control Action | Criterion | Block | Event |
|---|---|---|---|
| Cell Voltage Intervention | Temperature and Liquidus Measurement | LM<125 hours<br>AEKWH<8 hours<br>OAERR<br>BVINC<br>BVDEC<br>HOTLAL<br>HOTLAH<br>PBH<br>ANSPA<br>ANSPM<br>ANSPS | $\Delta V$ |
| $AlF_3$ Additions Intervention | Temperature and Liquidus Measurement | See Cell Voltage Intervention ($\Delta V$) | $F_{AlF3}$ |
| $Al_2O_3$ Feed Intervention | OACURV<br>Al2O3H | AE<5 hours<br>AC<12 hours<br>CBAN<12 hours<br>CBERR<12 hours<br>CBSPK<br>HOTAL | FA |
| $Al_2O_3$ Feed Intervention after AC | AC | CBAN<br>CBSPK<br>CBERR<br>CBDIST<br>OAERR<br>OACURV | FAC |

***Table 3.6*** *Automatic Control Actions*

Beside blockages listed in Table 3.6, the intervention is blocked according to the criteria for Al2O3H and OACURV as given by Table 3.4. In order to reduce the impact of an anode change close to a feeder hole related to dissolution characteristics locally, the alumina feed is redistributed (120/80% for 48 hours) over both point feed locations. This is only allowed when no hardware problems or abnormal alumina feeding conditions are present (Table 3.6).

#### 3.3.3.2 Human Intervention

In case of the detection of abnormalities as described in Sections 3.3.2.1 to 3.3.2.4 often human intervention is required to remove the underlying cause and restore normal process conditions (Table 3.7). Abnormalities related to anode conditions are measured by operators and listed in a database. Automatic detected spikes are also recorded in this database and once per shift these abnormalities are removed. A fast response to the detection of “plunger

hits anode" (CBAN) and "plugged feeder" (CBSPK) prevents unwanted anode effects. These alarms are automatically sent to the mobile phone of the operator. Other hardware problems (CBERR and CBDIST) are collected and automatically sent to the maintenance department.

If no cause-specific information is available, a list of "disturbed cells" is typically used in aluminium smelters to prioritize the investigation of these cells using a predefined decision-tree. In this thesis cells associated with the events listed under "overall process state" are checked by operators (Table 3.7).

| **Overall Process State** | **Anode Conditions** | **Alumina and $AlF_3$ Balance Control** | **Liquid Bath Mass** |
|---|---|---|---|
| HOTAH | CBAN | CBERR | BHCALC |
| PBH | ANSPA | CBSPK | BHL |
| TEMPKL | ANSPM | CBAN | BHH |
| TEMPKH | ANSPS | CBDIST | |
| LIQL | ANOFF | AlF3ERR | |
| LIQH | ANSLP | AEERR | |
| SHH | ANHGH | AEKWH | |
| NP | CLMVH | | |

***Table 3.7*** *Human Intervention Events*

Online Pareto analyses of the detected abnormalities support human decision-making and prioritize the corresponding corrective actions as shown in Figure 3.23. These analyses are continuously updated on the same time scale as the determination of the natural behaviour envelops (Section 3.3.1). As described in Sections 3.3.2.1 to 3.3.2.4 this thesis develops cause-specific protocols for feedback to engineers and operators, but the development of an integrated supervisory model is out of the scope of this work and is part of another research project (Gao *et al.*, 2009).

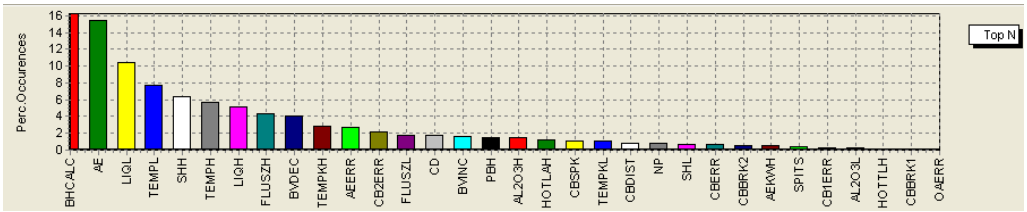


***Figure 3.23*** *Frequency of Detected Abnormalities at Aldel*

Frequently detected abnormalities and failure mechanisms provide a better understanding of the limiting components of the cell system and can be integrated into PDSA-cycle (Section 2.2.2). Improvements to the design of the operational work and control model are constantly needed to keep pace with rapidly varying economical and environmental conditions (Taylor *et al.*, 2010)

## 3.4 Architecture Principles

In this section a module-based architecture is developed which allows flexible configuration of the underlying control philosophy (Stam *et al.*, 2009). The architecture is designed along a sequence of control decisions. This sequence is built upon individual modules ordered by the control logic according to the characteristics of the smelting process. The architecture allows simple and fast adjustments to the control philosophy by the modification of existing modules, addition of new modules and elimination of old modules. In addition, all constants, parameters and targets are defined as variables, which provide maximum flexibility in the configuration of the required outcomes.

The architecture contains 3 different types of modules (statistical calculations[1)], detection of abnormalities[2)] and control responses[3)]) as shown in Figure 3.24. The first type of modules calculates the CUSUM of the ratio of alumina fed to a cell (Equation 3.3), CUSUM of $AlF_3$ additions, Hotelling $T^2$ (Equation 3.8), ellipsoid volume (Equation 3.10), pinballing (Equation 3.12) and metal height (Equation 3.13). The second type is designed for cause-specific detection of process abnormalities and failure mechanisms and consists of set of binary events as listed in Tables 3.2 to 3.5. The third type initiates associated control responses, which consists either root cause analysis based on a detected process abnormality or interventions to the cell voltage, $AlF_3$ additions and alumina feed control as depicted in Table 3.6.

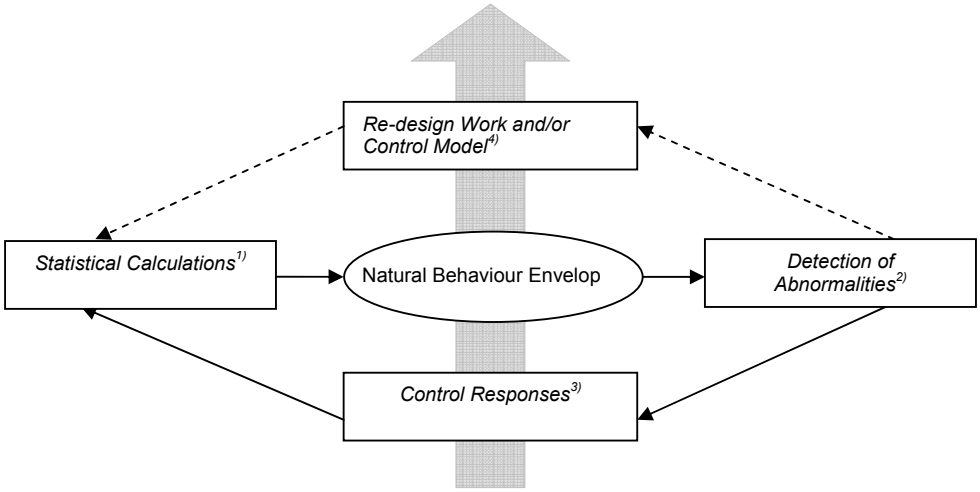


***Figure 3.24*** *Overall Control Philosophy (Stam et al., 2009, modified)*

The general routing of the control philosophy starts with statistical calculations[1)] in order to determine individual natural behaviour envelops for every cell (Section 3.3.1). After that the detection of abnormalities[2)] provides better understanding of potential failure mechanisms disturbing the underlying process stability (Section 3.3.2). Then the control model determines

associated control responses[3)] (Section 3.3.3). This practice is predicated on Deming's thinking that problems are best solved by attempting to correct or eliminate root causes. By eliminating causes, and implementing only corrective measures, recurrence of a variation will be minimized (Section 2.2.2). Ultimately continuous improvement is incorporated by Pareto analysis of frequently detected abnormalities in both system dynamics and control model, which results in re-design of people's work, cell/smelter hardware, or control modules[4)].

The general routing of the architecture is based on a predefined sequence of modules (Table 3.8). A sequence is activated by a trigger in order to initiate the calculation or determination of the module function. Firstly triggers are timer-based, e.g. once per minute, 5 minutes or day. Secondly triggers are based on operator measurements of bath and liquidus temperature, bath and metal height and anode current. Thirdly triggers are based on a range of activities or events. Discrete events like anode changing, metal tapping, beam raising, but also after an anode effect, current drop, power modulation and noise initiate a new module sequence.

| **Trigger Name** | **Sequence of Modules** | **Events** |
|---|---|---|
| Every Minute | Current Drop | CD |
| | Power Modulation | LM |
| Every 5 Minutes | Online CUSUM Calculations | |
| | Hotelling $T^2$ Calculation | |
| | Hotelling/pinballing Errors | HOTAL, HOTAH, PBH |
| | Alumina Feed Errors | OACURV, OAERR, Al2O3H, Al2O3L, CBAN |
| | Automatic Spike Detection | ANSPA |
| | Liquid Bath Mass Variations | BVINC, BVDEC |
| | $Al_2O_3$ Feed Intervention | FA |
| | $Al_2O_3$ Feed Intervention after AC | FAC |
| | Metal Height Calculation | |
| Daily Statistics | General Hardware Problems | CBERR, CBDIST, AlF3ERR |
| | Total Duration of Events | TOTEV |
| Temperature and Liquidus Measurements | Overall Process State Errors | TEMPL, TEMPKL, TEMPH, TEMPKH, LIQL, LIQH, SHL, SHH |
| | Cell Voltage Intervention | $\Delta V$ |
| | $AlF_3$ Intervention | $F_{AlF3}$ |
| Bath and Metal Height Measurements | Bath Height Calculation | |
| | Bath Height Calculation Errors | BHCALC, BHL, BHH |
| | Calculation of Tapped Metal | |
| Anode Measurements | | ANSPM, ANSPS, ANOFF, ANSLP, ANHGH, CLMVH, TOTAN |
| Anode Changing | | AC, CBAC, CBAN |
| Metal Tapping | | TP |
| Beam Raising | | BR |
| Anode Effect | | AE, AEERR, AEKWH |
| Noise | | NP |

***Table 3.8*** *Process Sequence and Triggers*

The 3 different types of modules have an identical architecture. Once a module sequence is triggered as indicated by Table 3.8, every module contains three individual steps and starts with a check whether this module is applicable to a particular cell (Figure 3.25) (Stam *et al.*, 2009). Modules are connected to pot lines, groups of cells or individual cells. This allows specific testing of new principles to a lead group of cells (Section 4.1.1). If a module is not valid for a cell, the sequence steps further to the next module (A1). The second step is a check whether a module is blocked, which can be initiated by cause-specific timers or other events (Table 3.2 to 3.6). If a module is blocked for a cell, the next module is entered (A2). Finally, the module function runs and after that the module sequence steps further to the next module (A3) according to Table 3.8.

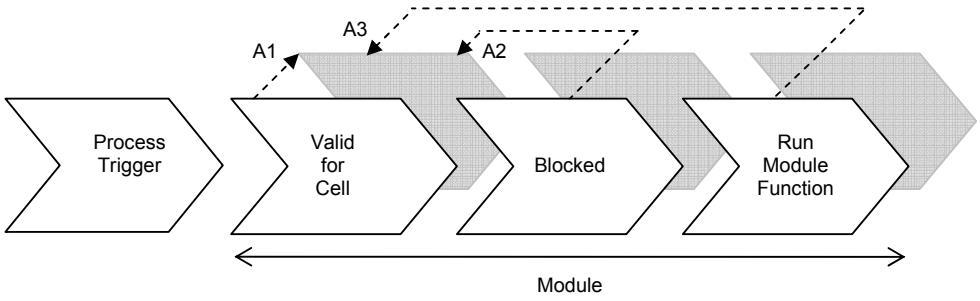


***Figure 3.25*** *Structure of Module Architecture (Stam et al., 2009)*

## 3.5 Hypotheses

The following hypotheses are formulated based on the theoretical development undertaken in this chapter:

1. A self-accelerating dominant sludge cycle caused by incomplete alumina dissolution drives liquid bath mass variations and increased alumina feeding until large and prolonged bath temperature and composition variation is produced. Preventing or breaking this cycle will reduce overall process variation (Section 3.1.1).

The widely varying observed responses of the cell to the same (repetitive) set of alumina feed events demonstrates that the longer term energy and mass balance of the cell (its process state) does have a profound influence on the process trajectory and subsequent cell outcomes (and control actions). This more general evidence of chaotic behaviour dictates that simple, linear or even compensatory multivariate control schemes will not be successful in the aluminium smelting process (Abraham and Shaw, 1987). This leads to a new control rationale:

2. A multivariate causally based control approach using natural behaviour envelops for individual cells and cause-specific detection and diagnosis of abnormalities will improve control and shrink the cell envelops (Section 3.2).

# Chapter 4 Experimental Design

This chapter presents the experimental design for industrial testing of the two hypotheses postulated in this thesis (Figure 4.1). The statistical basis for the industrial experiments using a test and reference group of cells is described in Section 4.1.1. The effectiveness of the new control philosophy is examined by the investigation of the underlying process behaviour envelops and abnormality detection (Section 4.1.2). These investigations serve as a basis for the determination of specific failure mechanisms and more complex multivariate statistical system dynamics. Based on these results the hypotheses are discussed in Section 4.1.3.

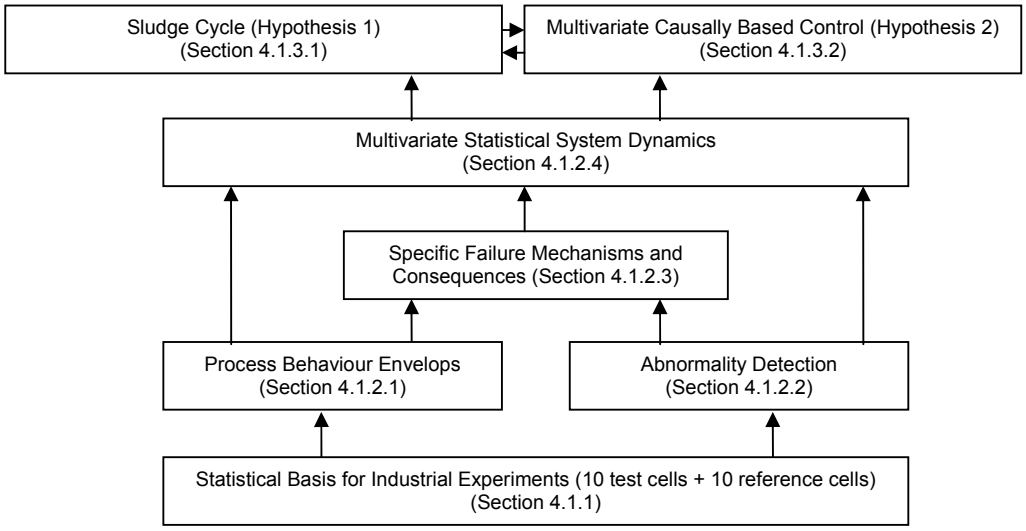


***Figure 4.1*** *Experimental Design and Data Analysis*

The second part of this chapter considers specific conditions and constraints associated with industrial testing. Variations in the energy input (Section 4.2.1) and variations in the supply and hence the properties and impurities of raw materials used (Section 4.2.2) are inevitable in industrial experiments. Actually, the motivation for advanced control is the necessity to increase the flexibility in energy input and raw material variations under rapid changes in economical and environmental circumstances as discussed in Section 1.1. The equipment and instruments involved in the tests are discussed in Section 4.2.3.

## 4.1 Methodology for Industrial Experiments

### 4.1.1 Statistical Basis

Scientific investigations undertaken under industrial circumstances require some additional precautions regarding the significance of the outcomes. The effectiveness of the new control strategy developed in this thesis is studied using a test group and control or reference group

of cells (Rutledge, 2008). The new strategy is applied to 10 test cells and compared with 10 reference cells. The application of a control group reduces the influence of global variations introduced through time like changes in the line current, raw materials and other operating conditions, since these are common to both groups. The Before-After-Control-Impact method is applied to remove the portion of the variance in each cell group due to the substantial variation between individual cells. In this respect the current and energy efficiency of the two groups of cells are also analysed before and after the experiment.

In order to minimize additional variations between the two groups of cells the location of the reference group is chosen next to the test group as demonstrated in Figure 4.2. At Aldel, the operating sequence follows the odd-numbered cells (2001→2183) and returns via the even-numbered cells (2184→2002). It is built upon a series of process measurements followed by discrete events: metal tapping, anode changing and covering (Sections 2.1.3 and 3.1.3). The interval between each activity is equal to one shift (8 hours), whereas the whole sequence takes 56 hours. This results in a 24 hours period without activities to stabilize the ensuing system dynamics.

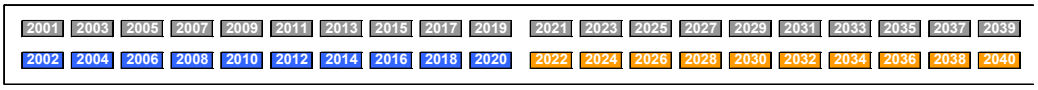


***Figure 4.2*** *Location of Test Cells (2002-2020) and Reference Cells (2022-2040) in Line 2 at Aldel*

The operational activities are planned based on the above-mentioned sequence. The test and reference cells are connected to the same secondary alumina silo and are applied with anodes from the same supplier (Section 4.2.2). Due to the rotating schedule, both groups are operated by all five working crews.

The experimental period must be long enough to ensure significant differences between the two groups rather than within one group. Typically a period of 200 to 400 days is used in the aluminium industry (Rutledge, 2008). The new control philosophy developed in this thesis is tested for a period of one full year. For the test and reference cells, the underlying process behaviour envelops and abnormality detection are not only studied separately, but also their mutual interactions are investigated (Sections 4.1.2.1 and 4.1.2.2).

A one-tailed paired t-test is used to identify significant differences in the means of the studied variables and abnormalities (Johnson, 1994). The relative variation is used to compare the variations in the two data sets. This is represented by the coefficient of variation, calculated as the standard deviation divided by the average. Differences in the variability between both groups of cells are determined using a paired F-test. A confidence level of 95% is used to distinguish between significant and trivial variations ($p\text{-value}<0.05$). This is then compared with the p-values for both differences in the mean and in relative variation.

The employment of the multivariate causally based control approach results in distinguished process behaviour and abnormality detection within the test and reference cells respectively. The variation within each group of cells is studied in relation to the productivity, and the current and energy efficiency. The main contributors to these variations are determined by correlation coefficients using linear regression (Johnson, 1994). In this respect a confidence level of 95% is used to distinguish between significant and trivial correlations.

However, correlation between 2 variables does not automatically imply a causal relationship. A detailed investigation of the paired correlations embedded in the theoretical development undertaken in Chapter 3 provides additional information about specific failure mechanisms and their consequences. These mechanisms are studied for both groups separately in order to determine the effectiveness of the new control philosophy based on the comparison of the group-specific behaviours (Section 4.1.2.3). This gives a better understanding of the main drivers for the observed process variability within these groups.

In case of highly correlated data as is present in the smelting process, Hotelling $T^2$ statistic has been found to be an appropriate control charting and analysis tool (Section 2.2.6). In this thesis Hotelling $T^2$ statistic is used to calculate three-dimensional natural behaviour envelops for every cell (Section 3.2.1.2). The calculations are based on a period of 30 measurements to eliminate short term variations and incorporate medium term variations like a continuous increase in the line current and variations in raw materials used (Section 3.3.1). The natural behaviour envelop is computed at a 95% confidence interval. Moreover, quantifiable, minor variations due to inevitable measurement errors and short term alumina feeding variations are incorporated in the core of the natural behaviour envelop.

Multivariate statistical projection methods (PCA and PLS) are applied to study the interplay in respect to the underlying process behaviour envelops, abnormality detection and specific failure mechanisms holistically (Section 4.1.2.4).

### 4.1.2 Experimental Set-Up

As discussed in Section 4.1.1 the new multivariate causally based control strategy is tested on 10 test cells and compared with 10 reference cells. The operational circumstances as well as the information generated by the new control philosophy are identical for both groups of cells. Also, both groups have the same control targets and the same information is available for data analysis. However, automatic control actions and the new diagnostic interventions (except from routine operations) are only applied to the test cells (Tables 3.6 and 3.7).

#### 4.1.2.1 Process Behaviour Envelops

The process variables of both groups of cells measured during the industrial experiments are listed in Table 4.1. Much of the required process data are recorded by cell-specific micro-computers automatically like the line current, cell voltage and noise. The alumina feeding is also registered online by the number of alumina shots and overfeeds per day. The number of $AlF_3$ shots is used to track the bath chemistry additions. Both the numbers of alumina and $AlF_3$ shots are based on volumetric dosing devices. Anode effects are detected by an abrupt and rapid increase of the cell voltage above 8 volts (Section 2.1.1).

| Process Parameters | Units | Method and Frequency |
|---|---|---|
| Line Current | kA | Continuously/electronically, 1 per 60 ms |
| Cell Voltage | V | Continuously/electronically, 1 per 60 ms |
| Noise | μΩ | Continuously/electronically, 1 per 60 ms |
| Alumina Shots | dumps/day | Continuously/electronically, per event |
| $AlF_3$ Shots | dumps/day | Continuously/electronically, per event |
| Number of Overfeeds | 1/day | Continuously/electronically, per event |
| Anode Effects | 1/cell·day | Continuously/electronically, per event |
| Bath Height | cm | Manual, 1 per 56 h |
| Iron | wt% | Manual, 1 per 56 h |
| Temperature | °C | Manual, 1 per 56 h |
| Liquidus | °C | Manual, 1 per 56 h |
| Superheat | °C | Manual, 1 per 56 h |
| Silicon | wt% | Manual, 1 per 56 h |
| $AlF_3$ Concentration | % | Manual, 1 per week |
| Cathode Resistance | μΩ | Manual, 1 per week |
| Anode Current Distribution | kA | Manual, 1 per week |
| Cathode Current Distribution | kA | Manual, 1 per week |

***Table 4.1*** *Measured Process Variables*

The remaining process variables are measured by a dedicated team of process operators. Cry-O-Therm measurements are carried out to determine the bath and liquidus temperatures (Figure 2.13). Additional bath samples are analysed to trace the $AlF_3$ concentration (Section 2.3.1.2). The liquid bath levels are determined with the iron rod method (Section 2.3.1.3), whereas the metal height is calculated using Equation 2.22. Extra measurements like the bottom resistance (Section 2.3.1.4), and anode and cathode current distributions are carried out to detect abnormalities in alumina feeding, anode and cathode conditions (sludge/ridge). Metal samples analyse the iron and silicon content of the aluminium produced.

In order to investigate the process behaviour for the test and reference cells systematically five groups of variables are composed (Figure 4.3). Due to the importance of good stability in the alumina concentration related to the overall process stability as stated in Section 3.1.1, the first group of variables is linked to alumina feed control (Group P1). Alumina feeding is

assessed based on the average and variability in the number of alumina shots, overfeeds and anode effects. The amount of sensible heat for alumina dissolution is influenced by the bath height. Iron levels in the metal are a crosscheck for high bath levels due to stub attack.

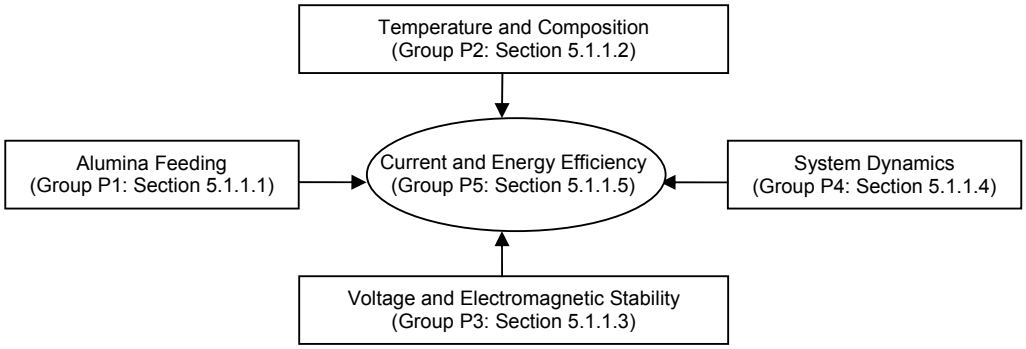


***Figure 4.3*** *Process Behaviour Groups and their Relationship*

The second group of variables (P2) is associated with the complex interactions between the mass and energy balance as demonstrated in Figure 3.11. The system dynamics are studied based on the development of the average and variability in the bath temperature, liquidus temperature and superheat. Together with the $AlF_3$ concentration these process variables also play an important role in the alumina dissolution effectiveness. In this respect silicon levels in metal are a crosscheck for the absence of side ledge protection. These interactions are studied in relation to the operating window for good cell performance (Figure 3.17).

The third group (P3) contains the cell voltages and electromagnetic stability. The variability in the bottom resistance and cathode current distribution may be related to dynamics in sludge and ridge formation and dissolution. The cell voltage incorporates the alumina concentration and heat generation within the cells (Section 1.3.2). The anode current distribution is linked to the accuracy of anode changing and therefore the electromagnetic stability of a cell.

The fourth group of variables (P4) contains the overall process stability represented by the ellipsoid volume and pinballing values as derived in this thesis (Sections 3.2.1.2 and 3.2.1.3).

The fifth group of variables (P5) contains the productivity, and current and energy efficiency and evaluate the effectiveness of the new control philosophy. Process variations within the test and reference cells related to the current and energy efficiency demonstrate the main process mechanisms acting within both groups of cells. A comparison between these group-specific behaviours is used to investigate these mechanisms in respect to the interventions of the new strategy. The results of the industrial experiments regarding the process behaviour envelops are discussed in Section 5.1.1.

#### 4.1.2.2 Abnormality Detection

An essential part of the new control philosophy is the detection, correction and eventual removal of process abnormalities. In order to investigate the role of process abnormalities in the test and reference cells five groups of abnormalities are composed (Figure 4.4). The first group (A1) studies predefined abnormalities to restrict the operating window according to its most efficient zone as given by Figure 3.17 and Table 3.2. Hotelling $T^2$ statistic is used to detect minor variations due to inevitable measurement errors and short term alumina feeding variation in Figure 3.12 and out of control behaviour (Section 3.2.1.3). High process velocity or "pinballing" as given by Equation 3.12 indicates the existence of an abnormality (event).

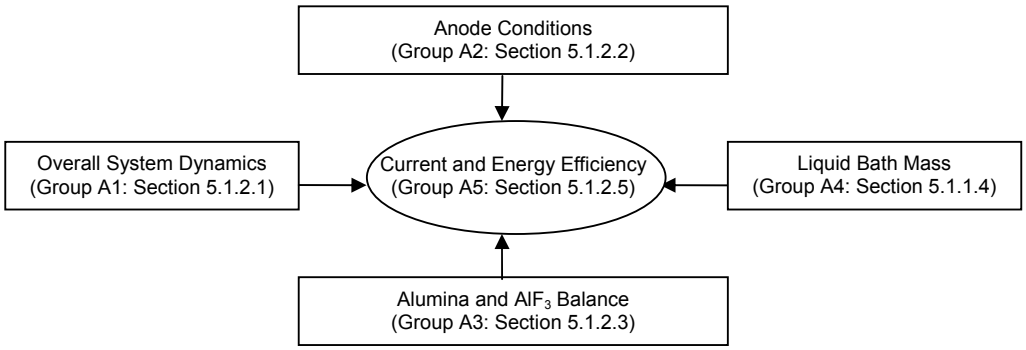


***Figure 4.4*** *Abnormality Detection Groups and their Relationship*

The total duration of abnormalities is one measure of the time the smelting process was not operating at its maximum potential. Further destabilizing of the self-regulating characteristics of the smelting process occurs if the original abnormality is not diagnosed or corrected. Under these process conditions the sensitivity and specificity of the detection of root causes of abnormality are hindered over time. Furthermore, the subsequent abnormalities provide no direct information of their origin and therefore root cause analysis is then less effective in identifying the original cause of variation.

The second group of abnormalities (A2) lists specific problems in the anode conditions (Table 3.3). This table lists a number of soft sensors which are used to identify abnormalities regarding anode setting procedures ("plunger hits anode") and automatic spike detection (ANSPA). Other abnormalities are based on voltage drop (clamp drop) and anode current distribution measurements (slipped anodes, anode spikes, anode drop off or clad failure and anode changing accuracy).

The third group (A3) contains abnormalities associated with alumina and $AlF_3$ feeding (Table 3.4). This table lists a number of direct automatic sensors and predefined soft sensors which

are used to identify hardware problems of the alumina and $AlF_3$ feed equipment. In addition, abnormal process conditions regarding the alumina dissolution effectiveness are detected.

The fourth group (A4) is linked to abnormalities in liquid bath mass and height calculations, which are also detected by soft sensors as listed in Table 3.5. These abnormalities are related to the variability in the liquid bath mass and therefore relate back to the effectiveness of alumina feeding, as well as control of the anode cathode distance (and therefore current efficiency) due to resistance regulation to the target value.

As discussed in Section 4.1.2.1 the effectiveness of the new control strategy is examined against the current and energy efficiency. The fifth group (A5) contains the most important abnormalities which result in losses in current and energy efficiency. Online Pareto analysis is used to identify the most frequent abnormalities (Figure 3.23). Moreover, group-specific detected abnormalities provide information about common abnormalities involved in the overall system dynamics within the test and reference cells respectively. The results of the industrial experiments regarding abnormality detection are discussed in Section 5.1.2.

#### 4.1.2.3 Specific Failure Mechanisms and Consequences

As identified in Figure 4.1 variables related to both process behaviour and to abnormality detection feed into the specific failure mechanisms. Chapter 3 identifies strong interactive multivariate characteristics of the smelting process resulting in complex system dynamics. The complex interactions between the bath temperature, composition and current distribution imbalances are exacerbated by the employment of power modulation, increased line current and increased variability in raw materials used. Therefore imbalances must be sensed quickly and their causes corrected or removed in a timely manner. Paired correlations between process behaviours and abnormality detection within either the test or reference cells provide a complete picture of their group-specific failure mechanisms.

In order to verify these group-specific failure mechanisms for the test and reference cells five groups of paired correlations are composed. The statistically significant paired correlations (in Tables 5.9 and 5.10) will be used to confirm the diagnosis of causes for the multivariate control system. The first group of correlations (F1) is linked to alumina feeding with respect to the stability of the smelting process. The most important paired correlations between the averages, variability and abnormalities in the number of alumina shots, overfeeds and anode effects are verified.

The second group (F2) lists the many significant correlations between the mass and energy balance related variables. Although the underlying root causes are complex (Figure 3.11),

abnormalities in these dynamics can be related back to cause-specific failure mechanisms in the control system.

The third group (F3) is linked to liquid bath mass variations. In general, liquid bath mass variations are connected to variations in the bath levels or superheat. However, a weak correlation between bath levels and inventory and between superheat and inventory were found in other studies (Figure 2.8). In this thesis soft sensors are developed to trace rapid changes in liquid bath mass (Section 3.2.2.2). Correlations between process variables and a detected increase or decrease in the bath mass investigate the reliability of these soft sensors.

The most efficient operating zone for smelting cells is associated with maximum process stability (Welch, 1998). The fourth group (F4) deals with paired correlations between the cell voltage, noise, bottom resistance, ellipsoid volume, pinballing and other measured process variables. This provides a better understanding of the underlying failure mechanisms causing increased variations.

The last group (F5) contains paired correlations in relation to cause-specific abnormalities in alumina feeding and anode conditions. The results of the industrial experiments regarding the specific failure mechanisms are discussed in Section 5.1.3.

#### 4.1.2.4 Multivariate Statistical System Dynamics

Principal component analysis (PCA) is used to identify the significant principal components and their individual contributors involved in the system dynamics for the test and reference cells respectively. These group-specific variations are compared with the underlying process behaviour envelops, abnormality detections, and specific failure mechanisms (Figure 4.1). The effectiveness of the new philosophy developed in this thesis is examined using partial least square analysis (PLS) against the quality data represented by the productivity, current efficiency and energy consumption (Groups P5, A5). A 95% confidence interval is used to describe the multivariate statistical system dynamics for the two groups of cells. The results are discussed in Section 5.1.4.

### 4.1.3 Hypothesis Testing

As described in Section 4.1.2 the industrial experiments examine the underlying process behaviour envelops, abnormality detection, specific failure mechanisms and more complex multivariate statistical system dynamics for the test and reference cells. These investigations are used to test the two hypotheses postulated in Chapter 3. The first hypothesis is a prevailing sludge cycle caused by incomplete alumina dissolution driving liquid bath mass

variations and increased alumina feeding until large and prolonged bath temperature and composition variation is produced. Section 4.1.3.1 details the experimental design for the investigation of this hypothesis.

The second hypothesis is that multivariate statistically defined envelops for individual cell behaviour can provide detection and causal diagnosis of process abnormalities which then improve the ability to control the system dynamics in Hypothesis 1. Continual recalculation of the natural behaviour envelops is designed to trigger earlier detection of abnormalities and improve decision-making over time as the operational variation reduces. Section 4.1.3.2 describes the experimental and control design for the investigation of this hypothesis.

#### 4.1.3.1 Sludge Cycle Driving Liquid Bath Mass Variations

The existence of a sludge cycle within the system dynamics of the test and reference cells is investigated in detail in this thesis. For the test cell, the effectiveness of the alumina feeding is incorporated into the new control philosophy, including the three-dimensional natural behaviour envelop, cause-specific detection of abnormalities and additional control actions to the basic alumina feeding strategy (Section 3.3.3.1). This leads to recognised process behaviours such as accelerated feeding cycles due to poor alumina dissolution, and specific abnormality detection such as breaker or feeder mechanical malfunction for the test cells. Through this process of statistical system identification, the dominance of the sludge cycle in the overall system dynamics in the two groups of cells is determined (Hypothesis 1).

In addition to the industrial experimentation with the new control philosophy (Hypothesis 2), liquid bath and metal measurements of medium term variations are carried out. These medium term effects are followed over a period of 2 anode rotas for one cell. The liquid bath mass is determined using strontium carbonate ($SrCO_3$) as a tracer and the metal mass is measured with a metal tracer (Cu) as described in Section 2.3.1.3. These measurements are carried out before and after the employment of the new control philosophy. The results of the industrial experiments regarding the sludge cycle and the additional measurements of liquid mass variations within smelting cells are discussed in Section 5.2.1.

#### 4.1.3.2 Multivariate Causally Based Control

The employment of a multivariate causally based control approach is investigated based on the effectiveness of the abnormality detection and control responses to the overall process state for the test cells. In this thesis the ellipsoid volume and pinballing value are used as measures of the stability of the underlying system dynamics. The correlations between these variables, and other process variables and detected abnormalities as discussed in Section 4.1.2 identity the benefit of this control approach.

The incorporation of an advanced system for abnormality detection follows Deming's thinking that problems are best solved by attempting to correct and eventually eliminate the root causes. Online Pareto analysis is used to identify the most frequent abnormalities interfering in the overall system dynamics for the test and reference cells. The results of the industrial experiments regarding the effectiveness of the multivariate causally based control approach to smelting cells are discussed in Section 5.2.2.

## 4.2 Conditions for Industrial Experiments

In comparison with laboratorial experiments additional variations are embedded in industrial testing. These variations are not only related to the scale, but are also linked to variations in the energy and raw material inputs, disturbances in the overall equipment effectiveness, changing environmental conditions and human interference (Rutledge, 2008). Actually, the motivation for advanced control is the necessity to increase the flexibility in energy input and raw material variations as discussed in Section 1.1 and during tests many such variations occurred. Therefore the new control philosophy is examined based on the performance of a test group compared with a reference group (Section 4.1.1). However, the system dynamics of the two groups of cells are also monitored over time in order to detect improvements in their internal process stability. The response of the two groups forms part of the assessment of the effectiveness of the control system (Hypothesis 2).

### 4.2.1 Variations in Energy Input

The operating window of the smelting process is set by the intensity and variations in the line current. As emphasized in Section 1.1, smelters have increased their current substantially in order to increase the productivity. An increase in line current has a profound impact to the system dynamics and associated process stability. Moreover, power modulation has been introduced to increase the flexibility of the energy use. Under these conditions the current is reduced or switched off for a particular period of time resulting in large energy deficiencies. The experiments are carried out at a historically maximum current (for Aldel) and a variety of energy management scenarios (Sections 4.2.1.1 and 4.2.1.2).

#### 4.2.1.1 Line Current

At Aldel, the line current has been increased by 41 kA after the commissioning of a hugely complex retrofit of the base technology (Figure 4.5). Although a significant reduction in the energy consumption was realised, the total internal heat generation has gone up by 36% to a level of 340 kW. Due to the implementation of larger anodes to keep the anode current density within acceptable operating limits (0.83 $A \cdot cm^{-2}$ in 2008), the liquid bath mass has

been reduced by 10%. The combination of a higher line current in a lower bath mass has led to an increase in the heat dissipation and alumina dissolution per cubic centimetre of liquid bath of 60%.

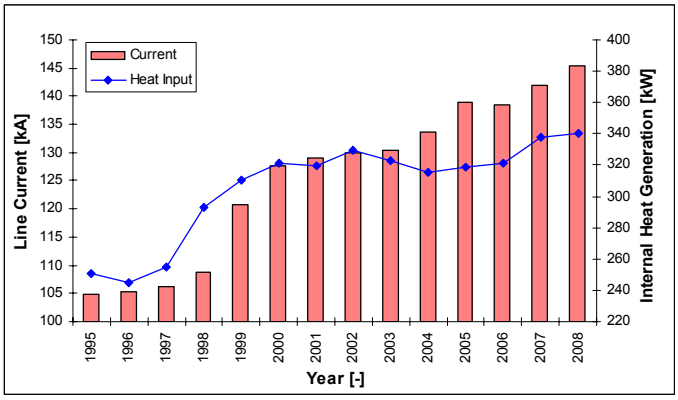


***Figure 4.5*** *Development of Line Current versus Internal Heat Generation at Aldel*

In order to withstand the increased heat dissipation within the cells two major changes have been implemented in 2003. The ventilation design of the cells at Aldel was improved in order to maintain sufficient ledge to protect the sidewall lining against corrosive electrolyte (Figure 2.5). A significant reduction in the air and steel temperature and a growth of the average side ledge was achieved (Section 2.1.2). Furthermore, Cry-O-Term measurements have been implemented to control the electrolyte and liquidus temperatures (and thus the superheat) simultaneously (Section 2.3.1.2). At Aldel, the cells are operated well above the theoretical calculated MHD stability limit of 135 kA (Stam and Kloetstra, 2004). During the experiments, from January to March 2008, the current was increased to 147 kA. By the end of the year the current was reduced to 137 kA due to the (upcoming) economic crisis (Figure 4.6).

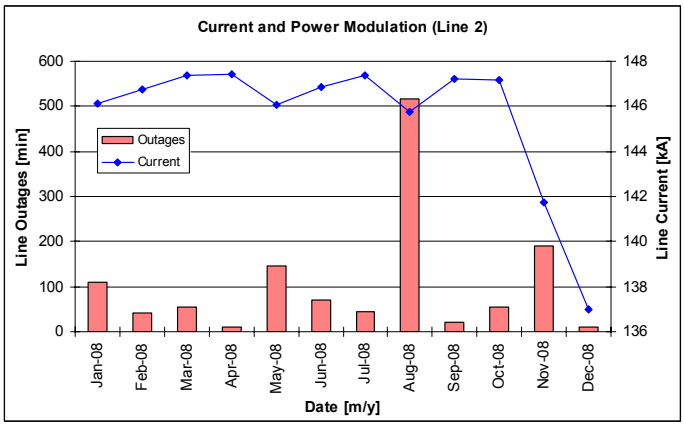


***Figure 4.6*** *Development of Line Current and Current Outages in Line 2 at Aldel*

#### 4.2.1.2 Power Modulation

While energy demand has strong temporal variation (from minutes up to seasonal effects), Aldel has built up a power management strategy in order to reduce its overall energy costs (Stam and Schaafsma, 2007). In general, this regulation comprises a few different scenarios. The employment of a day-night rhythm results in a continuous difference in base load over the lines between the day and night. A difference of 5 kA results in a variation in the bath and liquidus temperature of 5°C (Figure 4.7). It is also evident from these measurements that the reaction in the increase of the temperature is predominant, and initiates a temporary rise of the superheat (see blue dotted circle). This indicates a slower, but a more smooth adjustment of the bath chemistry. From January to October 2008 a day-night rhythm of 10 kA was applied to the cells at Aldel.

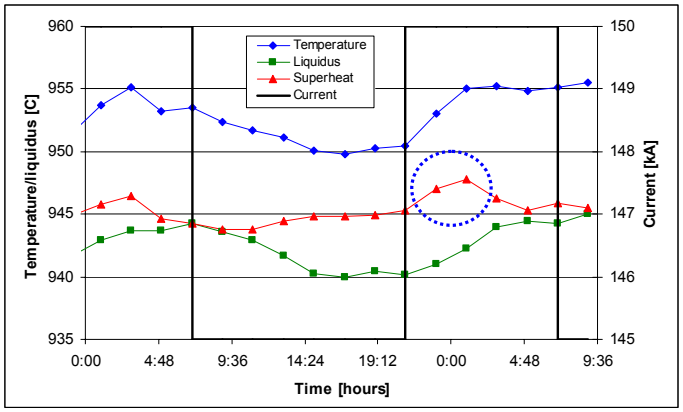


***Figure 4.7*** *Process State Variations due to Day-Night Rhythm (Stam et al. 2007)*

Other energy management scenarios applied at Aldel contains a current reduction and/or outages in the range of 15 MWh/day up to 560 MWh/day (with and without a pre-warning) (Stam and Schaafsma, 2007). Figure 4.8 shows the corresponding process state variations for a line current interruption of one hour. Initially a decrease in bath temperature leads to an identical decrease in the superheat. According to the self-regulating mechanism as depicted in Figure 2.4 ledge formation slows down the decrease in bath and liquidus temperature due to reduced heat losses through the sides and bath chemistry adjustments.

As described in case of day-night rhythm a predominant increase in the bath temperature is found over an increase in the liquidus point after the restart of the line current. A temporary different relationship between mass and energy balance indicates the existence of time lags within the smelting process. Precautionary mass and energy balance adjustments like an increase of the cell voltage and alumina feeding are used to counteract the ensuing system dynamics and promote a quick recovery of the smelting process to its original state (Section

3.2.2.4). During the experiments the total duration of current interruptions added up to 1268 minutes as demonstrated in Figure 4.6.

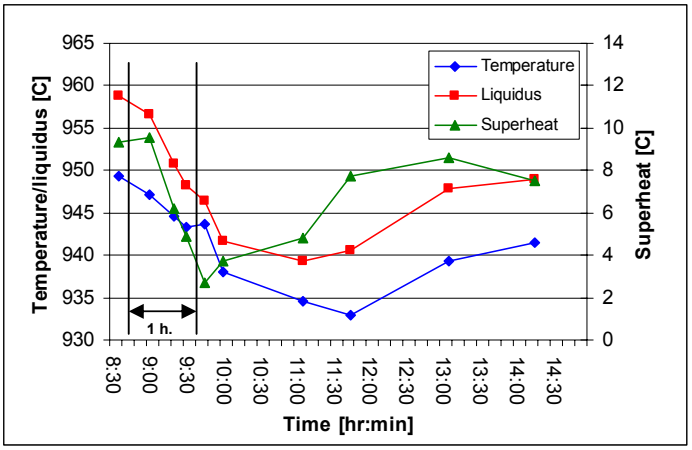


***Figure 4.8*** *Process State Variations due to 1 h Shutdown (Stam and Schaafsma, 2007)*

### 4.2.2 Variations in Raw Material Inputs

Alumina and carbon anodes are the main raw material inputs to the smelting process as derived from the primary reaction given by Equation 1.1. There is a gradual degradation and variability in the quality of some of the raw materials used in the process (Section 1.1). This has a profound impact to the system dynamics and associated process stability. However, the industrial experiments are carried out within the specification limits for regular operations at Aldel (Tables 4.2 and 4.3).

| | Specification | Average | Stdeviation | |
|---|---|---|---|---|
| **$SiO_2$** | <0.015 | 0.012 | 0.002 | % |
| **$Fe_2O_3$** | <0.025 | 0.023 | 0.003 | % |
| **CaO** | <0.030 | 0.011 | 0.003 | % |
| **$Na_2O$** | 0.30-0.40 | 0.34 | 0.017 | % |
| **LOI (300-1100C)** | <0.8 | 0.7 | 0.1 | % |
| **Alpha** | <8.0 | 2.6 | 1.2 | % |
| **B.E.T.** | 65-75 | 73.2 | 2.6 | $m^2/g$ |
| **> 150 um** | <5.0 | 3.1 | 1.0 | µm |
| **> 75 um** | | 66.5 | 4.1 | µm |
| **< 45 um** | <8.0 | 6.8 | 1.1 | µm |
| **< 20 um** | <1.5 | 0.9 | 0.3 | µm |
| **Bulk Density** | >1.0 | 1.17 | 0.03 | $kg/dm^3$ |
| **Attrition index** | <12.0 | 11.4 | 1.7 | % |

***Table 4.2*** *Primary Alumina Data based on 11 ktons Shipments from Auginish (2008)*

| | Specification | Average | Stdeviation | |
|---|---|---|---|---|
| **Apparent Density** | >1.59 | 1.60 | 0.015 | kg/dm$^3$ |
| **Electr. Resistance** | <56 | 53.3 | 2.1 | µΩm |
| **Flexural Strength** | >10 | 11.9 | 1.6 | MPa |
| **Air Permeability** | <1.5 | 1.21 | 0.37 | nPm |
| **CO2 Reactivity** | >90 | 92.2 | 1.8 | % |
| **Dust** | <3 | 1.3 | 0.8 | % |
| **Air Reactivity Residue** | >86 | 91.1 | 0.4 | % |
| **Dust** | <2 | 0.5 | 1.8 | % |
| **S** | <1.3 | 0.98 | 0.03 | % |
| **Si** | <200 | 153 | 25 | ppm |
| **Fe** | <350 | 316 | 14 | ppm |
| **Na** | <120 | 70 | 12 | ppm |

***Table 4.3*** *Anode Data based on 1.1 ktons Shipments from Rheinfelden (2008)*

### 4.2.3 Industrial Testing Equipment and Instruments

The industrial experiments are carried out under normal operating conditions regarding the application of the equipment and instruments. Section 4.2.3.1 discusses the underlying cell design applied to the test and reference cells. In this respect the cell design is adjusted to a continuous increase of the line current and employment of power modulation as discussed in Section 4.2.1. Furthermore, the devices applied for control and additional measurements are described in Section 4.2.3.2.

#### 4.2.3.1 Cell Design

As shown in Figure 4.5 the current is steadily increased over time resulting in a significantly increase in the internal heat generation in the cells at Aldel. In order to handle the increased heat generation several changes to the cells have been implemented. From November 2001 the quality of the cathode blocks was changed from 100% graphitic into graphitized blocks, which have a significant higher thermal conductivity. Also, the quality of the cathode bars were changed from steel-37 into ultra low carbon steel (C<0.01%) and the width of the bars was increased from 70 to 100 mm. These changes result in an increase in heat dissipation and a reduction in heat generation due to a lower cathode resistance (Figure 4.9).

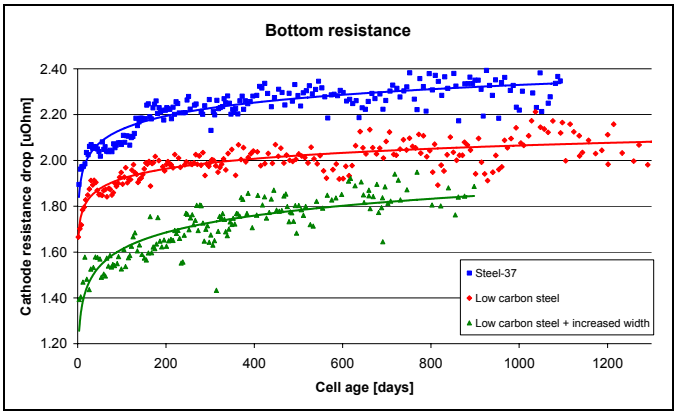


***Figure 4.9*** *Cathode Resistance at Aldel (normal, low C steel, thicker bars)*

The individual ages of the test and reference cells at the start of the industrial experiments are presented in Table 4.4. The cell ages at the end of the trail are depicted in Table 4.5. In 2008 the average failure age of the cells at Aldel was 2128 days. During 2008 one test cell was changed for a new design. Three reference cells were replaced during the trail, whereas one new cell was started up at the start of the experiments. The start-up phase of new cells incorporates increased process variability. Especially chemistry control is difficult due to an increased accumulation of sodium in the cathode blocks early in its lifetime; however, the application of graphitized blocks minimizes these effects (Figure 2.3). In order to eliminate the impact of the start-up and early operation of the new cells in the investigation the process data of the first month of operation are excluded from the analyses.

| Test Cells | Age [days] | Reference Cells | Age [days] |
|---|---|---|---|
| **2002** | 1200 | **2022** | 541 |
| **2004** | 1130 | **2024** | 458 |
| **2006** | 440 | **2026** | 549 |
| **2008** | 451 | **2028** | 1140 |
| **2010** | 1095 | **2030** | 744 |
| **2012** | 1101 | **2032** | - |
| **2014** | 845 | **2034** | 2343 |
| **2016** | 298 | **2036** | 1917 |
| **2018** | 1171 | **2038** | 1900 |
| **2020** | 905 | **2040** | 975 |
| **AVG** | 864 | **AVG** | 1174 |

***Table 4.4*** *Cell Age at January 1st, 2008*

| Test Cells | Age [days] | Reference Cells | Age [days] |
|---|---|---|---|
| **2002** | 192 | **2022** | 907 |
| **2004** | 1496 | **2024** | 824 |
| **2006** | 806 | **2026** | 915 |
| **2008** | 817 | **2028** | 1506 |
| **2010** | 1461 | **2030** | 1110 |
| **2012** | 1467 | **2032** | 361 |
| **2014** | 1211 | **2034** | 216 |
| **2016** | 664 | **2036** | 74 |
| **2018** | 1537 | **2038** | 94 |
| **2020** | 1271 | **2040** | 1341 |
| **AVG** | 1092 | **AVG** | 735 |

***Table 4.5*** *Cell Age at January 1st, 2009*

At Aldel, the cell design has one major constraint associated with alumina feeding. Originally the cells were equipped with side feed technology. This technology requires sufficient space between the side ledge and anodes, which results in limited distance between both rows of anodes (Figure 1.1). As discussed in Section 1.1 the cells were upgraded with point feed technology to minimize the alumina doses to 2 kg per dump (Section 2.1.3). However, the centre channel stayed at the limited width of 110 mm due to the necessity of larger anodes to maintain acceptable anode current densities (0.83 $A \cdot cm^{-2}$ in 2008) (Figure 4.10). This channel width is approximately half the recognized minimum for feeding channel width in other smelting technologies.

***Figure 4.10*** *Point Feed Hole for Alumina Feeding at Aldel*

#### 4.2.3.2 Measurement Devices

As stated in Section 4.1.1 the operational sequence is built upon a series of measurements followed by discrete events: metal tapping, anode changing and corresponding covering. At Aldel, the duration of this sequence is derived from the anode changing rota. An anode rota of 28 days was applied to the cells during the industrial experiments. Due to a double anode changing procedure and 24 anodes per cell, this leads to a 56 hours cycle (Section 3.1.3).

The bath and liquidus temperature (and therefore the superheat) are measured with the Cry-O-Therm system (Figure 4.11). The sensor and temperature curve are presented in Figure 2.13. Both the disposable couples and equipment are monitored with predefined calibrating procedures to minimize variations between sensors as well as over time. Bath compositions are analysed with XRD, but are not applied for regular control actions (Section 2.3.1.2).

***Figure 4.11*** *Bath and Liquidus Temperature Measurements at Aldel*

The bath and metal heights are measured using the iron rod method as described in Section 2.3.1.3). At Aldel, these rods are calibrated daily with a preformed template by the operators of the measurement team. For control purposes the metal height is also calculated using Equation 2.22 (Section 2.3.2). The operators also check devices for voltage drop, anode, and cathode current distribution measurements. The cathode condition is examined using a combined sensor for temperature and voltage drop (Section 2.3.1.4). The moment of the process measurements related to the operating cycle is important and therefore a fixed point provides the lowest and most predictable influence to the system dynamics (Sections 2.3.1.5 and 4.1.1).

# Chapter 5 Results and Discussion

In this chapter the main results of the industrial experiments with the new control philosophy are presented and discussed. These experiments are carried out on a group of 10 test cells and compared with 10 reference cells as described in Section 4.1.1. The main results are discussed in Section 5.1. In Section 5.2 these results are used to test the hypotheses postulated in this thesis. In order to investigate these hypotheses additional measurements were carried out and these are discussed. It is shown that the alumina dissolution effectiveness plays an essential role in achieving maximum current and energy efficiency. The sludge cycle postulated earlier drives liquid bath mass variations and increased alumina feeding. Moreover, advanced detection of abnormalities using the multivariate control approach as described in Section 3.3 is shown to dampen overcorrection by automatic control actions and also to improve subsequent human decision-making on individual cells.

## 5.1 Main Results

Section 5.1.1 presents the main results of the industrial experiments regarding the ensuing process behaviour for both the test and reference cells. The detection and removal or cause-specific correction of abnormalities leads to more stable and predictable system dynamics as discussed in Section 5.1.2. Furthermore, specific failure mechanisms are identified for both groups of cells separately (Section 5.1.3), and multivariate statistical analyses identify the driving parameters in the more complex system dynamics of both cell groups (Section 5.1.4).

### 5.1.1 Process Behaviour Envelops

The measured process variables of the test cells (2002-2020) and the reference cells (2022-2040) are listed in Tables 5.1 and 5.3 respectively and are divided into five groups (P1-P5) (Section 4.1.2.1). The averages (AVG) and coefficients of variation (CV) of these variables are determined to investigate the process behaviour with respect to the ability to control the cells to a given target and within a tight window (Figure 3.17). A confidence level of 95% (p-value <0.05) is used to identify significant differences between both groups (Section 4.1.1).

Group P1 (process variables 1-10) is linked to alumina feeding (Section 5.1.1.1). Group P2 (variables 11-20) contains bath temperatures and compositions, which define the complex interactions between the mass and energy balance in smelting cells (Section 5.1.1.2). Group P3 (variables 21-28) represents cell voltages and electromagnetic stability (Section 5.1.1.3). Group P4 (variables 29-32) is related to the system dynamics and contains the ellipsoid volume and pinballing (Section 5.1.1.4). Group P5 (variables 71-73) summarizes the current and energy efficiency, and the productivity.

| | | | | Test Cells | | | | | | | | | | | | |
|---|---|---|---|---|---|---|---|---|---|---|---|---|---|---|---|---|
| Gr. | Nr. | Process Variables | | 2002 | 2004 | 2006 | 2008 | 2010 | 2012 | 2014 | 2016 | 2018 | 2020 | AVG | Units | P-value |
| Group P1 | 1 | Alumina Shots | AVG | 1955 | 2030 | 2013 | 2011 | 1978 | 1966 | 2009 | 2037 | 2036 | 1994 | 2005 | kg/day | 0.000 |
| | 2 | | CV | 0.11 | 0.08 | 0.08 | 0.08 | 0.08 | 0.10 | 0.09 | 0.08 | 0.07 | 0.09 | 0.09 | - | 0.233 |
| | 3 | Number of Overfeeds | AVG | 13.4 | 14.6 | 14.6 | 14.7 | 13.9 | 14.0 | 14.7 | 14.9 | 15.2 | 14.3 | 14.5 | 1/day | 0.000 |
| | 4 | | CV | 0.26 | 0.23 | 0.22 | 0.23 | 0.23 | 0.25 | 0.25 | 0.21 | 0.20 | 0.25 | 0.23 | - | 0.004 |
| | 5 | Anode Effects | AVG | 0.23 | 0.39 | 0.25 | 0.18 | 0.17 | 0.31 | 0.21 | 0.32 | 0.16 | 0.22 | 0.25 | 1/cellday | 0.000 |
| | 6 | | CV | 3.0 | 1.8 | 2.6 | 2.6 | 2.9 | 2.1 | 2.9 | 2.6 | 2.5 | 2.3 | 2.5 | - | 0.000 |
| | 7 | Bath Height | AVG | 19.9 | 19.9 | 20.0 | 19.9 | 19.3 | 19.5 | 19.6 | 20.0 | 19.6 | 19.4 | 19.7 | cm | 0.000 |
| | 8 | | CV | 0.14 | 0.13 | 0.12 | 0.14 | 0.13 | 0.13 | 0.13 | 0.14 | 0.12 | 0.13 | 0.13 | - | 0.237 |
| | 9 | Iron | AVG | 0.23 | 0.15 | 0.14 | 0.12 | 0.11 | 0.13 | 0.15 | 0.18 | 0.17 | 0.12 | 0.15 | % | 0.056 |
| | 10 | | CV | 0.63 | 0.27 | 0.19 | 0.19 | 0.22 | 0.31 | 0.26 | 0.21 | 0.62 | 0.20 | 0.13 | - | 0.000 |
| Group P2 | 11 | Temperature | AVG | 966.6 | 966.7 | 963.4 | 964.9 | 968.5 | 968.6 | 966.4 | 962.1 | 967.7 | 966.3 | 966.1 | °C | 0.453 |
| | 12 | | CV | 0.021 | 0.017 | 0.017 | 0.019 | 0.015 | 0.015 | 0.021 | 0.018 | 0.015 | 0.018 | 0.018 | - | 0.034 |
| | 13 | Liquidus | AVG | 952.2 | 954.9 | 951.5 | 952.9 | 957.2 | 954.7 | 954.7 | 950.1 | 958.2 | 954.5 | 954.3 | °C | 0.021 |
| | 14 | | CV | 0.020 | 0.017 | 0.018 | 0.020 | 0.015 | 0.015 | 0.021 | 0.018 | 0.015 | 0.018 | 0.018 | - | 0.042 |
| | 15 | Superheat | AVG | 14.5 | 11.9 | 11.9 | 12.5 | 11.2 | 12.5 | 11.7 | 11.9 | 9.8 | 11.8 | 11.9 | °C | 0.000 |
| | 16 | | CV | 0.54 | 0.49 | 0.45 | 0.50 | 0.46 | 0.49 | 0.59 | 0.51 | 0.53 | 0.56 | 0.52 | - | 0.000 |
| | 17 | $AlF_3$ | AVG | 11.4 | 11.9 | 12.3 | 11.6 | 10.9 | 10.9 | 11.3 | 12.1 | 10.8 | 11.2 | 11.3 | % | 0.113 |
| | 18 | | CV | 0.16 | 0.18 | 0.23 | 0.21 | 0.23 | 0.21 | 0.21 | 0.24 | 0.21 | 0.19 | 0.21 | - | 0.486 |
| | 19 | Silicon | AVG | 0.069 | 0.051 | 0.063 | 0.050 | 0.052 | 0.053 | 0.053 | 0.054 | 0.057 | 0.052 | 0.055 | % | 0.405 |
| | 20 | | CV | 0.41 | 0.27 | 0.28 | 0.19 | 0.22 | 0.31 | 0.26 | 0.21 | 0.62 | 0.20 | 0.34 | - | 0.477 |
| Group P3 | 21 | Cell voltage | AVG | 4.481 | 4.468 | 4.467 | 4.462 | 4.463 | 4.448 | 4.456 | 4.468 | 4.452 | 4.454 | 4.461 | V | 0.000 |
| | 22 | | CV | 0.016 | 0.016 | 0.013 | 0.014 | 0.014 | 0.014 | 0.013 | 0.015 | 0.012 | 0.014 | 0.014 | - | 0.000 |
| | 23 | Cathode Resistance | AVG | 1.41 | 1.43 | 1.62 | 1.54 | 1.55 | 1.49 | 1.59 | 1.43 | 1.58 | 1.54 | 1.52 | μΩ | 0.035 |
| | 24 | | CV | 0.13 | 0.09 | 0.06 | 0.07 | 0.09 | 0.05 | 0.09 | 0.22 | 0.06 | 0.14 | 0.12 | - | 0.000 |
| | 25 | Noise | AVG | 0.096 | 0.096 | 0.077 | 0.059 | 0.057 | 0.064 | 0.064 | 0.074 | 0.058 | 0.066 | 0.070 | μΩ | 0.004 |
| | 26 | | CV | 1.05 | 0.61 | 0.69 | 0.66 | 0.57 | 0.63 | 0.63 | 0.77 | 0.55 | 0.76 | 0.75 | - | 0.005 |
| | 27 | Anode Current | CV | 0.20 | 0.18 | 0.20 | 0.19 | 0.17 | 0.18 | 0.19 | 0.19 | 0.18 | 0.19 | 0.19 | - | |
| | 28 | Cathode Current | CV | 0.17 | 0.14 | 0.15 | 0.15 | 0.14 | 0.14 | 0.16 | 0.14 | 0.16 | 0.14 | 0.15 | - | |
| Group P4 | 29 | Ellipsoid Volume | AVG | 132473 | 64381 | 95839 | 116828 | 79186 | 112186 | 167167 | 118377 | 76840 | 124292 | 107733 | $°C^2$ | 0.000 |
| | 30 | | CV | 0.73 | 1.00 | 0.30 | 0.82 | 0.41 | 1.04 | 0.35 | 0.67 | 0.51 | 0.90 | 0.83 | - | 0.000 |
| | 31 | Pinballing | AVG | 19.1 | 18.1 | 20.0 | 20.4 | 19.6 | 20.7 | 19.8 | 20.3 | 18.6 | 20.7 | 19.8 | $°C^{2/3}$ | 0.011 |
| | 32 | | CV | 0.72 | 1.00 | 0.56 | 0.98 | 0.59 | 0.98 | 0.62 | 0.97 | 0.58 | 1.00 | 0.63 | - | 0.000 |
| Group P5 | 71 | Productivity | AVG | 1104 | 1134 | 1111 | 1135 | 1075 | 1103 | 1112 | 1143 | 1141 | 1104 | 1116 | kg/cellday | 0.165 |
| | 72 | Current Efficiency | AVG | 93.45 | 96.19 | 94.17 | 96.34 | 91.11 | 93.59 | 94.21 | 96.89 | 96.82 | 93.54 | 94.63 | % | 0.162 |
| | 73 | Energy | AVG | 14.29 | 13.84 | 14.14 | 13.80 | 14.60 | 14.16 | 14.09 | 13.74 | 13.70 | 14.19 | 14.05 | kWh/kg | 0.303 |

*(AVG): Average; (CV): Coefficient of Variation (=Standard Deviation/Average); AVG(CV): Average Coefficient of Variation for Full Data Set*

***Table 5.1*** *Process Variables of the Test Cells (2002-2020)*

| Current Efficiency | | | Energy Consumption | | |
|---|---|---|---|---|---|
| Nr. | Process Variable | Correlation Coefficient | Nr. | Process Variable | Correlation Coefficient |
| 1 | Alumina Shots | 0.80 | 3 | Number of Overfeeds | -0.82 |
| 3 | Number of Overfeeds | 0.79 | 1 | Alumina Shots | -0.80 |
| 4 | Number of Overfeeds (CV) | -0.64 | 4 | Number of Overfeeds (CV) | 0.63 |

***Table 5.2*** *Correlation between Process Variables and Overall Efficiency in the Test Group*

| | | | | Reference Cells | | | | | | | | | | | | |
|---|---|---|---|---|---|---|---|---|---|---|---|---|---|---|---|---|
| Gr. | Nr. | Process Variables | | 2022 | 2024 | 2026 | 2028 | 2030 | 2032 | 2034 | 2036 | 2038 | 2040 | AVG | Units | P-value |
| Group P1 | 1 | Alumina Shots | AVG | 2027 | 1899 | 1941 | 1985 | 1951 | 1858 | 1987 | 1843 | 1972 | 1891 | 1938 | kg/day | 0.000 |
| | 2 | | CV | 0.07 | 0.08 | 0.08 | 0.09 | 0.08 | 0.09 | 0.07 | 0.11 | 0.10 | 0.08 | 0.09 | - | 0.233 |
| | 3 | Number of Overfeeds | AVG | 14.8 | 11.6 | 12.9 | 13.8 | 13.0 | 11.4 | 14.0 | 10.4 | 13.1 | 11.4 | 12.7 | 1/day | 0.000 |
| | 4 | | CV | 0.22 | 0.26 | 0.25 | 0.25 | 0.26 | 0.30 | 0.22 | 0.33 | 0.30 | 0.24 | 0.28 | - | 0.004 |
| | 5 | Anode Effects | AVG | 0.11 | 0.07 | 0.15 | 0.16 | 0.15 | 0.07 | 0.10 | 0.11 | 0.20 | 0.06 | 0.12 | 1/cellday | 0.000 |
| | 6 | | CV | 3.2 | 4.5 | 3.1 | 2.7 | 3.0 | 3.8 | 3.8 | 4.1 | 2.6 | 4.8 | 3.4 | - | 0.000 |
| | 7 | Bath Height | AVG | 18.9 | 19.5 | 18.2 | 19.2 | 18.6 | 18.9 | 19.5 | 19.2 | 19.6 | 19.3 | 19.0 | cm | 0.000 |
| | 8 | | CV | 0.13 | 0.17 | 0.17 | 0.16 | 0.17 | 0.17 | 0.22 | 0.19 | 0.15 | 0.14 | 0.14 | - | 0.237 |
| | 9 | Iron | AVG | 0.11 | 0.20 | 0.12 | 0.14 | 0.11 | 0.13 | 0.22 | 0.23 | 0.23 | 0.13 | 0.16 | % | 0.056 |
| | 10 | | CV | 0.67 | 0.71 | 0.72 | 0.87 | 0.82 | 0.78 | 0.81 | 0.77 | 0.57 | 0.66 | 1.24 | - | 0.000 |
| Group P2 | 11 | Temperature | AVG | 965.0 | 964.1 | 963.9 | 966.6 | 966.6 | 969.7 | 964.6 | 970.1 | 966.5 | 966.4 | 966.2 | °C | 0.453 |
| | 12 | | CV | 0.017 | 0.016 | 0.015 | 0.016 | 0.017 | 0.017 | 0.014 | 0.020 | 0.022 | 0.016 | 0.017 | - | 0.034 |
| | 13 | Liquidus | AVG | 953.1 | 951.0 | 950.2 | 953.7 | 954.1 | 956.3 | 953.3 | 954.4 | 951.4 | 954.5 | 953.1 | °C | 0.021 |
| | 14 | | CV | 0.017 | 0.017 | 0.016 | 0.016 | 0.017 | 0.016 | 0.015 | 0.019 | 0.022 | 0.017 | 0.017 | - | 0.042 |
| | 15 | Superheat | AVG | 11.8 | 13.4 | 13.7 | 13.0 | 12.4 | 13.8 | 11.8 | 15.6 | 14.9 | 11.9 | 13.2 | °C | 0.000 |
| | 16 | | CV | 0.48 | 0.51 | 0.49 | 0.52 | 0.50 | 0.57 | 0.49 | 0.64 | 0.64 | 0.45 | 0.54 | - | 0.000 |
| | 17 | $AlF_3$ | AVG | 10.7 | 10.6 | 12.0 | 10.6 | 10.3 | 10.9 | 12.6 | 10.4 | 11.5 | 10.9 | 11.0 | % | 0.113 |
| | 18 | | CV | 0.23 | 0.21 | 0.27 | 0.18 | 0.18 | 0.14 | 0.24 | 0.27 | 0.23 | 0.23 | 0.22 | - | 0.486 |
| | 19 | Silicon | AVG | 0.048 | 0.052 | 0.048 | 0.054 | 0.049 | 0.051 | 0.082 | 0.069 | 0.061 | 0.046 | 0.055 | % | 0.405 |
| | 20 | | CV | 0.14 | 0.19 | 0.15 | 0.34 | 0.16 | 0.22 | 0.39 | 0.38 | 0.29 | 0.29 | 0.34 | - | 0.477 |
| Group P3 | 21 | Cell voltage | AVG | 4.419 | 4.442 | 4.440 | 4.427 | 4.427 | 4.456 | 4.452 | 4.425 | 4.426 | 4.412 | 4.431 | V | 0.000 |
| | 22 | | CV | 0.029 | 0.015 | 0.013 | 0.014 | 0.012 | 0.017 | 0.015 | 0.018 | 0.015 | 0.012 | 0.017 | - | 0.000 |
| | 23 | Cathode Resistance | AVG | 1.37 | 1.46 | 1.72 | 1.66 | 1.70 | 1.61 | 1.82 | 1.62 | 1.91 | 1.50 | 1.59 | μΩ | 0.035 |
| | 24 | | CV | 0.04 | 0.09 | 0.15 | 0.11 | 0.05 | 0.41 | 0.34 | 0.08 | 0.14 | 0.03 | 0.18 | - | 0.000 |
| | 25 | Noise | AVG | 0.058 | 0.063 | 0.071 | 0.077 | 0.064 | 0.059 | 0.081 | 0.066 | 0.081 | 0.058 | 0.067 | μΩ | 0.004 |
| | 26 | | CV | 0.67 | 0.73 | 0.82 | 0.90 | 0.66 | 0.69 | 0.85 | 0.57 | 0.85 | 0.66 | 0.78 | - | 0.005 |
| | 27 | Anode Current | CV | n/a | n/a | n/a | n/a | n/a | n/a | n/a | n/a | n/a | n/a | n/a | - | |
| | 28 | Cathode Current | CV | n/a | n/a | n/a | n/a | n/a | n/a | n/a | n/a | n/a | n/a | n/a | - | |
| Group P4 | 29 | Ellipsoid Volume | AVG | 99109 | 83805 | 110989 | 142474 | 135685 | 155961 | 82944 | 91524 | 335935 | 78186 | 128375 | $°C^2$ | 0.000 |
| | 30 | | CV | 0.67 | 1.00 | 0.38 | 0.78 | 0.29 | 0.91 | 1.53 | 1.48 | 0.23 | 1.99 | 1.11 | - | 0.000 |
| | 31 | Pinballing | AVG | 21.6 | 18.9 | 22.5 | 20.9 | 19.7 | 21.0 | 19.5 | 17.8 | 26.1 | 20.3 | 20.9 | $°C^{2/3}$ | 0.011 |
| | 32 | | CV | 0.65 | 1.00 | 0.52 | 1.08 | 0.69 | 0.99 | 0.66 | 1.11 | 0.50 | 1.04 | 0.65 | - | 0.000 |
| Group P5 | 71 | Productivity | AVG | 1169 | 1138 | 1096 | 1126 | 1115 | 1093 | 1084 | 1050 | 1064 | 1097 | 1103 | kg/cellday | 0.165 |
| | 72 | Current Efficiency | AVG | 98.99 | 96.57 | 92.83 | 95.55 | 94.40 | 93.02 | 92.60 | 88.29 | 89.32 | 92.99 | 93.45 | % | 0.162 |
| | 73 | Energy | AVG | 13.30 | 13.71 | 14.25 | 13.81 | 13.98 | 14.28 | 14.33 | 14.94 | 14.77 | 14.14 | 14.13 | kWh/kg | 0.303 |

***Table 5.3*** *Process Variables of the Reference Cells (2022-2040)*

| Current Efficiency | | | Energy Consumption | | |
|---|---|---|---|---|---|
| Nr. | Process Variable | Correlation Coefficient | Nr. | Process Variable | Correlation Coefficient |
| 2 | Alumina Shots (CV) | -0.76 | 2 | Alumina Shots (CV) | 0.76 |
| 15 | Superheat | -0.71 | 15 | Superheat | 0.73 |
| 16 | Superheat (CV) | -0.69 | 16 | Superheat (CV) | 0.71 |
| 4 | Number of Overfeeds (CV) | -0.67 | 4 | Number of Overfeeds (CV) | 0.69 |
| 23 | Cathode resistance | -0.66 | 23 | Cathode resistance | 0.67 |
| 9 | Iron Content | -0.63 | 9 | Iron Content | 0.66 |

***Table 5.4*** *Correlation between Process Variables and Overall Efficiency in the Reference Group*

#### 5.1.1.1 Alumina Feeding (Group P1)

Comparing Table 5.1 and Table 5.3 a significantly higher number of alumina shots (variable 1) and overfeeds (variable 3) are found for the test group. The variability of the number of overfeeds (variable 4) is, however, significantly lower for the test cells. This has significant effects on the alumina dissolution effectiveness as discussed in Section 2.1.1. The average and the variation in the underfeed duration *(UF)* are also significantly lower for these cells. The underfeed duration ($h \cdot day^{-1}$) is an indication of the alumina concentration band and is connected to the number of overfeeds *(OA)* and duration (0.5 h.) as given by Equation 5.1.

$$UF = 24 - 0.5 \cdot OA \tag{5.1}$$

For the test cells, a significantly lower underfeed duration, higher number of anode effects and lower variability (variables 5, 6) indicate a lower and more stable alumina concentration in the bath as described in Section 2.1.1. This favours better alumina dissolution according to Equation 2.1 and therefore improves the controllability of the alumina feeding strategy. However, a higher anode effect frequency for the test cells causes extra evolution of greenhouse gases (Section 2.1.1) and the triggers for these anode effects there need further analysis.

Although the targets for the bath height are the same for the test and reference group, a significantly higher bath height (variable 7) is achieved for the test cells. This also allows better alumina dissolution as more bath provides more sensible heat required for dissolution (Section 2.1.1). At Aldel, the centre channel (space between the two rows of anodes in a cell) is very narrow which could be the main limiting factor in the alumina dissolution at higher line current and larger anodes (Section 4.2.3.1).

Although a higher bath height is found for the test cells, Table 5.1 shows a significantly lower variation in the iron content in the metal (variable 10) which is normally associated with stub attack by the higher bath levels (Section 3.1.5). Reduced bath height variability is a strong correlator for increased current efficiency and potentially reduced voltage in smelting cells (Tarcy and Sorensen, 1991), due to the higher and less variable ACD which accompanies it.

#### 5.1.1.2 Temperature and Composition (Group P2)

Both temperature and composition affect the solubility of aluminium in the electrolyte (Table 1.1). In this respect a lower temperature and a higher $AlF_3$ concentration favour a higher current efficiency. However, it is generally recognized that the most efficient operating zone is associated with maximum process stability (Welch, 1998). A better compositional stability reduces current distribution and metal interfacial disturbances within the cell. This results in a

decrease in the mass transfer of dissolved metal into the electrolyte (Taylor and Chen, 1997), which is accelerated by the pumping action of large bubbles of gas that are being released (Figure 1.2). Table 5.1 demonstrates no significant differences in the temperature (variable 11) and $AlF_3$ concentration (variable 17) between the test and the reference group. However, a significantly higher liquidus temperature and lower variability (variables 13, 14) are found for the test cells. Again, this indicates a lower average alumina concentration in these cells. Based on the substitution of the $AlF_3$ concentration and liquidus temperature of the two groups in Equation 2.21, a difference in alumina concentration of 0.5% is found.

Figure 3.17 shows the operating window for good cell performance. This window is not only limited by a given range of electrolyte and liquidus temperatures, but the combination of both determines the superheat. Figure 5.1 demonstrates a lower average and variability of the superheat (variables 15, 16) for the test group. Less variable superheat should result in improved alumina dissolution and maintenance of a more protective side wall ledge. Less superheat variation also favours better process stability due to stability of liquid volume caused by a reduced influence of sludge and ridge formation (Sections 1.3.5 and 3.1.5). This reduced ridge or ledge formation has not manifested itself in the formation of sidewall attack and the silicon levels show no significant differences between both groups.

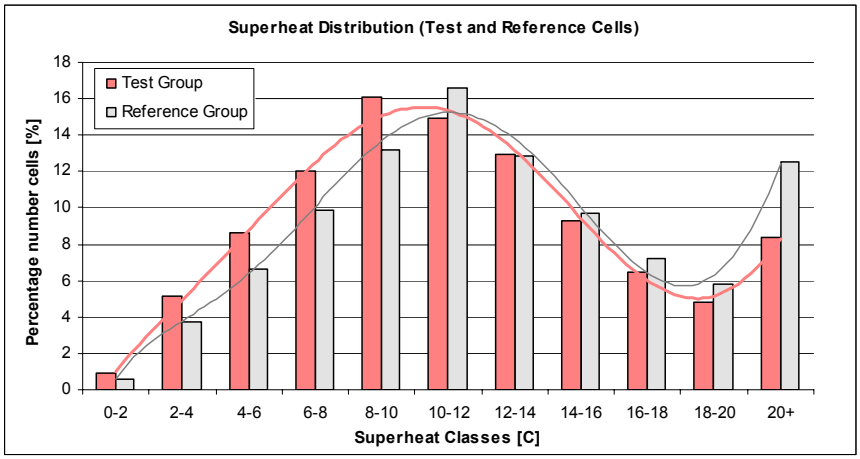


***Figure 5.1*** *Superheat Distribution (Test and Reference Cells)*

### 5.1.1.3 Voltage and Electromagnetic Stability (Group P3)

By comparing process variables 21 and 22 in Table 5.1 and Table 5.3, it is obvious that the test cells have a significantly higher average voltage, but lower variability. The cell voltage is made up of three groups of components as shown in Equation 1.5. The decomposition potential, anode polarisation, bubble and electrolyte resistances are increased marginally with reduced alumina concentration in the bulk electrolyte (Section 2.1.1). In this respect a lower alumina concentration requires a slightly higher cell voltage (estimated as ~5 mV). In

addition, a higher cell voltage is necessary to compensate for the lower heat generation within a cell at constant heat balance and higher current efficiency (Sections 1.3.4 and 5.1.1.5). However, since no significant correlation between the voltage and current efficiency is found for the test and the reference cells in this thesis, it is possible that the higher cell voltages of the test group were simply the result of target voltages being set higher than necessary.

The average noise is significantly higher for the test cells, whereas the variability in noise is significantly lower as shown by process variables 25 and 26. Although a lower noise level indicates higher electromagnetic stability, it is also associated with operating at higher energy consumption as discussed in Section 5.1.1.5. At Aldel, the cathode resistance (variable 23) is measured with a disposable sensor as described in Section 2.3.1.4 and is closely related to the cell design (Section 4.2.3.1). However, a lower variability in the cathode resistance (variable 24) and noise for the test cells indicates less dynamics in sludge and ridge formation and dissolution. This confirms the observations of a more stable control of the alumina concentration and superheat for the test cells (Sections 5.1.1.1 and 5.1.1.2).

#### 5.1.1.4 Overall System Dynamics (Group P4)

In this thesis alumina feeding characteristics are incorporated into the new process control philosophy. A natural behaviour envelop is derived for every cell and the ellipsoid volume is calculated with Equation 3.11. It is hypothesised in this thesis that better control should reduce the volume over time. Furthermore, the abnormal characteristic of pinballing is defined by high process velocity between two successive measurements in the three-dimensional space (bath temperature, liquidus temperature, CUSUM of ratio of alumina fed to a cell). Pinballing is signalled graphically as large vectors in this ellipsoidal space (Section 3.2.1.3) and is calculated with Equation 3.13. Table 5.1 shows a significantly better stability for the test cells based on both lower average and variability of both ellipsoid volume and pinballing (variables 29-32). This is confirmatory data for the earlier hypothesis about the effective of removing abnormalities through the new control philosophy on the degree of variation in a complex multivariate system (Hypothesis 2).

#### 5.1.1.5 Current and Energy Efficiency (Group P5)

Process variables 72 and 73 in Tables 5.1 and 5.3 show a higher average current efficiency (+1.18%) and a lower energy consumption (-0.081 kWh/kg) for the test cells compared to the reference cells. Analysis of the experimental period only indicates that the probability of committing a Type I error is 16% for the current efficiency and 30% for the energy efficiency. A more comprehensive analysis is required to remove the portion of the variance in each cell

group due to differences between individual cells. As discussed in Section 4.1.1 this is called the Before-After-Control-Impact statistical design.

Using this method each cell group is compared before and after the implementation of the experiment (years 2007 versus 2008). The variation within each group is studied in relation to the current and energy efficiency. The test cells show a higher current efficiency (+2.0%, p=0.075) and lower energy consumption (-0.42 kWh/kg, p=0.034) as given by Table 5.5. The test cells also show a significantly lower variation between the cells within the group before and after the experiment.

For the reference cells, Table 5.5 shows a lower current efficiency (-1.5%) and higher energy consumption (+0.11 kWh/kg) in 2008 compared to 2007. The deterioration in current and energy efficiency may be linked to increased variations in the energy input. For the reference cells the current efficiency in 2008 is equal to the average of the whole pot line. In 2008 the line current was increased by 3.6 kA and the total duration of interruptions added up to 1268 minutes (Figures 4.5 and 4.6). However, these differences are not significant at a confidence level of 95%. Also, the variability within the reference cells shows no significant differences.

| | Test Cells | | | Reference Cells | | |
|---|---|---|---|---|---|---|
| | **2007** | **2008** | **p-value** | **2007** | **2008** | **p-value** |
| Current Efficiency [%] | 92.6 | 94.6 | 0.075 | 95.0 | 93.5 | 0.148 |
| Current Efficiency (CV) [%] | 4.2 | 2.0 | 0.019 | 3.3 | 3.4 | 0.477 |
| Energy Consumption [kWh/kg] | 14.47 | 14.05 | 0.034 | 14.04 | 14.15 | 0.305 |
| Energy Consumption (CV) [%] | 4.2 | 2.0 | 0.017 | 3.2 | 3.4 | 0.429 |

***Table 5.5*** *Current Efficiency and Energy Consumption for the Test and Reference Cells (2007 and 2008)*

Table 5.2 identifies the main factors affecting the current and energy efficiency within the test group. The average current efficiency is clearly correlated with a higher number of alumina shots (variable 1) and a higher average and lower variability of overfeeds (variables 3, 4) usually associated with the rate of alumina dissolution, along with lower variability in the underfeed duration for the test cells which is the absolute measure of variation in alumina concentration.

Table 5.4 identifies the main contributors to the process variation within the reference group. The variables associated with current efficiency and energy consumption are the variability in alumina shots (variable 2) and number of overfeeds (variable 4). The variability in cathode resistance (variable 23) is also lower for the test group, indicating the influence of less sludge and bottom ridge, which supports the hypothesis of improved alumina feeding through breaking the sludge cycle (Hypothesis 1). The correlation of the average iron content (variable 9) with lower current efficiency for the reference cells also indicates the importance

of good control of the total liquid level in cells, since poor liquid level control is the major driver of higher iron content in the metal.

Moreover, a higher cathode resistance (variable 23) for the reference cells, combined with a lower average voltage (variable 21) is certain confirmation of lower ACD operation. This has led to an increase in the back reaction of aluminium to alumina for these cells lowering the current efficiency (Section 1.3.2). A higher average and higher variability of the superheat (variables 15, 16) indicates the existence of significant process excursions for the reference cells. This supports the hypothesis of improved detection and removal of abnormalities to improve both the current efficiency and energy consumption (Hypothesis 2).

### 5.1.2 Abnormality Detection

The abnormalities and associated failure mechanisms (events) for the test and reference cells are presented in Tables 5.6 and 5.8 respectively. The total duration of abnormalities is one measure of the time the smelting process was not operating at its maximum potential. A confidence level of 95% is used to distinguish between significant and trivial variations (p-value<0.05) (Section 4.1.1).

These abnormalities are divided in five groups (A1-A5) as discussed in Section 4.1.2.2. Group A1 (events 33-45) is connected to the overall system dynamics. Group A2 (events 46-54) contains abnormalities regarding the anode conditions. Furthermore, Group A3 (events 55-65) is linked to the detection of failure mechanisms related to the alumina feeding. In addition, hardware failures in the alumina and $AlF_3$ feeding are signalled. Group A4 (events 66-70) highlights abnormalities related to liquid bath mass variations. Group A5 (variables 71-73) summarizes the productivity, and the current and energy efficiency.

#### 5.1.2.1 System Dynamics (Group A1)

Comparing Tables 5.6 and 5.8 significantly lower number of high pinballing events (PBH, event 34) indicates better process stability for the test cells. This underlines the observed lower average and variability in the ellipsoid volume and pinballing value (variables 29-32) for these cells (Section 5.1.1.4). Furthermore, a significantly higher number of high liquidus temperature events (LIQH, event 41) are found which is in line with the significantly higher liquidus temperature (variable 13) for the test cells (Section 5.1.1.2). Also, a lower number of superheat excursions (SHH, event 43) indicates a better process stability for the test cells compared to the reference cells. This is also in line with a lower average and variability of the superheat (variables 15, 16) for the test cells (Section 5.1.1.2). As discussed in Section 5.1.1.4 this confirms the effect of removing abnormalities through the new control strategy on the degree of variation in a complex multivariate system (Hypothesis 2).

| | | | Test Cells | | | | | | | | | | | | |
|---|---|---|---|---|---|---|---|---|---|---|---|---|---|---|---|
| Gr. | Nr. | Events | 2002 | 2004 | 2006 | 2008 | 2010 | 2012 | 2014 | 2016 | 2018 | 2020 | AVG | Units | P-value |
| Group A1 | 33 | HOTLAH | 0.103 | 0.150 | 0.143 | 0.155 | 0.143 | 0.171 | 0.197 | 0.150 | 0.127 | 0.140 | 0.148 | 1/cellday | 0.212 |
| | 34 | PBH | 0.127 | 0.149 | 0.164 | 0.188 | 0.189 | 0.202 | 0.193 | 0.199 | 0.136 | 0.205 | 0.175 | 1/cellday | 0.007 |
| | 35 | TOTEV | 3.03 | 2.11 | 2.64 | 2.58 | 2.40 | 2.44 | 2.40 | 2.04 | 1.84 | 2.06 | 2.36 | 1/cellday | 0.192 |
| | 36 | TEMPL | 0.126 | 0.084 | 0.127 | 0.126 | 0.060 | 0.032 | 0.128 | 0.131 | 0.055 | 0.071 | 0.094 | 1/cellday | 0.394 |
| | 37 | TEMPKL | 0.030 | 0.000 | 0.000 | 0.014 | 0.000 | 0.000 | 0.014 | 0.008 | 0.000 | 0.011 | 0.008 | 1/cellday | 0.188 |
| | 38 | TEMPH | 0.238 | 0.177 | 0.174 | 0.207 | 0.219 | 0.228 | 0.240 | 0.143 | 0.238 | 0.171 | 0.204 | 1/cellday | 0.323 |
| | 39 | TEMPKH | 0.131 | 0.114 | 0.080 | 0.100 | 0.096 | 0.090 | 0.115 | 0.069 | 0.110 | 0.065 | 0.097 | 1/cellday | 0.069 |
| | 40 | LIQL | 0.166 | 0.130 | 0.204 | 0.180 | 0.085 | 0.085 | 0.177 | 0.186 | 0.057 | 0.125 | 0.140 | 1/cellday | 0.375 |
| | 41 | LIQH | 0.169 | 0.152 | 0.196 | 0.199 | 0.198 | 0.210 | 0.262 | 0.151 | 0.228 | 0.205 | 0.197 | 1/cellday | 0.003 |
| | 42 | SHL | 0.019 | 0.000 | 0.009 | 0.011 | 0.014 | 0.000 | 0.016 | 0.005 | 0.005 | 0.014 | 0.009 | 1/cellday | 0.388 |
| | 43 | SHH | 0.181 | 0.097 | 0.087 | 0.101 | 0.050 | 0.070 | 0.101 | 0.087 | 0.052 | 0.077 | 0.090 | 1/cellday | 0.028 |
| | 44 | NP | 0.001 | 0.000 | 0.000 | 0.000 | 0.000 | 0.000 | 0.000 | 0.000 | 0.000 | 0.000 | 0.000 | 1/cellday | 0.082 |
| | 45 | CD | 0.003 | 0.003 | 0.003 | 0.003 | 0.003 | 0.003 | 0.003 | 0.003 | 0.003 | 0.003 | 0.003 | 1/cellday | 0.465 |
| Group A2 | 46 | CBAN | 0.012 | 0.037 | 0.019 | 0.024 | 0.006 | 0.085 | 0.018 | 0.007 | 0.028 | 0.006 | 0.024 | 1/cellday | 0.351 |
| | 47 | ANSPA | 0.093 | 0.071 | 0.060 | 0.044 | 0.066 | 0.060 | 0.049 | 0.022 | 0.022 | 0.049 | 0.054 | 1/cellday | 0.000 |
| | 48 | ANSPM | 0.109 | 0.082 | 0.104 | 0.060 | 0.041 | 0.068 | 0.117 | 0.123 | 0.098 | 0.134 | 0.094 | - | |
| | 49 | ANSPS | 0.096 | 0.025 | 0.046 | 0.030 | 0.016 | 0.025 | 0.077 | 0.057 | 0.038 | 0.082 | 0.049 | - | |
| | 50 | ANSLP | 0.016 | 0.022 | 0.019 | 0.014 | 0.022 | 0.033 | 0.016 | 0.030 | 0.003 | 0.022 | 0.020 | - | |
| | 51 | ANOFF | 0.008 | 0.005 | 0.014 | 0.005 | 0.003 | 0.005 | 0.000 | 0.000 | 0.003 | 0.005 | 0.005 | - | |
| | 52 | ANHGH | 0.003 | 0.000 | 0.005 | 0.000 | 0.000 | 0.000 | 0.003 | 0.000 | 0.000 | 0.000 | 0.001 | - | |
| | 53 | CLMVH | 0.000 | 0.000 | 0.005 | 0.003 | 0.000 | 0.003 | 0.000 | 0.008 | 0.000 | 0.005 | 0.002 | - | |
| | 54 | TOTAN | 0.372 | 0.240 | 0.284 | 0.178 | 0.180 | 0.224 | 0.287 | 0.251 | 0.175 | 0.322 | 0.251 | - | |
| Group A3 | 55 | CBERR | 0.092 | 0.000 | 0.508 | 0.019 | 0.032 | 0.041 | 0.006 | 0.047 | 0.311 | 0.056 | 0.111 | 1/cellday | 0.198 |
| | 56 | CBSPK | 0.380 | 0.003 | 0.000 | 0.279 | 0.145 | 0.016 | 0.156 | 0.014 | 0.005 | 0.131 | 0.113 | 1/cellday | 0.361 |
| | 57 | CBDIST | 0.000 | 0.000 | 0.044 | 0.000 | 0.000 | 0.000 | 0.000 | 0.008 | 0.000 | 0.000 | 0.005 | 1/cellday | 0.152 |
| | 58 | ALFERR | 0.000 | 0.000 | 0.003 | 0.011 | 0.014 | 0.003 | 0.000 | 0.000 | 0.000 | 0.000 | 0.003 | 1/cellday | 0.178 |
| | 59 | AL2O3H | 0.098 | 0.182 | 0.127 | 0.143 | 0.078 | 0.127 | 0.155 | 0.147 | 0.136 | 0.106 | 0.130 | 1/cellday | 0.001 |
| | 60 | AL2O3L | 0.111 | 0.081 | 0.083 | 0.067 | 0.133 | 0.154 | 0.081 | 0.035 | 0.042 | 0.106 | 0.089 | 1/cellday | 0.068 |
| | 61 | OACURV | 0.048 | 0.033 | 0.055 | 0.032 | 0.045 | 0.075 | 0.040 | 0.043 | 0.025 | 0.052 | 0.045 | 1/cellday | 0.000 |
| | 62 | OAERR | 0.117 | 0.040 | 0.098 | 0.110 | 0.126 | 0.136 | 0.109 | 0.090 | 0.072 | 0.101 | 0.100 | 1/cellday | 0.066 |
| | 63 | AE | 0.000 | 0.001 | 0.000 | 0.000 | 0.000 | 0.000 | 0.000 | 0.000 | 0.000 | 0.000 | 0.000 | 1/cellday | 0.152 |
| | 64 | AEERR | 0.394 | 0.345 | 0.362 | 0.305 | 0.529 | 0.503 | 0.163 | 0.179 | 0.063 | 0.125 | 0.297 | 1/cellday | 0.016 |
| | 65 | AEKWH | 0.000 | 0.000 | 0.000 | 0.000 | 0.000 | 0.000 | 0.000 | 0.000 | 0.000 | 0.000 | 0.000 | 1/cellday | 0.146 |
| Group A4 | 66 | BHCALC | 0.298 | 0.240 | 0.094 | 0.200 | 0.188 | 0.172 | 0.129 | 0.222 | 0.077 | 0.187 | 0.181 | 1/cellday | 0.069 |
| | 67 | BHL | 0.060 | 0.016 | 0.029 | 0.034 | 0.005 | 0.014 | 0.041 | 0.038 | 0.025 | 0.022 | 0.028 | 1/cellday | 0.202 |
| | 68 | BHH | 0.033 | 0.035 | 0.014 | 0.028 | 0.005 | 0.004 | 0.000 | 0.036 | 0.010 | 0.005 | 0.017 | 1/cellday | 0.379 |
| | 69 | BVDEC | 0.018 | 0.006 | 0.000 | 0.035 | 0.025 | 0.000 | 0.048 | 0.012 | 0.000 | 0.050 | 0.019 | 1/cellday | 0.000 |
| | 70 | BVINC | 0.062 | 0.025 | 0.007 | 0.009 | 0.000 | 0.001 | 0.000 | 0.024 | 0.029 | 0.007 | 0.016 | 1/cellday | 0.000 |
| Group A5 | 71 | PROD | 1104 | 1134 | 1111 | 1135 | 1075 | 1103 | 1112 | 1143 | 1141 | 1104 | 1116 | kg/cellday | 0.165 |
| | 72 | CE | 93.45 | 96.19 | 94.17 | 96.34 | 91.11 | 93.59 | 94.21 | 96.89 | 96.82 | 93.54 | 94.63 | % | 0.162 |
| | 73 | ENERGY | 14.29 | 13.84 | 14.14 | 13.80 | 14.60 | 14.16 | 14.09 | 13.74 | 13.70 | 14.19 | 14.05 | kWh/kg | 0.303 |

*) The abbreviations are listed on page (xviii)

***Table 5.6*** *Abnormality Detection (Events) for the Test Cells (2002-2020)*

| Current Efficiency | | | Energy Consumption | | |
|---|---|---|---|---|---|
| Nr. | Event | Correlation Coefficient | Nr. | Event | Correlation Coefficient |
| 60 | AL2O3L | -0.85 | 60 | AL2O3L | 0.82 |
| 59 | AL2O3H | 0.78 | 59 | AL2O3H | -0.79 |
| 62 | OAERR | -0.67 | 47 | ANSPA | 0.65 |
| | | | 62 | OAERR | 0.64 |

***Table 5.7*** *Correlation between Abnormality Detection with Overall Efficiency for the Test Group*

| | | | Reference Cells | | | | | | | | | | | | |
|---|---|---|---|---|---|---|---|---|---|---|---|---|---|---|---|
| Gr. | Nr. | Events | 2022 | 2024 | 2026 | 2028 | 2030 | 2032 | 2034 | 2036 | 2038 | 2040 | AVG | Units | P-value |
| Group A1 | 33 | HOTLAH | 0.110 | 0.202 | 0.139 | 0.200 | 0.147 | 0.095 | 0.117 | 0.239 | 0.253 | 0.120 | 0.162 | 1/cellday | 0.212 |
| | 34 | PBH | 0.184 | 0.176 | 0.257 | 0.192 | 0.163 | 0.325 | 0.209 | 0.211 | 0.332 | 0.156 | 0.221 | 1/cellday | 0.007 |
| | 35 | TOTEV | 2.13 | 2.02 | 2.58 | 2.41 | 2.47 | 3.12 | 2.46 | 3.79 | 2.90 | 2.27 | 2.61 | 1/cellday | 0.192 |
| | 36 | TEMPL | 0.081 | 0.096 | 0.085 | 0.059 | 0.052 | 0.046 | 0.044 | 0.118 | 0.186 | 0.064 | 0.083 | 1/cellday | 0.394 |
| | 37 | TEMPKL | 0.011 | 0.010 | 0.008 | 0.000 | 0.000 | 0.000 | 0.000 | 0.005 | 0.036 | 0.000 | 0.007 | 1/cellday | 0.188 |
| | 38 | TEMPH | 0.189 | 0.150 | 0.153 | 0.185 | 0.165 | 0.335 | 0.281 | 0.303 | 0.180 | 0.252 | 0.219 | 1/cellday | 0.323 |
| | 39 | TEMPKH | 0.059 | 0.047 | 0.074 | 0.095 | 0.080 | 0.143 | 0.155 | 0.176 | 0.084 | 0.053 | 0.097 | 1/cellday | 0.069 |
| | 40 | LIQL | 0.131 | 0.143 | 0.189 | 0.125 | 0.151 | 0.102 | 0.135 | 0.156 | 0.270 | 0.132 | 0.153 | 1/cellday | 0.375 |
| | 41 | LIQH | 0.149 | 0.132 | 0.143 | 0.128 | 0.161 | 0.143 | 0.196 | 0.244 | 0.163 | 0.228 | 0.169 | 1/cellday | 0.003 |
| | 42 | SHL | 0.019 | 0.000 | 0.014 | 0.005 | 0.000 | 0.014 | 0.000 | 0.005 | 0.000 | 0.000 | 0.006 | 1/cellday | 0.388 |
| | 43 | SHH | 0.091 | 0.115 | 0.168 | 0.114 | 0.117 | 0.276 | 0.260 | 0.194 | 0.184 | 0.063 | 0.158 | 1/cellday | 0.028 |
| | 44 | NP | 0.000 | 0.000 | 0.000 | 0.001 | 0.000 | 0.000 | 0.000 | 0.000 | 0.000 | 0.000 | 0.000 | 1/cellday | 0.082 |
| | 45 | CD | 0.003 | 0.003 | 0.003 | 0.003 | 0.003 | 0.003 | 0.003 | 0.003 | 0.003 | 0.003 | 0.003 | 1/cellday | 0.465 |
| Group A2 | 46 | CBAN | 0.000 | 0.013 | 0.006 | 0.018 | 0.000 | 0.000 | 0.019 | 0.000 | 0.000 | 0.013 | 0.007 | 1/cellday | 0.351 |
| | 47 | ANSPA | 0.022 | 0.011 | 0.016 | 0.011 | 0.027 | 0.033 | 0.016 | 0.016 | 0.033 | 0.011 | 0.020 | 1/cellday | 0.000 |
| | 48 | ANSPM | 0.011 | 0.014 | 0.014 | 0.016 | 0.022 | 0.025 | 0.046 | 0.030 | 0.030 | 0.005 | 0.021 | - | |
| | 49 | ANSPS | 0.101 | 0.046 | 0.063 | 0.079 | 0.087 | 0.060 | 0.117 | 0.068 | 0.093 | 0.027 | 0.074 | - | |
| | 50 | ANSLP | 0.033 | 0.019 | 0.014 | 0.011 | 0.019 | 0.044 | 0.016 | 0.003 | 0.019 | 0.027 | 0.020 | - | |
| | 51 | ANOFF | 0.005 | 0.008 | 0.003 | 0.014 | 0.000 | 0.005 | 0.005 | 0.003 | 0.016 | 0.005 | 0.007 | - | |
| | 52 | ANHGH | 0.000 | 0.000 | 0.000 | 0.000 | 0.000 | 0.003 | 0.000 | 0.005 | 0.000 | 0.003 | 0.001 | - | |
| | 53 | CLMVH | 0.003 | 0.003 | 0.003 | 0.003 | 0.005 | 0.000 | 0.005 | 0.003 | 0.003 | 0.000 | 0.003 | - | |
| | 54 | TOTAN | 0.186 | 0.107 | 0.120 | 0.139 | 0.175 | 0.186 | 0.216 | 0.137 | 0.210 | 0.085 | 0.156 | - | |
| Group A3 | 55 | CBERR | 0.000 | 0.013 | 0.006 | 0.098 | 0.024 | 0.042 | 0.019 | 0.798 | 0.000 | 0.013 | 0.101 | 1/cellday | 0.198 |
| | 56 | CBSPK | 0.347 | 0.071 | 0.284 | 0.115 | 0.128 | 0.016 | 0.049 | 0.000 | 0.158 | 0.424 | 0.159 | 1/cellday | 0.361 |
| | 57 | CBDIST | 0.000 | 0.000 | 0.000 | 0.003 | 0.000 | 0.000 | 0.000 | 0.205 | 0.000 | 0.000 | 0.021 | 1/cellday | 0.152 |
| | 58 | ALFERR | 0.011 | 0.011 | 0.030 | 0.120 | 0.101 | 0.008 | 0.005 | 0.008 | 0.008 | 0.000 | 0.030 | 1/cellday | 0.178 |
| | 59 | AL2O3H | 0.133 | 0.010 | 0.048 | 0.101 | 0.049 | 0.033 | 0.065 | 0.005 | 0.091 | 0.006 | 0.054 | 1/cellday | 0.001 |
| | 60 | AL2O3L | 0.085 | 0.175 | 0.116 | 0.111 | 0.141 | 0.222 | 0.123 | 0.329 | 0.138 | 0.165 | 0.161 | 1/cellday | 0.068 |
| | 61 | OACURV | 0.035 | 0.090 | 0.104 | 0.061 | 0.079 | 0.094 | 0.090 | 0.135 | 0.093 | 0.082 | 0.086 | 1/cellday | 0.000 |
| | 62 | OAERR | 0.083 | 0.140 | 0.160 | 0.153 | 0.198 | 0.200 | 0.172 | 0.348 | 0.145 | 0.202 | 0.180 | 1/cellday | 0.066 |
| | 63 | AE | 0.000 | 0.000 | 0.000 | 0.000 | 0.000 | 0.000 | 0.000 | 0.000 | 0.000 | 0.000 | 0.000 | 1/cellday | 0.152 |
| | 64 | AEERR | 0.026 | 0.040 | 0.160 | 0.121 | 0.111 | 0.585 | 0.035 | 0.008 | 0.142 | 0.000 | 0.123 | 1/cellday | 0.016 |
| | 65 | AEKWH | 0.000 | 0.000 | 0.000 | 0.000 | 0.000 | 0.000 | 0.000 | 0.000 | 0.000 | 0.000 | 0.000 | 1/cellday | 0.146 |
| Group A4 | 66 | BHCALC | 0.164 | 0.181 | 0.254 | 0.128 | 0.286 | 0.164 | 0.271 | 0.011 | 0.202 | 0.172 | 0.183 | 1/cellday | 0.069 |
| | 67 | BHL | 0.040 | 0.016 | 0.058 | 0.024 | 0.062 | 0.044 | 0.056 | 0.011 | 0.027 | 0.017 | 0.036 | 1/cellday | 0.202 |
| | 68 | BHH | 0.008 | 0.021 | 0.005 | 0.020 | 0.035 | 0.005 | 0.030 | 0.000 | 0.016 | 0.005 | 0.015 | 1/cellday | 0.379 |
| | 69 | BVDEC | 0.082 | 0.101 | 0.091 | 0.112 | 0.098 | 0.060 | 0.114 | 0.104 | 0.093 | 0.057 | 0.091 | 1/cellday | 0.000 |
| | 70 | BVINC | 0.052 | 0.055 | 0.016 | 0.055 | 0.101 | 0.134 | 0.016 | 0.115 | 0.054 | 0.038 | 0.064 | 1/cellday | 0.000 |
| Group A5 | 71 | PROD | 1169 | 1138 | 1096 | 1126 | 1115 | 1093 | 1084 | 1050 | 1064 | 1097 | 1103 | kg/cellday | 0.165 |
| | 72 | CE | 98.99 | 96.57 | 92.83 | 95.55 | 94.40 | 93.02 | 92.60 | 88.29 | 89.32 | 92.99 | 93.45 | % | 0.162 |
| | 73 | ENERGY | 13.30 | 13.71 | 14.25 | 13.81 | 13.98 | 14.28 | 14.33 | 14.94 | 14.77 | 14.14 | 14.13 | kWh/kg | 0.303 |

*) *The abbreviations are listed on Page (xviii)*

***Table 5.8*** *Abnormality Detection (Events) for the Reference Cells (2022-2040)*

| Current Efficiency | | | Energy Consumption | | |
|---|---|---|---|---|---|
| Nr. | Event | Correlation Coefficient | Nr. | Event | Correlation Coefficient |
| 61 | OACURV | -0.84 | 61 | OACURV | 0.86 |
| 35 | TOTEV | -0.81 | 35 | TOTEV | 0.83 |
| 62 | OAERR | -0.72 | 62 | OAERR | 0.72 |
| | | | 39 | TEMPKH | 0.64 |

***Table 5.9*** *Correlation between Abnormality Detection with Overall Efficiency for the Reference Group*

#### 5.1.2.2 Anode Conditions (Group A2)

A significantly higher number of automatic detected anode spikes (ANSPA, event 47) was found for the test group (Table 5.6). This is associated with the new detection algorithm (soft sensor) in the control system for identifying this abnormality as well as the lower superheat as identified in Section 5.1.1.2. A considerable mass of cryolite freezes around and under a newly set anode. The rate of melting of this freeze depends mainly on the volume and superheat of the liquid bath around the anode (Sections 2.1.3 and 2.3.2). A lower superheat retards the melting of freeze under particular parts of the anode resulting in a higher risk of the formation of anode spikes. Increases in line current create a higher sensitivity for energy imbalances due to larger bath mass variations, lower liquid bath mass and consequently an increased sensitivity to anode setting (Section 2.3.2).

The total number of anode spikes detected by shift operators (ANSPS, event 49) and members of the measurement team (ANSPM, event 48) are considerable higher for the test cells (523 versus 350). This supports the employment of a causally based control approach in which abnormalities are detected and removed or corrected in order to improve the overall process stability (Hypothesis 2). In this respect the higher number of correctly detected anode spikes for the test cells has enabled the operators to remove them and restore the cell efficiency, highlighting the importance of the new system for abnormality detection as used for the test cells. Other detected abnormalities in anode conditions like slipped anodes (ANSLP, event 50), anode burn-offs (ANOFF, event 51), anode too high (ANHGH, event 52) and high clamp voltage (CMPVH, event 53) show no differences between the two groups, probably because these abnormalities are easily detected by operators without the new control system's assistance.

#### 5.1.2.3 Alumina and $AlF_3$ Balance (Group A3)

For the test cells, Table 5.6 demonstrates a significantly higher number of alumina ratio high events (AL2O3H, event 59). This underlines the observed higher average in alumina shots (variable 1) and overfeeds (variable 3) combined with a lower variability in the number of overfeeds (variable 4) as discussed in Section 5.1.1.1. Furthermore, a significantly lower number of abnormalities in the reaction of the cell resistance to overfeed (OACURV, event 61) are found for these cells (Section 3.3.2.3). This abnormality is linked to sludge formation. For the test cells, the number of repeated anode effects (AEERR, event 64) is significantly higher than found for the reference group. This is in line with the higher anode effect frequency (variable 5), lower average and variability in superheat (variable 15, 16) and lower alumina concentration for the test cells as discussed in Sections 5.1.1.1 and 5.1.1.2.

#### 5.1.2.4 Liquid Bath Mass (Group A4)

As described in Section 3.3.2.4 a soft sensor is developed in order to detect rapid changes in liquid bath mass. This sensor is based on a predefined process behaviour indicated by the ratio of alumina additions to metal production rate and the CUSUM of $AlF_3$ additions (Figure 3.2). For the test cells, Table 5.6 shows significantly lower number of liquid bath mass variations indicated by a lower number of increases (BVINC, event 70) and a lower number of decreases (BVDEC, event 69) in the liquid bath mass. A higher number of abnormalities associated with a fast decrease in liquid bath mass for the reference cells are in line with the lower average bath height (variable 7) (Section 5.1.1.1). The ratio of BVDEC over BVINC is also considerable higher for the reference cells indicating a tendency for running at low bath levels (2.62 versus 1.19).

#### 5.1.2.5 Current and Energy Efficiency (Group A5)

A higher average current efficiency and lower average energy consumption are found for the test cells as discussed in Section 5.1.1.5. Based on the overall investigation of abnormality detection as listed in Table 5.7 and confirmed by the observations as discussed in Section 5.1.1.5, a major contributing factor is believed to be due to a better control of the alumina feeding (Section 5.1.2.3). The lower variations within the test group are linked to less alumina ratio low (AL2O3L, event 60) and more alumina ratio high occurrences (AL2O3H, event 59). In addition, a low number of overfeed errors (OAERR, event 62) is associated with a high current efficiency.

A poorer control of the alumina feeding is also considered to be a major cause in higher variation within the reference group. Based on the investigation of abnormality detection as listed in Table 5.9, a higher number of abnormalities in the reaction of the cell resistance to overfeed (OACURV, event 61) and higher number of overfeed errors (OAERR, event 62) result in both lower current and energy efficiency. These abnormalities (OACURV, OAERR) are linked to sludge formation and dissolution respectively as described in Section 3.3.2.3.

A negative correlation is also found between the total number of detected abnormalities and the current and energy efficiency within the reference group. In particular, a higher number of critical high temperature events (TEMPKH, event 39) results in higher energy consumption. The detection and subsequent correction or removal of these abnormalities prevents cells to move out of their most efficient operating window. This is also supported by the absence of significant correlation between the total number of abnormalities (TOTEV, event 35) with the current and energy efficiency between the cells within the test group. Actually, this is one of the important rationales of this thesis (Hypothesis 2).

### 5.1.3 Specific Failure Mechanisms and Consequences

In this section specific failure mechanisms involved in the system dynamics within the test and reference cells are discussed. This analysis investigates the process variability within each group with respect to the paired correlations between process variables and/or process abnormalities as discussed in Sections 5.1.1 and 5.1.2. These mechanisms are divided in five groups (F1-F5) (Section 4.1.2.3). Group F1 is linked to failure mechanisms involved in the controllability of the alumina feeding (Section 5.1.3.1). Group F2 incorporates process behaviour and abnormalities in mass and energy balance control (Section 5.1.3.2). Group F3 is related to liquid bath mass control (Section 5.1.3.3). Group F4 is linked to the underlying process stability (Section 5.1.3.4). General abnormalities are discussed in Group F5 (Section 5.1.3.5).

#### 5.1.3.1 Alumina Feeding (Group F1)

For the test cells, a list of process variables and/or events is separately correlated and the correlation coefficients are given in Table 5.10. It is clear that there is a significant correlation between the average and variability in the number of alumina shots with the number of overfeeds (variables 1-4). The average and variability in the number of alumina shots (variables 1, 2) are inversely correlated. These variables are associated with the alumina dissolution effectiveness as discussed in Section 5.1.1.1. The total number of alumina shots is inversely linked to the number of low alumina events (AL2O3L, event 60). These variables and events are also identified as the main contributors to the current and energy efficiency as shown in Tables 5.2 and 5.7. Thus a good control of the alumina feeding results in an improved efficiency of the smelting process.

Paired correlations between the average and variability in the number of alumina shots and overfeeds (variables 1-4) are also found for the reference cells (Table 5.11). These cells also show a stronger correlation with respect to alumina feeding. The number of alumina shots (variable 1) and overfeeds (variables 3) with alumina low events (AL2O3L, event 60) and alumina high events (AL2O3H, 59) are correlated. Also, a paired correlation between low alumina events (AL2O3L, event 60) with low overfeed events (OAERR, event 62) is found. The average and variability in the anode effect frequency (variables 5, 6) are correlated. For the reference cells, a higher variability and more paired correlations between the process behaviour envelops and detected abnormalities related to alumina feeding are found than for the test cells.

| | Nr. | Parameter 1 (Variable or Event) | Nr. | Parameter 2 (Variable or Event) | Correlation Coefficient |
|---|---|---|---|---|---|
| Alumina Feeding | 3 | Number of Overfeeds | 1 | Alumina Shots | 0.94 |
| | 2 | Alumina Shots (CV) | 1 | Alumina Shots | -0.91 |
| | 4 | Number of Overfeeds (CV) | 2 | Alumina Shots (CV) | 0.89 |
| | 60 | AL2O3L | 1 | Alumina Shots | -0.88 |
| Mass and Energy Balance | 12 | Temperature (CV) | 14 | Liquidus (CV) | 0.96 |
| | 36 | TEMPL | 40 | LIQL | 0.94 |
| | 37 | TEMPKL | 12 | Temperature (CV) | 0.90 |
| | 11 | Temperature | 17 | $AlF_3$ | -0.88 |
| | 36 | TEMPL | 14 | Liquidus (CV) | 0.87 |
| | 43 | SHH | 37 | TEMPKL | 0.87 |
| | 40 | LIQL | 13 | Liquidus | -0.87 |
| | 43 | SHH | 15 | Superheat | 0.86 |
| Liquid Bath Mass | 66 | BHCALC | 22 | Cell Voltage (CV) | 0.96 |
| | 9 | Iron Content | 70 | BVINC | 0.92 |
| | 66 | BHCALC | 8 | Bath Height (CV) | 0.88 |
| | 67 | BHL | 12 | Temperature (CV) | 0.86 |
| | 67 | BHL | 37 | TEMPKL | 0.86 |
| | 7 | Bath Height | 17 | $AlF_3$ | 0.85 |
| | 68 | BHH | 41 | LIQH | -0.85 |
| Process Stability | 10 | Iron Content (CV) | 20 | Silicon Content (CV) | 0.91 |
| | 22 | Cell Voltage (CV) | 23 | Cathode resistance | -0.91 |
| | 30 | Ellipsoid Volume (CV) | 32 | Pinballing (CV) | 0.90 |
| | 44 | NP | 26 | Noise (CV) | 0.90 |
| | 5 | Anode Effect | 25 | Noise | 0.89 |
| | 68 | SHH | 44 | NP | 0.88 |
| | 9 | Iron Content | 44 | NP | 0.87 |
| | 43 | SHH | 26 | Noise (CV) | 0.86 |
| Abnormalities | 23 | Cathode resistance | 66 | BHCALC | -0.88 |
| | 54 | TOTAN | 49 | ANSPS | 0.88 |
| | 39 | TEMPKH | 53 | CLMVH | -0.88 |
| | 37 | TEMPKL | 56 | CBSPK | 0.87 |

***Table 5.10*** *Main Paired Correlations between Process Variables with Events for the Test Cells*

| | Nr. | Parameter 1 (Variable or Event) | Nr. | Parameter 2 (Variable or Event) | Correlation Coefficient |
|---|---|---|---|---|---|
| Alumina Feeding | 3 | Number of Overfeeds | 1 | Alumina Shots | 0.98 |
| | 4 | Number of Overfeeds (CV) | 2 | Alumina Shots (CV) | 0.95 |
| | 59 | AL2O3H | 3 | Number of Overfeeds | 0.91 |
| | 6 | Anode Effect (CV) | 5 | Anode Effect | -0.91 |
| | 62 | OAERR | 60 | AL2O3L | 0.90 |
| | 59 | AL2O3H | 1 | Alumina Shots | 0.90 |
| | 60 | AL2O3L | 1 | Alumina Shots | -0.88 |
| | 60 | AL2O3L | 3 | Number of Overfeeds | -0.87 |
| Mass and Energy Balance | 15 | Superheat | 2 | Alumina Shots (CV) | 0.94 |
| | 12 | Temperature (CV) | 14 | Liquidus (CV) | 0.94 |
| | 37 | TEMPKL | 36 | TEMPL | 0.93 |
| | 36 | TEMPL | 14 | Liquidus (CV) | 0.93 |
| | 15 | Superheat | 4 | Number of Overfeeds (CV) | 0.93 |
| | 16 | Superheat (CV) | 2 | Alumina Shots (CV) | 0.93 |
| | 16 | Superheat (CV) | 15 | Superheat | 0.91 |
| | 16 | Superheat (CV) | 4 | Number of Overfeeds (CV) | 0.89 |
| | 37 | TEMPKL | 40 | LIQL | 0.89 |
| | 12 | Temperature (CV) | 16 | Superheat (CV) | 0.87 |
| | 40 | LIQL | 36 | TEMPL | 0.87 |
| | 36 | TEMPL | 12 | Temperature (CV) | 0.86 |
| Liquid Bath Mass | 70 | BVINC | 11 | Temperature | 0.86 |
| Process Stability | 43 | SHH | 24 | Cathode resistance (CV) | 0.91 |
| | 24 | Cathode resistance (CV) | 21 | Cell Voltage | 0.87 |
| | 25 | Noise | 23 | Cathode resistance | 0.85 |
| Abnormalities | 55 | CBERR | 57 | CBDIST | 0.99 |
| | 19 | Silicon Content | 48 | ANSPM | 0.91 |
| | 60 | Al2O3L | 52 | ANHGH | 0.91 |
| | 62 | OAERR | 52 | ANHGH | 0.87 |
| | 54 | TOTAN | 49 | ANSPS | 0.87 |
| | 62 | OAERR | 55 | CBERR | 0.86 |
| | 2 | Alumina Shots (CV) | 35 | TOTEV | 0.85 |
| | 62 | OAERR | 57 | CBDIST | 0.85 |

***Table 5.11*** *Main Paired Correlations between Process Variables with Events for the Reference Cells*

#### 5.1.3.2 Mass and Energy Balance (Group F2)

For the test group, Table 5.10 shows a clear relation between the temperature with the $AlF_3$ concentration (variables 11, 17). This paired correlation is not found for the reference cells, which indicates a better control of the superheat (variable 15) and therefore the mass and energy balance for the test cells (Table 5.11). As discussed in Section 5.1.3.1 this behaviour is most likely the result of less occurrences of the hypothesized sludge cycle, partly in combination with a reduced destabilizing effect, resulting in low sludging, low variability in the number of overfeeds, and better alumina dissolution consistency (Section 5.2.1.1).

A number of paired correlations between process variables and/or events regarding the mass and energy balance are found for the test cells. Paired correlations are found between the variability in the bath temperature with the liquidus temperature (variables 12, 14), between the variability in the temperature (variable 12) with critical high temperature events (TEMPKL, event 37), between the variability in liquidus temperature (variable 14) with low temperature events (TEMPL, event 36), between the liquidus temperature (variable 13) with low liquidus temperature events (LIQL, event 40), between the superheat (variable 15) with number of superheat events (SHH, event 43), and between the number of low liquidus temperature events (LIQL, event 40) with low bath temperature events (TEMPL, event 36). These paired correlations are part of the self-regulation mechanism of the mass and energy balance via the side ledge as shown in Figures 2.4 and 3.18.

Furthermore, the test group underlines an important failure mechanism, which is linked to a critical low bath temperature (TEMPKL, event 37) and high number of superheat excursions (SHH, event 43) (Section 3.2.1.1). This correlation has been identified earlier as part of the sludge cycle (Section 5.2.1.1). Ordinary control strategies - not measuring the superheat or using a univariate control approach as represented by the yellow region in Figure 3.18 - increase the cell voltage under these conditions resulting in fast melting of the side ledge. Simultaneous bath and liquidus temperature measurements distinguish between mass and energy imbalances and improve underlying control decisions. An addition of soda ash as given by Equation 2.13 is the most appropriate, although costly remedial control action, because it restores the bath chemistry and alumina dissolution characteristics.

The reference cells show a positive paired correlation between the variability in the alumina shots (variable 2) and overfeeds (variable 4) with the average and variability in the superheat (variables 15, 16). A correlation between the average superheat with its variability is also found. Again, these correlations has been identified earlier as part of the sludge cycle as given by Figure 3.5. The variability in the liquidus point and superheat (variables 14, 16) are correlated with the variability in the bath temperature (variable 12). The variability in the bath and liquidus temperatures (variables 12, 14) are linked to low temperature event (TEMPL,

event 36). Table 5.11 shows a clear interdependency between TEMPKL (event 37), TEMPL (event 36) and LIQL (event 40). As identified for the test cells, these correlations highlight the relation between the mass and energy balance via the side ledge.

#### 5.1.3.3 Liquid Bath Mass (Group F3)

Table 5.10 demonstrates a number of paired correlations regarding the liquid bath mass for the test cells. Abnormalities in the calculated bath height (BHCALC, event 66) are connected to variations in the cell voltage and bath height (variables 22, 8). In this respect variations in the voltage initiate variations in the corresponding ACD and therefore in the stability of the bath height. Under these conditions the calculation of the bath height via the plungers is not reliable enough for control purposes (Section 3.2.2.2).

A clear correlation is found between a sensed increase in bath mass (BVINC, event 70) with the iron content (variable 9), which is linked to stub attack. This confirms the reliability of the soft sensor for bath mass increase detection (Section 5.1.2.4). Low bath height excursions (BHL, event 67) are linked to the variability in bath temperature (variable 12) and critical low temperature events (TEMPKL, event 37). This is associated with sludge formation leading to a decrease in liquid bath mass and increased energy demand due to an increase in alumina additions (Section 3.1.1). Furthermore, it is connected to an increase in the cell voltage (and therefore the ACD) due to automatic control actions. Also, it is linked to increased ridge formation because of a low temperature of the cathode surface (Section 3.1.5).

High bath height excursions (BHH, event 68) are inversely correlated to high liquidus temperature events (LIQH, event 41). A positive correlation between the bath height with the $AlF_3$ concentration in the electrolyte (variables 7, 17) is found. This is in line with a slope-based alumina feeding strategy in which the average concentration will decrease at higher liquid mass inventory (Section 3.1.1, point 13). The $AlF_3$ concentration will increase due to the mass balance control at a fixed target liquidus temperature (Equations 2.19 and 3.4).

For the reference cells, the only significant correlation regarding the liquid electrolyte mass is found between the bath temperature (variable 11) with a detected increase in bath mass (BVINC, event 70) as shown in Table 5.11. A high temperature is linked to increased energy dissipation within a smelting cell with associated melting of side cryolite (especially near the cathode surface). In both groups no significant correlations between the bath superheat and liquid bath mass variations are found showing that side ledge variations is not a major driver of bath mass in the Aldel cell (Section 2.1.4).

#### 5.1.3.4 Process Stability (Group F4)

Table 5.10 demonstrates a clear correlation between high noise events (NP, event 44) with the variability in noise (variable 26), high superheat events (SHH, event 68) and the average iron content (variable 9) for the test group. Also, the variability in noise (variable 26) is linked to high superheat excursions (SHH, event 43) and the anode effect frequency (variable 5) is related to the average noise (variable 25). These observations are closely connected to process instabilities. Typically noisy cells are observed to have an increased cell voltage and are therefore associated with increased heat generation resulting in a high superheat with corresponding melting of side ledge. A higher anode effect frequency is connected to the deterioration in the controllability of the alumina feeding strategy due to an unpredictable development in the resistance over time (Section 2.1.1).

The positive correlation between the variability in the iron with the silicon content (variables 10, 20) identifies a failure mechanism resulting in a fast increase in the liquid bath mass (stub attack) due to losing protective side ledge (Section 5.1.3.3). The correlation between the variability in the ellipsoid volume with the variability in pinballing (variables 30, 32) is in line with these observations. A negative correlation between the cathode resistance with the variability in the voltage (variables 23, 22) could indicate less stable energy balance control in smelting cells which are equipped with increased cathode bar dimensions as discussed in Section 4.2.3.1. The instabilities are exacerbated with the employment of power modulation, but could reduce at higher line current due to a higher cathode surface temperature.

The cathode resistance and noise (variables 23, 25) are correlated in the reference cells as shown in Table 5.11. In this respect a higher cathode resistance is linked to higher levels of sludge and ridge resulting in a decline in the electromagnetic stability induced by increased horizontal currents in the metal (Section 1.3.5). The variability in the cathode resistance (variable 24) is linked to the number of high superheat excursions (SHH, event 43) and the average cell voltage (variable 21).

#### 5.1.3.5 Abnormalities (Group F5)

Different and mainly independent failure mechanisms are identified in the test and reference cells. For the test cells, Table 5.10 demonstrates a negative correlation between errors in the bath height calculation (BHCALC, 66) with the cathode resistance (variable 23). This is in line with a less stable energy balance control on the smelting cells with increased cathode bar dimensions resulting in more cathode ridge formation (Section 5.1.3.4).

Furthermore, a positive correlation between plugged feeders (CBSPK, event 56) with a critical low temperature (TEMPKL, event 37) highlights the effects of uncontrolled alumina

feeding. Under these process conditions alumina collects on top of the point feed hole and enters the electrolyte as a big chunk if the hole opens up (naturally or by human intervention at anode setting). This leads to large energy imbalances with a rapid decrease in the bath temperature.

Anode spikes detected by the shift operators (ANSPS, event 49) are connected to the total number of anode spikes (TOTAN, event 54). The number of critical high temperature events (TEMPKH, event 39) is inversely linked to the number of high positioned anodes during changing (ANHGH, event 52). However, the occurrence of this abnormality is almost zero and has therefore no significant contribution to the failure mechanisms for the test cells. In general, the formation of anode spikes (with a corresponding raise in the bath temperature) is linked to the accuracy of anode setting (Section 5.1.2.2).

For the reference cells, process abnormalities are closely linked to hardware failures and anode problems (Table 5.11). A general hardware failure of the alumina feeding equipment (CBERR, event 55) and a slow plunger (CBDIST, event 57) are correlated to a low number of overfeeds per day (OAERR, event 62). These correlations indicate uncontrolled alumina feeding. A lower number of overfeeds (OAERR) is associated to sludge dissolution which is a result of poor control of the alumina feeding (Section 3.3.2.3). The variability in alumina shots is linked to the total number of abnormalities (TOTEV, event 35). Again, this indicates a positive effect of an advanced system for abnormality detection combined with appropriate actions to correct or remove these abnormalities (Hypothesis 2).

The correlation between the number of anode spikes detected by the measurement team (ANSPM, event 48) with the silicon content (variable 19) for the reference cells is a result of inadequate spike detection by normal procedures. An increase in silicon levels is connected to the absence of side ledge (locally) due to excessive heat generation. The number of anode spikes detected by the shift operators (ANSPS, event 49) is linked to the total number of anode spikes (TOTAN, event 54). Also, less alumina ratio low events (AL2O3L, event 60) and overfeeds (OAERR, event 62) are linked to the number of high positioned anodes during changing (ANHGH, event 52). However, the occurrence of the ANHGH event is almost zero and has therefore no significant contribution to the group-specific failure mechanisms for the reference cells.

### 5.1.4 Multivariate Statistical System Dynamics

In this section a multivariate statistical analysis is carried out as described in Section 2.2.6. This investigation identifies the principal components in both the test and reference cells respectively. A PLS analysis explains the captured variance per principal component for the quality data. This quality data is represented by the productivity per cell per day, the current

efficiency and energy consumption (Sections 5.1.1.5 and 5.1.2.5). Based on the individual principal components and their contribution to the current efficiency and energy consumption the predominant system dynamics on both groups of cells are determined.

### 5.1.4.1 Test Cells

Figure 5.2 shows the five principal components capturing the variance for the quality data for the test cells (variables 71-73, Tables 5.1 and 5.6). These components are built upon the process variables (variables 1-32, Table 5.1) and abnormality detection (events 33-70, Table 5.6). The total variance between cells within the test group related to the productivity, current efficiency and energy consumption is explained by three principal components (PC1-PC3), representing 97.4% of the total variance. Figure 5.3 shows the individual contributors in the order of importance to the principal components.

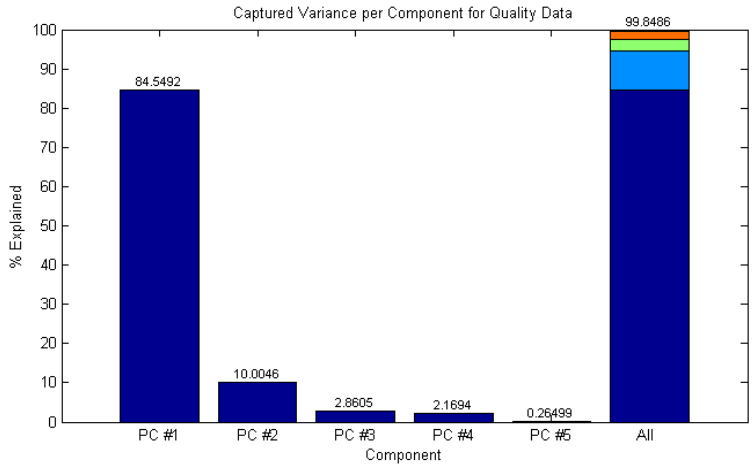


***Figure 5.2*** *Principal Components Related to the Overall Efficiency for the Test Cells*

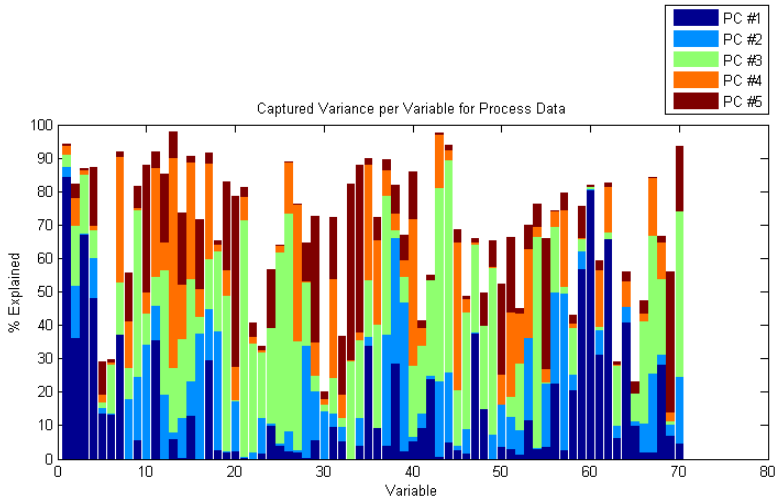


***Figure 5.3*** *Individual Contributors to the Principal Components for the Test Cells*

Alumina feeding plays a predominant role in PC1, which captures 84.5% of the variance. Table 5.12 shows the individual contributors to the main principal components. The first six contributors (variables/events 1, 3, 4, 59, 60, 62) are also identified as the main causes of variation for the process variables and abnormalities in relation to the current efficiency and energy consumption (Tables 5.2 and 5.7). The remaining contributors regarding alumina feeding are the average bath height (variable 7), the variability in alumina shots (variable 2) and the detected abnormalities AEERR, OACURV (variables 61, 64). These observations are in line with the observations in Sections 5.1.1.1 and 5.1.2.3. A higher bath height and a lower number of AEERR and OACURV events are associated with better alumina dissolution effectiveness.

| Nr. | PC1 (84.5%) | CONT | Nr. | PC2 (10.0%) | CONT | Nr. | PC3 (2.9%) | CONT |
|---|---|---|---|---|---|---|---|---|
| 1 | Alumina Shots | 0.85 | 57 | CBDIST | 0.47 | 21 | Cell Voltage | 0.71 |
| 60 | AL2O3L | 0.81 | 39 | TEMPKH | 0.45 | 26 | Noise (CV) | 0.65 |
| 3 | Overfeeds | 0.67 | 38 | TEMPH | 0.38 | 44 | NP | 0.63 |
| 62 | OAERR | 0.66 | 16 | Superheat (CV) | 0.37 | 54 | TOTAN | 0.63 |
| 59 | Al2O3H | 0.57 | 18 | $AlF_3$ Conc. (CV) | 0.35 | 43 | SHH | 0.58 |
| 4 | Overfeeds (CV) | 0.48 | 10 | Iron Content (CV) | 0.34 | 25 | Noise | 0.57 |
| 64 | AEERR | 0.41 | 28 | Cathode Current (CV) | 0.33 | 9 | Iron Content | 0.50 |
| 47 | ANSPA | 0.38 | 37 | TEMPKL | 0.33 | 70 | BVINC | 0.50 |
| 7 | Bath Height | 0.37 | | | | 49 | ANSPS | 0.50 |
| 2 | Alumina Shots (CV) | 0.37 | | | | 19 | Silicon Content | 0.47 |
| 11 | Temperature | 0.36 | | | | 37 | TEMPKL | 0.42 |
| 35 | TOTEV | 0.34 | | | | 67 | BHL | 0.41 |
| 61 | OACURV | 0.31 | | | | 12 | Temperature (CV) | 0.37 |
| 17 | $AlF_3$ concentration | 0.30 | | | | 46 | CBAN | 0.35 |
| | | | | | | 22 | Cell Voltage (CV) | 0.33 |
| | | | | | | 27 | Anode Current (CV) | 0.33 |
| | | | | | | 36 | TEMPL | 0.31 |
| | | | | | | 66 | BHCALC | 0.31 |
| | | | | | | 15 | Superheat | 0.31 |

***Table 5.12*** *Individual Contributors of the PC's Related to the Current and Energy Efficiency for the Test Cells*

Furthermore, the temperature and $AlF_3$ concentration (variables 11, 17) are also identified as main contributors to PC1. These variables show a clear paired correlation and are linked to better alumina feed control resulting in a tighter alumina concentration band as discussed in Section 5.1.3.2. The number of automatic detected anode spikes (ANSPA, event 47) and the total duration of detected abnormalities (TOTEV, event 35) are also significant contributors to PC1. A significant contribution of these parameters to the current and energy efficiency indicates a positive effect of an advanced system for abnormality detection combined with appropriate actions to correct or remove these abnormalities.

PC2 captures 10.0% of the variance for cells within the test group and relates to the sludge cycle disturbances specifically. CBDIST (event 57) is related to hardware failures of the alumina feed equipment. These hardware failures are connected to uncontrolled alumina

feeding and associated mass and energy imbalances (Section 5.1.3.5). These imbalances lead to abnormalities in the bath temperature (events 37-39) and higher variability in the cell superheat and $AlF_3$ concentration (variables 16, 18). The variability in the cathode current distribution (variable 28) may be linked to dynamics in sludge formation and dissolution. The contribution of the variability in the iron content (variable 10) due to large liquid bath height variations is part of the prevailing sludge cycle (Hypothesis 1).

PC3 captures only 2.9% of the variance and incorporates process stability (Section 5.1.3.4) and abnormalities (Section 5.1.3.5). Abnormalities in anode conditions (events 46, 49, 54) are recognized as important contributors to PC3. These problems - if not detected in an early stage - lead to process instabilities (variables/events 21, 22, 25, 26, 27, 44) with associated disturbances in mass and energy balance (variables/events 12, 15, 19, 36, 37, 43; Section 5.1.3.2) and liquid bath mass variations (variables/events 9, 66, 67, 10; Section 5.1.3.3).

### 5.1.4.2 Reference Cells

Figure 5.4 shows the five principal components capturing the variance for the quality data on the reference cells (variables 71-73, Tables 5.1 and 5.6). These components are built upon the averages (AVG) and the coefficients of variation (CV) of the process behaviour (variables 1-32, Tables 5.1) and abnormality detection (events 33-70, Table 5.6). The variance within the reference cells related to the productivity per cell per day, current efficiency and energy consumption is explained by three principal components, representing 98.4% of the variance (P1-P3). The individual contributors are given by Figure 5.5 in the order of importance to the principal components.

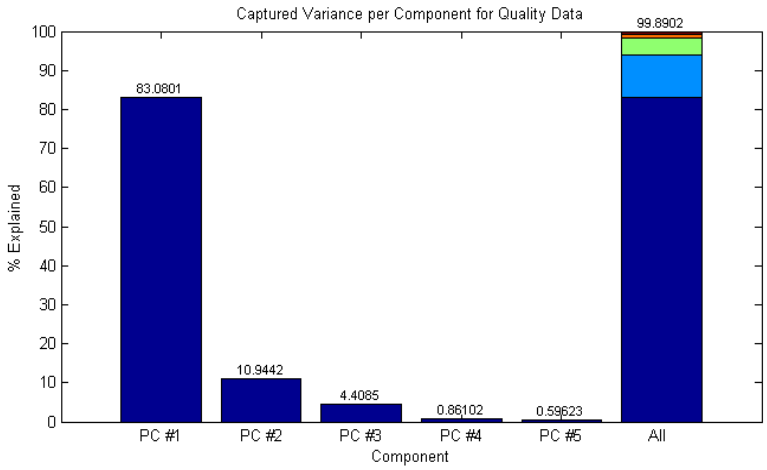


***Figure 5.4*** *Principal Components Related to the Overall Efficiency for the Reference Cells*

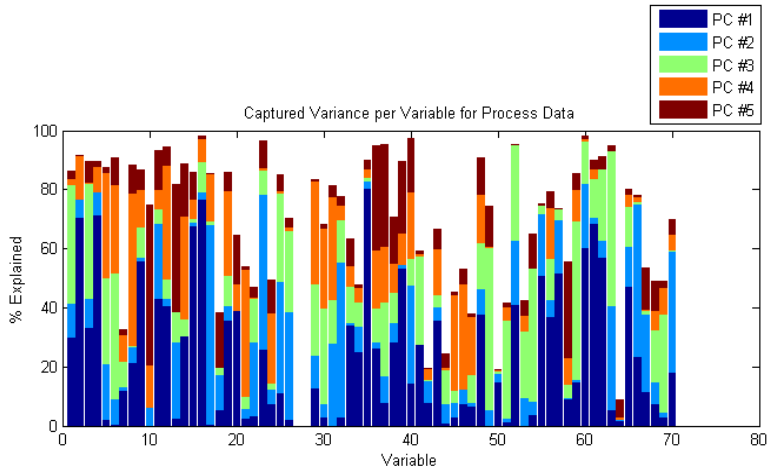


***Figure 5.5*** *Individual Contributors to the Principal Components for the Reference Cells*

| Nr. | PC1 (83.1%) | CONT | Nr. | PC2 (10.9%) | CONT | Nr. | PC3 (4.4%) | CONT |
|---|---|---|---|---|---|---|---|---|
| 35 | TOTEV | 0.80 | 17 | $AlF_3$ concentration | 0.68 | 49 | ANSPS | 0.55 |
| 16 | Superheat (CV) | 0.77 | 32 | Pinballing (CV) | 0.52 | 59 | Al2O3H | 0.54 |
| 4 | Overfeeds (CV) | 0.72 | 23 | Cathode resistance | 0.52 | 5 | Anode Effect | 0.52 |
| 2 | Alumina Shots (CV) | 0.71 | 66 | BHCALC | 0.52 | 54 | TOTAN | 0.45 |
| 61 | OACURV | 0.69 | 70 | BVINC | 0.41 | 6 | Anode Effects (CV) | 0.42 |
| 15 | Superheat | 0.68 | 25 | Noise | 0.38 | 1 | Alumina Shots | 0.40 |
| 60 | Al2O3L | 0.60 | 26 | Noise (CV) | 0.36 | 3 | Overfeeds | 0.39 |
| 62 | OAERR | 0.57 | 5 | Anode Effects | 0.35 | 69 | BVDEC | 0.33 |
| 9 | Iron Content | 0.56 | 40 | LIQL | 0.33 | 51 | ANOFF | 0.33 |
| 39 | TEMPKH | 0.53 | | | | 30 | Ellipsoid Volume (CV) | 0.32 |
| 57 | CBDIST | 0.52 | | | | 52 | ANHGH | 0.32 |
| 55 | CBERR | 0.51 | | | | 25 | Noise | 0.30 |
| 65 | AEKWH | 0.47 | | | | 41 | LIQH | 0.30 |
| 11 | Temperature | 0.43 | | | | | | |
| 52 | ANHGH | 0.41 | | | | | | |
| 12 | Temperature (CV) | 0.41 | | | | | | |
| 20 | Silicon (CV) | 0.39 | | | | | | |
| 48 | ANSPM | 0.38 | | | | | | |
| 56 | CBSPK | 0.37 | | | | | | |
| 19 | Silicon | 0.36 | | | | | | |
| 43 | SHH | 0.36 | | | | | | |
| 33 | HOTLAH | 0.34 | | | | | | |
| 3 | Overfeeds | 0.33 | | | | | | |
| 14 | Liquidus (CV) | 0.30 | | | | | | |
| 1 | Alumina Shots | 0.30 | | | | | | |

***Table 5.13*** *Individual Contributors of the PC's Related to the Current and Energy Efficiency for the Reference Cells*

Contrary to the multivariate statistical analysis for the test cells, the principal components for the reference cells do not show similar univocal process behaviour (Table 5.13). Although PC1 explains 83.1% of the variance, it contains a wide range of detected abnormalities. Actually, the most important contributor to PC1 is the total duration of detected abnormalities (TOTEV, event 35) (Hypothesis 2). The controllability of the alumina feeding also plays a

significant role (variables/events 1-4, 60-62, 65). This is also confirmed by the observations as discussed in Sections 5.1.1.5 and 5.1.2.5.

Hardware problems in the alumina feeding equipment (events 55-57) are an important failure mechanism with respect to the contribution in the deterioration of the current and energy efficiency for the reference cells. These abnormalities lead to uncontrolled alumina feeding resulting in large energy imbalances as described in Section 5.1.3.5.

Furthermore, PC1 incorporates abnormalities in the anode conditions (events 48, 52). These anode problems are correlated to abnormal behaviour in the process variables (variables 9, 11, 12, 14-16, 19, 20) and abnormalities (33, 39, 43). In this respect hardware failures of feeding equipment and anode problems lead to destabilizing of the self-regulating characteristics of the smelting process as given by Figure 3.11.

PC2 captures 10.9% of the variance for the quality data within cells in the reference group and it is linked to electromagnetic stability. The $AlF_3$ concentration (variable 17), low liquidus temperature (event 40), cathode resistance (variable 23), the average and variability in noise (variables 25, 26) and the number of anode effects (variable 5) indicate problems with sludge and ridge formation resulting in a decrease in the stability of the smelting process. These problems result in an increase in the variability in pinballing (variable 32), abnormalities in the calculation of the bath height (event 66) and liquid bath mass variations.

PC3 captures only 4.4% of the variance. This component contains abnormalities in anode conditions (events 49, 51, 52, 54). These abnormalities result in excursions in the control of the mass and energy balance control (event 41 and variable 30). There is also a contribution of the alumina feeding to PC3 (variable/event 1, 3, 5, 6, 25, 59). The decrease in the liquid bath mass combined with the alumina feeding observations indicates potential problems with the alumina dissolution. The combination of both mechanisms (anode and alumina feeding problems) suggests a slow detection of anode problems resulting in an overcompensation of the control model. This leads to a reduction in energy supply to the cells and a reduction of the alumina dissolution rate.

## 5.2 Hypotheses

Based on the theoretical development undertaken in Chapter 3, two main hypotheses are postulated in this thesis (Section 3.5). These hypotheses are evaluated in the context of the main results of the industrial experiments as presented in Section 5.1. The first hypothesis constructed in this thesis is a self-accelerating sludge cycle caused by incomplete alumina dissolution. This sludge cycle drives liquid bath mass variations and increased alumina

feeding until large and prolonged bath temperature and composition variation is produced. This is discussed in Section 5.2.1.

The widely varying observed responses of the cell to the same (repetitive) set of alumina feed events demonstrates that the longer term energy and mass balance of the cell (its process state) does have a profound influence on the process trajectory and subsequent cell outcomes (and control actions). This more general evidence of chaotic behaviour dictates that simple, linear or even compensatory multivariate control schemes will not be successful in the aluminium smelting process (Abraham and Shaw, 1987).

This leads to the second hypothesis constructed in this thesis. A multivariate causally based control approach using natural behaviour envelops for individual cells and cause-specific detection and diagnosis of abnormalities will improve control and shrink the cell envelops. Continual improvement is supported by recalculation of natural behaviour envelops leading to improved decision-making. This is discussed in Section 5.2.2.

### 5.2.1 Sludge Cycle Driving Liquid Bath Variations

One self-accelerating mechanism being hypothesised is a prevailing sludge cycle caused by incomplete alumina dissolution driving liquid bath mass variations and increased alumina feeding (Sections 3.1.1 and 3.1.5). For the test cells, a number of precautions to the control strategy are implemented to reduce the associated deterioration in the stability of the mass and energy balance. In general, the alumina feeding is incorporated in the natural behaviour envelop of a cell (Section 3.3.1). More specifically, additional control actions are carried out during accumulation of alumina within a cell and anode changing (Table 3.6). Furthermore, the alumina mass fed during overfeed and duration are minimized (Section 3.1.3).

The investigations undertaken in Section 5.1 related to the underlying process behaviour envelops, detected abnormalities, paired correlations and the multivariate statistical analyses of the overall system dynamics within the test and reference cells provide information about the hypothesized phenomena. Section 5.2.1.1 discusses the results of the industrial experiments with respect to the sludge cycle. Supporting measurements of liquid mass variations before and after the implementation of the new control philosophy are presented in Section 5.2.1.2.

#### 5.2.1.1 Results of the Industrial Experiments

A significantly higher number of alumina shots (variable 1), higher average and lower variability in overfeeds (variables 3, 4), lower average and variability in underfeed duration and superheat (variables 15, 16), more AL2O3H (event 59) and less OACURV events (event

61) are found for the test group in comparison with the reference group (Tables 5.1, 5.3, 5.6 and 5.8). For the test cells, the current efficiency and energy consumption are correlated to the alumina shots, Al2O3L and Al2O3H events. The current and energy efficiency are also linked to a higher average and lower variability of overfeeds usually associated with the rate of alumina dissolution, along with lower variability in underfeed duration which is the absolute measure of variation in the alumina concentration (Sections 5.1.1.5 and 5.1.2.5).

Except for the variability in the number of overfeeds (variable 4), these variables are not identified as significant contributors to the current and energy efficiency for the reference cells. The variability in alumina shots (variable 2), average and variability in the superheat (variable 15, 16), average cathode resistance (variable 23), iron content (variable 9), and the events OACURV, OAERR and AEKWH (events 61, 62, 65) are correlated to the current and energy efficiency. These variables and events show different paired correlations indicating a clear interactive behaviour between the effectiveness of the alumina feeding strategy and the stability in the mass and energy balance (Figure 3.11).

The test cells operate at a lower alumina concentration than the reference cells as indicated by a significantly lower underfeed duration, higher average and lower variability in the anode effect frequency (variables 5-6), higher number of AEERR events (event 64) combined with higher liquidus temperature (variable 13) and LIQH events (event 41) (Tables 5.1, 5.3, 5.6 and 5.8). In this respect a higher average and lower variability in the cell voltage (variables 21, 22) result in a higher and more stable ACD. In the case of alumina feed control based on slope triggers a lower and more stable alumina concentration can be achieved as described in Section 2.1.1. These process conditions favour alumina dissolution according to Equation 2.1 and improve the effectiveness of the alumina feeding strategy as discussed in Section 5.1.1.1.

A significantly higher bath height (variable 7) is achieved for the test cells (Section 5.1.1.1). However, the variability in the iron content (variable 10) is significantly lower for these cells. A lower number of liquid bath mass variations for the test cells is confirmed by a significantly lower number of increased (BVINC, event 70) and decreased (BVDEC, event 69) liquid bath mass events (Section 5.1.2.4). The BVINC event is correlated to the iron content (variable 9) for the test cells, whereas it is correlated with the temperature (variable 11) for the reference cells (Section 5.1.3.3). The ratio of BVDEC over BVINC is also considerable higher for the reference cells indicating the tendency for running low bath levels.

For the test cells, low bath height excursions (BHL, event 67) are linked to the variability in bath temperature (variable 11) and the number of critical low temperature events (TEMPKL, event 37) (Section 5.1.3.3). These correlations are associated with sludge formation, which results in a decrease in the liquid bath mass combined with an increase in energy demand

due to more alumina additions. Furthermore, Section 5.1.3.2 identifies a positive correlation between critical low temperature events (TEMPKL, event 37) with high superheat events (SHH, event 43). Under these conditions sludge formation is delayed due to an increase in sensible heat for dissolution due to high superheat, but it is accelerated due to an increase in the alumina concentration and decrease in bath temperature.

High bath height events (BHH, event 68) are inversely linked to high liquidus temperature events (LIQH, event 41). Also, a positive correlation between the bath height (variable 7) with the $AlF_3$ concentration (variable 17) is found. This is in line with a slope-based alumina feeding strategy in which the average alumina concentration will decrease at higher liquid bath mass favouring the dissolution characteristics (Section 3.1.1, point 13). However, mass balance control based on a fixed target liquidus temperature will lead to an increase in the average $AlF_3$ concentration, which deteriorates alumina dissolution (Equation 2.21).

A significantly lower number of abnormalities in the reaction of the cell resistance to overfeed (OACURV, event 61) are found for the test cells. For the reference cells, the abnormalities OACURV and OAERR (events 61, 62) events are determined as significant contributors to the current efficiency and energy consumption (Table 5.9). These abnormalities are inversely correlated to the current and energy efficiency. A low number of overfeeds (OAERR) is linked to hardware failures of the alumina feeding equipment (CBERR and CBDIST; events 55, 57) for these cells (Section 5.1.3.5). In this respect the integrity of the alumina feeding equipment is essential for maintaining stable operating conditions and avoiding uncontrolled feeding.

The average cathode resistance and noise (variables 23, 25) are correlated for the reference cells (Section 5.1.3.4). For the test cells, a significantly lower variability in these variables is found. These observations indicate fewer extremes in sludge formation and dissolution for the test cells. A significantly lower number of high pinballing events (PBH, event 34), along with lower average and variability in the calculated ellipsoid volume and pinballing (variables 29-32) confirm a more stable and predictable process behaviour for the test group.

As described in Section 5.1.4 the multivariate statistical analysis provide an overview of the more complex interplay between the process behaviour, detected abnormalities and specific failure mechanisms. For the test cells, alumina feeding and associated variables and events play a predominant role in the main principal component in the variance of the quality data as given by Table 5.12. The effectiveness of the alumina feeding plays also a significant role for the reference cells, but the overall system dynamics are dominated by the total duration of detected abnormalities (TOTEV, event 35).

Hardware failures of alumina feed equipment also play a significant role in self-accelerating destabilizing mechanisms leading to intensified complex system dynamics. PC2 captures 10.0% of the variance for the test cells (Section 5.1.4.1). The incorporated hardware failures are linked to uncontrolled alumina feeding and associated mass and energy imbalances. This leads to abnormalities in the bath temperature and higher variability in superheat and $AlF_3$ concentration. The cathode current distribution is linked to dynamics in sludge formation and dissolution. The variability in the iron content is associated with large liquid bath height variations, which is part of the sludge cycle.

As discussed in this section the results of the industrial experiments confirm the existence of a prevailing sludge cycle in aluminium smelting cells (Hypothesis 1). The contribution of the sludge cycle to the underlying process variation for the test cells is significantly less than for the reference cells. This is verified by a significantly lower and more stable average alumina concentration (variables/events 5, 6, 13, 41, 64) and superheat (variables 15, 16), better process stability (variables/events 21, 22, 24-26, 29-32, 34), lower number of abnormalities in alumina feeding (61) and a higher and more stable liquid bath mass (variables/events 7, 10, 69, 70). In this respect a more stable and predictable behaviour is achieved for the test cells, based on the self-regulating side ledge mechanism as shown in Figure 2.4. However, a sludge cycle is still part of the process variation for these cells as shown in the contributors to PC1 and PC2 (Table 5.12).

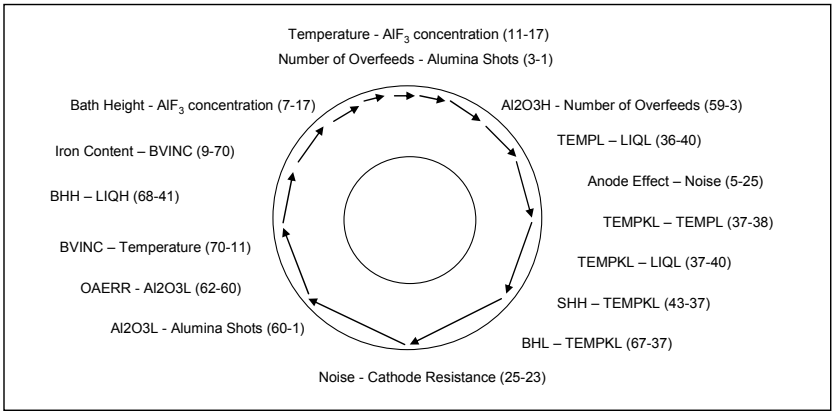


***Figure 5.6*** *Process Variables and Abnormalities Plotted in Sludge Cycle*

Figure 5.6 overlays the significant correlations found for the test and reference cells plotted in the sludge cycle as demonstrated in Figure 3.5. Points 1-14 in Section 3.1.1 describe the influences of the sludge cycle to the compositional and electromagnetic stability of the smelting process. Preferential sludge formation over sludge dissolution results in more alumina additions to the cell resulting in an increase in energy demand. This leads to a decrease in the bath and liquidus temperature. The liquid bath mass also decreases over time. The dissolution of sludge is accelerated halfway through the cycle due to an increase in

the electromagnetic instability (horizontal current flow in the metal) and therefore an increase in turbulences in the metal. Under these conditions the bath and liquidus temperature will increase rapidly leading to an increase in the liquid bath mass.

#### 5.2.1.2 Supporting Liquid Mass Measurements

Figure 5.7 shows earlier data of liquid bath mass variations for a cell and confirms significant medium term variations in both liquid bath and metal inventories. These measurements were undertaken before the implementation of the new control philosophy (Stam *et al.*, 2008). An average bath mass of 4.65 tonnes is found with a coefficient of variation of 0.16 using a Sr-tracer (Section 2.3.1.3). The measured liquid bath inventory varies between 3.58 and 5.99 tonnes. The black arrows indicate bath tapping. The total variation in bath mass of 50% is in line with other studies (Section 2.1.4).

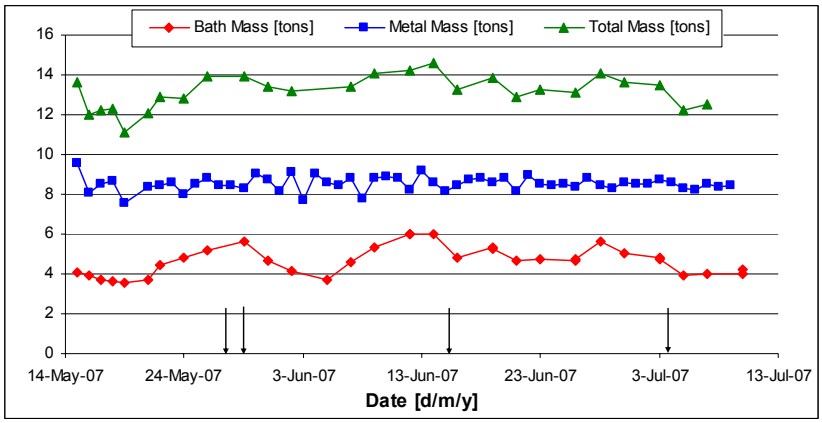


***Figure 5.7*** *Medium Term Variations of Bath and Metal Mass at Aldel (Stam et al., 2008)*

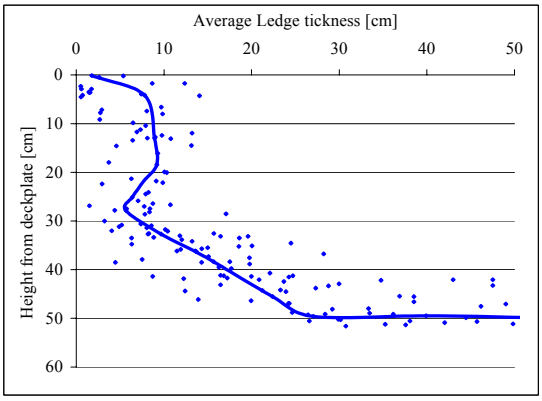


***Figure 5.8*** *Typical Ledge Profile at 140 kA at Aldel (Stam et al., 2008)*

Figure 5.8 shows an average minimum ledge thickness of 5.6 cm with a range of 1.5 to 11 cm and it can be concluded that the ramming paste is partly replaced by side ledge. The

measurements are consistent with the available liquid bath volume based on cell and anode dimensions, average ledge profile and a bath density of 2100 kg/m$^3$ ($AlF_3$=11%, $Al_2O_3$=3%, $CaF_2$=4% at $T_B$=960°C).

The average metal inventory is 8.55 tonnes with a coefficient of variation of 0.04 using a Cu-tracer (Section 2.3.1.3). This inventory is also consistent with the existing dimensions of the Aldel cell and a density of 2360 kg/m$^3$ ($T_{Al}$=950°C). The metal mass varies between 7.52 and 9.58 tonnes, which implies a total variation of 24%. Based on the copper analyses a current efficiency of 94% is found for this cell.

Figure 5.9 shows the results of measurements of medium term variations in both liquid bath and metal mass undertaken after the implementation of the new control philosophy. For Cell 2008, an average bath mass of 4.45 tonnes is found with a coefficient of variation of 0.10. The liquid bath mass varies between 3.53 and 5.59 tonnes, which represents a total variation of 45%. At a confidence level of 99.5% an F-test shows a significantly lower variation in bath mass after the implementation of the new control philosophy. However, the variation is still substantial with respect to both the effectiveness of the alumina feeding strategy and the controllability of the ensuing bath chemistry (Section 2.1.2 and 2.1.4). This shows the further potential for control improvement in this system.

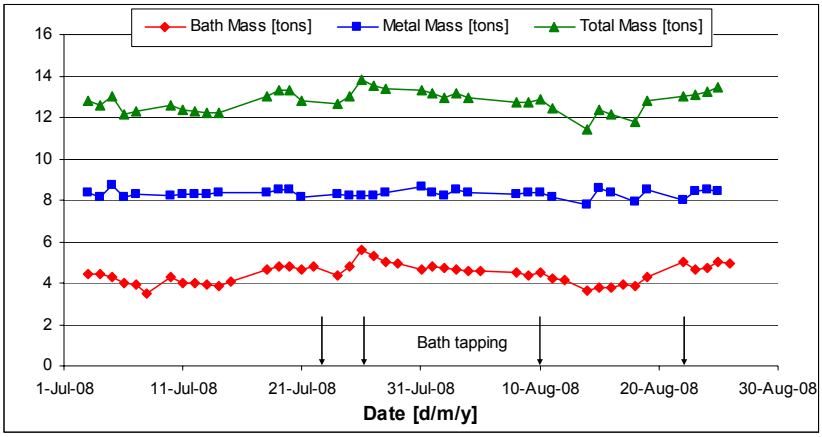


***Figure 5.9*** *Medium Term Variations of Bath and Metal Mass at Aldel (Cell 2008)*

The average metal mass is 8.32 tonnes with a coefficient of variation of 0.02. The range in inventory varies between 7.78 and 8.74 tons, which is a variation of 12%. The coefficient of variation in the total liquid mass has been reduced from 0.07 to 0.04. Both the average and variability in the metal mass are significantly lower with the employment of the new control philosophy. Again, this indicates less dynamics in sludge formation and dissolution as metal tapping is based on the calculated metal height at Aldel (Section 2.3.2). A more stable liquid

metal mass within the test cells reduces the variation in heat dissipation dynamics at a given cell voltage and line current.

Line current outages influence process stability significantly (Section 4.2.1.1). The total duration of outages during the period of the measurement of the liquid bath and metal inventory for Cell 2008 (July and August 2008) is 10:30 hours (Table 5.14). After a line current drop, a higher number of abnormalities in alumina feeding (CBERR, CBSPK; events 55-56) are found (Table 5.15). Under these process conditions plugged feeders are caused by increased freezing of the feeder holes with the absence of frequent breaking. Plugged feeders (CBSPK, event 56) result in uncontrolled alumina feeding and therefore to a higher number of critical low temperature events (TEMPKL, event 37) (Section 5.1.3.5).

| Date | Duration |
|---|---|
| 01-Jul-08 | 0:45 |
| 04-Jul-08 | 0:10 |
| 16-Jul-08 | 0:50 |
| 18-Jul-08 | 0:10 |
| 01-Aug-08 | 1:25 |
| 06-Aug-08 | 0:10 |
| 08-Aug-08 | 0:55 |
| 16-Aug-08 | 0:44 |
| 20-Aug-08 | 1:59 |
| 23-Aug-08 | 0:55 |
| 25-Aug-08 | 2:10 |
| 27-Aug-08 | 0:15 |
| **Total** | **10:30** |

***Table 5.14*** *Line Current Shut Downs*

| Date | Event |
|---|---|
| 02-Jul-08 | CBSPK |
| 05-Jul-08 | CBSPK |
| 09-Jul-08 | CBERR |
| 11-Jul-08 | CBERR |
| 13-Jul-08 | CBSPK |
| 15-Jul-08 | CBSPK |
| 26-Jul-08 | CBSPK |
| 03-Aug-08 | CBSPK |
| 06-Aug-08 | CBSPK |
| 13-Aug-08 | CBSPK |

***Table 5.15*** *Abnormalities in Alumina Feeding*

### 5.2.2 Multivariate Causally Based Control

The second hypothesis postulated in this thesis is that a multivariate causally based control approach using Hotelling $T^2$ statistic combined with cause-specific detection and diagnosis of abnormalities will improve the control of smelting cells. In the new control strategy automatic control responses are only allowed under specific conditions (Table 3.6). These conditions correspond to the space between the natural and mechanistic or structural behaviour envelop. In this region, $AlF_3$ additions and cell voltage are controlled according to Equations 3.4 and 3.5 respectively.

If a smelting cell is located outside the 95% confidence interval of the natural behaviour envelop or within the structural envelop, mass and energy balance controls are switched off and the control settings are returned to their targets. This avoids overcorrection and restricts unwanted variations. Pinballing is also defined as out of control behaviour (Section 3.3.3.1). Section 5.2.2.1 discusses the development of the overall process state over time for the test and reference cells. The effectiveness of advanced detection and correction of abnormalities in relation to the current and energy efficiency is discussed in Section 5.2.2.2.

#### 5.2.2.1 Overall Process State

The development of the ellipsoid volume over time for the test and reference cells is shown in Figure 5.10. At the start of the experiments the process stability for the test cells compared to the reference cells is worse according to a larger volume of the ellipsoid envelop. After the employment of the new control strategy for the test cells, the ensuing ellipsoid volume starts to decrease over time. After 2 months of experimentation the metal tapping strategy is re-designed as part of a continuous improvement project (route 4 in Figure 3.24). The interval between two successive tapping events is cut in half to run the cells close to their metal set-points. Unfortunately the metal set-point of the cells was also reduced by 1 cm for the test and reference cells.

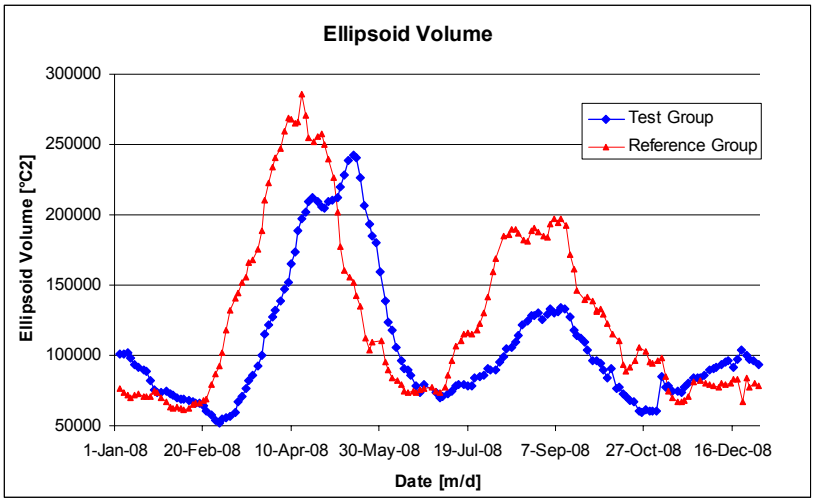


***Figure 5.10*** *Development of the Ellipsoid Volume over Time (Test and Reference Cells)*

A rapid increase in the ellipsoid volume from 20$^{th}$ February indicates a deterioration of the process stability over time. The rise in the ellipsoid volume was initially delayed for the test cells by avoiding overcorrecting control actions. However, the heat imbalance caused by reduction in metal height disturbed the natural behaviour envelops with respect to bath temperature and liquidus point. The larger cell envelops reduced the ability of the control system to detect abnormalities over the subsequent 3 months. Under these circumstances cause-specific detection and diagnosis of abnormalities is required. For the test cells, a second, higher peak (mid May) is linked to another heat balance disturbances due to power modulation (Figure 4.6). The test cells show a faster recovery as indicated by a shorter time period between the highest and lowest ellipsoid volume. The recovery of the process stability is accelerated by an internal self-checking and reinforcing mechanism at a continuous reducing ellipsoid volume.

For the test cells, additional interventions to the alumina feeding strategy (FA and FAC) are introduced in June (Table 3.6). At the beginning of July the overall process stability for the test and reference cells deteriorates and gets worse in August due to severe power modulation (515 minutes of current outages). Again, the rise in the ellipsoid volume was initially delayed by avoiding overcorrections, in the new control strategy for the test cells. Furthermore, the total impact of the underlying disturbance is significantly lower according to the lower peak in the ellipsoid volume. The additional interventions in the alumina feeding strategy suppress sludge formation with its ensuing cyclic process behaviour.

| | | October-08 | | | | | | | | | | | | | | | | | | | | | | | | | | | | |
|---|---|---|---|---|---|---|---|---|---|---|---|---|---|---|---|---|---|---|---|---|---|---|---|---|---|---|---|---|---|---|
| Nr. | Events | 1 | 2 | 3 | 4 | 5 | 6 | 7 | 8 | 9 | 10 | 11 | 12 | 13 | 14 | 15 | 16 | 17 | 18 | 19 | 20 | 21 | 22 | 23 | 24 | 25 | 26 | 27 | 28 | 29 | 30 | 31 |
| 33 | HOTLAH | | | | | | | | | | | | | | | | | | | | | | | | | | | | | | | |
| 34 | PBH | | | | | | | | | | | | | | | | | | | | | | | | | | | | | | | |
| 36 | TEMPL | | | | | | | | | | | | | | | | | | | | | | | | | | | | | | | |
| 37 | TEMPKL | | | | | | | | | | | | | | | | | | | | | | | | | | | | | | | |
| 38 | TEMPH | | | | | | | | | | | | | | | | | | | | | | | | | | | | | | | |
| 40 | LIQL | | | | | | | | | | | | | | | | | | | | | | | | | | | | | | | |
| 41 | LIQH | | | | | | | | | | | | | | | | | | | | | | | | | | | | | | | |
| 43 | SHH | | | | | | | | | | | | | | | | | | | | | | | | | | | | | | | |
| 45 | CD | | | | | | | | | | | | | | | | | | | | | | | | | | | | | | | |
| 55 | CBERR | | | | | | | | | | | | | | | | | | | | | | | | | | | | | | | |
| 56 | CBSPK | | | | | | | | | | | | | | | | | | | | | | | | | | | | | | | |
| 58 | ALFERR | | | | | | | | | | | | | | | | | | | | | | | | | | | | | | | |
| 59 | AL2O3H | | | | | | | | | | | | | | | | | | | | | | | | | | | | | | | |
| 60 | AL2O3L | | | | | | | | | | | | | | | | | | | | | | | | | | | | | | | |
| 61 | OACURV | | | | | | | | | | | | | | | | | | | | | | | | | | | | | | | |
| 62 | OAERR | | | | | | | | | | | | | | | | | | | | | | | | | | | | | | | |
| 63 | AE | | | | | | | | | | | | | | | | | | | | | | | | | | | | | | | |
| 65 | AEKWH | | | | | | | | | | | | | | | | | | | | | | | | | | | | | | | |
| 66 | BHCALC | | | | | | | | | | | | | | | | | | | | | | | | | | | | | | | |
| 67 | BHL | | | | | | | | | | | | | | | | | | | | | | | | | | | | | | | |
| 68 | BHH | | | | | | | | | | | | | | | | | | | | | | | | | | | | | | | |

***Table 5.16*** *Sequence of Detected Abnormalities in October 2008 for Cell 2008*

| | | November-08 | | | | | | | | | | | | | | | | | | | | | | | | | | | | |
|---|---|---|---|---|---|---|---|---|---|---|---|---|---|---|---|---|---|---|---|---|---|---|---|---|---|---|---|---|---|---|
| Nr. | Events | 1 | 2 | 3 | 4 | 5 | 6 | 7 | 8 | 9 | 10 | 11 | 12 | 13 | 14 | 15 | 16 | 17 | 18 | 19 | 20 | 21 | 22 | 23 | 24 | 25 | 26 | 27 | 28 | 29 | 30 |
| 33 | HOTLAH | | | | | | | | | | | | | | | | | | | | | | | | | | | | | | |
| 34 | PBH | | | | | | | | | | | | | | | | | | | | | | | | | | | | | | |
| 36 | TEMPL | | | | | | | | | | | | | | | | | | | | | | | | | | | | | | |
| 37 | TEMPKL | | | | | | | | | | | | | | | | | | | | | | | | | | | | | | |
| 38 | TEMPH | | | | | | | | | | | | | | | | | | | | | | | | | | | | | | |
| 40 | LIQL | | | | | | | | | | | | | | | | | | | | | | | | | | | | | | |
| 41 | LIQH | | | | | | | | | | | | | | | | | | | | | | | | | | | | | | |
| 43 | SHH | | | | | | | | | | | | | | | | | | | | | | | | | | | | | | |
| 45 | CD | | | | | | | | | | | | | | | | | | | | | | | | | | | | | | |
| 55 | CBERR | | | | | | | | | | | | | | | | | | | | | | | | | | | | | | |
| 56 | CBSPK | | | | | | | | | | | | | | | | | | | | | | | | | | | | | | |
| 58 | ALFERR | | | | | | | | | | | | | | | | | | | | | | | | | | | | | | |
| 59 | AL2O3H | | | | | | | | | | | | | | | | | | | | | | | | | | | | | | |
| 60 | AL2O3L | | | | | | | | | | | | | | | | | | | | | | | | | | | | | | |
| 61 | OACURV | | | | | | | | | | | | | | | | | | | | | | | | | | | | | | |
| 62 | OAERR | | | | | | | | | | | | | | | | | | | | | | | | | | | | | | |
| 63 | AE | | | | | | | | | | | | | | | | | | | | | | | | | | | | | | |
| 65 | AEKWH | | | | | | | | | | | | | | | | | | | | | | | | | | | | | | |
| 66 | BHCALC | | | | | | | | | | | | | | | | | | | | | | | | | | | | | | |
| 67 | BHL | | | | | | | | | | | | | | | | | | | | | | | | | | | | | | |
| 68 | BHH | | | | | | | | | | | | | | | | | | | | | | | | | | | | | | |

***Table 5.17*** *Sequence of Detected Abnormalities in November 2008 for Cell 2008*

From 1st November the line current is reduced by 2 kA per week for a period of 5 weeks (Figure 4.6). This reduction in the line current results in a deterioration of the process stability for both groups according to the rise in the ellipsoid volume. At the beginning of November a step increase in the ellipsoid volume for the test cells indicates severe problems with the underlying process stability (Figure 5.10). This can be tracked to one cell in the test group. In

this period Cell 2008 shows an instantaneous rise in the ellipsoid volume by a factor of 1.8. In order to investigate the underlying process mechanisms acting in this cell Table 5.16 and Table 5.17 show the sequence of the detected abnormalities in October and November.

For Cell 2008, increased alumina feeding (AL2O3H, event 59) is observed for the first two weeks of October. This is most likely related to plugged or blocked feeders (CBSPK, event 56) and problems with the alumina dissolution effectiveness (OACURV, AE, AEKWH; events 61, 63, 65). Thereafter uncontrolled alumina feeding to Cell 2008 results in sludge formation and low bath levels (22→15 cm) as identified in case of the sludge cycle (Section 5.2.1). Periods with back feeding (OAERR, event 62) are most likely initiated by large disturbances in the metal pad during the termination of anode effect by lowering the ACD (Figure 1.8). After two weeks of October these problems are signalled with high Hotelling (HOTAH, event 33) and high pinballing (PBH, event 34).

In the third week of October low bath levels (average 16 cm) and high sludge levels initiate a rapid increase in the temperature (961→986°C) and superheat (9→19°C) due to increased heat generation. The reduction in the line current (November 1$^{st}$) and a line current outage for 150 minutes (November 3$^{rd}$) swings Cell 2008 from the high temperature region into long period of cold temperatures (986→926°C). This behaviour is mirrored in the rapid increase in the ellipsoid volume.

Figure 5.11 shows the development of pinballing over time for the test and reference cells. Pinballing is presented as a 70 days moving average to synchronize the time period with the 30 measurements which are used in the calculation of the ellipsoid volume (Section 3.3.1). As discussed in Section 5.2.3 blockages in control actions under abnormal conditions avoid overcorrection. For the test cells, less rapid changes in bath temperature and liquidus point underline the effectiveness of this approach. Furthermore, the occurrence of pinballing shows a faster and earlier response to abnormalities than the development of the ellipsoid volume over time. In addition, pinballing signals out of control behaviour inside the ellipsoid.

The existing control strategy applied to the reference cells clearly results in overcorrecting actions. These cells operate at a lower cell voltage than the test cells as demonstrated in Figure 5.12. Independently of the cause of abnormality, the cell voltage is adjusted based on compensation for high temperatures in the reference group (Equation 3.6). As described in Section 1.3.2 a lower cell voltage results in a lower ACD. This leads to an increase in the back reaction of aluminium to alumina, primarily due to a decrease in the distance between the anode and the metal pad. Under these conditions the current efficiency deteriorates over time as given by a decrease in the ratio of alumina shots fed to the reference cells related to the line current (Figure 5.13)

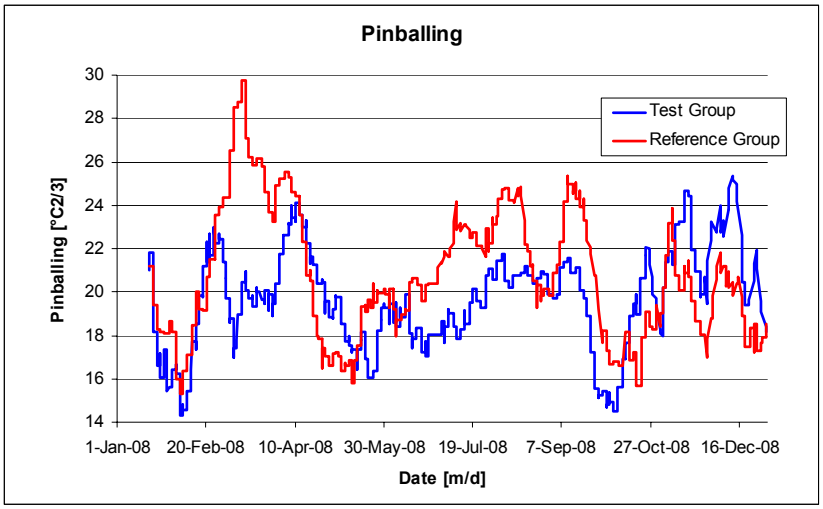


***Figure 5.11*** *Development of Pinballing over Time (Test and Reference Cells)*

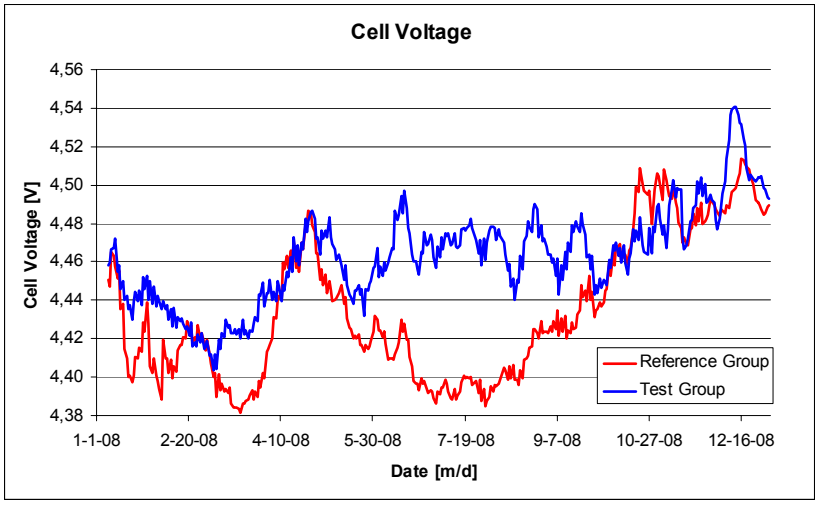


***Figure 5.12*** *Development of Cell Voltage over Time (Test and Reference Cells)*

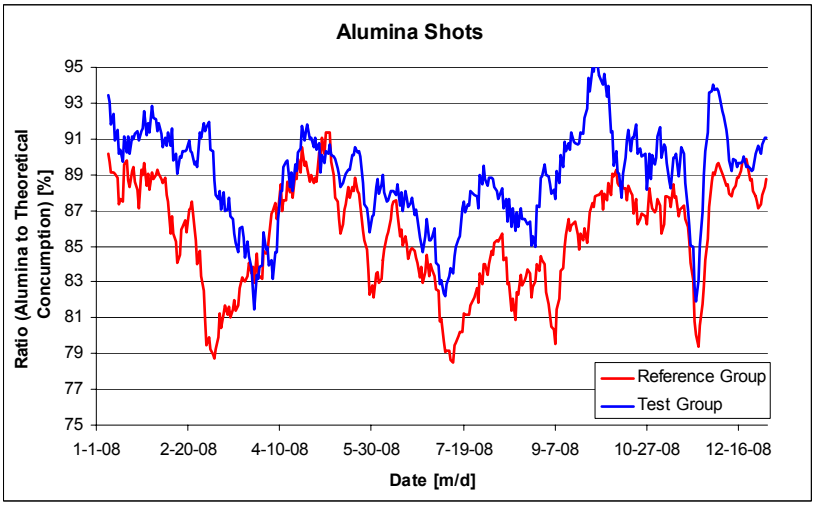


***Figure 5.13*** *Development of Alumina Shots over Time (Test and Reference Cells)*

Table 5.18 shows the significant correlations between the ellipsoid volume (variable 29) and pinballing (variable 31) with other variables and events for the test cells. By its definition the ellipsoid volume is positively correlated to the variability in the bath and liquidus temperature, and superheat. Low bath levels (BHL, event 67) and critical low temperatures (TEMPKL, even 37) are also positively correlated with the ellipsoid volume. Together with the positive correlation between pinballing with OAERR and OACURV (events 61, 62), this indicates a relation to the sludge cycle (Section 5.2.1). Abnormalities in anode conditions like anode spikes (ANSPS, event 49) also lead to increased variability in the ellipsoid volume. Because of their indirect effect the correlations between ellipsoid volume or pinballing and the current and energy efficiency are weaker.

| Ellipsoid Volume | | | Pinballing | | |
|---|---|---|---|---|---|
| **Nr.** | **Process Variable or Event** | **Correlation Coefficient** | **Nr.** | **Process Variable or Event** | **Correlation Coefficient** |
| 12 | Temperature (CV) | 0.77 | 34 | PBH | 0.82 |
| 14 | Liquidus (CV) | 0.76 | 62 | OAERR | 0.70 |
| 16 | Superheat (CV) | 0.74 | 53 | CLMVH | 0.65 |
| 49 | ANSPS | 0.72 | 61 | OACURV | 0.62 |
| 37 | TEMPKL | 0.70 | | | |
| 67 | BHL | 0.65 | | | |
| 69 | BVDEC | 0.64 | | | |

***Table 5.18*** *Correlation between Ellipsoid Volume and Pinballing with Variables and Events for the Test Cells*

| Ellipsoid Volume | | | Pinballing | | |
|---|---|---|---|---|---|
| **Nr.** | **Process Variable or Event** | **Correlation Coefficient** | **Nr.** | **Process Variable or Event** | **Correlation Coefficient** |
| 31 | Pinballing | 0.83 | 29 | Ellipsoid Volume | 0.83 |
| 37 | TEMPKL | 0.79 | 37 | TEMPKL | 0.76 |
| 40 | LIQL | 0.76 | 40 | LIQL | 0.72 |
| 12 | Temperature (CV) | 0.74 | 5 | Anode Effect | 0.67 |
| 14 | Liquidus (CV) | 0.74 | 34 | PBH | 0.66 |
| 34 | PBH | 0.72 | 32 | Pinballing (CV) | -0.66 |
| 5 | Anode Effect | 0.70 | 6 | Anode Effect (CV) | -0.65 |
| 36 | TEMPL | 0.69 | | | |
| 47 | ANSPA | 0.69 | | | |
| 51 | ANOFF | 0.67 | | | |
| 65 | AEKWH | 0.66 | | | |

***Table 5.19*** *Correlation between Ellipsoid Volume and Pinballing with Variables and Events for the Reference Cells*

Table 5.19 shows the significant correlations between the ellipsoid volume (variable 29) and pinballing (variable 31) with other variables and events for the reference cells. Abnormalities in the alumina feeding (anode effects, AEKWH; variable/event 5, 65) and anode conditions (ANSPA, ANOFF; events 47, 51) are correlated to the ellipsoid volume. These abnormalities, if not corrected or removed, result in a deterioration of the ensuing mass and energy balance

(variability in the bath and liquidus temperatures, TEMPL, TEMPKL, LIQL; variables/events 12, 14, 36, 37, 40). For the reference cells, a weak correlation between the ellipsoid volume and current efficiency (R = -0.40) is found.

According to Hypothesis 1 liquid bath mass variation is driven primarily by the sludge cycle as confirmed by liquid bath mass measurements for Cell 2008 (Section 5.2.1.2). Figure 5.14 shows the development of the ellipsoid volume and pinballing for this cell over the same period as the liquid bath measurements. The ellipsoid volume is weakly and inversely linked to the liquid bath mass as derived from Figures 5.9 and 5.14 (R = -0.44). This implies better process stability at higher liquid bath mass, which may be linked to the effectiveness of alumina dissolution. No significant correlation between the liquid bath mass with the cell superheat is observed. Pinballing shows an oscillating pattern of low and high process velocity in Cell 2008. This pattern is linked to an increase in the average amount of alumina additions (1850→2175 kg/day) and increased variation in alumina additions (±100→±210 kg/day), mainly due to increased current interruptions in August (Figure 4.6)

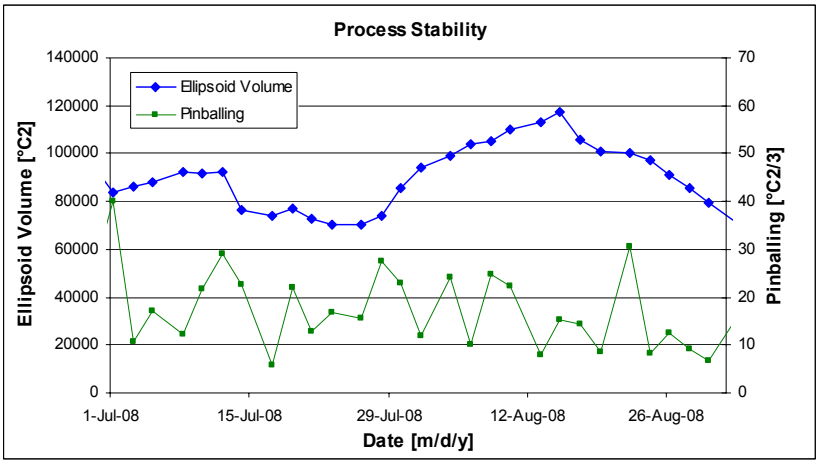


***Figure 5.14*** *Development of the Ellipsoid Volume and Pinballing (Cell 2008)*

### 5.2.2.2 Abnormality Detection

The multivariate statistical analyses undertaken in Section 5.1.4 confirm and characterize the following mechanisms of abnormality: for the test cells, alumina feeding, hardware failures of the alumina feed equipment and anode problems. For the reference cells, however, principal component 1 contains a wide range of detected abnormalities resulting in intensified variation. Evidently the cause-specific detection and diagnosis of abnormalities in the test cells has led to a more stable and predictable process behaviour (Section 5.2.3).

For the reference cells, the total duration of abnormalities (TOTEV, event 35) is significantly increased and correlated with a lower productivity, lower current efficiency and higher energy

consumption (Table 5.9). The number of abnormalities in the reaction of the cell resistance to an overfeed (OACURV, event 61), overfeed errors (OAERR, event 62), high energy anode effects (AEKWH, event 65) and critical high temperature events (TEMPKH, event 39) are inversely correlated with the current and energy efficiency. Figure 5.15 shows a Pareto chart of the duration (calculated per cell·day) of the detected abnormalities for the reference cells.

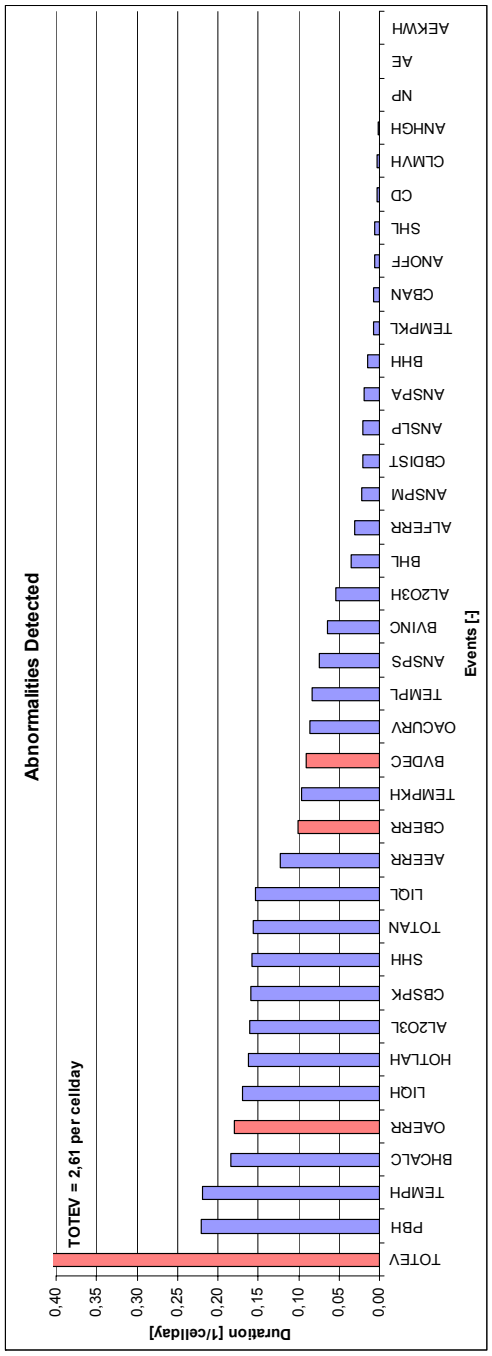


***Figure 5.15*** *Abnormalities for the Reference Cells*

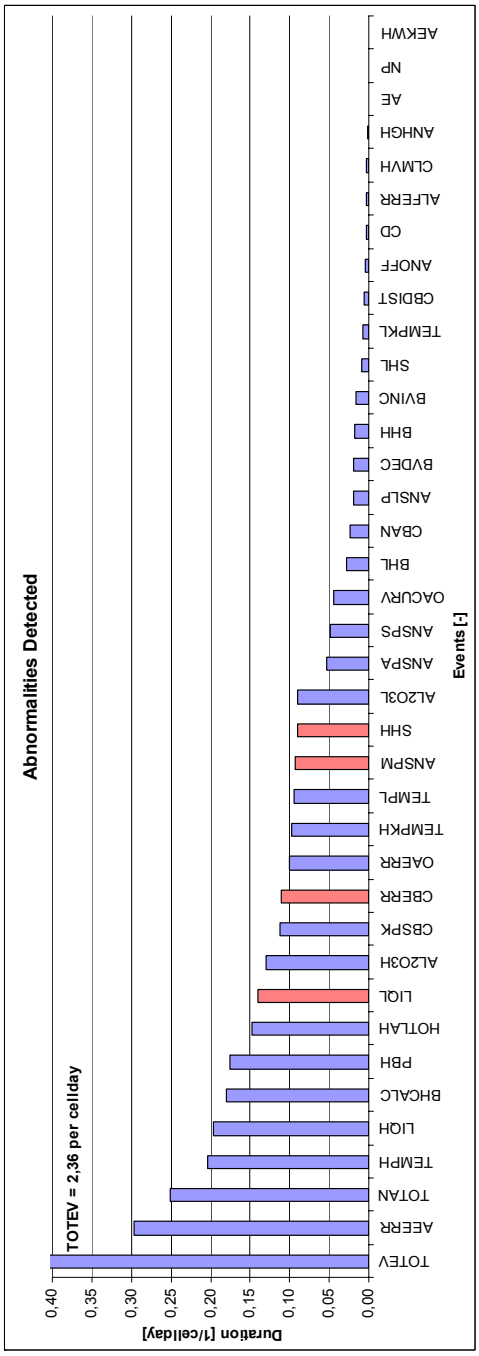


***Figure 5.16*** *Abnormalities for the Test Cells*

This causal correlation is not found for the test cells indicating the effectiveness of the more advanced abnormality detection system there for maintaining these cells within their most efficient operating window. A low number of overfeed errors (OAERR, event 62) and the automatic detected anode spikes (ANSPA, event 47) are identified as significant individual contributors to the productivity, current efficiency and energy consumption on these cells (Section 5.1.2.5). The numbers of high and low CUSUM of the ratio of alumina fed (AL2O3H, AL2O3L; events 59, 60) are also linked to the overall performance for the test cells. Figure 5.16 shows a Pareto chart of the duration of the abnormalities for these cells.

Other abnormalities are problems with the anode conditions (Figure 5.17). For the test cells, anode problems are recognized as main contributors to PC3, however, this PC captures only 2.9% of the variance (Section 5.1.4.1). A higher number of correctly detected anode spikes for these cells have enabled the operators to remove them and restore the cell efficiency, highlighting the importance of the new system for abnormality detection (Section 5.1.2.2). Moreover, the paired correlation between anode spikes detected by the measurement team (ANSPM, event 48) in stead of the routine check by shift operators with the silicon content in the metal assumes inadequate spike detection by normal procedures (Section 5.1.3.5).

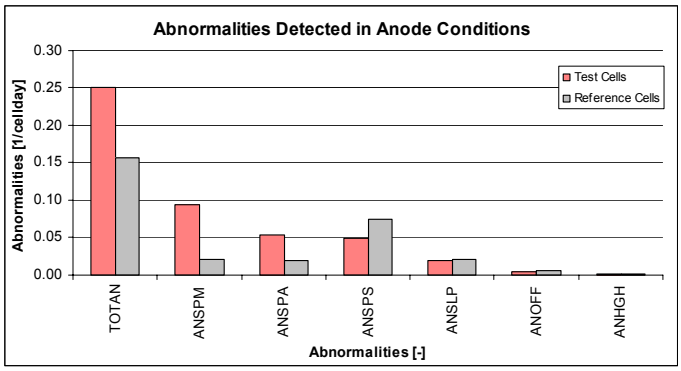


***Figure 5.17*** *Abnormalities Detected in Anode Conditions (Test and Reference Cells)*

For the reference cells, PC3 also incorporates abnormalities in anode conditions (Section 5.1.4.2). These abnormalities result in excursions in mass and energy balance control. There is also a contribution of the alumina feeding. The decrease in the liquid bath mass combined with increased alumina feeding indicates potential problems with alumina dissolution. The combination suggests a slow detection of anode problems, resulting in an overcompensation of the control model. This leads to a reduction in energy supply to the cells and a reduction of the alumina dissolution rate.

# Chapter 6 Conclusions and Further Developments

This chapter presents the conclusions of the industrial experiments carried out with the new control philosophy as described in the previous chapters. For the test cells, the employment of the new control approach has resulted in a higher current efficiency (+2.0%, p=0.075) and significantly lower energy consumption (-0.42 kWh/kg, p=0.034) for 2008 compared to 2007. The variations in current and energy efficiency between the cells within the test group have been halved. Section 6.1 discusses the two hypotheses postulated in this thesis. Section 6.2 considers further developments in maximizing the still unutilized potential of the system and its operational flexibility under the currently changing smelter operating conditions.

## 6.1 Hypotheses

This section presents the conclusions regarding the two hypotheses postulated in this thesis. Hypothesis 1 deals with a prevailing sludge cycle caused by incomplete alumina dissolution driving liquid bath mass variations and increased alumina feeding as discussed in Section 6.1.1. Hypothesis 2 involves the improvement of the stability of the smelting process using natural behaviour envelops for individual cells and cause-specific detection and diagnosis of process abnormalities (Section 6.1.2).

### 6.1.1 Sludge Cycle Driving Liquid Bath Mass Variations

This thesis has identified a prevailing sludge cycle caused by incomplete alumina dissolution as a major self-accelerating deterioration mechanism within smelting cells. The effectiveness of the alumina feeding plays a predominant role in maintaining maximum current and energy efficiency at increased variations in energy and raw material inputs. A tight control of the superheat, bath height and alumina concentration have been identified as main parameters to minimize the sludge cycle (Section 5.2.1).

Multivariate statistical analysis has identified the necessity of a good control of the interaction between the bath temperature, composition, bath height and alumina feeding characteristics for the test cells (PC1=84.5%). These cells operate at a 0.5% lower and more stable alumina concentration. This is confirmed by a significantly lower average and variability in underfeed duration, higher number and lower variability in anode effects (variables 5, 6 in Table 5.1), and higher liquidus temperature (variable 13 in Table 5.1). For the test cells, a tighter control of the superheat and alumina concentration is confirmed by a significant correlation between the bath temperature with the $AlF_3$ concentration (variables 11, 17 in Table 5.1). This paired correlation represents the self-regulating mechanism within smelting cells as demonstrated in Figure 2.4.

Furthermore, the test cells show a significantly lower number of abnormalities in the reaction of the cell resistance to overfeed (OACURV, event 61 in Table 5.6). This is linked to reduced sludge formation for the test cells. The reference cells on the other hand had a higher number of these abnormalities and consequently lower current and energy efficiency. Similarly the number of overfeed errors (OAERR, event 62 in Table 5.6) is linked to sludge dissolution and these abnormalities are higher for the reference cells compared to the test cells.

The integrity of the alumina feeding hardware has been identified as a major factor in the loss in the current and energy efficiency for the test cells (PC2=10.0%). Reliable soft sensors for the detection of these failures have been designed (CBERR, CBSPK, CBDIST; events 55-57 in Table 5.6). Hardware failures are related to poor control of alumina feeding through a low number of overfeeds (OAERR, event 62 in Table 5.6). These hardware failures are partly influenced by line current outages due to plugged and frozen feeder holes. Plugged feeder holes (CBSPK, event 37 in Table 5.6) result in critical low bath temperatures (TEMPKL, event 56 in Table 5.6) because uncontrolled feeding is occurring under these circumstances.

The sludge cycle has also been proven to cause (rapid) liquid bath mass variations. This was previously unknown. The control approach used here reduces these liquid bath mass variations. This is confirmed by liquid bath mass measurements before and after the employment of the new control philosophy and sensors. A reliable soft sensor for the detection of rapid increase in liquid bath mass (BVINC, event 70 in Table 5.6) has been developed in this research. This is confirmed by a significant correlation between the new sensor and the iron content (variable 9 in Table 5.1) due to bath contact with anode stubs. The test cells show a significantly lower variability in the liquid bath mass (BVDEC, BVINC; events 69, 70 in Table 5.6). However, the observed variations in bath mass are still substantial. This has a detrimental effect on the control of the test cells within their optimum operating window (Figure 3.17). It is also important that no significant correlations between superheat and liquid bath mass variations are found for either cell group, because the side wall ledge dynamics are not the cause of the liquid bath mass variations.

### 6.1.2 Multivariate Causally Based Control

Diagnoses of abnormalities and subsequent correction or removal of the underlying causes have resulted in more stable and predictable system dynamics (Section 5.2.2). This is confirmed by the inverse correlation between the number of abnormalities (TOTEV, event 35 in Table 5.6) with the current and energy efficiency for the reference cells and the absence of this correlation for the test cells.

For the reference cells, a higher average and more variable superheat (variables 15, 16 in Table 5.1) indicate the presence of severe process excursions within the system. Conversely the test cells had significantly lower number of rapid variations in temperature/liquidus point (PBH, event 34 in Table 5.6), lower variability in cell voltage (variable 21 in Table 5.1) and therefore in the ACD, voltage noise (variable 25 in Table 5.1) and cathode resistance (variable 23 in Table 5.1). These all demonstrate better process stability for the test cells.

Soft sensors for the detection of abnormalities in the anode conditions have been developed in this work. Anode problems (ANSPA, ANSPM, ANSPS; event 47-49 in Table 5.6) have been identified as major contributors to losses in current and energy efficiency. For the reference cells where these sensors were not employed, the paired correlation between the anode spikes with the silicon content in the metal (variable 19 in Table 5.1) shows inadequate spike detection. The increase in the silicon content (variable 19 in Table 5.1) is linked to the absence of side ledge (locally) due to excessive heat generation and superheat.

As discussed in Section 6.1.1 a prevailing sludge cycle has been identified as a major driver of deterioration in process stability. Hardware failures in the feeding equipment and problems in the anode conditions further contribute to losses in the current and energy efficiency. A sequence of abnormal behaviours often leads to more complex interactions between the mass and energy balance for aluminium smelting cells. These conditions are captured by the development of the natural behaviour envelop of each cell over time.

Periodic recalculation of the ellipsoid envelop adds an internal self-checking and reinforcing mechanism to the control model. The multidimensional envelops shrink over time if the abnormalities are corrected or removed one by one. In turn the smaller envelop results in better detection of abnormalities and a process state closer to optimality. This is confirmed by a significantly lower average and variability of the ellipsoid volume and lower pinballing for the test cells (variables 29-32 in Table 5.1). However, the detection of abnormalities using the natural behaviour envelop deteriorates if the envelop increases in size due to poorer process stability for example after line amperage outages or raw material changes. Under these conditions cause-specific detection using the soft sensors is necessary to restore the required process conditions.

## 6.2 Further Developments

This section proposes further developments based on the conclusions and outcomes of this thesis. Further improvements in the alumina feeding strategy, but also better knowledge of the chemical and physical properties involved in the alumina dissolution effectiveness within smelting cells are required (Section 6.2.1). A further extension of the dimensionality of the

multivariate control approach may maximize the system potential and operational flexibility in respect to the stability of the process behaviour and abnormality detection (Section 6.2.2). Furthermore, the development of an advanced system for the guidance of human decisions further improves the effectiveness of the multivariate causally based control approach within smelting cells (Section 6.2.3).

### 6.2.1 Alumina Feeding

The alumina dissolution effectiveness has been established as a major factor in achieving maximum current and energy efficiency for smelting cells. The controllability of the system dynamics including the alumina concentration deteriorates with increased variation in energy input and raw material quality. Advanced mass balance control is required at these varying conditions. However, indirect control of the alumina concentration via the pseudo-resistance as applied in industrial smelting cells is a major constraint regarding advanced mass balance control because variations in the liquid bath mass are not taken into account. Direct measurements of the effectiveness of the alumina feeding process would fundamentally change controllability of the cell mass balance.

The liquid bath mass is still unknown in the traditional control approach resulting in incorrect control where undetected liquid bath mass variations is occurring, e.g. in the sludge cycle. A sensor for the determination of the liquid bath mass in smelting cells would provide extra information about the alumina dissolution effectiveness over time. Such a sensor may also detect alumina accumulation through its presence in the sludge. In this respect an automatic calculation of the metal height as described in Equation 2.22 can be used to detect sludge formation by monitoring differences in the rate of metal height increase. The reliability of this metal height sensor is currently insufficient for its deployment.

### 6.2.2 Multivariate Causally Based Control

Despite improvements in the efficiency and stability of the test cells, large variations in the underlying process behaviour envelops are still present (variable 30 in Table 5.1 and Figure 5.10). Some of these variations are influenced by power modulation and undetected abnormalities. Therefore extension of the multivariate control approach to these factors would further improve control.

For example the incorporation of $AlF_3$ additions, energy input, superheat and tapped metal in the control envelop would provide this extra abnormality detection capability. In order to detect changes in these process variables a CUSUM could be used as in the case of alumina feeding. Hotelling $T^2$ statistic can still be used to derive the three control zones

representing structural variation, out of control behaviour and the zone in which compensatory control actions are applied (Section 3.2.1.3).

### 6.2.3 Human Feedback Loops

This thesis demonstrates how a multivariate causally based approach is able to improve the controllability of smelting cells. The control philosophy combines the multivariate interactive characteristics of the smelting process with advanced detection of abnormalities and specific failure mechanisms. Detection of abnormalities by the control system does not in itself change the control outcome of the process. Correction or removal of these abnormalities by humans is often required. Therefore the behaviour of each person in the process is critical to the effectiveness of the control approach.

The development of a supervisory control system as part of the multivariate control approach may assist in making better human decisions. The information generated by the control system needs to be made available in a visual way to guide operator decisions. Additional feedback from the operators into the control system is essential to close the PDSA-cycle. Better understanding of psychologically related factors such as intuitive reasoning, operator response characteristics, perception of risk and implication of reward may support advanced detection of abnormalities and specific failure mechanisms.

# References

Abbas, H., Taylor, M.P., Farid, M., Chen, J.J.J., "The Impact of Cell Ventilation in the Top Heat Losses and Fugitive Emissions in an Aluminium Smelting Cell", Light Metals, 2009, pp. 551-556

Abraham, R.H., Shaw, C.D., "Dynamics: A Visual Introduction." In F. Eugene Yates, ed., *Self-Organizing Systems: The Emergence of Order*. New York: Plenum Press, 1987, pp. 543-597

Alusuisse Electrolysis Seminar, Chippis, Switzerland, 1998

Andrews, E.W., "A Controllable Continuous Mass-Feed System for Aluminium Smelters", Ph.D. Thesis, University of Auckland, New Zealand, 1998

Andrews, E.W., Taylor, M.P., Johnson, G.L., Coad, I. "The Impact of Anode Cover Control and Anode Assembly Design on Smelting Cell Performance – Part 2", Light Metals 2005, pp. 357-362

Atkins, P.W., "Physical Chemistry", 4th edition, 1990

Bearne, G., "Reduction Lines Process Control Development", Proc. 6th Australasian Aluminium Smelting Technology Conference and Workshops, 1998, pp. 91-130

Bearne, G., Whitfield, D., "Improving Smelting Cell Metal Level Measurement and Control", Light Metals, 2005, pp. 413-418

Berezin, A.I., Polyakov, P.V., Rodnov, O.O., Yasinski, V.L., Stont, P.D., "FMEA-based Expert System for Electrolysis Diagnosis", Light Metals, 2005, pp. 429-434

Brant Filho, A.C. et al., "The Operation of a Smelter with Power Modulation", Light Metals, 1992, pp. 357-362

Brisk, M.J., "Process Control: Potential Benefits and Wasted Opportunities", Control Conference, 2004, Vol. 1, pp. 10-16

Bruggeman, J.R., "Pot Heat Balance Fundamentals", Proc. 6th Australasian Aluminium Smelting Technology Conference and Workshops, 1998, pp. 167-190

Chen, J.J.J. and Taylor, M.P., "Control of Temperature and Aluminium Fluoride in Aluminium Reduction", Aluminium, Vol. 81 (7/8), 2005, pp. 678-682

Cheng, C.S., "A Neural Network Approach for the Analysis of Control Chart Patterns", Int. J. Prod. Res., Vol. 35, No. 3, 1997, pp. 667-697

Cooksey, M., Taylor, M.P., Chen, J.J.J., "Resistance Due to Gas Bubbles in Aluminum Smelting cells", JOM, 2008, pp. 51-57

Creemers, M.R., Leijendeckers, P.H.H., Maarschalkerwaart, M.C.M. van, Tysma, Sj., "Poly-technisch Zakboekje, 1987

Crowley, J.L., Demazeau, Y., "Principles and Techniques for Sensor Data Fusion", Signal Processing, Volume 23, 1993

Dando, N.R., "Using Fume Duct Temperatures for Minimizing Open Holes in Pot Cover", Light Metals, 2004, pp. 245-248

Deming, W.E., "Out of Crisis", 1st Edition, Massachusetts Institute of Technology, Center for Advanced Engineering Study, Cambridge, MA, 1982

Deming, W.E., "The New Economics for Industry, Government, Education", 2nd Edition, 2000

Drengstig, T., "On Process Model Representation and $AlF_3$ Dynamic of Aluminium Electrolysis Cells", PhD Thesis, Norwegian University of Science and Technology, Trondheim, 1997

Dupas, N., "Increasing Electrolysis Pot Performances through New Crustbreaking and Feeding Solutions", Light Metals, 2009, pp. 337-340

Eisma, D. and Patel, P., "Challenges in Power Modulation", Light Metals 2009, pp. 327-332

Entner, P., "Control of $AlF_3$ Concentration", Light Metals, 1992, pp. 369-374

Ferreira, H., Nagem, N.F., Braga, C., Leite, P., Coimbra, B., Batista, E., Bessa, E., Maia, E., Kato, C., Camara, J., "Smart Feeders at Alumar Plant", Light Metals, 2008, pp. 339-341

Frost, F., Karri, V., "Identifying Significant Parameters for Hall-Heroult Process Modelling using General Regression Neural Network", 13th International Conference on Industrial and Engineering Applications of Artificial Intelligence and Expert Systems, 2000, pp. 73-78

Gao, Y.S., Gustafsson, M., Taylor, M.P., Chen, J.J.J., "The Control Ellipse as a Decision Making Support Tool to Control Temperature and Aluminium Fluoride in Aluminium Reduction", Proc. 9th Australasian Aluminium Smelting Technology Conference and Workshops, 2007, pp. 265-275

Gao, Y., Taylor, M.P., Chen, J.J.J., Hautus, M.J., "Operational Decision Making in Aluminium Smelters", Engineering Psychology and Cognitive Ergonomics, Volume 5639, 2009, pp. 167-178

Graduate Certificate Course in Aluminium Smelting Process Technology, University of New South Wales, 2003

Graduate Certificate in Aluminium Smelting Technology, University of Auckland, 2008

Green, J.A.S., "Aluminium Recylcing and Processing for Energy Conservation and Sustainability", ASM International, Metals Park, OH, USA, 2007

Grjotheim, K., Kvande, H., "Introduction to Aluminium Electrolysis", Aluminium-Verlag, 2nd edition, Düsseldorf, 1993

Guðmundsson, G.A., "Automatic Determination of Metal Height in Electrolysis Cells", Light Metals, 1999, pp. 297-302

Gupta, P., "Six Sigma Business Score Card", McGraw-Hill, 2004

Haverkamp, R.G., Welch, B.J., "Alumina Concentration Measuring Device", NZ Patent, 272 913, 1995

Haupin, W., Kvande, H., "Thermodynamics of Electrochemical Reduction of Alumina", Light Metals, 2001, pp. 379-384

Holt, N., Anderson, N.M., Karlsen, M., Foosnaes, T., "Ventilation of Potrooms in Aluminium Production", Light Metals, 1999, pp. 263-268

Homsi P., "Alumina Requirements for Modern Smelters", Proc. 7th Australasian Aluminium Smelting Technology Conference and Workshops, 2001, pp. 426-455

Hvidsten, R., Rye, K.Å., "Smart" Feeders for Alumina in a Hall-Heroult Prebake Cell", Light Metals 2007, pp. 435-438

Hyland, M., Patterson, E., Welch, B.J., "Alumina Structural Hydroxyl as a Continuous Source of HF", Light Metals, 2004, pp. 361-366

Iffert, M., "Aluminium Smelting Cell Control and Optimalisation", Ph.D. Thesis, University of New South Wales, Sydney, Australia, 2007

ISO/TS16949: Quality Management Systems – Particular Requirements for the Application of ISO 9001:2000 for Automotive Production and Relevant Service Part Organizations", 2002

Johnson, R.A., "Miller & Freund's Probability & Statistics for Engineers", 5th Edition, Englewood Cliffs, 1994

Jounier, B.L., "Fourth Generation Management: The New Business Consciousness", 1st Edition, 1994

Karlsen, M., Kielland, V., Kvande, H., Vestre, S.B., "Factors Influencing Cell Hooding and Gas Collection Efficiencies", Light Metals, 1998, pp. 303-310

Keniry, J., Shaidulin, E., "Anode Signal Analysis - The Next Generation in Smelting cell Control", Light Metals, 2008, pp. 287-292

Kessler, W., Kessler, R.W., "Industrial On-line Quality Control of Thin Surface Layers on Metal Sheets by Spectral Interference in Combination with Multivariate Data Analysis", EuroPact, 2008

Kloetstra, K.R., Stam, M.A., "Optimisation of Aluminium Fluoride Control at Aluminium Delfzijl", Proc. 7th Australasian Aluminium Smelting Technology Conference and Workshops, 2001, pp. 506-514

Kosko, B., Isaka, S., "Fuzzy Logic", Scientific American, July 1993, pp. 76-81

Kourti, T., Lee, J., MacGregor, J.F., "Experiences with Industrial Applications of Projection Methods for Multivariate Statistical Process Control", Computers Chemical Engineering, Vol. 20, 1996, pp. S745-S750

Kvande, H. and Haupin, W., "Cell Voltage in Aluminium Electrolysis: a Practical Approach", JOM, 2000, pp. 31-37

Li, J., Ding, F., Zou, Z., Li, M., Liu, Y., Bian, Y., Wu, Z., Liu, G., "Development of Fuzzy Expert Control Technique for Aluminium Electrolysis", Light Metals, 2001

MacGregor, J.F., Kourti, T., “Statistical Process Control of Multivariate Processes”, Control Engineering Practice, Vol. 3, No. 3, 1995, pp. 403-414

Majid, N.A.A., Young, B.R., Taylor, M.P., Chen, J.J.J., “Detecting Abnormities in Aluminium Smelting Cells Based on Process Events using Multi-Way Principle Component Analysis (MPCA)”, Light Metals, 2009

Martin, O., Despinasse, S., Ritter, C., Santerre, R., Tomasino, T., “The FECRI Approach and the Lastest Developments in the AP3X Technology, Light Metals, 2008, pp. 255-260

Meghlaoui, A., Aljabri, N., “Aluminium Fluoride Control Strategy Improvement”, Light Metals, 2003, pp. 425-429

Metson, J.B., Hyland M.M. and Groutso, T., “Alumina Phase Distribution, Structural Hydroxyl and Performance of Smelter Grade Alumina in the Smelting Cell”, Light Metals, 2005, pp. 425-429

Moors, E., “Technology Strategies for Sustainable Metals Production Systems: A Case Study of Primary Aluminium Production in The Netherlands and Norway”, Journal of Cleaner Production 14, 2006, 1121-1138

Moxnes, B.P., Aga, B.E., Skaar, J.H., “How to Obtain Open Feeder Holes by Installing Anodes with Tracks”, Light Metals, 1998, pp. 247-255

Moxnes, B.P., Solheim, A., Støre, T., Aga, B.E., Støen, L. “The “Liquidus Enigma” Revisited”, Light Metals, 2006, pp. 285-290

Moxnes, B.P., Kvande, H. and Solheim, A., “Experience and Challenges with Amperage Increase in Hydro Aluminium Potlines”, Light Metals 2007, pp. 263-268

Moxnes, B.P., Solheim, A., Liane, M., Svinsås, E., Halkjelsvik, A., “Improved Cell Operation by Redistribution of the Alumina Feed”, Light Metals, 2009, pp. 461-466

Nelson, L.S., “Technical Aids”, Journal of Technology Quality, 16, no. 4, October 1984

Perander, L.M., Zujovic, Z.D., Hyland, M.H., Smith, M.E., O’Dell, L.A., Metson, J.B., “Short- and Long-Range Order in Alumina - Development of Nano- and Microstructures during the Calcination of Bayer Gibbsite”, Light Metals, 2008, pp. 29-35

Purdie, J.M., “Alumina Behaviour and Related Process Variations in Aluminium Smelting”, PhD Thesis, University of Auckland, 1993

Purdie, J.M., “The Effect of Feeder Design on the Alumina Concentration”, Proc. 5th Australasian Aluminium Smelting Technology Conference and Workshops, 1995

Rieck, T., Iffert, M., White, P., Rodrigo, R., Kelchtermans, R., “Increased Current Efficiency and Reduced Energy Consumption at the TRIMET Smelter Essen using 9 Box Matrix Control”, Light Metals, 2003, pp. 449-457

Roffel, B., “Introduction to Multivariate Process Control”, University of Groningen, 2008

Rolofs, B., Wai-Poi, N.,“The Effect of Anode Spike Formation on Operational Performance”, Light Metals, 2000, pp. 189-193

Rolseth, S., Verstreken, P., Kobbeltvedt, O., “Liquidus Temperature Determination in Molten Salts”, Light Metals, 1998, pp. 359-366

Rutledge, S., “Statistical Methods for Use in the Aluminium Smelting Industry”, Light Metals, 2008, pp. 325-327

Sadler, B.A., Welch, B.J., “Anode Consumption Mechanisms – A Practical Review of the Theory and Anode Property Considerations”, Proc. 7th Australasian Aluminium Smelting Technology Conference and Workshops, 2001, pp. 294-335

Saving Iceland, http://savingiceland.puscii.nl/?language=en, 2009

Shewhart, W.A., “Economic Control of Quality of Manufactured Product”, 1931

Sintef, www.sintef.no/static/mt/2423/light_metal/software/index.htm, 2009

Solheim, A., Sterten, Å., “Activity Data for the System NaF-$AlF_3$”, *Proceedings of the Ninth International Symposium on Light Metals Production,* Tromsø-Trondheim, Norway, August 18 - 21, 1997

Sølie, M., Øye, H.A., ”Cathodes in Aluminium Electrolysis”, 2nd Edition, Düsseldorf, 1994

Stam, M.A., Kloetstra, K.R., “Development of an Advanced Control Strategy at Aluminium Delfzijl”, Proc. 8th Australasian Aluminium Smelting Technology Conference and Workshops, 2004, pp. 314-318

Stam, M.A., Taylor, M.P., Chen, J.J.J., Dellen, S. van "Operational and Control Improvements in Reduction Lines at Aluminium Delfzijl", Light Metals, 2007, pp. 243-247

Stam, M.A., Schaafsma, J., "The Impact of Power Modulation on the Cell Dynamics", Proc. 9th Australasian Aluminium Smelting Technology Conference and Workshops, 2007, pp. 465-472

Stam, M.A., Taylor, M.P., Chen, J.J.J., Mulder, A., Rodrigo, R., "Common Behaviour and Abnormalities in Aluminium Reduction Cells", Light Metals, 2008, pp. 309-314

Stam, M.A., Taylor, M.P., Chen, J.J.J., Mulder, A., Rodrigo, R., "Development of a Multivariate Process Control Strategy for Aluminium Reduction Cells", Light Metals, 2009, pp. 311-315

Stevens McFadden, F.J., Welch, B.J., Whitfield, D., Skyllas-Kazacos, M., "Control of Temperature in Aluminium Reduction Cells - Challenges in Measurements and Variability, Light Metals, 2001

Stevens McFadden, F.J., Bearne, G.P., Austin, P.C., Welch, B.J., "Application of Advanced Process Control to Aluminium Reduction Cells – A Review", Light Metals, 2001, pp. 1233-1242

Stevens McFadden, F.J., Welch, B.J., Austin, P.C., "Improving the Control of the Non-Alumina Electrolyte Variables in Aluminium Reduction Cells: Application of Multivariable Model-Based Control", Proc. 9th Australasian Aluminium Smelting Technology Conference and Workshops, 2007, pp. 245-264

Rye, K.Å., Solberg, I., Eidet, T., Rolseth, S., "Aluminium fluoride dissolution and distribution – an investigation of the dynamic mass balance when adding large quantities to a prebake cell", Light Metals, 2001, pp. 529-534

Tabereaux, A.T., "Impact of AE Kill Strategies on $CF_4$ emissions", Proc. 9th Australasian Aluminium Smelting Technology Conference and Workshops, 2007, pp. 127-138

Tandon, G., Taylor, M.P., Chen, J.J.J., "A Case Study of Variation in Aluminium Smelting Cell Thermal State with Control Implications", Metallurgical and Materials Transactions B, August 2007, pp. 707-712

Tarcy, G.P., Sorensen, J., "Determination of factors affecting current efficiency in commercial Hall cells using controlled potential coulometry and statistical experiments", Light Metals 1991, pp. 453-459

Taylor, A., "Impact of Bayer Process Conditions on the Characteristics of Smelter Grade Alumina", Proc. 8th Australasian Aluminium Smelting Technology Conference and Workshops, 2004, pp.128-147

Taylor, M.P., "The Influence of Process Dynamics on the Heat Balance and Cell Operation in the Electro winning of Aluminium", PhD Thesis, University of Auckland, 1984

Taylor, M.P., Welch, B.J., Keniry, J.T., "Effect of Electrochemical Changes on the Heat Balance in Aluminium Smelting Cells", Journal of Electro analytical Chemistry, Vol. 168, Issues 1-2, 25 May 1984, pp. 179-192

Taylor, M.P., McKibbin, R., Welch, B.J., "Effect of Convective Heat Transfer and Phase Change on the Stability of Aluminium, Journal AIChE, 1986

Taylor, M.P., Liu, X., Fraser, K.J., Welch, B.J., "The Dynamics and Performance of Smelting cell Electrolytes, Light Metals 1990, pp. 259-266

Taylor, M.P., "Challenges in Optimising and Controlling the Electrolyte in Aluminium Smelters", Molten Slags, Fluxes and Salts Conference, 1997, pp. 659-674

Taylor, M.P., Johnson, G.L., Andrews, E.W., Welch, B.J., "The Impact of Anode Cover Control and Anode Assembly Design on Smelting cell Performance", Light Metals 2004, pp. 199-206

Taylor, M.P., Welch, B.J., "Improved Energy Management for Smelters", Proc. 8th Australasian Aluminium Smelting Technology Conference and Workshops, 2004, pp. 550-566

Taylor, M.P., "Anode Cover Material - Science, Practice and Future Needs", Proc. 9th Australasian Aluminium Smelting Technology Conference and Workshops, 2007, pp. 77-96

Taylor, M.P., Chen J.J.J., Hautus, M.J., "Operational Control Decisions in Smelters", Proc. 9th Australasian Aluminium Smelting Technology Conference and Workshops, 2007, pp. 277-290

Taylor, M.P., Chen, J.J.J., “Advances in Process Control for Aluminium Smelters”, Materials and Manufacturing Processes, Vol. 22, 2007

Taylor, M.P., Mulder, A., Hautus, M.J., Chen, J.J.J., Stam, M.A., “Analysis of Human Work Decisions in an Aluminium Smelter”, International Journal of Decision Sciences, Risk and Management”, 2010

Tessier, J., Duchesne, C., Gauthier, C., Dufour, G., “Image Analysis for Estimation of Anode Cover Material Composition”, Light Metals, 2008, pp. 293-298

Tessier, J., Zwirz, T.G., Tarcy, G.P., Manzini, R.A., “Multivariate Statistical Process Monitoring of Smelting cells”, Light Metals, 2009, pp. 305-310

Thonstad, J., Fellner, P., Haarberg, G.M., Híveš, J., Kvande, H., Sterten, Å., “Aluminium Electrolysis – Fundamentals of the Hall-Héroult Process”, 3rd Edition, 2001

Torremans, H., “Lean Management. Europees Onderzoek. Leiderschap, Mensen, Management, én een Sterke Methodologie”, Partner Rijnconsult, November 2008

U.S. Department of Health and Human Services *et al.*, “Guidance for Industry; PAT - A Framework for Innovative Pharmaceutical Development, Manufacturing and Quality Assurance”, 2004

Vanvoren, C., Homsi, P., Basquin, J.L., Beheregaray, T., “AP50: the Pechiney 500 kA Cell”, Light Metals, 2001

Verstreken, P., Benninghoff, S., “Bath- and Liquidus Sensor for Molten Salts”, Light Metals, 1996, pp. 437-444

Wai-Poi, N.S., Haverkamp, R.G., Kübler, S., Müller-Steinhagen H. and Welch, B.J., “Thermal Effects associated with Alumina Feeding in Aluminium Smelting cells”, Light Metals, 1994, pp. 219-225

Wai-Poi, N.S. and Welch, B.J., “Comparing Alumina Quality Specifications and Smelter Expectations”, Light Metals, 1994, pp. 345-350

Wang, X., Tarcy, G., Hosler, B., Slaugenhaupt, M., Albright, S., “Paradox in Cell Temperature Measurement using Type K Thermocouples”, Light Metals, 2006, pp. 279-284

Welch, B.J., "Technology of Electrolyte Reduction of Alumina by Hall-Heroult Process: I. A Voltage Analysis Under Conditions of Varying Alumina Concentrations", Proceedings Autr. I.M.&M (No 214), 1965

Welch, B.J, Stretch, D.J., Purdie, J.M., "Continuous Alumina Feeder", U.S. Patent Number 5,476,574, 1995

Welch, B.J., "Current Efficiencies in Aluminium Smelting Cells", The 17th International Course on Process Metallurgy of Aluminium, Trondheim, Norway, 1998, Chapter 15, 1-22.

Welch, B.J., "The Impact of Changes in Heat Balance and Operations on the Electrolyte Composition", Proc. 6th Australasian Aluminium Smelting Technology Conference and Workshops, 1998, pp. 191-204

Welch, B.J., Keniry, J.T., "Advancing the Hall Heroult Electrolytic Process", Light Metals, 2000

Westerterp, K.R., Swaaij, W.P.M. van and Beenackers, A.A.C.M., "Chemical Reactor Design and Operation", Amsterdam, the Netherlands, Reprinted in 1993

White, P., Wai-Poi, N., Rolofs, B., Verstreken, P., Kelchtermans, R., "Development and Application of a Novel Sensor for Combined Measurement of Bath Temperature and Cathode Voltage Drop in Aluminium Cells", Light Metals, 2001, pp. 1179-1186

Whitfield, D., Skyllas-Kazacos, M., Welch, B.J., Stevens Mc Fadden, F., "Aspects of Alumina Control in Aluminium Smelting cells", Light Metals, 2004, pp. 249-255

Whitfield, D., Skyllas-Kazacos, M., Welch, B.J., White, P., "Metal Pad Temperatures in Aluminium Smelting cells", Light Metals, 2004, pp. 239-244

Womack, J.P., Jones, D.T., "Lean Thinking", Free Press, 2003

Zhang, W.D., Chen, J.J.J., Taylor, M.P., Welch, B.J., Chemica 91, Proceedings of 19th Australasian Chemical Engineering Conference, Newcastle, 1991